

# Hijacking novel non-PROTACable E3 ligases for targeted protein degradation

Doctoral thesis at the Medical University of Vienna  
for obtaining the academic degree

**Doctor of Philosophy**

Submitted by

**MSc, Chrysanthi Kagiou**

Supervisor:  
PhD, Georg E. Winter

CeMM Research Center for Molecular Medicine of the Austrian  
Academy of Sciences  
Lazarettgasse 14, AKH BT 25.3, 1090 Vienna, Austria

Vienna, June 2025

*To my aunt,  
Alma.*

## Acknowledgements

This thesis marks the end of the most exciting and enriching journey of my life so far – defined not only by scientific but also deep personal growth. The trajectory has been far from linear; starting a PhD during Covid-19 in a new city and restarting in a new lab and scientific field midway, were challenging experiences. What carried me through these moments was the incredible support I received from so many people, to whom I am extremely grateful.

First and foremost, I would like to thank my supervisor and mentor, Georg Winter, for his support from the moment I joined his lab. His words on my first lab meeting as a Winter lab member, referring to the lab change and restarting my PhD, will always stay with me:

*“Chrysa is on a soul finding - and I hope not soul crushing - journey.”*

Despite the hurdles that I came across, from transitioning into a new field to the pressure of being “scooped”, Georg always had my back, offering the encouragement I needed to keep going. Thank you, Georg, for believing in me, for being an inspiring scientific role model, and for helping me avoid the “soul crushing”.

I would like to extend my gratitude to the whole CeMM community - from Faculty, to PhDs, PostDocs and administrative staff - for supporting my PhD in countless ways. The scientific feedback, the fruitful collaborations and the many thoughtful exchanges greatly enriched and facilitated my PhD journey. Thank you to CeMM directors, Giulio and Anita, for the support during a time when the future of my PhD was uncertain. Being part of the CeMM community has truly made this PhD experience a one-in-a-lifetime and taught me the value of a vibrant and collaborative environment where science thrives through mutual support.

Along the way, I learnt that a PhD is not a lonely endeavor, and I owe a great deal to all the past and present members of the Winter lab. Thank you, guys, for welcoming me so warmly and making sure that I get all the support that I needed to find my way in the lab. I’ve made friends here that made the PhD experience unforgettable. In particular, thank you, Marko, for all the scientific and emotional support you provided throughout my whole PhD journey, from day one that you were assigned as my lab “buddy”, to the day we co-celebrated the publications of our papers, even to this day that you helped me translate my thesis abstract.

Of course, I am very grateful to Joanna Loizou, all the members of the Loizou lab and for my experience during the first 2 years of my PhD. Thank you, Joanna, for giving me the chance to begin this PhD in your lab, and for being a supportive mentor up to this day. My earliest steps as a PhD student were supported by so many generous Loizou lab members - thank you Jo, Sara, Anna, Goncalo and everyone else who taught me how to work in the lab and how to start thinking like a scientist. While the lab closing was a difficult chapter, it taught me resilience, dedication, and accelerated my personal and professional growth.

To my fellow “Pandemic cohort” – my incredible PhD companions – thank you for being by my side through all the challenges and the unforgettable moments we shared.

Finally, to my dear friends from home Σοφία and Γωγώ and all the friends that made Vienna feel like home, as well as my brother Άγγελο – thank you for supporting every crazy decision I’ve made. Your constant encouragement has been my anchor throughout this experience.

## Declaration

This doctoral thesis is cumulative containing the research manuscript published by Kagiou et. al. Chrysanthi Kagiou is the only author of this thesis, for which she received input by her supervisor Georg Winter. The abstract was written by Chrysanthi Kagiou in English and translated in German using ChatGPT and curated by Marko Cigler. Chrysanthi Kagiou is the first author of the included publication and performed the majority of the experiments and analysis in the laboratory of Georg Winter at CeMM Research Center for Molecular Medicine of the Austrian Academy of Sciences, in Vienna, Austria. The work shown here was supported by several members of the Winter group, as well as collaborators in the laboratory of Brenda Schulman at the Max Planck Institute of Biochemistry, in Martinsried, Germany. Detailed author contributions are outlined in the prologue of the results section and in the original research article in the author contribution section.

The manuscript in Chapter 2.3 was published at Nature Communications and is an open access article distributed under the Creative Commons CC BY licence, permitting unrestricted use, distribution and reproduction, if properly cited.

Kagiou, C., Cisneros, J.A., Farnung, J. *et al.* Alkylamine-tethered molecules recruit FBXO22 for targeted protein degradation. *Nat Commun* **15**, 5409 (2024). <https://doi.org/10.1038/s41467-024-49739-3>



# Table of Contents

|   |     |
|---|-----|
| Declaration .....   | ii  |
| Table of Contents .....   | iii |
| List of figures .....   | v   |
| List of tables .....  | v   |
| List of algorithms.....   | v   |
| Abstract .....  | vi  |
| Zusammenfassung .....   | vii |
| Abbreviations .....   | ix  |
| 1. Introduction .....   | 1   |
| 1.1 The power of proximity in biology .....   | 1   |
| 1.2 Manipulating proximity – early steps.....   | 2   |
| 1.2.1 First compounds to modulate proximity.....  | 2   |
| 1.2.2 Controlling protein destabilization .....   | 3   |
| 1.3 Induced degradation of endogenous proteins – targeted protein degradation.....            | 8   |
| 1.3.1 Can small molecules induce endogenous protein destabilization in mammalian cells? ..... | 8   |
| 1.3.2 The concept of PROTACs .....  | 9   |
| 1.3.3 The identification of CRBN as thalidomide’s target – molecular glues for TPD            | 10  |
| 1.3.4 Field expansion & clinical application .....  | 14  |
| 1.4 The multifaceted mechanisms of proximity-induced degradation .....                        | 19  |
| 1.4.1 Learnings from nature’s degraders.....  | 19  |
| 1.4.2 Unique mechanisms of synthetic small molecule-induced degradation via the UPS .....     | 21  |
| 1.4.3 Redirecting alternative proteolytic pathways - TPD beyond the UPS.....                  | 31  |
| 1.5 Advances in E3 ligase discovery to broaden the scope of TPD .....                         | 33  |
| 1.5.1 Current E3s for TPD.....  | 33  |
| 1.5.2 Discovery methods of novel TPD-amenable E3 ligases .....                                | 38  |
| 1.5.3 Unlocking new opportunities with novel E3 ligases .....                                 | 40  |
| 1.5.4 Challenges in identifying and utilizing novel E3 ligases .....                          | 41  |
| 1.5.5 Thesis aims.....  | 42  |
| 2. Results.....   | 42  |
| 2.1 Preliminary results.....  | 42  |

|   |     |
|---|-----|
| 2.2 Prologue for published manuscript .....                                     | 44  |
| 2.3 Results .....   | 45  |
| 3. Discussion .....   | 76  |
| 3.1 Alkylamine-based molecules as a novel class of degraders.....               | 76  |
| 3.2 FBXO22's role in cancer and implications .....                              | 78  |
| 3.3 FBXO22's role in redox homeostasis and implications .....                   | 79  |
| 3.4 FBXO22's liability to covalent engagement and implications .....            | 81  |
| 3.5 Metabolic liability of alkylamine-tethered molecules and implications ..... | 83  |
| 3.6 FBXO22 expands the TPD toolbox.....   | 86  |
| 3.7 Conclusion and outlook .....  | 87  |
| 4. Materials and Methods.....   | 90  |
| References .....  | 91  |
| Appendix & CV .....   | 123 |

## List of figures

|   |    |
|---|----|
| <b>Figure 1.</b> The E1-E2-E3 cascade. ....   | 4  |
| <b>Figure 2.</b> E3 ligase classification. ....   | 6  |
| <b>Figure 3.</b> Early synthetic systems for UPS-mediated protein degradation. ....   | 7  |
| <b>Figure 4.</b> PROTACs and MGDs.....  | 14 |
| <b>Figure 5.</b> Examples of natural degraders.....   | 21 |
| <b>Figure 6.</b> MGD-induced neointeractions.....   | 25 |
| <b>Figure 7.</b> PROTACs redirecting different UPS components.....  | 27 |
| <b>Figure 8.</b> Chaperone-mediated degradation and hydrophobic tagging. ....   | 28 |
| <b>Figure 9.</b> Alternative degradation strategies. ....   | 29 |
| <b>Figure 10.</b> Unconventional degradation mechanisms with non-obvious bifunctional molecules. ....                         | 31 |
| <b>Figure 11.</b> General principles of hijacking the lysosomal pathway for TPD.. ....  | 33 |
| <b>Preliminary Data Figure 1.</b> Preliminary screen identifies the starting material SP3N as a putative FKBP12 degrader..... | 43 |

## List of tables

|   |    |
|---|----|
| <b>Table 1.</b> E3 ligase subunits with at least one application in TPD with small molecule PROTAC or MGD. Applications with peptidic-based compounds were excluded. .... | 38 |
|---|----|

## List of algorithms

|              |          |
|--------------|----------|
| ChatGPT..... | vii-viii |
|--------------|----------|

## Abstract

Targeted protein degradation (TPD) is a pharmacological strategy based on the principle that chemical compounds can be used to bridge a protein of interest (POI) with an E3 ligase, ultimately marking the POI for degradation. Two major categories of degraders dominate the field, bifunctional molecules binding both the E3 ligase and the POI, known as proteolysis targeting chimeras, and monovalent molecular glue degraders that usually bind to either partner and facilitate protein-protein interactions. Both classes enable the recruitment of an E3 ligase to a POI for degradation and have opened novel therapeutic avenues with a few clinical successes. In contrast to the traditional inhibitor-based pharmacology, TPD offers a few advantages, including the ability to target “undruggable” proteins without the need for binding pockets, as well as the enhanced biological effects through event-driven mechanisms and elimination of any catalytic and non-catalytic protein functions.

Despite the human proteome encoding more than 600 E3 ligases, only a small fraction has been utilized in TPD applications, with a few degraders advancing into clinical development. However, reliance on a small pool of E3s in cancer treatment has led to resistance mechanisms, often driven by genetic alterations of the E3 ligase. In addition to overcoming resistance, an expanded E3 ligase repertoire could offer advantages such as access to a broader range of protein targets and selectivity arising from tissue or cell-type specific expression patterns. These underscore the need for exploration of novel E3s, yet the lack of small molecule ligands to recruit E3 ligases remains the major bottleneck in expanding the TPD toolbox.

This work attempts to bridge this gap by developing a reporter-based screening platform to discover degraders that could recruit unexplored E3 ligases. This effort led to the identification of the chemical compound SP3N, a small molecule that induced the degradation of the prolyl isomerase FKBP12. The compound SP3N is derived from the established FKBP12 ligand SLF, conjugated to a flexible alkylamine tail. This small modification proved to be sufficient to transform the ligand into a degrader, inducing selective and proteasome-dependent FKBP12 degradation. Using CRISPR-based genetic screens coupled to FACS sorting we identified the E3 ligase complex SKP1-Cullin1-FBXO22 (SCF<sup>FBXO22</sup>) as responsible for the SP3N-mediated FKBP12 degradation. Metabolomic profiling revealed that the primary NH<sub>2</sub> of SP3N undergoes metabolic conversion into an active aldehyde, which covalently engages the cysteine residue 326 of FBXO22. Importantly, we showed that this mechanism is generalizable to two recently reported degraders that target the methyltransferase NSD2 and the E3 ligase XIAP, respectively.

Collectively, these findings establish FBXO22, which was previously a non-hijackable E3 ligase, as a new avenue for TPD applications. Given FBXO22's reported roles in cancer and redox homeostasis, co-opting this E3 ligase for TPD could offer new opportunities to overcome resistance and expand the clinical utility of degrader-based therapies.

## Zusammenfassung

Der gezielte Proteinabbau (Targeted Protein Degradation, TPD) ist ein moderner pharmakologischer Ansatz, bei dem chemische Verbindungen ein Zielprotein in die räumliche Nähe einer E3 Ubiquitin-Ligase bringen, um dessen Ubiquitinierung und anschließenden proteasomalen Abbau zu fördern. Aktuell stehen dabei zwei Hauptklassen von Degradern im Fokus: bifunktionale Moleküle, sogenannte Proteolysis Targeting Chimeras (PROTACs), die gleichzeitig an das Zielprotein und eine E3 Ligase binden, sowie monovalente kleine Moleküle, sogenannte Molekulare Kleber (Molecular Glue Degraders, MGD), die durch Stabilisierung spezifischer Protein-Protein-Wechselwirkungen die Rekrutierung der Ligase ermöglichen. Beide Strategien haben neuartige therapeutische Möglichkeiten eröffnet – einige davon befinden sich bereits in klinischer Erprobung. Im Gegensatz zur klassischen, inhibitorbasierten Pharmakologie ermöglicht TPD die gezielte Ausschaltung von Proteinen, selbst wenn diese keine Bindetaschen aufweisen („undruggable targets“). Durch den ereignisgetriebenen Mechanismus lassen sich sowohl katalytische als auch nicht-katalytische Funktionen eines Zielproteins gleichzeitig ausschalten, was oft zu stärkeren, nachhaltigen biologischen Effekten führt.

Obwohl das menschliche Proteom über 600 E3 Ligasen umfasst, kommen in der TPD bislang nur wenige davon zum Einsatz. Der starke Fokus auf eine begrenzte Auswahl an E3 Ligasen – insbesondere im onkologischen Kontext – führt jedoch häufig zur Entstehung von Resistenzmechanismen, die meist auf genetischen Veränderungen der jeweiligen E3-Ligase beruhen. Eine breitere Nutzung weiterer E3 Ligasen könnte solche Resistenzen überwinden, neue Zielproteine zugänglich machen und durch gewebespezifische Expression zusätzliche Selektivität bieten. Der entscheidende Engpass bleibt dabei das Fehlen geeigneter kleiner Moleküle, mit denen sich diese alternativen Ligase-Systeme gezielt rekrutieren lassen.

In dieser Arbeit wurde deshalb eine neue, reporterbasierte Screening-Plattform entwickelt, um Degradere zu identifizieren, die das Potenzial besitzen, bisher unerforschte E3-Ligasen nutzen zu können. Dabei wurde die SP3N entdeckt – eine niedermolekulare chemische Verbindung, die gezielt den Abbau der Prolyl-Isomerase FKBP12 auslöst. SP3N leitet sich vom bekannten FKBP12-Liganden SLF ab, wurde jedoch durch einen flexiblen Alkylamin-Linker erweitert. Diese scheinbar kleine strukturelle Modifikation reichte aus, um aus einem klassischen Liganden einen selektiven, proteasomabhängigen FKBP12 Degradere zu machen. Durch Kombination von CRISPR-basierten genetischen Screens mit FACS-Sortierung konnte der E3 Ligase Komplex SKP1-Cullin1-FBXO22 ( $SCF^{FBXO22}$ ) als entscheidender Vermittler dieses Abbaus identifiziert werden. Weiterführende metabolische Analysen zeigten, dass die primäre Aminogruppe von SP3N enzymatisch in ein reaktives Aldehyd umgewandelt wird, welches kovalent mit Cystein 326 von FBXO22 reagiert. Bemerkenswert ist, dass dieser Mechanismus auf zwei weitere Degradere übertragbar ist, die die Methyltransferase NSD2 bzw. die E3 Ligase XIAP gezielt abbauen.

Diese Ergebnisse zeigen, dass FBXO22 – bisher nicht als Ziel für TPD genutzt – ein vielversprechender neuer Ansatzpunkt für Degradere-Strategien ist. Aufgrund ihrer bekannten Rolle in der Krebsbiologie und im zellulären Redox-Gleichgewicht könnte die

gezielte Nutzung von FBXO22 neue Wege zur Überwindung von Therapieresistenzen und zur Erweiterung des klinischen Einsatzes von Degradier-Wirkstoffen eröffnen.

## Abbreviations

AID, auxin inducible degron

AO, amine oxidase

AOC, amine oxidase copper containing

AR, androgen receptor

As<sub>2</sub>O<sub>3</sub>, arsenic trioxide

ATP, adenosine triphosphate

ATTEC, autophagy-tethering compound

AUTAC, autophagy targeting chimera

BACH1, BTB and CNC homology 1

BAG3, Bcl2-associated athanogene 3

BCL6, B-cell lymphoma 6

BCL-XL, B cell lymphoma extra-large

BET, bromodomain and extra terminal

BMI1, B lymphoma Mo-MLV insertion region 1 homolog

BRD4/9, bromodomain-containing protein 4/9

BSAO, bovine serum amine oxidase

BTK, Bruton's tyrosine kinase

CAO, copper-containing amine oxidase

CDK, cyclin-dependent protein kinase

cGMP, cyclic guanosine monophosphate

clAP1, cellular inhibitor of apoptosis protein 1

CI-MPR, cation-independent mannose-6-phosphate receptor

CIP, chemically induced proximity

CK1 $\alpha$ , casein kinase 1 $\alpha$

CoREST, co-repressor complex

CRABPs, cellular retinoic acid binding proteins

CRBN, cereblon

CRL, cullin RING ligases

CsA, cyclosporin A

CTLH, C-terminal to LisH

DAO, diamine oxidase

DCAF16, DDB1 and CUL4 associated factor 16

DDB1, damage-specific DNA binding protein 1

DEL, DNA-encoded library

E6-AP, E6-associated protein

EED, embryonic ectoderm development protein

ERR $\alpha$ , estrogen-related receptor  $\alpha$

ER $\alpha$ , estrogen receptor  $\alpha$

FAD, flavin adenine dinucleotide

FAO, FAD-containing amine oxidase

FEMB1, fem-1 homologue B

FGFR1/2, fibroblast growth factor receptor 1/2

FKBP12, 12-kDa FK506-binding protein

FNIP1, folliculin-interacting protein 1

GSPT1, G1 to S phase transition 1

HDAC1, histone deacetylase 1

HECT, homologous to the E6AP carboxyl terminus

HIF-1 $\alpha$ , hypoxia-inducible factor-1 $\alpha$

HO-1, heme oxygenase -1

|  |   |
|--|---|
| IAA, indole-3-acetic acid  | NUP98, nucleoporin 98   |
| IDO1, indoleamine-2,3-dioxygenase 1  | ORF, open-reading frame   |
| IKZF1/3, Ikaros zinc finger proteins 1/3   | PAO, polyamine oxidase  |
| IMiD, immunomodulatory drug  | PML-RAR $\alpha$ , promyelocytic leukemia – retinoid acid receptor alpha fusion protein |
| InsP <sub>6</sub> , inositol hexakisphosphate  | POI, protein of interest  |
| isoTOP-ABPP, isotopic tandem orthogonal proteolysis-enabled activity-based protein profiling | PPI, protein - protein interaction  |
| I $\kappa$ B $\alpha$ , NF- $\kappa$ B inhibitor- $\alpha$                                   | PRC1, polycomb repressive complex 1   |
| KBTBD4, kelch repeat and BTB domain containing 4   | PROTAC, proteolysis targeting chimera   |
| KEAP1, Kelch-like ECH-associated protein 1   | PTMs, post-translational modifications  |
| KLF4, Krüppel-like factor 4  | RBM39, RNA binding motif protein 39   |
| LPS, lipopolysaccharide  | RBR, RING-in-between-RING   |
| LSD1/2, lysine-specific demethylase 1/2  | RING, really interesting new gene   |
| LYTAC, lysosome-targeting chimeras   | ROS, reactive oxygen species  |
| M6P, mannose-6-phosphate   | SALL4, Sal-like protein 4   |
| MAO, monoamine oxidase   | SCF, SKP1-Cullin1-F-box   |
| MaRap, C20-methyl-rapamycin  | SERD, selective estrogen receptor degrader  |
| MDM2, double minute 2 homologue  | SMARCA2, SWI/SNF related BAF chromatin remodeling complex subunit ATPase 2              |
| MetAP-2, methionine aminopeptidase 2   | SMO, spermine oxidase   |
| MGD, molecular glue degrader   | SNIPER, specific and non-genetic IAP-dependent protein eraser                           |
| MHC, major histocompatibility complex  | SP3N, SLF-PEG3-NH <sub>2</sub>  |
| mTOR, mechanistic target of rapamycin  | SR, substrate receptor  |
| MTX, methotrexate  | SSAO, semicarbazide-sensitive oxidase   |
| NF- $\kappa$ B, nuclear factor kappa-light-chain-enhancer of activated B cells               | STAT5, signal transducer and activator of transcription 5                               |
| NHR, nuclear hormone receptors   | SuFEx, Sulfur(VI) Fluoride Exchange   |
| NRF2, nuclear factor erythroid 2-related factor 2  | TCI, targeted covalent inhibitor  |



|  |  |
|--|--|
| TCR, T cell receptor                                     | UPS, ubiquitin proteasome system                                   |
| TF, transcription factor                                 | VHL, Von-Hippel-Lindau   |
| TIR1, transport response inhibitor 1                     | XIAP, X-linked inhibitor of apoptosis protein                      |
| TPD, targeted protein degradation                        | YPEL5, Yippee-like 5   |
| TRIM21, tripartite motif-containing protein 21           | ZBTB16, zinc finger and BTB domain 16                              |
| Ub, ubiquitin  | $\beta$ -TRCP, $\beta$ -transducin repeat-containing F-box protein |
| UBR5, ubiquitin protein ligase E3 component N-recognin 5 |  |

# 1. Introduction

## 1.1 The power of proximity in biology

Biological systems rely on highly controlled and precisely organized principles to sustain life. Among the multiple factors underlying this complexity, proximity stands out as a fundamental force shaping interactions at multiple levels, from nanoscale molecular dynamics to macroscale coordination of multicellular organisms (Beck et al., 2011). Proximity does not occur by chance but is an actively regulated process to achieve specificity and efficiency (Good et al., 2011; Kholodenko, 2006). At the molecular scale, processes such as enzymatic catalysis, signaling cascades or membrane receptor activation are orchestrated by proximity, mediated by localization and enabling protein - protein interactions (PPIs) (Stanton et al., 2018). Spatial and temporal concentration of molecules, cellular compartmentalization, tissue organization and organ communication all rely on dynamic regulation of the localization of individual components in relation to each other (Beck et al., 2011).

The realization of the critical role of proximity in biology has fueled years of research to understand the principles of how the physical closeness of molecules can affect biological output. Early in the process, it was clear that post-translational modifications (PTMs) of proteins, meaning the addition of chemical groups to amino acids, change the protein's fate mainly by affecting interactions with other cellular components, resulting in a multitude of outputs such as protein stability, PPIs, complex assemblies, (in)activation or localization changes (Venne et al., 2014).

A major milestone for our understanding of spatial relationships among molecules was achieved with the introduction of chemically induced proximity, that is the use of chemical compounds to control or manipulate biomolecular interactions (Liu et al., 1991). Chemical compounds, akin to PTMs, could serve as chemical marks that rewire PPI networks, affecting the biological output (Schreiber, 2019). Leveraging proximity has emerged as a powerful tool in chemical biology and medicine, not only for our understanding of endogenous processes, but also as a promising therapeutic modality (Békés et al., 2022; Stanton et al., 2018).

The realization that chemical modulation of proximity can be harnessed to rewire cellular processes paved the way for the concept of targeted protein degradation (TPD), where small molecules hijack the cellular degradation machinery to eliminate proteins of interest (POIs) (Sakamoto et al., 2001). Approximately two decades of research in this field has shown

that TPD could expand the druggable proteome beyond traditional inhibitors, thus offering new therapeutic opportunities (Békés et al., 2022).

This thesis builds on the foundational principles of chemically induced proximity, with a specific focus on hijacking the cellular proteolytic system to induce protein degradation, that has revolutionized drug development. Building on unsolved challenges and knowledge gaps in TPD, our work has enabled the identification of a novel generalizable mechanism for the recruitment of an uncharted E3 ligase, thus expanding the TPD toolbox. In this context, it is evident that future efforts will be necessary to unlock TPD's full potential.

## **1.2 Manipulating proximity – early steps**

### **1.2.1 First compounds to modulate proximity**

The central role of proximity in regulating PPIs and biological outcome has inspired scientists to explore approaches for harnessing this natural principle. Pioneering research in the 1990s laid the groundwork for chemically induced proximity, setting the stage for modern chemical modulation approaches.

Initial efforts were not focused on manipulating proximity but on understanding the mode of action of certain immunosuppressant natural chemical compounds including Cyclosporin A (CsA), rapamycin and FK506 (Liu et al., 1991; Michnick et al., 1991; Zheng et al., 1995). These compounds were known to act as immunosuppressants, and their clinical use was introduced before the discovery of their direct targets or the underlying mechanisms of action. Later, it was revealed that these compounds bind directly to endogenous proteins, with the 12-kDa FK506-binding protein (FKBP12) as target of both FK506 and rapamycin, and cyclophilin as target of CsA (Liu et al., 1991; Michnick et al., 1991).

Interestingly, in 1991, FK506 and CsA were shown to induce complex formation between the phosphatase calcineurin and FKBP12 or cyclophilin, respectively (Liu et al., 1991). The term “molecular glue” was first introduced in 1992 to describe the “gluing” activity of FK506 and CsA in protein complexes, analogous to the way that antigens form complexes with the major histocompatibility complex (MHC) and the T cell receptor (TCR) (Schreiber, 1992). The gluing activity of rapamycin, similarly to FK506 and CsA, was confirmed later, with the identification of the mechanistic target of rapamycin (mTOR) as the binding partner (Banaszynski et al., 2005; Sabatini et al., 1994; Zheng et al., 1995).

These initial studies paved the way for a new tool to study biology, the chemical induction of proximity (Belshaw et al., 1996; Ho et al., 1996; Luo et al., 1996; Pruschy et al., 1994; Spencer et al., 1993). Prototype homo-bifunctional molecules comprising two FK506 moieties were demonstrated to glue copies of chimeric proteins fused to FKBP12 (Spencer et al., 1993). With these glue compounds at hand, researchers were presented with the opportunity to study the mechanisms that control proximity by engineering ways to modulate it.

Following studies by Crabtree and Schreiber realized the idea that chemical compounds can be used to modulate endogenous pathways, such as receptor-mediated signal transduction (Pruschy et al., 1994; Spencer et al., 1993). To showcase this, analogues of FK506 were used to induce the intracellular di- and oligomerization of FKBP12-fused-TCR chimeras lacking the transmembrane domains (Pruschy et al., 1994). This chimeric platform achieved precise compound-mediated regulation of TCR target-gene transcription. Additional examples of dimerizing compounds targeting FKBP12-fused activator or repressor proteins shed more light into transcriptional regulation, and further established chemical induced proximity as means of controlling cellular functions (Ho et al., 1996). With these studies, chemically induced proximity emerged as an effective tool to modulate biochemical processes in a controllable and temporary fashion, thereby opening novel ways for modulation of cellular functions.

### **1.2.2 Controlling protein destabilization**

The initial studies on chemical modulation of PPIs coincided with pioneering biochemical work by Hershko, Ciechanover, Rose and others in the 1980s and 1990s that led to the discovery and characterization of one of the major cellular proteolytic pathways called the ubiquitin proteasome system (UPS) (Chau et al., 1989; Ciechanover et al., 1980; Goldstein et al., 1975; Hershko et al., 1980; Wilkinson, 2005; Wilkinson et al., 1980). The growing knowledge on UPS not only revolutionized the understanding of protein quality control, but also inspired researchers to explore chemical modulation approaches to direct proteins toward degradation, primarily motivated by the idea that complete eradication of a protein from the cell could reveal deeper insights into its function (Wilkinson, 2005).

#### **1.2.2.i The ubiquitin proteasome system**

The UPS is based on a cascade of multiple molecular events that lead to marking cellular proteins with a highly conserved 76-amino-acid-residue protein, ubiquitin (Ub),

resulting in degradation through a multisubunit proteolytic complex, the 26S proteasome (Hershko and Ciechanover, 1998).

Mechanistically, Ub attachment to a protein requires an enzymatic cascade of reactions, namely E1-E2-E3 cascade (Fig. 1) (Hershko and Ciechanover, 1998; Pickart, 2001; Zheng and Shabek, 2017). Humans have only two E1 enzymes, or Ub-activating enzymes, and their role is to use adenosine triphosphate (ATP) to activate Ub. Following activation, Ub is transferred to one of the ~35 E2 Ub-conjugating enzymes, by the formation of a thioester bond with a cysteine in the E2 active site. The diversity of the E2 enzymes provides an initial level of regulation to the system, as different E2s demonstrate differential specificities for Ub linkages or substrates. At the final step of the cascade, the E3 Ub-ligases bridge the Ub-loaded E2 with a protein substrate and facilitate the formation of an isopeptide bond between the carboxyl-terminal of Ub and the side chain amine of the substrate's lysine residue.

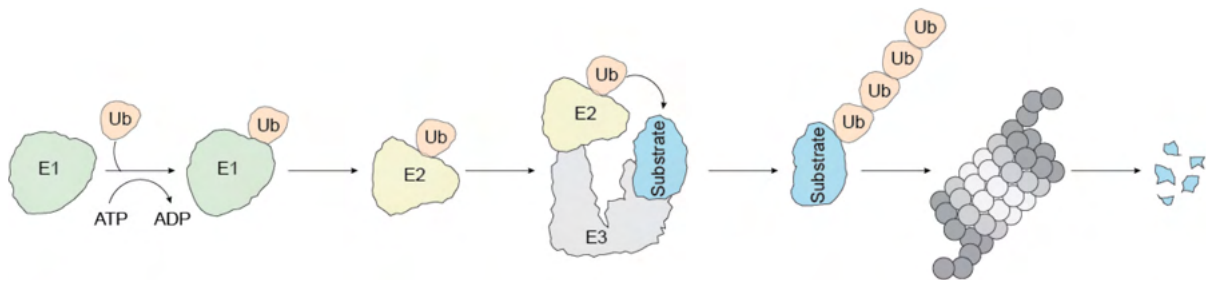


**Figure 1. The E1-E2-E3 cascade.** E1 enzymes use ATP to activate ubiquitin (Ub) that is subsequently transferred to the E2-Ub conjugating enzyme. E3 ligases bring E2-Ub in proximity to the substrate and facilitate the final substrate-Ub conjugation for subsequent substrate degradation via the 26S proteasome. Ub, Ubiquitin; ATP or ADP, adenosine tri- or di-phosphate.

Notably, the human proteome has more than 600 E3 ligases (Harper and Schulman, 2021; Hinterdorfer et al., 2025; Zheng and Shabek, 2017). This large family of enzymes demonstrates intricate mechanistic diversity and provides the highest degree of substrate specificity. E3 ligases differ in their structural organization, catalytic mechanisms and substrate recognition (Zheng and Shabek, 2017). Based on these features, E3 ligases can be grouped into different classes (Fig. 2):

- Homologous to the E6-AP carboxyl terminus (HECT) E3 ligases (Fig. 2A).

This class of enzymes employs a two-step mechanism for Ub transfer to the substrate (Buetow and Huang, 2016; Rotin and Kumar, 2009; Shah and Kumar, 2021). First, Ub is transferred to a conserved cysteine at the E3's active site and subsequently attached to the substrate through the formation of an isopeptide bond. The bi-lobal catalytic domain of the HECT E3s with the N-lobe interacting with the Ub-loaded E2 and the C-lobe containing the

E3's active site cysteine, allow for the efficient transfer of Ub to the E3 before attachment to the substrate. Notably, HECTs can either employ adaptor proteins or directly interact with different substrates and can control the type of Ub linkage they form (Buetow and Huang, 2016).

- Really interesting new gene (RING)-finger E3 ligases (Fig. 2A, 2B).

These E3 ligases are classified based on the presence of a RING domain and comprise the majority of E3 proteins. Mechanistically, they differ from the HECT E3s, as they directly transfer the Ub from the E2 to the substrate without the intermediate E3-Ub binding (Buetow and Huang, 2016; Plechanovová et al., 2012; Zheng and Shabek, 2017). They are further grouped into monomeric RING E3s that contain all domains necessary for their activity, or multi-subunit E3s, such as the cullin RING ligases (CRLs) (Fig. 2B) (Harper and Schulman, 2021). CRLs contain a cullin scaffold that allows them to interact with an adaptor protein at the N-terminus and a substrate receptor at the C-terminus. CRLs are the largest and most diverse family of E3 ligases, and their modular architecture allows for targeting a large number of proteins for degradation, making them central hubs of the UPS (Buetow and Huang, 2016; Harper and Schulman, 2021).

- U-box E3 ligases (Fig. 2A).

Characterized by the C-terminal U-box domain, this small class of E3 ligases also catalyzes the direct transfer of the Ub from the E2 to the substrate (Hatakeyama et al., 2001; Pruneda et al., 2012).

- RING-in-between-RING (RBR) E3 ligases (Fig. 2A)

The catalytic region of these ligases consists of two RING domains interspaced by an in-between-RINGs region (IBR) and have a two-step Ub transfer mode of action similar to the HECT E3s (Lechtenberg et al., 2016; Wenzel et al., 2011). In particular, the Ub-loaded E2 is recruited to the RING1 domain, and the Ub is transferred to a catalytic cysteine in the RING2 domain, before being attached to the substrate.

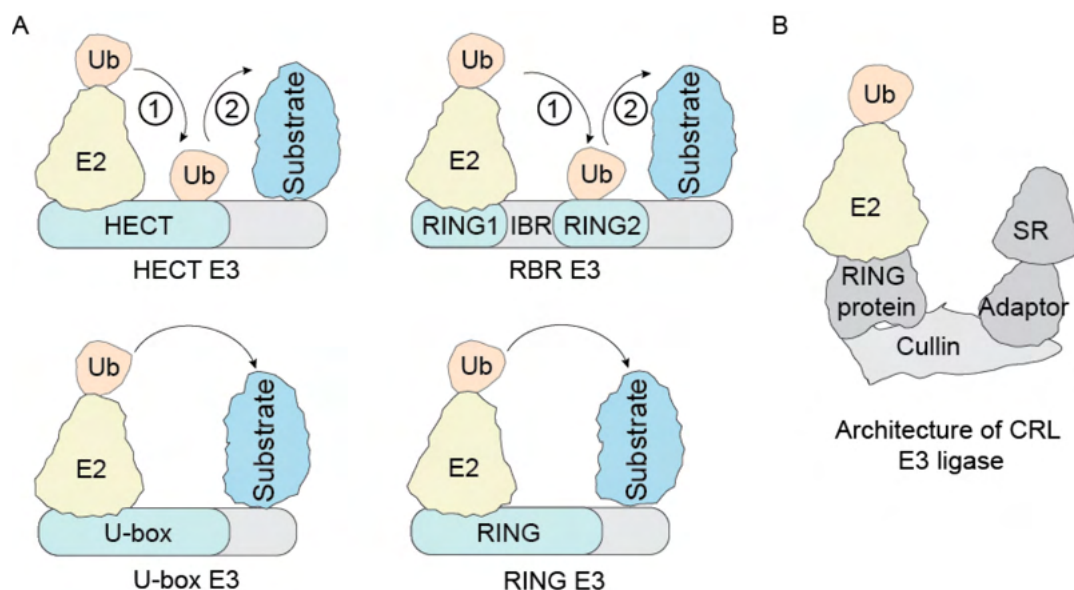


**Figure 2. E3 ligase classification.** A) HECT & RBR E3 ligases catalyze a 2-step reaction. Ub is first transferred from the E2 to the E3 and subsequently to the substrate. U-box and RING E3 ligases facilitate direct transfer from the E2 to the substrate. B) CRLs are the largest family of RING E3 ligases. They are multisubunit complexes with modular architecture usually consisting of a Cullin scaffold that directly interacts with an adaptor protein. The adaptor binds to different substrate receptors (SR), which mediate substrate binding. On the C-terminus, the RING finger protein interacts with the Ub-loaded E2. HECT, Homologous to the E6-AP carboxyl terminus; RING, really interesting new gene; CRL, cullin RING ligase; Ub, Ubiquitin; IBR, in-between-RING.

Continuous research in the UPS system has revealed an intricate regulatory network for proteolysis that serves as the cellular quality control system for aberrant proteins and mediates the temporal control of cellular processes by regulating protein half-lives (Pohl and Dikic, 2019). In addition, mechanistic understanding of the UPS system has set the foundations for the development of strategies to post-translationally control protein levels.

### 1.2.2.ii Early synthetic systems to induce protein destabilization via the UPS

Early research on using the UPS to control protein stability was focused on synthetic systems (Banaszynski and Wandless, 2006). Studies by Varshavsky and colleagues in the late 1980's described that protein stability is highly influenced by the amino acid composition of the N-terminus of a protein and established the N-end rule pathway (Bachmair et al., 1986). They designed ubiquitin- $\beta$ -galactosidase protein chimeras, which were liable to cleavage by the *S. cerevisiae* deubiquitinating proteases, revealing diverse amino acids at the N-terminus of the protein. With this system they demonstrated that exposing different N-terminal residues, such as arginine, led to rapid degradation of the  $\beta$ -galactosidase in a ubiquitin- and proteasome-dependent manner (Fig. 3A). This work laid the foundation for synthetically controlling POI chimeras.

Alternatively, Howley and Gosink groups independently introduced the concept of degradation by association, which was based on protein chimeras consisting of the target protein and a component of the ubiquitin-proteasome system, in particular an E2 or E3 (Fig. 3B) (Gosink and Vierstra, 1995; Zhou et al., 2000). These chimeras were unstable as opposed to the otherwise stable target protein, setting the foundations for direct hijacking of the UPS system to degrade a POI.

Even though both mentioned mechanisms to induce POI degradation were fundamental for expanding the available tools for post-translational protein regulation, they both lacked tunability and controllable induction of protein destabilization.

#### A. N-end rule pathway



#### B. Degradation by association

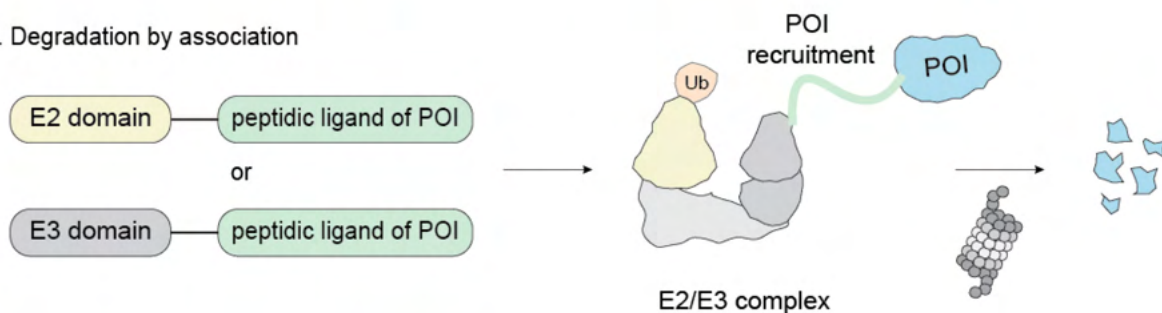


**Figure 3. Early synthetic systems for UPS-mediated protein degradation.** A) Ub-POI chimeras are cleaved by deubiquitinating enzymes of *S. cerevisiae* exposing arginine (Arg) on the POI's N-terminus, triggering proteasome-dependent degradation. B) Fusions of E2 or E3 enzymes with peptidic sequences known to bind to a target POI can lead to recruitment of the POI to the degradation machinery. POI, protein of interest.

### 1.2.2.iii Introducing small molecules to modulate protein stability via the UPS

Building on the early synthetic approaches focused on the N-end-rule pathway, researchers sought to achieve conditional control of protein stability. Varshavsky and colleagues developed a heat-inducible degron system that enabled temperature-dependent protein degradation (Dohmen et al., 1994), a method applied for systematically inducing conditional degradation of proteins in budding yeast (Kanemaki et al., 2003). This system was



adapted to respond to the chemical compound methotrexate (MTX): in the absence of MTX, the protein chimeras bearing the destabilizing N-terminus were degraded, whereas adding MTX would stabilize the fusions and protect them from degradation (Lévy et al., 1999). Despite its value as proof of principle for temporal control of proteolysis, this approach posed disadvantages, such as MTX toxicity and potential proteasome inhibition by the stabilized fusions.

In parallel, Crabtree and colleagues adapted the FK506-based dimerization system, to allow a tunable and reversible degradation of a POI upon chemical stimulation (Stankunas et al., 2003). Initially designed to circumvent rapamycin's toxicity due to TOR inhibition, they generated a mutant of the rapamycin binding domain of TOR protein (termed FRB\*) and synthesized a rapamycin analogue C20-methyl-rapamycin (MaRap) that could specifically bind to FRB\* (Liberles et al., 1997; Stankunas et al., 2003). Unexpectedly, it was revealed that FRB\* was significantly more unstable compared to the wild-type counterpart, while its stability could be restored by MaRap treatment, due to recruitment of FKBP12 (Stankunas et al., 2003). Utilizing this finding, they developed a rapidly reversible system, in which intrinsically unstable FRB\*-POI chimeras would be stabilized upon MaRap treatment offering an orthogonal and fully controllable platform for protein degradation. The tunability of this system enabled studies on different proteins, however the poor synthetic accessibility and pharmacokinetics of MaRap posed obstacles, particularly for in vivo studies.

Overall, these chemically induced degradation systems were powerful tools to study cellular processes and established the core principles for chemically controlled protein degradation. However, they relied on genetically modified proteins that required extensive engineering limiting broader applications. Importantly, these synthetic systems were far from achieving control of native cellular proteins, limiting their therapeutic potential.

### **1.3 Induced degradation of endogenous proteins – targeted protein degradation**

#### **1.3.1 Can small molecules induce endogenous protein destabilization in mammalian cells?**

While early studies (section 1.2.2.ii, iii) aimed at controlling protein levels through engineered systems, unexpected findings from pharmacological research revealed that small molecules could, in fact, induce degradation of endogenous proteins.

One of the earliest examples was arsenic trioxide (As<sub>2</sub>O<sub>3</sub>), an established treatment for acute promyelocytic leukemia, that has been shown to induce leukemia cell death through

multiple pathways including reactive oxygen species (ROS) production and transcription inhibition (Emadi and Gore, 2010). Interestingly, among the many effects, As<sub>2</sub>O<sub>3</sub> was demonstrated to induce the proteasome-dependent degradation of promyelocytic leukemia – retinoid acid receptor alpha fusion protein (PML-RAR $\alpha$ ), contributing to its therapeutic efficacy in acute promyelotic leukemia (Zhu et al., 1997). Similarly, fulvestrant, a selective estrogen receptor degrader (SERD) originally developed as an estrogen receptor  $\alpha$  (ER $\alpha$ ) antagonist, was shown to block ER $\alpha$  signaling and promote its degradation, suggesting that ER degradation could be an integral component of its mechanism of action (Wijayaratne and McDonnell, 2001).

Although these discoveries were not initially intended to harness degradation as a mode of action and despite the lack of complete mechanistic elucidation of their effects, they provided early indications that small molecules could trigger the selective elimination of endogenous disease-related proteins. This realization prompted a shift in focus from synthetic protein systems to chemically induced degradation of native proteins.

### **1.3.2 The concept of PROTACs**

The basis for the systematic investigation of induced degradation of endogenous proteins - beyond the synthetic proteolytic systems and the fragmented observations of drug-induced protein destabilization - was set in the early 2000s, when Crews and Deshaies laboratories introduced for the first time the concept of proteolysis targeting chimeras (PROTACs) (Sakamoto et al., 2001). PROTACs are synthetic bifunctional molecules acting as bridges of an endogenous E3 ligase to an endogenous POI, forcing the proximity to the UPS system required for POI degradation (Fig. 4) (Békés et al., 2022). PROTAC technology bypassed the need for ectopic expression and chimeric protein engineering and utilized the concept of using chemical molecules to finetune protein degradation in cells.

The first PROTAC, Protac-1, consisted of a 10-aa phosphopeptide – the recognition sequence of the nuclear factor kappa-light-chain-enhancer of activated B cells (NF- $\kappa$ B) inhibitor- $\alpha$  (I $\kappa$ B $\alpha$ ) by the  $\beta$ -transducin repeat-containing F-box protein ( $\beta$ -TRCP) – linked to ovalicin, a covalent inhibitor of the methionine aminopeptidase 2 (MetAP-2) (Sakamoto et al., 2001). This bifunctional synthetic molecule was shown to induce rapid MetAP-2 ubiquitination and degradation mediated by the SKP1-Cullin1-F-box $\beta$ -TRCP (SCF $\beta$ -TRCP) complex in a cell-free system of *Xenopus* eggs extracts. An obvious disadvantage was that Protac-1's size and properties compromised cell permeability, and thus efficacy in mammalian cells.

Nevertheless, this work was groundbreaking as it provided proof of concept that synthetic molecules could co-opt the UPS machinery to degrade chosen protein targets and paved the way for the development of chemical tools for degradation of endogenous proteins (Schneekloth et al., 2004).

Following studies with peptide-based PROTACs targeting the estrogen (ER) or androgen receptor (AR), opened new possibilities for addressing disease-relevant proteins (Rodriguez-Gonzalez et al., 2008; Sakamoto et al., 2003). Notably, these PROTACs were designed not only to degrade different targets, but also to recruit a different E3 ligase substrate receptor, the Von-Hippel-Lindau (VHL), demonstrating the modularity and versatility of this emerging technology. Nevertheless, both ER $\alpha$ - and AR-targeting PROTACs contained a pentapeptide degron from VHLs' endogenous target, the hypoxia-inducible factor-1 $\alpha$  (HIF-1 $\alpha$ ), posing permeability and synthetic limitations.

It was only in 2008 that non-peptidic small molecule-based PROTACs were introduced (Schneekloth et al., 2008). The Crews laboratory reported a cell-permeable PROTAC that could degrade the AR at micromolar range. This molecule was formed by linking an AR ligand to nutlin-3a, a known binder of the double minute 2 homologue (MDM2) E3 ligase (Schneekloth et al., 2008).

In the same year, Naito's group made an interesting discovery: the small molecule bestatin induced the auto-ubiquitination and degradation of the cellular inhibitor of apoptosis protein 1 (cIAP1), a known E3 ligase (Sekine et al., 2008). This finding made bestatin an attractive candidate for PROTAC development, as attaching bestatin to ligands of POIs could potentially induce proximity of POIs to cIAP1, leading to their degradation. Indeed, shortly after, several studies demonstrated that these cIAP1 recruiting heterobifunctional molecules, which were termed specific and non-genetic IAP-dependent protein erasers (SNIPERs), were able to degrade a diverse range of targets (Itoh et al., 2012, 2011a, 2011b; Naito, 2022; Ohoka et al., 2017; Okuhira et al., 2013, 2011).

These advances established PROTACs as promising tools for TPD, showcasing their versatility and opening novel therapeutic avenues.

### **1.3.3 The identification of CRBN as thalidomide's target – molecular glues for TPD**

Despite these initial successes, a major leap forward in TPD followed when researchers uncovered the mode of action of the immunomodulatory drug thalidomide (Ito et

al., 2010). Thalidomide, a synthetic glutamic acid derivative, was an FDA approved sedative in the late 1950s but became infamous for causing severe malformations in >8000 babies, after being prescribed to pregnant women for morning sickness (Franks et al., 2004; Smithells and Newman, 1992; Ward, 1962). In the 1960s, thalidomide was found to be effective against autoimmune diseases, and decades of research have revealed its immunosuppressive and direct anti-tumor activities (Bartlett et al., 2004; Franks et al., 2004; Melchert and List, 2007; Teo et al., 2002). Nearly 70 years since the first FDA approval, thalidomide and its derivatives - termed as immunomodulatory drugs (IMiDs), are widely used in the clinics to treat several autoimmune diseases and cancers (Bartlett et al., 2004).

Despite its diverse effects, the direct targets of thalidomide remained unknown until 2010, when the Handa laboratory immobilized thalidomide on beads to pull-down interacting proteins from HeLa extracts (Ito et al., 2010). They identified two main interactors via mass spectrometry, cereblon (CRBN) and the damage-specific DNA binding protein 1 (DDB1). They demonstrated that CRBN is a novel substrate receptor of the CUL4-DDB1 E3 Ub-ligase complex (Angers et al., 2006) and suggested that thalidomide inhibits CRBN's activity (Ito et al., 2010). This study shed light on the molecular mechanisms of thalidomide-induced teratogenicity, however, key questions remained regarding CRBN's substrates and the precise mechanisms by which thalidomide influenced CRBN's activity.

Subsequent genetic and biochemical studies revealed that CRBN is indispensable for the IMiD antiproliferative effects in various tumor cell lines (Lopez-Girona et al., 2012; Zhu et al., 2011). In 2013, two landmark independent studies by the laboratories of Ebert and Bradner & Kaelin revealed that lenalidomide leads to CRBN- and proteasomal- dependent degradation of Ikaros zinc finger proteins IKZF1 and IKZF3 (Krönke et al., 2014; Lu et al., 2014). To identify potential CRBN substrate downregulation upon lenalidomide treatment, Lu and colleagues designed a luciferase reporter library to monitor the stability of >15000 open-reading frames (ORFs) (Lu et al., 2014). They found IKZF1 as the main downregulated ORF, and further validation identified its paralogue IKZF3 as another target. In parallel, Krönke and colleagues used an orthogonal quantitative assay based on ubiquitinated-peptide enrichment coupled with mass-spectrometry to assess proteome changes in multiple myeloma cells upon lenalidomide treatment, revealing the decrease of both IKZF1 and IKZF3 (Krönke et al., 2014). Shortly after, independent studies showed that IMiDs induce IKFZ1/3 degradation in activated

T cells and in multiple myeloma patients, proposing this as an important mechanism underlying the immunomodulatory effects of IMiDs (Gandhi et al., 2014; Zhu et al., 2014).

Crystal structures of DDB1-CRBN in complex with different IMiDs shed light on the mode of binding of these compounds, proposing a mechanism where IMiDs occupy the endogenous substrate recognition site of CRBN and potentially introduce a new interaction surface (Fischer et al., 2014). This interaction surface could in turn facilitate the recruitment of IKZF1 and IKZF3, which inhibits the binding of endogenous substrates and therefore leads to their increased abundance. Following studies identified additional CRBN “neosubstrates” induced by thalidomide and its analogues (Krönke et al., 2015; Matyskiela et al., 2016; Petzold et al., 2016). Lenalidomide was reported to induce degradation of casein kinase 1 $\alpha$  (CK1 $\alpha$ ) in addition to IKZF1 and IKZF3, with subtle changes in IMiD structure being sufficient to alter substrate specificity (Krönke et al., 2015; Petzold et al., 2016). Other IMiD analogues, such as CC-885, were shown to induce CRBN-dependent G1 to S phase transition 1 (GSPT1) degradation (Matyskiela et al., 2016).

The structural elucidation of the ternary complexes of DDB1-CRBN-lenalidomide-CK1 $\alpha$  and DDB1-CRBN-CC-885-GSPT1 revealed that IMiDs bind to CRBN in a way that creates a cooperative interaction site (or hotspot) on the CRBN surface (Matyskiela et al., 2016; Petzold et al., 2016). The IMiD-modified CRBN surface facilitates simultaneous interaction of the substrate with both CRBN and the IMiD. This mechanism potentially explains how low molecular weight compounds are capable of mediating such protein-protein interactions. Despite the lack of sequence homology among different substrates like CK1 $\alpha$ , IKZF1 or GSPT1, they appear to share a common mechanism of recruitment to CRBN, relying on structural features rather than sequence similarity (Matyskiela et al., 2016; Petzold et al., 2016; Sievers et al., 2018).

These studies collectively demonstrated for the first time that previously undruggable transcription factors could be targeted via a different mechanism: chemically induced proteasomal degradation mediated by CRBN. This approach differed from the traditional inhibitor-based pharmacology and conceptually aligned with the use of PROTACs to repurpose E3 ligases to degrade POIs (Gadd et al., 2017). However, in contrast to the heterobifunctional nature of PROTACs, the IMiD-induced degradation did not rely on a clearly bifunctional design. The discovery that CRBN can be harnessed to degrade crucial hard-to-

target transcription factors paved the way for a new era in research and therapeutic development focused on chemically induced target degradation.

In 2015, the Bradner laboratory leveraged the ability of IMiDs to bind to CRBN to rationally design phthalimide-based PROTACs, envisioning a modular strategy to degrade different target proteins depending on the POI-recruiting small molecule attached to phthalimide moiety (Winter et al., 2015). As proof of concept, two different proteins were targeted, the bromodomain-containing protein 4 (BRD4) and FKBP12, by linking either JQ1 (BRD4 inhibitor, (Filippakopoulos et al., 2010)) or SLF (FKBP12 ligand) to phthalimide. These heterobifunctional molecules induced efficient CRBN-mediated and proteasomal-dependent degradation of their respective targets, highlighting the potential to expand to additional POIs (Winter et al., 2015). Notably, dBet1, the BRD4 degrader, outperformed the competitive bromodomain and extra terminal (BET) inhibitor JQ1 *in vivo*, suggesting that protein degradation may provide additional benefits over inhibition by disrupting potential scaffolding functions. These compounds offered a few additional advantages over previous peptide-based PROTACs, including lower molecular weight that improved cell permeability and eased synthetic efforts, while their efficacy was independent of the POI ligand's inhibitory activity.(Winter et al., 2015).

These initial studies revealed two distinct categories of degraders - PROTACs and molecular glue degraders (MGDs) (Fig. 4). Both leverage the UPS to induce TPD, however they differ in structure, design flexibility and mechanism of action (Békés et al., 2022). PROTACs, being bifunctional molecules, offer modularity and rational design, as in principle any (known) ligand of an E3 could be linked to a POI binder. However, they are relatively larger molecules, potentially posing challenges related to cell permeability and pharmacokinetics (Lipinski et al., 1997). In contrast, MGDs are generally smaller, monovalent molecules with no obvious bifunctionality, that facilitate PPIs(Dong et al., 2021). MGDs' structure potentially results in better drug-like properties, but their discovery is unpredictable and their tunability is more limited compared to PROTACs. Despite the inherent differences of these synthetic degraders, research into both classes has set the foundations for TPD and has allowed for a rapidly growing field with promising therapeutic applications.

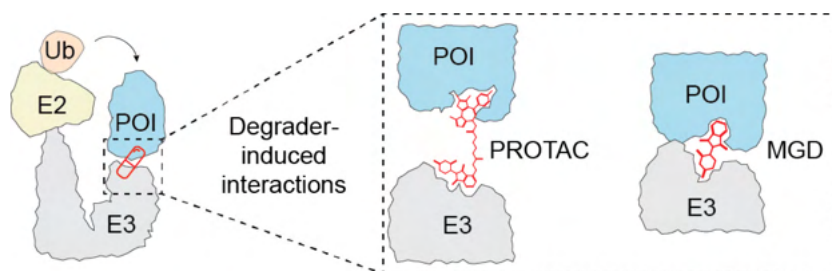


**Figure 4. PROTACs and MGDs.** PROTACs are heterobifunctional molecules containing ligands of the E3 and the POI connected by a chosen linker. MGDs are monovalent compounds facilitating PPIs between the E3 and the POI. The induced E3-POI interaction allows for POI ubiquitination.

### 1.3.4 Field expansion & clinical application

Since the first CRBN-recruiting PROTACs, the field of TPD has seen a substantial expansion on the number of therapeutically relevant targets that can be degraded, spanning diseases like cancer, neurodegenerative disorders, immune diseases and viral infections as well as cardiovascular diseases. With a history of approximately 25 years since the introduction of PROTACs, this emerging pharmacology offers the potential to expand the druggable proteome, and multiple efforts are employed to include them in the clinics as potential therapeutics (Békés et al., 2022; Hinterndorfer et al., 2025). Alongside PROTACs, MGDs with their lower molecular complexity have gained significant attention, particularly following the clinical success of IMiDs (Sasso et al., 2023). The complementary nature of these two degrader modalities and the therapeutic potential have accelerated their integration in drug development.

#### 1.3.4.i Comparison with inhibitor-based pharmacology

Accumulating research has shown that PROTACs and MGDs represent a paradigm shift in drug discovery, offering several advantages over the traditional inhibitor- and occupancy-based pharmacology (Bouvier et al., 2024).

First, degraders have the potential to expand the druggable proteome, as they allow for targeting proteins that lack enzymatic activity or druggable pockets (“undruggable”), two features that are usually required by the inhibitor-based therapeutics (Békés et al., 2022). A big class of such “undruggable” molecules are transcription factors that are major oncogenic drivers in several cancers (Wang et al., 2023). For instance, beyond the degradation of the Ikaros family transcription factors by thalidomide (Gandhi et al., 2014; Krönke et al., 2014; Lu et al., 2014), or the steroid receptors (AR and ER) by the initial PROTACs (Rodriguez-Gonzalez et al., 2008), degraders have demonstrated pre-clinical or clinical efficacy against several transcriptional regulators such as the signal transducer and activator of transcription

5 (STAT5 (Kaneshige et al., 2023)), B-cell lymphoma 6 (BCL6 (Słabicki et al., 2020b)), zinc finger and BTB domain 16 (ZBTB16 (Matyskiela et al., 2020)), p63 (Asatsuma-Okumura et al., 2019) and  $\beta$ -catenin (Gowans et al., 2024). Similarly, since the development of the initial BRD4 degrader by Winter and colleagues (Winter et al., 2015), several degraders have been developed against members of the BET family, such as BRD9 or SMARCA2, and are already under clinical investigation (Livingston et al., 2025; Poling et al., 2023; Qilu Pharmaceutical Co., 2023; Zhou et al., 2022).

The advantage of degraders to reach difficult-to-target proteins extends beyond oncology. TPD could offer significant benefits in neurodegenerative disorders, where protein aggregates are central to the disease pathology and effective treatments remain limited. Several degraders targeting Tau (Alzheimer's), huntingtin (Huntington's),  $\alpha$ -synuclein (Parkinson's) or TDP-43 (ALS), have shown encouraging pre-clinical efficacies (Wang et al., 2023).

A second advantage is the improved selectivity and specificity achieved by the requirement for simultaneous binding of the POI and the E3 ligase to form a ternary complex (Wurz et al., 2023). This step introduces an extra layer of selectivity, which could decrease off-target effects. For instance, degraders of STAT3, STAT5 or fibroblast growth factor receptor 1/2 (FGFR1/2) outperformed in selectivity compared to the inhibitors from which they were derived (L. Bai et al., 2019; Du et al., 2021; Kaneshige et al., 2023). Other studies with promiscuous pan-kinase inhibitors as starting materials for PROTAC development have shown that selectivity arises from the stability – or lack thereof – of the POI-PROTAC-E3 ternary complex (Donovan et al., 2020). These results highlight the potential of repurposing inhibitors with multiple off-target effects as starting point for PROTAC development, transforming them into more selective therapeutic agents. Interestingly, as exemplified with the case of p38 $\alpha$ , inhibitors with modest affinities could be transformed into high affinity PROTACs, potentially due to stabilization resulting from the cooperative nature of the ternary complex formation (Bondeson et al., 2018). Along these lines, MGDs also confer unique selectivity advantages, as they exploit natural binding interfaces to stabilize PPIs, offering increased potency without extensive modifications (Nowak et al., 2018).

Thirdly, degraders acutely deplete the POI rather than just blocking one of its functions, thus eliminating any additional scaffolding or non-catalytic activities that traditional inhibitors would leave intact. This was recently exemplified with the CRBN-based PROTAC, NX-2127,



targeting the Bruton's tyrosine kinase (BTK) (Montoya et al., 2024). NX-2127 was shown to completely eradicate inhibitor-resistant BTK mutants that retained scaffolding functions and thus uninterrupted B-cell receptor signaling. This degrader has entered clinical trials, showing promising responses of refractory chronic lymphocytic leukemia patients, and offering an alternative solution for the treatment of inhibitor-resistant tumors. IRAK4 is another example that has been targeted by degradation to disrupt both its kinase activity and scaffolding roles (Zheng et al., 2024). Therefore, TPD offers an alternative to targeting PPI-based functions of proteins, which has been proven to be a challenging effort in pharmacology (Lu et al., 2020).

Finally, in traditional occupancy-based approaches, the efficacy of an inhibitor relies on sustained binding of the target (Copeland et al., 2006). In contrast, degraders operate via event-driven pharmacology, where a transient interaction with the POI leads to a lasting effect (degradation) that can only be counteracted by cellular protein synthesis (Haid and Reichel, 2025). After a binding event, the POI is degraded and the small molecule can, in principle, be reused to degrade additional POI molecules. The reversibility of the binding, combined with the lack of a need for continuous occupancy, enables, in some cases, a catalytic-like mode of action (Gao et al., 2023). This allows for high efficacy at sub-stoichiometric concentrations and prolonged biological effects (Bondeson et al., 2015). Notably, the biological effect of degraders could be sustained even after drug removal, since cells require time to resynthesize the degraded protein. This prolonged effect has been shown to lead to a pharmacokinetic/pharmacodynamic decoupling, as therapeutic effects could persist despite undetectable drug levels in circulation (Bartlett and Gilbert, 2022; Mares et al., 2020).

Taken together, both PROTACs and MGDs share the ability to expand the druggable proteome, enhance selectivity and disrupt non-catalytic protein functions. By harnessing event-driven mechanisms, they can induce sustained effects with high potency, making them promising therapeutic modalities alongside traditional inhibitor-based pharmacology.

#### **1.3.4.ii Clinical development**

Driven by the promise of expanding the druggable proteome and overcoming limitations of traditional inhibitors, several degraders have progressed from preclinical discovery to clinical evaluation (Pliatsika et al., 2024; Tsai et al., 2024). In 2019, two PROTACs, ARV-110 against AR and ARV-471 against ER, became the first degraders to enter clinical trials, both showing promising clinical profiles (Békés et al., 2022; Gao et al., 2022; Hamilton et al., 2022). Since then, >50 PROTACs and MGDs have advanced into clinical development

with the majority targeting hematological tumors, prostate or breast cancer and a few targeting autoimmune diseases (Mario et al., 2025; Tsai et al., 2024).

TPD is a transformative therapeutic modality with numerous clinical applications. PROTACs have been used to target a diverse range of proteins such as the AR, ER, BRD9, B-cell lymphoma-extra-large (BCL-XL), IRAK4, STAT3, and BTK across diverse indications (Tsai et al., 2024). Beyond the FDA approved MGDs - thalidomide, pomalidomide and lenalidomide – MGDs targeting the Ikaros transcription factors or GSPT1 are predominant in clinical trials for the treatment of diverse malignancies (Hinterndorfer et al., 2025; Tsai et al., 2024). While MGDs offer pharmacokinetic advantages like enhanced bioavailability and tissue penetration, PROTACs provide broader applicability, due to their bifunctional nature and rational design.

Beyond oncology, TPD holds great promise in areas such as inflammatory, neurodegenerative and infectious diseases. For example, PROTACs targeting IRAK4 are being repurposed for autoimmune diseases, while those degrading proteins such as Tau and Huntingtin are advancing pre-clinical neurodegenerative research (Zheng et al., 2024). In infectious diseases, PROTACs designed to degrade pathogen-specific proteins, like the hepatitis C NS3/4A protease, have demonstrated potential in combating resistant viral strains (de Wispelaere et al., 2019). Moreover, novel approaches like BacPROTACs leverage bacterial proteolytic systems, targeting proteins in pathogens such as *Mycobacterium tuberculosis* (Hoi et al., 2023; Morreale et al., 2022).

Collectively, these clinical developments reflect the potential of TPD in addressing therapeutic needs, however key challenges need to be addressed to achieve this promise.

#### **1.3.4.iii Challenges**

Although significant efforts have brought several degraders into clinical trials, with a few successes, the reality remains that only a minimal fraction progresses to approval, underscoring a gap between preclinical promise and clinical translation (Tsai et al., 2024). Many challenges persist, including unwanted drug toxicities, pharmacokinetic limitations and resistance occurrences.

1) Drug toxicity. Off-target effects of degraders remain a notable concern, with unpredictable engagement of alternative E3 ligases or target substrates. This issue is particularly critical for thalidomide-derived PROTACs, which can degrade unintended targets

such as Sal-like protein 4 (SALL4) or p63, posing risks of developmental toxicity (Asatsuma-Okumura et al., 2019; Donovan et al., 2018). Ensuring selectivity is crucial to minimizing these adverse effects and expanding the therapeutic window. Optimizing these properties requires innovative chemical strategies, such as engaging tissue-specific E3 ligases to minimize systemic exposure and off-target degradation.

2) Pharmacokinetic limitations. PROTACs usually present poor pharmacokinetic properties, including poor bioavailability and limited tissue penetration, which can hinder their therapeutic efficacy (Edmondson et al., 2019; Pike et al., 2020). Optimizing solubility, stability and cellular permeability require extended efforts (Chirnomas et al., 2023; Edmondson et al., 2019; Pike et al., 2020). MGDs on the other hand, by having a lower molecular weight, they demonstrate more attractive drug-like properties, although their discovery and lack of rational design pose limitations (Sasso et al., 2023).

3) Drug resistance. Several studies have shown that the use of CRBN- or VHL-based PROTACs poses the risk of resistance occurrences in cells and in clinical settings. While resistance can result from mutations on the binding site of the target POI, genetic studies upon degrader treatments have shown that aberrations in the degradation machinery components are frequent mechanisms of acquired resistance (Gooding et al., 2021; Gosavi et al., 2022; Hanzl et al., 2023; Lu Zhang et al., 2019). For instance, loss of CUL2 after treatment with VHL-based PROTACs or complete loss of CRBN are prominent examples of resistance mechanisms (Gooding et al., 2021; Lu Zhang et al., 2019). In refractory myeloma patients that had undergone lenalidomide or pomalidomide treatments, more than 30% of patients carried aberrations that directly or indirectly affected CRBN (Gooding et al., 2021). A recent deep mutagenesis study on CRBN and VHL mapped resistant hotspots in these two substrate receptors, providing a framework to predict clinically relevant mutations that could arise as resistance mechanisms in patients (Hanzl et al., 2023).

To fully harness the potential of TPD necessitates both improved molecular designs and more sophisticated preclinical models to better predict drug responses. In addition, a deeper understanding of the diverse mechanisms underlying proximity induced degradation is essential. The efficiency, selectivity and resistance profiles are intrinsically linked to how degraders exploit the cell's proteolytic systems. Dissecting the molecular determinants of induced degradation can help refine degrader design and expand the targetable space.

## **1.4 The multifaceted mechanisms of proximity-induced degradation**

The study of targeted protein degraders, including PROTACs and MGDs, has expanded our understanding of how induced proximity can rewire cellular networks in unexpected ways. While the conventional model of degrader function involves the recruitment of an E3 ligase to a POI for ubiquitination and proteasomal degradation (Fig. 4), the TPD discoveries of the last decade have revealed a diverse range of mechanistic variations beyond this simple paradigm (Tsai et al., 2024). These insights have not only identified new hijackable E3 ligases but have also uncovered alternative molecular events leading to degradation. The increasing complexity of degrader mechanisms underscores their potential as more than just inducers of targeted degradation; they actively reshape endogenous circuits revealing new layers of biological regulation.

### **1.4.1 Learnings from nature's degraders**

Induced degradation is not a foreign concept in nature. Living organisms have employed sophisticated mechanisms to regulate protein homeostasis and have evolved diverse strategies to degrade proteins in response to cellular cues (Fig. 5) (Tsai et al., 2024). By studying these natural pathways, we gain valuable insight into the fundamental principles of degraders that could shape the development of next generation TPD strategies.

Long before TPD was introduced, the Howley laboratory, through their work on the human papillomavirus (HPV), described an intriguing mechanism (Huibregtse et al., 1991). They demonstrated that the viral E6 protein, by associating with the host's p53 and the newly identified E6-associated protein (E6-AP), induced ubiquitin-dependent p53 degradation (Fig. 5.4). Essentially, in this process, the viral peptide acted as a bridge to facilitate the interaction between the E6-AP, a novel E3 ligase, and p53, to promote viral survival by uncontrollable proliferation (Martinez-Zapien et al., 2016). Since the initial discovery, a growing number of virus families, such as adenoviruses, paramyxoviruses or retroviruses, have been identified to hijack several components of the host's UPS (KyungWon et al., 2007; Li et al., 2010; Mahon et al., 2014). This suggests that proximity-induced degradation is a general phenomenon in viral pathogenesis, highlighting how nature had long exploited proximity-induced degradation for cellular control.

Contrary to viruses that hijack the host's degradation system, plants have evolved an endogenous hormone-responsive proteolytic pathway to regulate their growth. Seminal work by Estelle and colleagues uncovered a pathway that relied on the plant hormone indole-3-

acetic acid (IAA or auxin) to trigger proteasome-dependent degradation of Aux/IAA proteins via the SCF-transport response inhibitor 1 (SCF<sup>TIR1</sup>) complex (Fig. 5.3) (Gray et al., 2001, 1999; Tan et al., 2007). Similarly to auxin, jasmonate acts as a molecular glue to induce degradation of jasmonate-zim domain proteins via the SCF<sup>COI1</sup> E3 complex (Chini et al., 2007).

Although no similar mechanism has been reported in mammalian cells so far, the identification of endogenous molecular glues in plants reinforced the idea that small molecules can be utilized for induced degradation and inspired the development of synthetic biology tools for controllable protein degradation. In particular, the Kanemaki laboratory engineered an orthogonal synthetic system, called auxin inducible degron (AID), to rapidly and reversibly degrade mammalian proteins (Nishimura et al., 2009). By ectopic expression of TIR1 and a chimeric POI-auxin-responsive degron (67aa), researchers could orthogonally modulate protein stability, without the requirement of large synthetic ligands.

Mammalian cells, on the other hand, have evolved a different mechanism to regulate their nuclear hormone receptors (NHRs) via ligand-controlled ubiquitin-mediated degradation (Nawaz et al., 1999; Wallace and Cidlowski, 2001; Zhu et al., 1999). Several NHRs share a C-terminal ligand-binding domain that, upon binding of the respective hormone, undergoes conformational changes leading to degron exposure, recognized by the E3 ubiquitin protein ligase UBR5 (Fig. 5.2) (Tsai et al., 2023).

As mentioned earlier (section 1.3.1), the ER-targeting SERDs have been reported to act via a mechanism where E3-SERD complex is targeted for UPS-mediated degradation (Gheysen et al., 2024; Long and Nephew, 2006). The E3 ligases UBR5 or RNF111 have been implicated to participate in this process, although the precise mechanisms remain elusive (Hilmi et al., 2012). Even though the endogenous-hormone-induced and SERD-induced degradation likely follow distinct pathways, these examples show how synthetic molecules can mimic natural compounds, ultimately converging on ligand-induced targeted degradation as a powerful regulatory strategy.

Learnings from nature have shown that virtually any molecule, even a simple metal ion, could act as a molecular glue (Henning et al., 2022). Work from the Rape laboratory proposed a mechanism where zinc (Zn) facilitates the assembly of the CUL2-FEM1B-FNIP1 complex upon reductive stress (FEM1B, fem-1 homologue B; FNIP1, folliculin-interacting protein 1). In this context, reduction of residues on FNIP1 are detected by FEM1B via atomic

interactions stabilized by Zn. Thus, Zn acts as a molecular bridge stabilizing the FEM1B-Zn-FNIP1<sup>reduced</sup> complex and facilitating FNIP1 degradation (Fig. 5.1) This intriguing mechanism expands the scope of natural glues beyond peptides or small molecule hormones, suggesting that even chemical elements can serve as proximity-inducing factors for degradation.

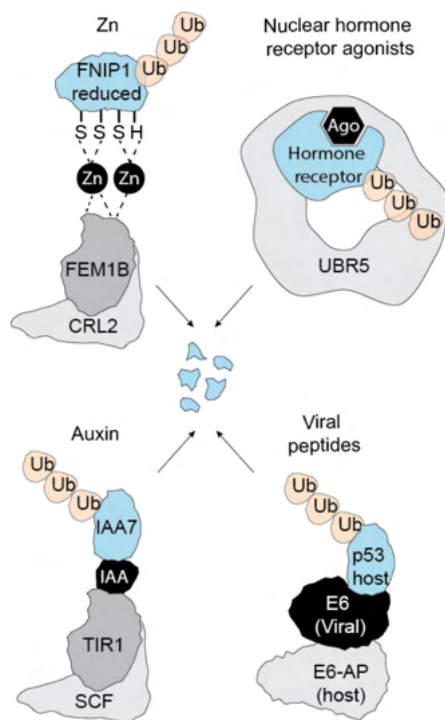


**Figure 5. Examples of natural degraders.** 1) Under reductive stress, Zn facilitates the assembly of CUL2-FEM1B-FNIP1<sup>reduced</sup>, promoting FNIP degradation. 2) Upon agonist (Ago) binding, nuclear hormone receptors undergo conformational changes, exposing hidden degrons that can be recognized by E3 ligases (e.g. UBR5), triggering degradation. 3) In plant cells, the growth hormone auxin (indole-3-acetic acid, IAA) acts as a MGD, inducing interactions between TIR1 (substrate receptor of SCF complex) and Auxin proteins (i.e. IAA7). 4) The HPV protein E6 bridges two host proteins, the tumor suppressor p53 and the E3 ligase E6-AP, to induce p53 degradation. All shown interactions induce ubiquitination and subsequent degradation. FEM1B, Fem-1 homologue B; FNIP1, Folliculin-interacting protein 1; UBR5, Ubiquitin Protein Ligase E3 Component N-Recognin 5; Ub, ubiquitin; TIR1, transport response inhibitor 1; E6-AP, E6-associated protein

#### 1.4.2 Unique mechanisms of synthetic small molecule-induced degradation via the UPS

Similarly to nature's diverse mechanisms for induced degradation, synthetic degraders have further expanded this landscape by revealing mechanisms that go beyond the classical E3 ligase-substrate interaction. Recent discoveries in the TPD field have demonstrated a growing number of unconventional rewiring of cellular pathways ultimately leading to degradation. From a mechanistic perspective, these uncovered mechanisms give valuable insights into the biology of TPD, that can be leveraged for expanding the targetable scope. In this section, several representative examples will be described that showcase the complexity of TPD and highlight the potential of expanding the field in different directions.

##### 1.4.2.i Neo-interactions induced by MGDs

IMiDs and their function as MGDs that bridge CRBN with IKZF1/3 for degradation have set the paradigm of classical glues (Fig. 6.1) (Chamberlain et al., 2014; Gandhi et al., 2014; Krönke et al., 2014; Lu et al., 2014; Zhu et al., 2014). However, many recent reports have

demonstrated examples of non-classical glue-induced degradation. One such example is the MGD-induced degradation of cyclin K, in which the DDB1- cell-cycle-dependent protein kinase 12 (CDK12) gluing allows for optimal cyclin K positioning for ubiquitination (Fig. 6.2) (Kozicka et al., 2024; Lv et al., 2020; Mayor-Ruiz et al., 2020; Słabicki et al., 2020a). In this example, cyclin-K being the “cargo” of CDK12, becomes the indirect target for degradation. This paradigm expanded the mechanistic diversity of MGDs, showing that POI degradation can be achieved via indirect substrate recruitment.

Efficient POI degradation requires both right conformation for efficient ternary complex formation, and sufficient stability of the ternary complex (Bondeson et al., 2018; Du et al., 2019). Growing evidence suggests that MDGs not only act by inducing novel interactions, but also by re-enforcing existent low-affinity ones (Cao et al., 2022; Hanzl et al., 2025; Hsia et al., 2024; Y.-D. Li et al., 2024; Rui et al., 2023; Słabicki et al., 2020b). For instance, the interaction of DDB1 and CUL4 associated factor 16 (DCAF16) with BRD4 is typically weak and does not lead to degradation (Hsia et al., 2024).

A few studies have shown that MGDs can solidify the BRD4-DCAF16 interaction via different mechanisms. For example, a joint study by the Winter and Ciulli laboratories introduced the concept of intramolecular glue degraders (Fig. 6.6) (Hsia et al., 2024). They showed that the compound IBG1 induced a neosurface by the two bromodomains of BRD4 that facilitated the stabilization of BRD4-DCAF16 complex, ultimately leading to BRD4 degradation. Their biophysical data showed that IBG1 stabilized the pre-existing low affinity BRD4-DCAF16 interaction, demonstrating that MGDs can enhance transient interactions to induce degradation. With this knowledge at hand, the authors tested rationally designed intramolecular glues, revealing an unprecedented potency at picomolar range, supporting the potential of expanding towards this methodology.

To harness these weak intrinsic interactions to rationally design degraders, the Ebert laboratory introduced a mechanism termed template-assisted covalent modification (Fig. 6.3) (Y.-D. Li et al., 2024). In brief, they presented a method to overcome the inconsequential BRD4 - DCAF16 low affinity interaction, by using a BRD4 ligand carrying a covalent handle. In this model, BRD4 served as a carrier, delivering a covalent warhead within reach of a DCAF16 cysteine, enabling covalent modification and complex stabilization. This, in turn, led to BRD4's own degradation, demonstrating how small molecules can be rationally designed to enforce PPIs if positioned correctly. Combined, these studies highlight how uncovering the mode of

action of MGDs can inform the rational transformation of transient PPIs to stable complexes, driving wanted biological outcomes.

In line with the notion that MGDs can harness or enhance endogenous circuits to exert their activity, Slabicki and colleagues identified a distinct MGD-driven degradation mechanism based on POI polymerization (Slabicki et al., 2020b). Their compound, BI-3802, induced symmetrical BCL6 homodimer clustering, forming high molecular-weight helical structures. Following genetic screens and biochemical assays revealed that the BCL6 polymers were recognized by the E3 ligase seven in absentia homolog 1 (SIAH1), which was shown to be an endogenous E3 for BCL6. These compound-induced BCL6 polymers enhanced the intrinsic recognition by SIAH1 leading to the observed degradation (Fig. 6.4). This mechanism showcased the mechanistic versatility of TPD and introduced a novel degradation paradigm in which POI polymerization can be harnessed to reinforce endogenous proteolytic circuits. Notably, the identification of SIAH1 as an endogenous BCL6 ligase highlights the value of exploring synthetic-compound-induced effects, as they can uncover previously unknown regulatory pathways.

Looking at the other side of the coin, studying protein mutations can reveal how MGDs induce PPIs. A recent study by the Liao laboratory exemplified this by the identification of cancer-associated gain-of-function mutations on the E3 ligase substrate receptor kelch repeat and BTB domain containing 4 (KBTBD4) that forced aberrant co-repressor complex (CoREST) degradation (Xie et al., 2025). Using deep mutational scanning and structural elucidation they demonstrated direct interaction with the histone deacetylase 1 (HDAC1), mediated by surface complementarity introduced by the mutated residues of KBTBD4, leading to stabilization and degradation. Intriguingly, they showed that this mechanism was mimicked by the small molecule UM171, inducing similar surface interactions (Fig. 6.5). Notably, the HDAC1/2 cofactor inositol hexakisphosphate (InsP6), that stabilizes HDAC1-CoREST interactions, was also required for the degradation phenotype. This study, parallelizing small-molecule effects to mutation-driven outcomes, opens new possibilities for drug design by using lessons learned from mutant-induced neointeractions.

Finally, recent reports on MGDs have revealed mechanisms that require additional cellular components, beyond an E3 ligase and POI, for the activity. Many small molecules carry moieties that present metabolic liabilities at the organismal or cellular level, with a lot of research focusing on prodrug development for improving drug delivery (Fralish et al., 2024).



Studies of small molecules acting as degraders have revealed interesting mechanistic events that convert precursor molecules to active MGDs in the cells leading to observed target degradation. For instance, a joint study by the Schulman and Gray labs, reported a first-in-class type of molecular glue that was termed charged glue (c-Glue) (Zhuang et al., 2024). Combining genetics, proteomics and structural/biochemical studies, they identified the small molecule ZZ1, which contains a covalent handle metabolized into a charged moiety. This, in turn, is indispensable for the electrostatic interactions with the Yippee like 5 (YPEL5) subunit of the E3 ligase C-terminal to LisH (CTLH) (Fig. 6.7). This study introduced a unique metabolic MGD mechanism and described in atomic detail how electrostatic interactions mediate interactions of a POI with an E3 ligase that has not been used in TPD before.

Along the lines of metabolically converted drugs, the Han laboratory identified the mode of action of the antipsychotic drug acepromazine (ACE) (Lu et al., 2024). In brief, cellular enzymes induced the reduction of ACE to the active counterpart (S)-ACE-OH, that in turn caused nucleoporin 98 (NUP98) degradation via the E3 ligase tripartite motif-containing protein 21 (TRIM21). Following ACE-based PROTAC development, the researchers demonstrated that TRIM21 can be redirected towards degradation of multimeric proteins only when present in nuclear condensates and not in the monomeric form. Although degradation of endogenous proteins localized in the condensates was not shown, the potential of this mechanism is invaluable, as it could allow for degradation of disease-causing protein aggregates.

Collectively, these examples of uncovering diverse MGD mechanisms underscore the versatility of small-molecule-induced degradation and the complexity of modulating the UPS system. However, these discoveries have mainly originated from serendipity. In contrast, the modularity of PROTAC technology has inspired efforts beyond the standard paradigm of E3 ligase recruitment.

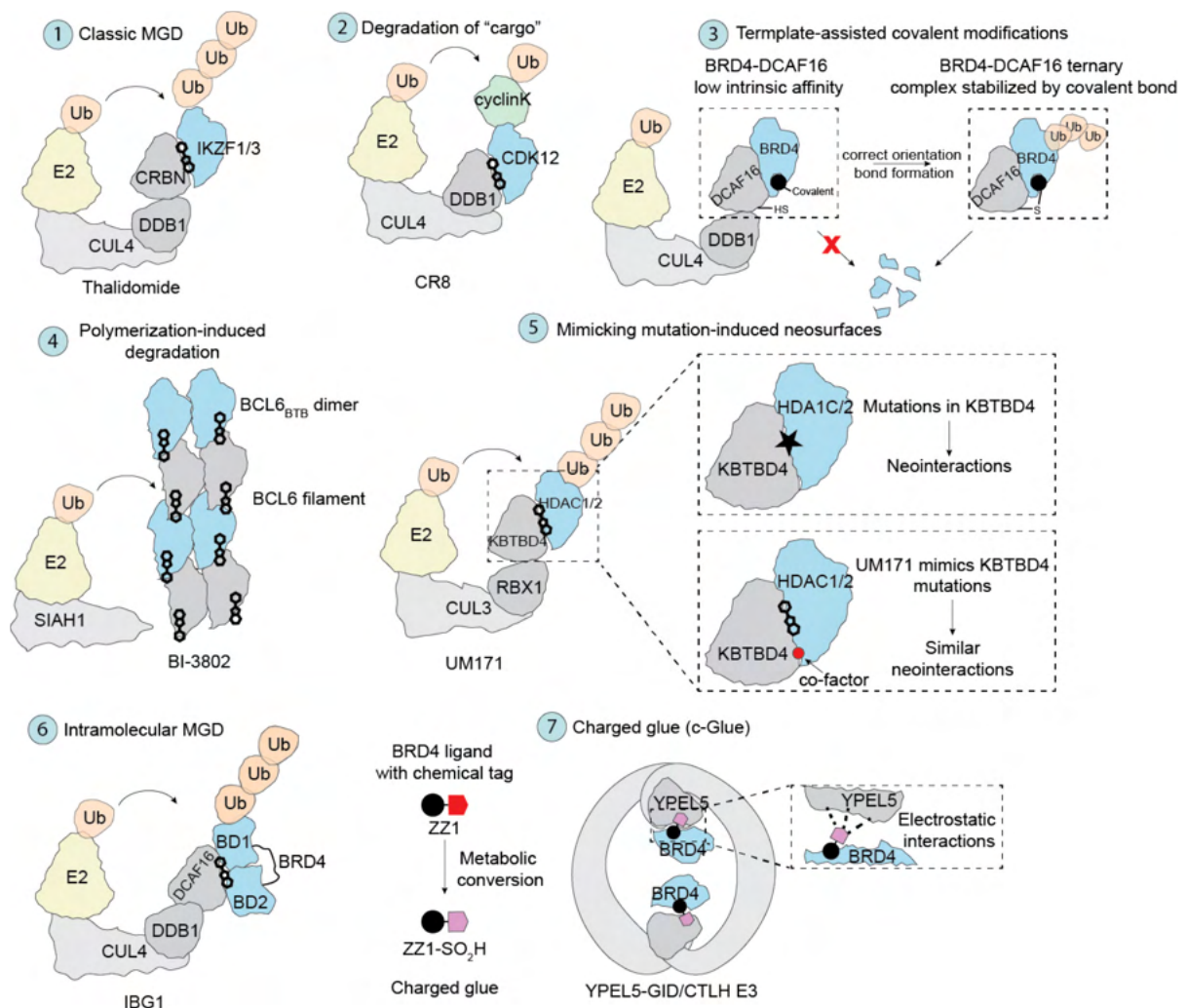


**Figure 6. MGD-induced neointeractions.** 1) Classical example of MGD, as exemplified by the first identified IMiD thalidomide, that induces CRBN-IKZF1/3 neointeractions, leading to degradation. 2) Degradation of cargo by CR8 molecular glue that induces DDB1-CDK12 interaction, thereby positioning cyclin K ("cargo") at the reach of ubiquitination. 3) Template-assisted covalent modification. Weak intrinsic interactions between DCAF16 and BRD4 are normally insufficient to induce degradation. By attaching a covalent handle to JQ1 (BRD4-ligand), BRD4 facilitates covalent modification of a Cys on DCAF16 during the transient interaction. This covalent "gluing" stabilizes the complex and induces BRD4 degradation. 4) Polymerization-induced degradation. The compound BI-3802 induces BCL6-homodimer polymerization leading to filamentous structures recognized by the endogenous BCL6 E3 ligase SIAH1. 5) UM171 mimics the gain-of-function mutations on the E3 ligase KBTBD4 that induce neointeractions with the HDAC1 component of the CoREST complex. The co-factor InsP6 (red) is required for CoREST degradation. 6) IBG1 acts as an intramolecular glue degrader creating a neosurface consisting of bromodomains BD1 and BD2 of BRD4 and DCAF16, leading to degradation. 7) The compound ZZ1 is metabolized to the charged ZZ1-SO<sub>2</sub>H, (charged molecular glue or c-Glue) facilitating electrostatic interactions between YPEL5 and BRD4. IKZF1/3, Ikaros zinc finger proteins 1/3; BRD4, bromodomain-containing protein 4; BCL6, B-cell lymphoma 6; CDK12, cell cycle-dependent protein kinase 12; CoREST, co-repressor complex; CRBN, cereblon; CRL, cullin RING ligases; DDB1, damage-specific DNA binding protein 1; DCAF16, DDB1 and CUL4 associated factor 16; HDAC1,

histone deacetylase 1; KBTBD4, kelch repeat and BTB domain containing 4; SIAH1, seven in absentia homolog 1; YPEL5, Yippee like 5; CTLH, C-terminal to LisH.

#### **1.4.2.ii Redirecting alternative UPS components**

Traditional PROTACs and MGDs primarily function by recruiting an E3 ligase substrate receptor (SR) like CRBN, to the POI. However, the inherent modularity allows for more flexible engagement of the UPS system. As the field tries to expand beyond the conventional CRBN or VHL-based approaches, researchers have employed diverse PROTAC strategies to recruit different components of the UPS system (Fig. 7).

As mentioned above, MGDs acting via the recruitment of DDB1 were the first proof that bypassing substrate receptor recruitment is a viable strategy to induce degradation (Lv et al., 2020; Mayor-Ruiz et al., 2020; Słabicki et al., 2020a). More recent studies have expanded this concept by hijacking alternative components of the UPS system. Several studies by the Nomura laboratory using a ligand-first approach employed chemoproteomics that resulted in the identification of covalent binders for the adaptor proteins DDB1 and SKP1, as well as for the E2 Ub conjugating enzyme UBE2D (Fig. 7) (Belcher et al., 2023; Forte et al., 2023; Hong et al., 2024; Meyers et al., 2024). In all cases, these novel covalent binders were subsequently incorporated into PROTACs targeting AR or BRD4, demonstrating promising degradation properties. Although these strategies offer opportunities to expand the TPD field, further mechanistic understanding of the underlying molecular events is needed to assess their applicability and versatility.

Interestingly, a recent study reported a TPD strategy for directly targeting a POI to the proteasome without the need of intermediate components (Fig. 7) (Bashore et al., 2023). It was shown that peptidic macrocycles could directly bind PSMD2, a 26S proteasome subunit, without inhibiting its function. Incorporating them into bifunctional molecules with BRD4 ligand resulted in efficient BRD4 degradation. Despite limitations arising from the high molecular weight, these chimeras could reach proteins with limited (or no) available lysines for ubiquitination and overcome resistance mutations in the ubiquitination cascade. However, their full potential remains significantly unexplored and could be further developed by identifying novel proteasomal-subunit ligands.

These examples of harnessing the UPS via alternative ways could push the boundaries of TPD, yet there is still room for further exploration of the mechanistic underpinnings and implementation in drug development.

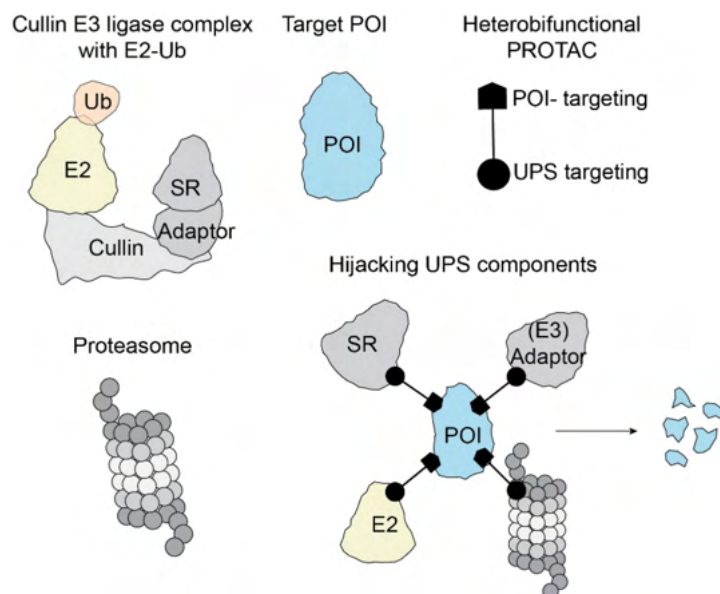


**Figure 7. PROTACs redirecting different UPS components.** PROTAC designs to target a POI for degradation via the UPS. Different components of the cullin E3 ligases have been recruited, such as substrate receptors (SR) and adaptor proteins. Alternatively, components upstream the E3s such as E2s, or downstream the ubiquitination cascade, such as proteasomal subunits, have been shown to be successfully hijacked.

### 1.4.2.iii Chaperone mediated degradation

#### Chaperone-recruiting PROTACs

An alternative UPS-dependent TPD strategy has been inspired by the ability of chaperones to recognize misfolded proteins and facilitate their degradation by recruiting different E3 ligases (Fig. 8). Interestingly, the chaperone HSP90 has been reported to interact with ~30% of the E3 ligases (Taipale et al., 2012). In principle, heterobifunctional molecules bridging a POI with the HSP90 chaperone could induce POI degradation, with proof-of-concept studies demonstrating successful applications CDKs' degradation in cells and in vivo (Li et al., 2023). Although different variations of this platform (HEMTACs, HIM-PROTACs, CHAMPS etc) have been introduced, all follow the same principle of HSP90 chaperone-mediated TPD, yet the exact underlying mechanisms of this approach have not been fully elucidated (Dong et al., 2024; Foley et al., 2021; Li et al., 2023).

#### Hydrophobic tags

An extension to a potentially chaperone-mediated TPD approach is hydrophobic tagging, where lipophilic and hence hydrophobic tags are appended to ligands of POIs (Fig. 8) (Cheng et al., 2025; L. Ma et al., 2024; Xie et al., 2023). This approach is based on the principle that binding of a hydrophobic tag to a POI could mimic the misfolded protein state which would be recognized by the quality control machinery (especially chaperones), subsequently leading to POI degradation. This platform has been used to target a few POIs,

yet the precise mechanism of action is not fully understood, with limited evidence for chaperone and E3 involvement.

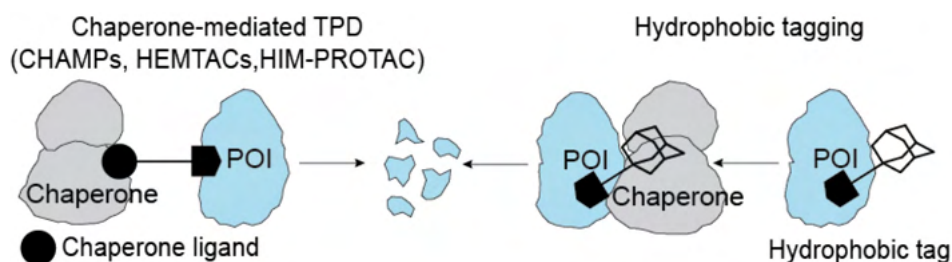


**Figure 8. Chaperone-mediated degradation and hydrophobic tagging.** Left: heterobifunctional molecules built from a chaperone ligand and a POI ligand can recruit various E3 ligases to induce chaperone-mediated degradation. Right: attachment of a hydrophobic moiety on a POI-ligand resembles the unfolded state of a protein, potentially recruiting a chaperone and E3 ligases for POI degradation. The mechanism is mostly speculative and not elucidated.

#### 1.4.2.iv Other unconventional degradation strategies

Several unconventional TPD approaches have emerged, involving more intricate molecular mechanisms beyond bifunctional designs. One such approach is collateral degradation, where targeting a primary POI, when part of a multisubunit complex, triggers the degradation of interacting proteins, or complex collapse (Fig. 9.1) (Hsu et al., 2020; Padovani et al., 2022; Pla-Prats and Thomä, 2022; Zhang et al., 2023). This phenomenon has been observed in repressor complexes, although its precise molecular mechanisms are not fully elucidated.

Other emerging strategies exploit unique recruitment mechanisms for target degradation. For instance, nucleic-acid-mediated degradation is based on oligonucleotide-small-molecule chimeras, in which E3-recruiting ligands are attached to oligonucleotides to recruit RNA- or DNA- binding proteins for degradation (Fig. 9.2) (Ghidini et al., 2021; Samarasinghe et al., 2022; Shao et al., 2021). This approach has been applied to degrade RNA-binding proteins (RNA-PROTACs, (Ghidini et al., 2021)) or transcription factors (oligoTRAFTACs, (Samarasinghe et al., 2022) and O'PROTACs, (Shao et al., 2021)), paving the way for degrading targets that are otherwise challenging to recruit by small molecules. In contrast, Trim-away technology employs the endogenous function of the TRIM21 E3 ligase, which naturally degrades antibodies as part of the immune response (Mallery et al., 2010). By introducing antibodies against a wanted POI, Trim-away allows for rapid proteasome-dependent degradation of the POI, expanding the TPD toolkit beyond small molecule-driven strategies (Fig. 9.3) (Clift et al., 2017).

Finally, experimental designs such as trivalent PROTACs that simultaneously recruit two distinct E3 ligases for POI degradation, offer an alternative approach to potentially overcome resistances (Fig. 9.5) (Bond et al., 2024). Alternatively, bridged-PROTACs could also support a “degradation of cargo” mechanism – similarly to cyclin K degraders (Lv et al., 2020; Mayor-Ruiz et al., 2020; Słabicki et al., 2020a) – as exemplified by compound 1 (MS181) that binds to the embryonic ectoderm development protein (EED) but degrades EED-associated components of the polycomb repressive complex 1 (PRC1), B lymphoma Mo-MLV insertion region 1 homolog (BMI1) and RING1B (Fig. 9.4) (Kabir et al., 2024).

These emerging strategies, either intentionally designed or as a result of unexpected observations, showcase the versatility of TPD and provide new tools to control degradation. Nevertheless, more research is required to fully understand their underlying molecular mechanisms and assess their translational potential beyond preclinical efficacy.

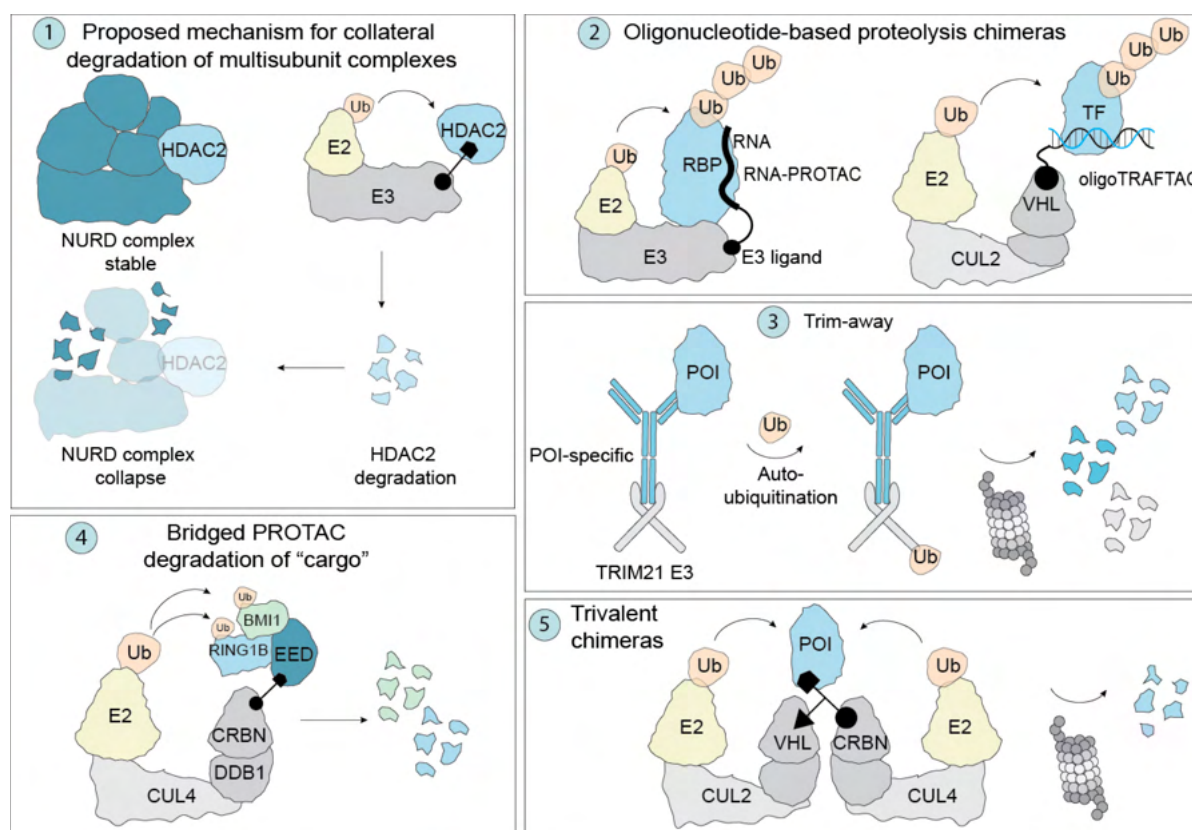


**Figure 9. Alternative degradation strategies.** 1) Targeted degradation of one component of multisubunit complexes leads to complex degradation/collapse. 2) RNA-small-molecule- (RNA-PROTACs) or DNA-small-molecule- (oligo-TRAFTACs) chimeras to recruit E3 ligases to RNA-binding proteins (RBPs) or DNA-binding proteins such as transcription factors (TFs), respectively. 3) Antibodies against an endogenous POI can trigger recognition by the TRIM21 E3 ligase. 4) Bridged PROTAC



recruits EED to CRBN and induces degradation of the EED-associated subunits BMI1 and RING1B ("cargo"). 5) Chimeras consisting of CRBN-, VHL- and POI- ligands recruit two E3 ligases simultaneously for POI degradation. EED, embryonic ectoderm development protein; PRC1, polycomb repressive complex 1; BMI1, B lymphoma Mo-MLV insertion region 1 homolog; RING1B, really interesting new gene 1B; TRIM21, tripartite motif-containing protein 21

#### **1.4.2.v Degraders with non-obvious bifunctionality beyond MGDs**

##### **Inhibitors increasing endogenous turnover**

Beyond PROTACs and MGDs, many small-molecule inhibitors have been unexpectedly found to act as destabilizers, triggering degradation. In addition to the previously mentioned SERDs that induce ER degradation (Gheysen et al., 2024), kinase inhibitors often exhibit destabilizing effects (Jones, 2018). A large-scale study investigating this phenomenon identified an overarching mechanism that involved inhibitor-induced exacerbating (or "supercharging") of the natural degradation pathway of the kinase targets (Fig. 10A) (Scholes et al., 2024). This process was driven by inhibitor-induced hyperactivation (Fig. 10A.1), mislocalization (Fig. 10A.2) or multimerization (Fig. 10A.3), which in turn activated endogenous kinase proteolytic circuits. This mechanism is extended beyond kinase inhibitors, covering inhibitors of the enzyme indoleamine-2,3-dioxygenase 1 (IDO1) (Hennes et al., 2025). These examples involve much more intricate mechanisms, posing challenges for rational design and mechanistic elucidation.

##### **Small molecule ubiquitination**

Notably, another study reported an unconventional mechanism in which the E3 ligase X-linked inhibitor of apoptosis protein (XIAP) could directly ubiquitinate its own ligand that carried an aliphatic chain with a terminal primary amine (den Besten et al., 2021). This mechanism was based on the principle that the small molecule mimicked the side chain of lysine, which is the primary amino acid for Ub attachment (Fig. 10B). In vitro assays detected the small molecule-Ub conjugates, suggesting a mechanism of auto-degradation where an E3 ligase could ubiquitinate a bound small molecule, thereby indirectly marking itself for degradation (den Besten et al., 2021). Ubiquitination of non-protein substrates has also been shown by Otten and colleagues, who demonstrated that the bacterial lipopolysaccharide (LPS) can be directly ubiquitinated by the eukaryotic E3 ligase RNF213, contributing to antibacterial defense (Otten et al., 2021).

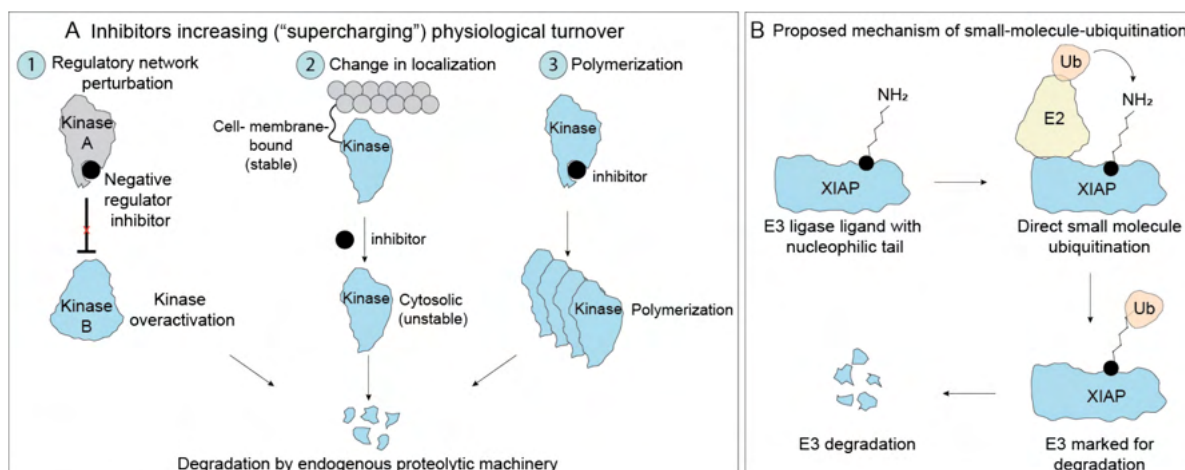


**Figure 10. Unconventional degradation mechanisms with non-obvious bifunctional molecules.**

A) Examples of how kinase inhibitors induce destabilization by enhancing kinase physiological turnover. (1) Inhibition of a negative regulator (kinase A) leads to kinase B overactivation and subsequent degradation by its endogenous E3. (2) An inhibitor can induce change in localization from a stable membrane-bound state to an unstable free cytosolic state, triggering degradation. (3) An inhibitor could trigger kinase polymerization that is cleared by the kinase's endogenous turnover pathway. B) Proposed mechanism for small molecule ubiquitination. Attaching an aliphatic chain with a terminal amine on XIAP's ligand induces XIAP autodegradation. The amine-tethered small molecule mimics lysine's side chain (primary ubiquitination residue), triggering XIAP-mediated ubiquitin attachment on the small molecule, marking the XIAP-small-molecule-Ub complex for degradation. XIAP, X-linked inhibitor of apoptosis protein.

The exploration of molecules that modulate proximity has uncovered a variety of unconventional modes of action and has offered significant insights into drug design. These findings emphasize the importance of investigating diverse chemical compounds and unconventional design strategies to expand the targetable proteome.

### 1.4.3 Redirecting alternative proteolytic pathways - TPD beyond the UPS

While degraders harnessing the UPS have revolutionized TPD, their function is inherently limited to intracellular or membrane-anchored proteins. In addition to the UPS, lysosomal degradation is the other major pathway for maintaining protein homeostasis (Mutvei et al., 2023; Pohl and Dikic, 2019). Lysosome-based strategies complement UPS-based degraders by enabling the degradation of transmembrane receptors, extracellular proteins, protein aggregates or even whole organelles and pathogens, making them attractive in areas such as neurodegenerative diseases and immune modulation (Wells and Kumru, 2024; Zhao et al., 2022).

In 2019, autophagy targeting chimeras (AUTACs) were introduced, combining small-molecule POI ligands and a cyclic guanosine monophosphate (cGMP) to tether proteins to the autophagosomes for lysosomal degradation (Takahashi et al., 2019). Subsequent approaches



(AUTOTACs, ATTECs), despite the name discrepancies, follow a similar principle: hijacking different autophagy-related factors to direct a POI to the autophagy-lysosome pathway (Fig. 11) (Ji et al., 2022; Z. Li et al., 2020). Notably, compounds called alkenyl oxindoles, repeatedly reported as autophagy-tethering compound (ATTECs), were shown by independent studies that can induce DCAF11- and proteasome-dependent degradation when incorporated into BRD4-targeting PROTACs (Wang et al., 2024; Xue et al., 2023). These contradictory results potentially suggest differential pathway involvement that could be dictated by the different target POIs or cellular backgrounds (Zhong et al., 2024).

Alternatively, the Bertozzi laboratory pioneered lysosome-targeting chimeras (LYTACs), to engage the endosome-lysosome pathway (Fig. 11) (Banik et al., 2020). LYTACs were heterobifunctional molecules bridging target proteins with a lysosomal receptor called cation-independent mannose-6-phosphate receptor (CI-MPR) (Ghosh et al., 2003). This receptor was known to bind mannose-6-phosphate (M6P)-modified proteins to facilitate their lysosomal degradation (Banik et al., 2020). As proof of concept, the researchers conjugated poly-M6Pn to antibodies targeting EGFR or PDL1 - targets with therapeutic value – and demonstrated effective degradation. This technology offered versatility, in addition to potential tissue-specificity dictated by the differential expression of lysosomal receptors, as was shown in following studies (Ahn et al., 2021; Caianiello et al., 2021; Paulk, 2021; Xiao et al., 2025).

Notably, most lysosome-mediated TPD strategies rely on biologics, such as antibodies and peptide-based chimeras, rather than small molecules (Zhao et al., 2022). Despite this distinction, they have opened therapeutic avenues for previously inaccessible targets.

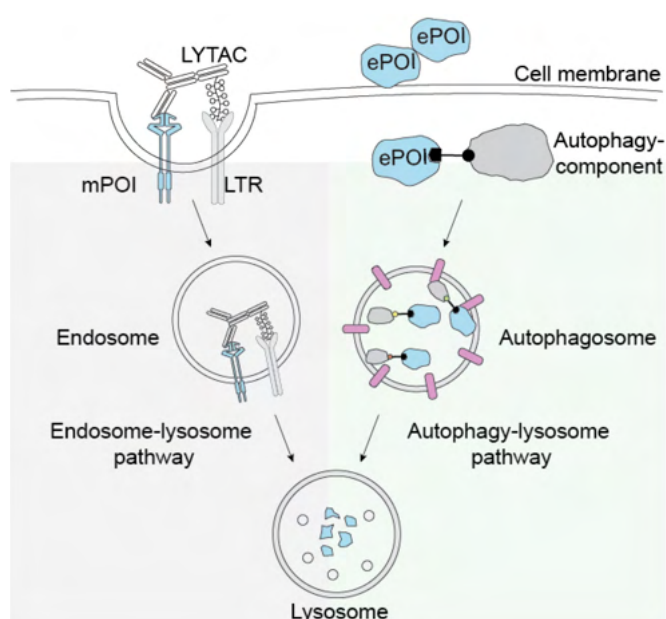


**Figure 11. General principles of hijacking the lysosomal pathway for TPD.**

Extracellular POIs (ePOIs) or membrane bound POIs (mPOIs) can be redirected to the endosome-lysosome (grey) or autophagy-lysosome (green) pathways for subsequent lysosomal-mediated degradation. Lysosome-targeting chimeras (LYTACs) are POI-targeting antibodies linked to poly-M6Pn, a substrate of lysosome receptors (LTR). The mPOI-LYTAC-LTR complex is transferred to the lysosome via endosomal trafficking (grey). Autophagy-targeting chimeras bridge diverse autophagy

components with a POI, leading to autophagosome formation and subsequent lysosomal degradation.

## 1.5 Advances in E3 ligase discovery to broaden the scope of TPD

Having highlighted the multifaceted mechanisms of TPD, the next question is how we could further expand these approaches to address novel proteins and therapeutic needs. For that, it is important to direct the focus towards the E3 ligases, the critical component mediating the POI degradation. Most TPD strategies so far rely on a limited number of well-characterized E3 ligases, posing several limitations. Therefore, the field recognizes that to achieve the full TPD potential, broadening the E3 ligase repertoire is required.

### 1.5.1 Current E3s for TPD

Recent work in the field has led to the discovery of molecules to recruit novel E3 ligases for TPD, in addition to the well-characterized ones, CRBN and VHL (Ishida and Ciulli, 2021; Rodríguez-Gimeno and Galdeano, 2024; Xiao et al., 2024). The most prominent examples of E3 ligases utilized for TPD will be outlined in this section, highlighting the efforts that led to their identification, advantages they might offer and remaining challenges in their wider application.

#### CRBN

As already discussed (section 1.3.3), CRBN is the dominant E3 ligase used in TPD, both in terms of MGD and PROTAC development, as well as in terms of clinical applications. The well-characterized mechanism of action, supported by extensive structural insights and

the availability of ligands from various drug-development campaigns by academia and industry have allowed a broad target scope. Several studies pursuing CRBN-glue protein targets in an unbiased way have revealed previously unknown interactions (Baek et al., 2024; Petzold et al., 2024). Nevertheless, limitations such as ubiquitous expression, mutation accumulation and target (in)accessibility of CRBN, undermine the potential to expand the druggable space if CRBN remains the only E3 ligase utilized for TPD applications (Békés et al., 2022).

## VHL

VHL was one of the first E3 ligases used in PROTAC development, when HIF1 $\alpha$ -derived peptidic molecules known to recruit VHL were linked to the FKBP12<sup>F36V</sup> ligand AP21998 (Schneekloth et al., 2004). These molecules performed better at entering the cells compared to the Protac-1 from the Crews laboratory in 2001 (Sakamoto et al., 2001), but still required improvements of the pharmacokinetics and structural simplification.

In 2012, work from the Crews and Ciulli laboratories led to the discovery of small molecule inhibitors of VHL (Buckley et al., 2012; Van Molle et al., 2012), which entered the TPD momentum in 2015 with a series of VHL-based degraders targeting BRD4 (Zengerle et al., 2015), estrogen-related receptor alpha (ERR $\alpha$ ), and the serine-threonine receptor-interacting-protein kinase 2 (RIPK2) (Bondeson et al., 2015). Their studies revealed a few of the properties of PROTACs, including the concept of event-driven pharmacology, the modularity for different targets, the reversibility of PROTAC effects depending on protein synthesis and structural determinants of their activity (i.e. linker composition) (Bondeson et al., 2015). Several VHL-recruiting PROTACs against a variety of targets have shown efficient pre-clinical effectiveness (Ishida and Ciulli, 2021).

A notable example of a VHL-based PROTAC is DT2216, designed for the degradation of the anti-apoptotic protein B-cell lymphoma extra-large (BCL-XL), an attractive target in hematological malignancies (He et al., 2020; Zhang et al., 2019). Clinical success of BCL-XL inhibitors such as ABT263 has proven to be challenging, primarily due to thrombocytopenia, a severe side effect of inhibition of BCL-XL in platelets (Kaefer et al., 2014). DT2216, a bifunctional molecule bridging a VHL ligand and ABT263, appeared to be superior to the inhibitor alone (He et al., 2020). Specifically, it efficiently degraded BCL-XL in malignant T-cells, but spared platelets as they express low levels of VHL. This added on-target specificity directed by the E3 ligase offers therapeutic advantages over inhibitor-based pharmacology and further supports the value of expanding the E3 ligase toolbox for TPD.

## AhR

The Naito laboratory has achieved hijacking of the arylhydrocarbon receptor (AhR), a ligand-responsive E3 ligase (Ohtake et al., 2007). By synthesizing heterobifunctional molecules based on the AhR agonist  $\beta$ -naphthoflavone and ligands of either the cellular retinoic acid binding proteins (CRABPs) or BET bromodomains, they demonstrated efficient degradation (Ohoka et al., 2019), with potential applications for anti-cancer therapy and inflammatory diseases, in which AhR is overexpressed (Nguyen et al., 2013; Safe et al., 2017).

## MDM2

MDM2, the endogenous E3 ligase regulating the levels of the tumor-suppressive factor p53 (Wu et al., 1993) was the first E3 ligase used in small-molecule-based PROTAC development, because of the availability of its agonist, nutlin-3 (Schneekloth et al., 2008). These first small-molecule PROTACs had favorable features compared to the earlier non-cell-permeable peptidic PROTACs (Sakamoto et al., 2001; Schneekloth et al., 2004). A decade after the first MDM2-based AR degraders, the Crews laboratory synthesized bifunctional molecules that combined nutlin-3 with JQ1, to effectively degrade BRD4 (Hines et al., 2019). This study revealed the dual function of this heterobifunctional molecule: it simultaneously degraded BRD4, thus disrupting oncogenic transcription, and deprived p53 of MDM2, thereby releasing the tumor suppressor. These combined effects showed additive antiproliferative activity compared to previous VHL-based BRD4 degraders. The example of MDM2 really highlights additional advantages of TPD technology: 1) it demonstrated that the endogenous roles of novel PROTACable-E3 ligases could offer more potent cellular effects and 2) there might be clinical advantages, as treatment-evading mutations are less likely to abolish both PROTAC functions (Hines et al., 2019).

## DCAF15

Two independent studies from 2017 focusing on sulfonamides (i.e. indisulam, E7820, CQS) demonstrated that thalidomide and analogues are not the only molecules that act as MGDs (Han et al., 2017; Uehara et al., 2017). Indisulam had shown some efficacy in clinical trials in solid tumors, yet the underlying mechanism of action of this compound was unresolved (Baur et al., 2007). By developing and sequencing resistant-to-indisulam clones, Han and colleagues identified the splicing factor RNA binding motif protein 39 (RBM39, also known as

CAPER $\alpha$ ) as the main target of the drug (Han et al., 2017), while Uehara and colleagues used orthogonal MS-based assays that led to the same conclusion (Uehara et al., 2017).

With a series of biochemical and proteomics methods, both groups revealed the mode of action of indisulam: this compound facilitates the ternary complex formation between the CUL4A/B-DCAF15 and RBM39, a mechanism akin to thalidomide for CUL4-CRBN-IKZF1/3 (Han et al., 2017; Sievers et al., 2018; Uehara et al., 2017). RBM39 degradation resulted in splicing defects in cancer cells, contributing to the anti-cancer activity of these compounds (Han et al., 2017; Uehara et al., 2017). Han and colleagues, additionally showed that aryl sulfonamides were particularly effective against cancers with hematological origin that highly expressed DCAF15, providing both a mechanistic understanding and a potential screening method for drug efficiency (Han et al., 2017).

Structural resolution of the ternary complex DCAF15-indisulam-RBM39 indicated mechanistic differences compared to CRBN-thalidomide that posed challenges in further developing indisulam-based molecular glues or PROTACs for other targets (Bussiere et al., 2020). More specifically, indisulam binds very weakly to DCAF15 and requires RBM39's amino acid side chains for strong binding. Hindrances in the ternary complex formation might be another limiting factor. Thus, efforts to make aryl-sulfonamide based PROTACs, apart from few examples, have been limited (L. Li et al., 2020).

## **KEAP1**

As the first pre-clinical application of TPD in neurodegenerative diseases, Lu and colleagues used peptidic-stretches that bind Tau protein on the one side and the Kelch-like ECH-associated protein 1 (KEAP1) E3 ligase on the other side, thus forming bifunctional molecules for Tau degradation (Lu et al., 2018). KEAP1, as a responder to oxidative stress, is particularly interesting in the context of neurodegenerative diseases, where oxidative stress is a prominent factor of disease pathology (Zhang et al., 2004). Further studies have demonstrated the utility of KEAP1 for TPD through small-molecule-based PROTACs (Tong et al., 2020a; Wei et al., 2021).

## **DCAF16**

The Cravatt laboratory devised a method to identify novel E3 ligases, using electrophilic heterobifunctional molecules with high promiscuity, generally termed as “covalent scouts” (Backus et al., 2016; Crowley et al., 2021). This approach identified DCAF16 as a

novel E3 ligase that could degrade nuclear proteins (Zhang et al., 2019b). Their strategy, on the one hand, provided a viable framework for identifying new E3 ligases for TPD that has been widely used ever since (Xiao et al., 2024), and on the other hand introduced a method to study degradation in specific cellular compartments, potentially expanding specificity options.

Since the first study by Cravatt, several DCAF16-targeting compounds have been introduced, expanding both targets and identified modes of action (Hassan et al., 2024; Lim et al., 2024; Shergalis et al., 2023). Nomura and Gray teams have reported covalent handles for DCAF16 recruitment, achieving degradation of several targets (Hassan et al., 2024; Lim et al., 2024). Interestingly, DCAF16 has been repeatedly identified as a “frequent hitter” E3 ligase involved in diverse mechanisms such as intramolecular glue degraders and template-assisted covalent modification (trans)-labeling (Hassan et al., 2024; Hsia et al., 2024; Zhang et al., 2025).

## **RNF114**

Parallel to the identification of electrophilic compounds targeting DCAF16, a joint study by two groups, Maimone and Nomura, discovered another covalently engaged E3, RNF114 (Spradlin et al., 2019). Their study was focused on understanding the mechanism of action of the natural product nimbolide (from *Azadirachta indica* tree), which features a cysteine-reactive moiety (Cohen et al., 1996). To map potential nimbolide-targeted cysteines across the proteome, the researchers used an unbiased chemoproteomic method called isotopic tandem orthogonal proteolysis-enabled activity-based protein profiling (isoTOP-ABPP) (Weerapana et al., 2010). In brief, mass spectrometry was used to map proteome-wide binding of pan-reactive cysteine probes, excluding those residues “protected” by compound (nimbolide) binding. Their approach uncovered the exact cysteine engaged by nimbolide and allowed for PROTAC development against chosen POIs (Luo et al., 2021; Tong et al., 2020b).

## **Others**

Beyond the aforementioned examples, a few additional E3 ligases have been shown to have potential TPD applications, although their wider applicability warrants additional research. Table 1 summarizes all E3 ligases with at least one case of TPD application with small-molecule degraders (PROTACs or MGDs).

**Table 1.** E3 ligase subunits with at least one application in TPD with small molecule PROTAC or MGD. Applications with peptidic-based compounds were excluded.

| #  | E3 ligase                              | Type of degrader                                  | E3 family |
|----|--|---|-----------|
| 1  | CRBN                                   | MGD & PROTAC                                      | CRL4      |
| 2  | DCAF15                                 | MGD   | CRL4      |
| 3  | VHL                                    | MGD & PROTAC                                      | CRL2      |
| 4  | DCAF1 (Schröder et al., 2024)          | PROTAC  | CLR4      |
| 5  | DCAF11 (Zhang et al., 2021)            | PROTAC  | CLR4      |
| 6  | clAP1                                  | PROTAC (SNIPERs)                                  | RING      |
| 7  | DCAF16                                 | PROTAC  | CLR4      |
| 8  | RNF114                                 | PROTAC  | RING      |
| 9  | MDM2                                   | PROTAC  | RING      |
| 10 | AhR                                    | PROTAC  | CLR4B     |
| 11 | KEAP1                                  | MGD (Roy et al., 2024) & PROTAC (Du et al., 2022) | CLR3      |
| 12 | RNF4 (Ward et al., 2019)               | PROTAC  | RING      |
| 13 | GID4 (Li et al., 2025)                 | PROTAC  | RING      |
| 14 | TRIM21 (Lu et al., 2024)               | MGD & PROTAC                                      | RING      |
| 15 | XIAP (den Besten et al., 2021)         | Small-molecule autoubiquitination                 | RING      |
| 16 | $\beta$ -TrCP (Simonetta et al., 2019) | MGD   | CLR1      |
| 17 | KLDHC2 (Hickey et al., 2024)           | PROTAC  | CLR2      |
| 18 | KBTBD4 (Xie et al., 2025)              | MGD   | CLR3      |
| 19 | YPEL5 (Zhuang et al., 2024)            | MGD   | RING      |
| 20 | SPOP (Deng et al., 2025)               | Bridged-PROTAC                                    | CLR3      |

### 1.5.2 Discovery methods of novel TPD-amenable E3 ligases

Using insights from all identified ligases for TPD, generally the methods for the discovery of novel recruitable E3 ligases can be summarized into unifying categories (Jevtić et al., 2021; Rodríguez-Gimeno and Galdeano, 2024; Xiao et al., 2024):

**1) Serendipitous discovery via compound mode of action studies.** From the first discovery of compounds with gluing activity such as rapamycin, FK506 and cyclosporin A to the identification of the targets of IMiDs and indisulam, drugs with therapeutic effects but elusive mode of action, have been primary targets for mechanistic characterization (Z. Guo et al., 2019; Han et al., 2017; Ito et al., 2010; Liu et al., 1991). While this approach relies on

unexpected findings and cannot be used as a discovery tool, it might offer immediate therapeutic leads as the compounds are already in clinical use.

**2) Rational design using E3 binding peptidic motifs.** This approach is based on knowledge regarding the binding motifs for E3 ligases, as exemplified with the original peptidic PROTACs recruiting VHL or  $\beta$ -TRCP (Sakamoto et al., 2001; Schneekloth et al., 2004). Although there is clear rationale behind the development of these PROTACs, it depends on existing knowledge that is often lacking for most of the ~600 E3 ligases (Xiao et al., 2024). In addition, tedious synthetic efforts and poor pharmacokinetics of peptidic drugs might hinder therapeutic applications (Lipinski et al., 1997).

**3) Rational design using existing E3 ligands (“ligand-first” approach).** Existing E3 ligase ligands, for instance nutlin-3 for MDM2 (Hines et al., 2019), can be used for streamlined design of PROTACs. Although this approach is straightforward, it is limited by the availability of known compounds.

**4) Chemoproteomics with covalent scout fragments.** High-throughput screens with promiscuous covalent fragments have revealed ligandable sites for several E3 ligases that were successfully used for PROTAC development (Crowley et al., 2021; King et al., 2023; Lim et al., 2024; Luo et al., 2021; Resnick et al., 2019; Ward et al., 2019; Weerapana et al., 2010; Zhang et al., 2019). This approach has accelerated the discovery of novel E3 ligases and has demonstrated improved efficiencies in degradation. Nevertheless, starting from promiscuous fragments poses the risk of off-targets, and significant improvements are needed for downstream therapeutic applications.

All discovery approaches have been proven valuable in the exploration of E3 ligases for TPD, however they pose challenges that require careful consideration before translational investigation. Nevertheless, combining these strategies can maximize the chances of uncovering diverse and potentially more effective E3 ligases for TPD.

Another notable observation is that the majority of E3 ligases harnessed for TPD belong to the RING E3 ligase family, predominantly the cullin RING ligases (Békés et al., 2022). Although no definitive study has tested the reasons for this prevalence, it is probably multifactorial. Firstly, RING (and CRL) ligases comprise the majority of E3s, thus the numerical dominance might contribute to the more frequent identification (Harper and Schulman, 2021). In addition, they are highly modular, as they consist of multiple components such as diverse



SRs and adaptor proteins that could allow versatility (Harper and Schulman, 2021). Finally, the one-step catalytic mechanism of RING E3s might confer kinetic advantages for the event-driven pharmacology of TPD (Zheng and Shabek, 2017). Consequently, the combination of cellular abundance, modularity and efficient catalysis positions RING E3s at the forefront of TPD.

### 1.5.3 Unlocking new opportunities with novel E3 ligases

Significant progress in expanding the current milieu of E3 ligases has revealed how the inherent versatility of E3 ligases could contribute to the versatility of TPD. Exploiting novel E3s offers opportunities to fine-tune degradation, addressing a few of the challenges that TPD faces, such as resistance to widely used E3s and off target toxicities. Apart from these, inherent E3 ligase biology could unlock distinct advantages, stemming from specialized endogenous roles and expression patterns. More specifically, hijacking novel E3s for TPD could help:

**1) Overcoming drug resistance:** drug resistance remains a major challenge in the clinical application of CRBN- and VHL-based degraders, as tumors frequently evolve escape mechanisms by mutating or downregulating these ligases (Gooding et al., 2021; Gosavi et al., 2022; Hanzl et al., 2023). Therefore, broadening the E3 ligase pool could mitigate or delay resistance occurrences.

**2) Achieving cell type or tissue selectivity:** as exemplified by the VHL-based PROTAC DT2216 and thrombocytopenia, a wide variety of E3 ligases with differential tissue selectivity could offer degradation in target tissues while sparing healthy ones, a quality lacking from the ubiquitously expressed CRBN and VHL (He et al., 2020).

**3) Accessing alternative pathways.** The subcellular localization of different E3 ligases could offer the opportunity for differentiating in target specificity (Poirson et al., 2024). For instance, specificity for nuclear, mitochondrial or transmembrane targets could be achieved by organelle-specific E3s (Shah and Đikić, 2022; Simpson et al., 2022). Alternatively, E3 ligase specificity for misfolded proteins or aggregates could reach currently inaccessible targets.

**4) Tapping into synergistic effects:** even though in many cases, it is favorable to preserve the endogenous roles of the E3 ligases, there are situations where disrupting the natural substrate can induce synergistic therapeutic effects (Hines et al., 2019; Lu et al., 2018).

By redirecting an E3 away from its endogenous targets could lead to dual biological outcome - for instance by eliminating a disease-causing protein and by modulating the activity of its natural substrate. A compelling example is using MDM2-based PROTACs against BRD4 (Békés et al., 2022; Hines et al., 2019). Redirecting MDM2 from p53 towards the oncogenic driver BRD4 could inhibit cancer progression by removing the oncogenic signal and reactivating the tumor suppressor. Alternatively, a KEAP1- based PROTAC could offer a dual benefit by degrading, for instance, a neurotoxic protein while simultaneously releasing the antioxidant NRF2, leading to combinatorial cytoprotective effects (Lee and Hu, 2020; Lu et al., 2018).

#### **1.5.4 Challenges in identifying and utilizing novel E3 ligases**

As outlined above, there is a strong rationale to make more E3 ligases available for TPD, however several technical or biological challenges exist slowing down progress in that direction.

The primary limitation is the lack of available ligands for the majority of E3 ligases (Rodríguez-Gimeno and Galdeano, 2024). While recent developments in chemoproteomic tools and high-throughput screening have allowed the discovery of novel ligands (Kannt and Đikić, 2021), the majority remains inaccessible to small molecules, hindering the applicability in TPD. Moreover, when identifying or designing ligands for E3 ligases, it is crucial that these compounds do not interfere with essential functional domains - particularly those required for ligase complex assembly and activity.

Secondly, limited knowledge around most E3 ligases presents a significant challenge. Not many E3 ligases are well-characterized with the majority lacking information regarding their natural substrates, regulatory mechanisms or structural elucidation (Liu et al., 2023). This makes the identification of suitable E3 ligases for therapeutic development more complex, resource-intensive and unpredictable.

Finally, the unknown endogenous substrates profile of many E3s can pose additional risks in therapeutic development (Landré et al., 2014). For instance, in cases of multiple or essential endogenous substrates, redirecting an E3 ligase could lead to multiple off-target effects or broad proteome destabilization. Without a clear understanding of their natural degradation pathways, repurposing E3 ligases could disrupt cellular function, leading to adverse effects (Landré et al., 2014; Zheng and Shabek, 2017).

In summary, E3 ligases hold immense promise for TPD, but realizing their promise requires overcoming challenges in ligand discovery, structural characterization, functional elucidation and selective engagement.

### **1.5.5 Thesis aims**

Building on the insights outlined before and acknowledging the need for expanding the E3 ligase toolbox, the overarching aim of this thesis was to expand the scope of TPD beyond the few characterized E3 ligases. Given the momentum of covalent chemistry as a tool to identify ligandable E3s (Belcher et al., 2023; Crowley et al., 2021; Zhang et al., 2021, 2019), we employed a scout-fragment strategy and a reporter system with the goal of uncovering E3 ligases amenable to TPD strategies.

More specifically, this thesis was built on the following subaims:

1. Developing a luminescence-based strategy to screen covalent heterobifunctional molecules for the identification of novel degraders.
2. Elucidation of the degradation machinery involved in the hit compound's activity with specific focus on identifying the E3 ligase involved.
3. Detailed mechanistic characterization of the mode of action of the hit compound.

## **2. Results**

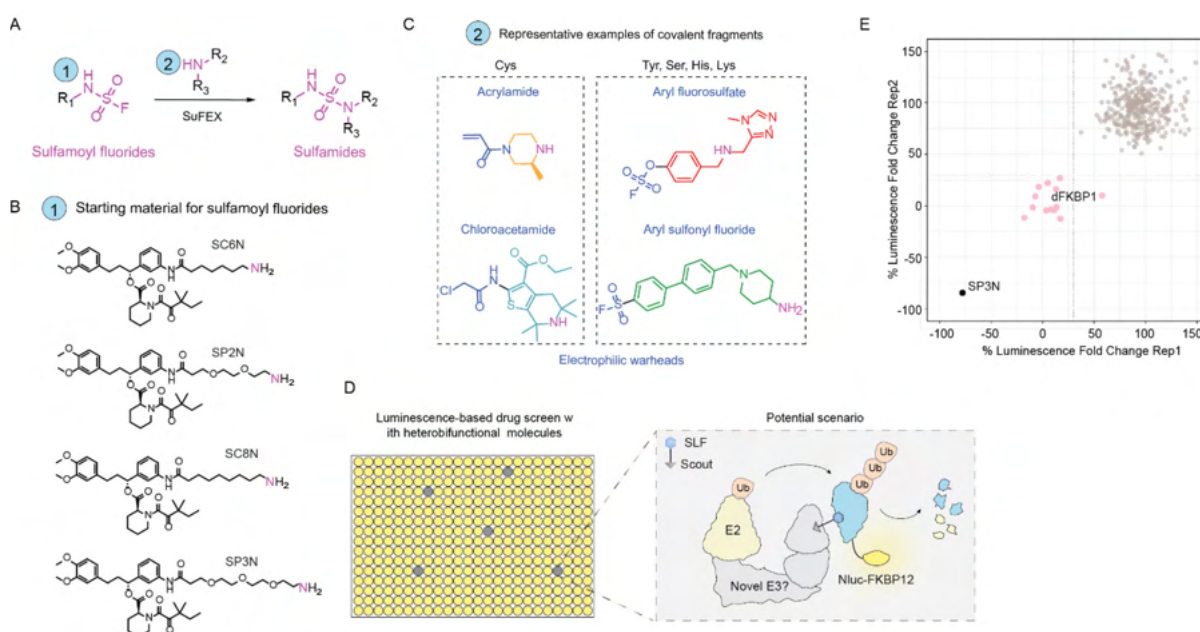
### **2.1 Preliminary results**

To discover novel degrader molecules and potentially identify new E3 ligases for TPD, we developed a luminescence-based reporter system by fusing the prolyl isomerase FKBP12 to nanoluciferase (Nluc-FKBP12), enabling luminescence readout as a proxy for degradation (Preliminary Data Fig.1D). Using this system, we screened an in-house library of heterobifunctional molecules, each consisting of the established FKBP12 ligand SLF, four different flexible linkers, and a diverse set of covalent fragments (available by Enamine, Preliminary Data Fig.1B, 1C). These compounds were synthesized previously via Sulfur(VI) Fluoride Exchange (SuFEx) reaction (Preliminary Data Fig.1A), with the fragment selection based on a few criteria:

- i) Presence of an amine required for the SuFEx reaction

- ii) Presence of a covalent warhead, that could theoretically engage different amino acid residues
- iii) Low molecular weight
- iv) Potential for promiscuous interactions to increase the chances of binding cellular proteins

The library of heterobifunctional molecules included a positive control, dFKBP1, which is a known CRBN-recruiting FKBP12 PROTAC (Winter et al., 2015), as well as negative controls, in which SLF was only bound to a linker with a terminal amine, serving as starting materials for the SuFEx reaction (Preliminary Data Fig. 1B). The results of the preliminary screen revealed an unexpected hit – the negative control, SLF-PEG3-NH<sub>2</sub> (SP3N), potently destabilized Nluc-FKBP12 despite lacking any obvious degradation moiety (Preliminary Data Fig.1E). Given SP3N's minimal structure, essentially consisting of only the ligand SLF (with no degradation properties) and an aliphatic linker ending on a primary amine, we set out to investigate its unexpected activity.



**Preliminary Data Figure 1. Preliminary screen identifies the starting material SP3N as a putative FKBP12 degrader** A) Schematic of SuFEx reaction occurring between sulfamoyl fluorides (1) and primary or secondary amines (2) B) Starting materials for the synthesis of SLF-based sulfamoyl fluorides for SuFEx reaction component (1) shown in A. SLF-linker-NH<sub>2</sub> compounds for the synthesis of the SC6N, SLF-C6-NH<sub>2</sub>; SC8N, SLF-C8-NH<sub>2</sub>; SP2N, SLF-PEG2-NH<sub>2</sub>; SP3N, SLF-PEG3-NH<sub>2</sub>. C) Examples of covalent fragments with primary or secondary amines for the SuFEx reaction component

(2) shown in A. Four different groups are distinguished: acrylamides and chloroacetamides theoretically able to engage cysteines and aryl fluorosulfates or aryl sulfonyl fluorides theoretically able to engage tyrosines, serines, lysines or histidines. D) Schematic overview of the luminescence-based drug screen. The heterobifunctional molecules were screened against a reporter cell line expressing nanoluciferase-tagged FKBP12 (Nluc-FKBP12). Luminescence was monitored as a proxy for FKBP12 levels. Compounds inducing Nluc signal reduction (grey wells) could be Nluc-FKBP12 degraders by potentially recruiting a novel E3 ligase. E) Luminescence-based screen in HEK293T cells expressing the Nluc-FKBP12 construct, treated with 396 FKBP12-targeting heterobifunctional molecules, at 10 $\mu$ M in duplicates. Percentage (%) luminescence fold change was calculated based on the DMSO treated controls. dFKBP1 is a CRBN-based FKBP12 degrader and was used as positive control. Black dot: SP3N, pink dots: dFKBP1, grey dots: heterobifunctional molecules. Dotted lines at 25% luminescence fold change.

## 2.2 Prologue for published manuscript

Given that our preliminary screen revealed a potential degrader with non-obvious bifunctionality, we aimed at elucidating its mode of action. At the time, two independent studies had reported a similar observation - small molecules with an aliphatic tail had degradation properties, although they provided minimal mechanistic insights. Specifically, den Besten and colleagues reported that attaching an aliphatic tail to the ligand of the E3 ligase XIAP induced XIAP autodegradation, by direct small molecule ubiquitination (Section 1.4.2v) (den Besten et al., 2021). Although the small molecule ubiquitination was an intriguing mechanism, the proof was limited to in vitro assays. On the contrary, Hanley and colleagues reported the alkylamine containing nuclear receptor binding SET domain protein 2 (NSD2) degrader UNC8153 to be dependent on the UPS system, however no further mechanistic elucidation was described (Hanley et al., 2023).

To explore the mode of action of our hit compound SP3N, we used diverse genetic, proteomic and biochemical approaches, which revealed that it recruits the SCF<sup>FBXO22</sup> E3 ligase complex to induce potent and selective FKBP12 degradation. Metabolomics experiments demonstrated that SP3N's activity relied on the metabolic conversion of the primary amine into a reactive aldehyde, SP3CHO, a process dependent on amine oxidases present in the fetal calf serum (FCS). Mutagenesis and in vitro biochemical studies revealed that SP3CHO forms an adduct with FBXO22, via its C326, suggesting a covalent interaction.

Our study successfully identified a novel PROTACable E3 ligase while uncovering a "minimal" PROTAC-like degradation mechanism. We further demonstrated the generalizability

of this strategy by showing that the other two alkylamine-based degraders targeting NSD2 and XIAP, also depended on FBXO22-C326 for their activity. This modular design of low molecular weight PROTACs engaging FBXO22 and depending on amine oxidases, both cancer-relevant factors, highlights a powerful strategy to expand TPD.

### **2.3 Results**


Our findings following up on the unexpected hit SP3N, which provide detailed mechanistic characterization of SP3N and serve as proof-of-concept for the utility of FBXO22 for TPD applications were published in the paper “Alkylamine tethered molecules recruit FBXO22 for targeted protein degradation” (Kagiou et al., 2024). The author of this thesis performed most mechanistic studies and analyses and together with Georg Winter conceptualized the study. JACT synthesized the heterobifunctional molecules for the preliminary screen and other compounds used subsequently, while biochemical studies and proteomics analyses were performed by collaborators. More details regarding the contributions can be found in the respective section of the paper.

# Alkylamine-tethered molecules recruit FBXO22 for targeted protein degradation

Received: 29 January 2024

Accepted: 18 June 2024

Published online: 26 June 2024

 Check for updates

Chrysanthi Kagiou<sup>1</sup>, Jose A. Cisneros<sup>1</sup>, Jakob Farnung<sup>2</sup>, Joanna Liwocha<sup>2</sup>, Fabian Offensperger<sup>1</sup>, Kevin Dong<sup>3</sup>, Ka Yang<sup>3</sup>, Gary Tin<sup>1</sup>, Christina S. Horstmann<sup>1,4</sup>, Matthias Hinterndorfer<sup>1</sup>, Joao A. Paulo<sup>3</sup>, Natalie S. Scholes<sup>1</sup>, Juan Sanchez Avila<sup>1</sup>, Michaela Fellner<sup>5</sup>, Florian Andersch<sup>5</sup>, J. Thomas Hannich<sup>1</sup>, Johannes Zuber<sup>5</sup>, Stefan Kubicek<sup>1</sup>, Steven P. Gygi<sup>3</sup>, Brenda A. Schulman<sup>2</sup> & Georg E. Winter<sup>1</sup>✉

Targeted protein degradation (TPD) relies on small molecules to recruit proteins to E3 ligases to induce their ubiquitylation and degradation by the proteasome. Only a few of the approximately 600 human E3 ligases are currently amenable to this strategy. This limits the actionable target space and clinical opportunities and thus establishes the necessity to expand to additional ligases. Here we identify and characterize SP3N, a specific degrader of the prolyl isomerase FKBP12. SP3N features a minimal design, where a known FKBP12 ligand is appended with a flexible alkylamine tail that conveys degradation properties. We found that SP3N is a precursor and that the alkylamine is metabolized to an active aldehyde species that recruits the SCF<sup>FBXO22</sup> ligase for FKBP12 degradation. Target engagement occurs via covalent adduction of Cys326 in the FBXO22 C-terminal domain, which is critical for ternary complex formation, ubiquitylation and degradation. This mechanism is conserved for two recently reported alkylamine-based degraders of NSD2 and XIAP, thus establishing alkylamine tethering and covalent hijacking of FBXO22 as a generalizable TPD strategy.

Targeted Protein Degradation (TPD) has gained significant attention in recent years as a therapeutic modality that promises to overcome the limitations of conventional, inhibitor-centric small-molecule design.

TPD is based on the principle that small molecules can induce molecular proximity between an E3 ubiquitin ligase and a target protein of interest (POI) to trigger POI ubiquitylation and ensuing degradation by the proteasome. On a high level, the field distinguishes two major classes of degraders.

Molecular glue degraders (MGDs) typically function by binding to either the E3 or the POI, modifying the protein surface to induce novel or stabilize existing protein–protein interactions. The resulting ternary

complex (POI-MGD-E3) is hence highly cooperative and the MGD orchestrates several protein–protein interactions at the binding interface. The most prominent MGDs are thalidomide and its analogs (commonly referred to as immunomodulatory drugs or IMiDs), which bind to the E3 ligase CRL4<sup>CRBN</sup> thereby causing recruitment and degradation of a suite of zinc finger transcription factors<sup>1–4</sup>. Noteworthy, the identification of IMiDs and other MGDs was serendipitous<sup>5</sup>, but an increasing toolbox of MGD discovery strategies promises to rationalize future MGD identification<sup>6–11</sup>. The other prominent class of degraders is heterobifunctional proteolysis targeting chimeras (PROTACs)<sup>12</sup>. PROTACs simultaneously bind the POI and the E3 ligase

<sup>1</sup>CeMM Research Center for Molecular Medicine of the Austrian Academy of Sciences, 1090 Vienna, Austria. <sup>2</sup>Department of Molecular Machines and Signaling, Max Planck Institute of Biochemistry, Martinsried, Germany. <sup>3</sup>Department of Cell Biology, Harvard Medical School, Boston, MA, USA. <sup>4</sup>St. Anna Children's Cancer Research Institute, Vienna, Austria. <sup>5</sup>Research Institute of Molecular Pathology, Vienna BioCenter, 1030 Vienna, Austria.

✉ e-mail: [gwinter@cemm.oeaw.ac.at](mailto:gwinter@cemm.oeaw.ac.at)



via dedicated ligands that are connected via a flexible linker. The chimeric nature of PROTACs allows their rational design but overall depends on the availability of well-defined ligands for the POI and the E3.

Around twenty degraders have entered human clinical investigation, all of which function by coopting either CRL4<sup>CRBN</sup> or CRL2<sup>VHL</sup><sup>13,14</sup>. This establishes the motivation to expand the set of actionable E3 ligases with several objectives in mind<sup>15</sup>. First, accessing new E3 ligases provides a strategy to address resistance mechanisms that are either already clinically observed or expected, particularly in oncology settings<sup>16–19</sup>. Second, VHL and CRBN are, with few exceptions ubiquitously expressed<sup>20</sup>, thus preventing tissue- or cell-type selective degradation strategies which would have the potential of an increased therapeutic index. Third, not all POIs are equally amenable to CRBN- or VHL-based degraders, possibly due to incompatibilities in surface topologies and hence an inability to form a productive ternary complex<sup>21–23</sup>. Over the last years, strategies employing electrophilic fragments either as affinity reagents or as putative E3 binders have been successful in unlocking several E3 ligases, including CRL4<sup>DCAF1</sup>, CRL4<sup>DCAF16</sup>, RNF4, or RNF114 for prototypic PROTAC design, but additional work will be required to understand or realize their translational potential<sup>24–28</sup>.

In addition to these two paradigmatic degrader classes, a suite of insufficiently characterized, seemingly “monovalent” degraders directly bind a POI through a well-defined molecular recognition yet induce POI degradation through elusive mechanisms. Functional annotation of these mechanisms promises to reveal novel strategies for degrader design and to unlock additional E3 ligases for chemical exploration. Among others, this has been exemplified by functional studies with the monovalent BRD2/4 degrader GNE-0011 that functionally depends on the CRL4<sup>DCAF18</sup> ligase<sup>29–31</sup>. Similarly, recent reports disclosed “compound 10”, a small-molecule degrader of XIAP that consists of a known XIAP binder appended to a flexible primary alkylamine<sup>32</sup>. Initial mechanistic characterization of compound 10 led to a model where the free amine would be directly polyubiquitinated by XIAP *in cis*, thereby inducing its proteasomal degradation<sup>33</sup>.

Here, we describe the mechanistic characterization of a serendipitously discovered degrader of the prolyl isomerase FKBP12. Akin to compound 10, it consists of an alkylamine tail that is appended on a target-binding ligand, here the synthetic ligand of FKBP12 (SLF) and is hence termed SLF-PEG3-NH2 (SP3N). To unravel the mechanism of action of SP3N, we coupled FACS-based CRISPR/Cas9 knockout screens with quantitative proteomics and biochemical reconstitutions. This led us to identify that SP3N recruits the SCF<sup>FBXO22</sup> ligase to induce FKBP12 polyubiquitylation and ensuing proteasomal degradation. In accordance with a recently reported alkylamine degrader targeting the histone methyltransferase NSD2<sup>33</sup>, we show that SP3N is a precursor that is metabolized into an active aldehyde species. Through targeted mutagenesis, functional reconstitutions, and intact mass spectrometry, we show that the aldehyde adducts a cysteine residue (C326) in the C-terminal domain of FBXO22, and that this covalent engagement is functionally required for ternary complex formation, productive ubiquitylation and degradation. Importantly, our data imply that compound 10, as well as the alkylamine-based degrader of NSD2 functionally converge on the same, PROTAC-like mechanism. Collectively, our data therefore outline a roadmap to rational degrader development and unlocking FBXO22 for TPD applications.

## Results

### SP3N-induced FKBP12 degradation depends on the primary amine and is UPS dependent

En route to the development of a PROTAC candidate library targeting the prolyl isomerase FKBP12, we serendipitously discovered a set of small molecule precursors with unexpected degradation activity. Active precursors merely consist of a free primary alkylamine attached

to the synthetic ligand of FKBP12 (SLF) (Supplementary Fig. 1a, b). Among the assayed molecules, attachment of a PEG3-NH2 moiety to SLF (SP3N) yielded the most potent degrader which was thus prioritized for ensuing studies (Fig. 1a). To monitor drug-induced changes in FKBP12 stability, we engineered KBM7 cells to express an FKBP12-BFP-P2A-mCherry reporter compatible with FACS analysis. Leveraging this reporter, we could show that SP3N efficiently degrades FKBP12 in a time- and dose-dependent manner (Fig. 1b). In addition, competition experiments with excess amount of SLF fully rescued from degradation, confirming the requirement of FKBP12 target engagement for productive degradation (Supplementary Fig. 1c). Degradation activity of SP3N was completely abrogated by acetylating the free primary amine (SP3NAc), thus confirming its relevance akin to previously disclosed alkylamine degraders targeting XIAP or NSD2 (Fig. 1a, c, d)<sup>32,34</sup>. To assay the proteome-wide degradation specificity of SP3N, we conducted MS-based whole proteome analysis using tandem mass tags in HEK293T cells. Among the 8958 identified proteins, SP3N selectively degraded FKBP12 after a 16 h incubation. In contrast, the acetylated analog SP3NAc did not prompt destabilization of FKBP12 or any other protein (Fig. 1e, Supplementary Data 1). To gain a better understanding of the mechanism of the SP3N-mediated degradation, we conducted chemical competition experiments with the proteasome inhibitor carfilzomib and the ubiquitin-activating enzyme (UAE) inhibitor TAK243. Both inhibitors fully prevented FKBP12 degradation, indicating a dependency on the ubiquitin-proteasome system (UPS) (Fig. 1f). In addition, pre-treatment with the NEDD8-activating enzyme (NAE) inhibitor MLN4924 fully rescued from degradation, highlighting a functional requirement on NEDD8 conjugation, and hence implying the functional involvement of a Cullin-RING ligase (CRL) in the SP3N-induced degradation of FKBP12<sup>35</sup>.

### SP3N recruits FBXO22 for FKBP12 degradation

To identify cellular effectors required for SP3N-induced FKBP12 degradation in an unbiased manner, we employed a FACS-based CRISPR/Cas9 knock-out screen with a UPS-focused sgRNA library (Supplementary Data 2). To this end, we transduced KBM7 cells expressing doxycycline-inducible Cas9 (iCas9) and the FKBP12-BFP-P2A-mCherry reporter with a UPS-focused sgRNA library. Three days post-doxycycline induction cells were treated with SP3N and sorted based on the FKBP12-BFP expression levels into three distinct populations—the highest and lowest 5% of BFP-expressing cells (FKBP12<sup>HIGH</sup> and FKBP12<sup>LOW</sup>, respectively), along with the 30% of cells expressing average levels of BFP (FKBP12<sup>MD</sup>). As a control degrader, we used dFKBP1, a previously reported SLF-based PROTAC that is dependent on the CUL4<sup>CRBN</sup> ligase<sup>36</sup>. As expected, FACS-based CRISPR/Cas9 screens of dFKBP1 revealed all components of the CUL4<sup>CRBN</sup> ligase complex alongside subunits of the proteasome as well as the COP9 signalosome in the FKBP12<sup>HIGH</sup> fraction. This implies that CRISPR/Cas9-mediated disruption of these genes abolishes dFKBP1 activity and thus establishes validity of our screening setup (Supplementary Fig. 2a, Supplementary Data 3). Turning our focus to screens treated with SP3N, we identified a profound enrichment of the substrate receptor FBXO22 and other components of the SCF<sup>FBXO22</sup> ligase complex in the FKBP12<sup>HIGH</sup> population, again accompanied by components of the proteasome and COP9 signalosome, thus corroborating chemical competition experiments (Fig. 2a, Supplementary Data 3). To validate the screen results, we proceeded with arrayed gene knockout and reconstitution experiments. Population-level FBXO22 disruption in KBM7 iCas9 cells completely rescued SP3N-induced FKBP12 degradation, as assayed via the FKBP12-BFP-P2A-mCherry stability reporter. In contrast, disruption of the control locus AAVS1 did not affect SP3N efficacy (Fig. 2b, Supplementary Fig. 2b). These results were further corroborated by comparing SP3N-induced FKBP12 degradation in HEK293T wildtype (WT) cells compared to an isogenic, clonal FBXO22 knockout line (FBXO22 KO; Fig. 2c). In addition, reconstitution of



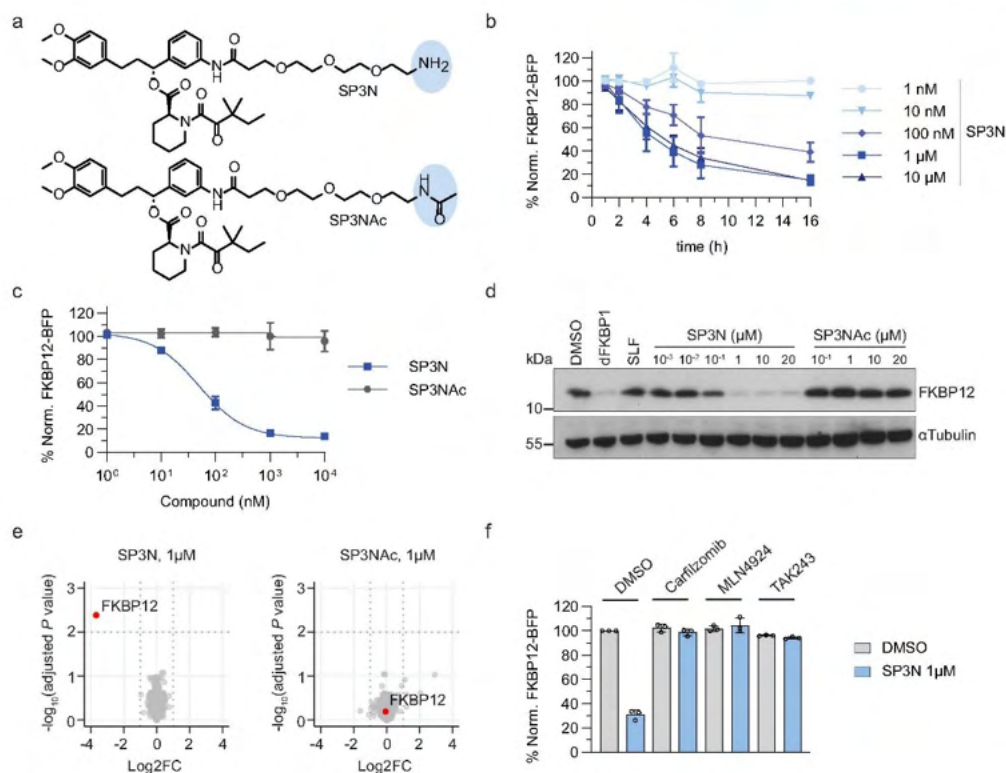


**Fig. 1 | SP3N-induced FKBP12 degradation depends on the primary amine and is UPS-dependent.** **a** Structures of SP3N and SP3Nac. **b** Flow-cytometry based degradation assay upon SP3N treatment. KBM7 iCas9 cells expressing the FKBP12-BFP-P2A-mCherry reporter were treated with the indicated concentrations of SP3N for 1–16 h. **c** Flow-cytometry based degradation assay in KBM7 iCas9 FKBP12-BFP-P2A-mCherry cells treated with SP3N or SP3Nac for 16 h. **d** Immunoblot of FKBP12 in HEK293T Nluc-3xFlag-FKBP12-NLS cells treated with DMSO, 1 μM dFKBP1, 10 μM SLF and the indicated concentrations of SP3N or SP3Nac for 16 h. αTubulin is the loading control. Representative image of  $n = 3$  independent experiments. **e** Whole

proteome analysis using tandem mass tag quantification in HEK293T cells treated with DMSO, 1 μM SP3N or 1 μM SP3Nac for 16 h. Log2 fold-changes (Log2FC) and  $-\log_{10}$ -transformed Benjamini-Hochberg adjusted one-way analysis of variance (ANOVA) P value compared with DMSO treatment. Data from  $n = 3$  replicates. **f** Flow-cytometry based degradation assay in KBM7 iCas9 FKBP12-BFP-P2A-mCherry cells pre-treated with DMSO, 1 μM carfilzomib, 1 μM MLN4924, or 500 nM TAK243 for 1 h before the addition of 1 μM SP3N for 6 h. For all the flow-cytometry based degradation assays (**b**, **c**, **f**), the BFP/mCherry ratio was normalized to DMSO and the data shown are from  $n = 3$  biological replicates, mean  $\pm$  s.d.

FBXO22 KO cells with FBXO22 cDNA restored degradation to levels comparable to WT cells (Fig. 2c). Finally, depletion of the FBXO22 adaptor protein SKP1 also rescued from SP3N-mediated FKBP12 degradation, further confirming that the SCF<sup>FBXO22</sup> complex is required for the degradation process (Supplementary Fig. 2c).

To assess if SP3N induces proximity between FBXO22 and FKBP12, we performed co-immunoprecipitation experiments of 2HA-tagged FBXO22 and 3xFlag tagged FKBP12. As expected, in the input fraction SP3N treatment induced FKBP12 degradation, which was abolished with carfilzomib treatment. In the IP fraction we observed an interaction of FKBP12 with FBXO22 exclusively upon treatment with SP3N in a dose-dependent manner (Fig. 2d). In line with a lack of SP3Nac-induced degradation, we did not observe an interaction between 2HA-FBXO22 and 3xFlag-FKBP12 upon cellular treatment with SP3Nac (Fig. 2d). To further corroborate these results, we developed a proximity assay that is compatible with measurements in intact cells. To this end, we turned to a nanoluciferase complementation assay (NanoBIT<sup>®</sup>) capable of assessing ternary complex formation between FBXO22 and FKBP12 (Fig. 2e). HEK293T cells were co-transfected with LgBIT-FKBP12

and SmBIT-FBXO22 followed by treatment with DMSO, SP3N or SP3Nac. Supporting co-IP data, we observed a pronounced and dose-proportional increase of bioluminescence after cellular SP3N treatment, indicative of drug-induced ternary complex formation (Fig. 2f). Noteworthy, the less potent degrader SP2N also induced FKBP12-FBXO22 complex formation, albeit at a lower magnitude (Supplementary Fig. 2d). As expected, SP3Nac treatment did not induce a bioluminescence signal (Fig. 2f). Competition of SP3N with excess SLF blocked luminescence induction, thus further corroborating the requirement for direct FKBP12 engagement (Fig. 2g). In conclusion, these data support a mechanism whereby SP3N induces proximity between FKBP12 and FBXO22 to prompt FKBP12 degradation by FBXO22.

**SP3N is a precursor metabolized to an active aldehyde species**  
Since primary alkylamines represent a potential metabolic liability, we sought to identify if SP3N might be converted into a functionally relevant metabolite. Of note, a similar mechanism has recently been disclosed for UNC8732, an alkylamine-based degrader targeting the

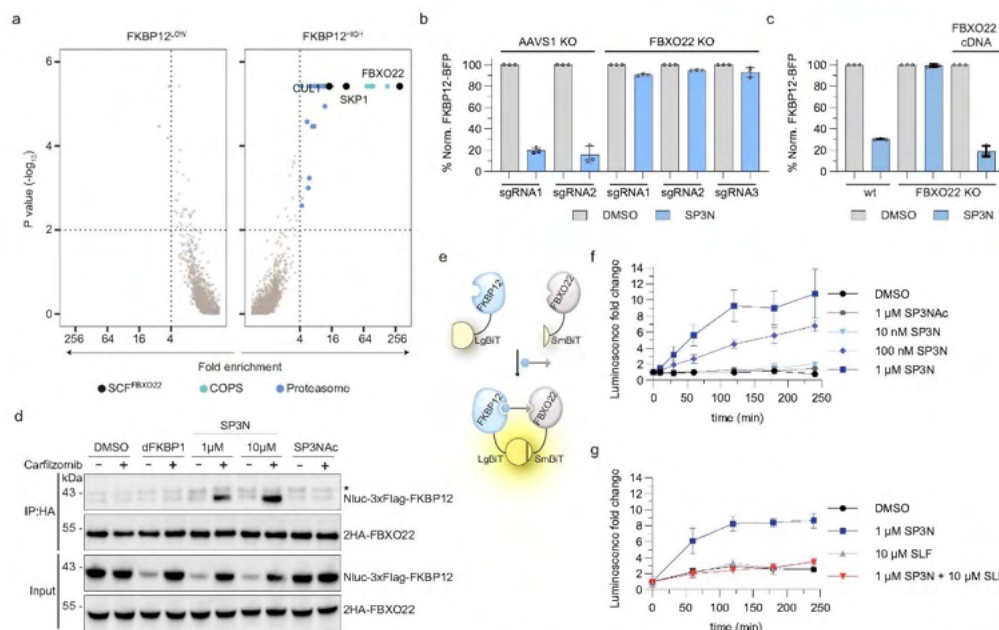


**Fig. 2 | SP3N recruits FBXO22 for degradation.** **a** FACS based CRISPR/Cas9 stability screen. KBM7 iCas9-FKBP12-BFP-P2A-mCherry reporter cells were transduced with a UPS-focused sgRNA library, treated with DMSO or 250 nM SP3N for 16 h and sorted based on the FKBP12-BFP levels. Fold changes and p-values of the FKBP12<sup>low</sup> and FKBP12<sup>high</sup> populations were calculated by comparison with the FKBP12<sup>med</sup> population using two-sided negative binomial test (MAGECK). Significant hits: fold-enrichment ≥ 4 and -log<sub>10</sub> P-values ≥ 2 (dotted lines). Cyan: COP9 signalosome; blue: proteasome subunits; black: SKP1-CUL1-FBXO22 complex. Data from  $n = 2$  replicates. **b** Flow cytometry-based degradation assay for screen validation. KBM7 iCas9-FKBP12-BFP-P2A-mCherry cells were transduced with sgRNAs targeting the control locus AAVS1 or FBXO22 and treated with DMSO or 1 μM SP3N for 16 h. **c** Flow cytometry-based degradation assay for FBXO22 reconstitution. FBXO22 clonal knock-out of HEK293T FKBP12-BFP-P2A-mCherry cells were reconstituted with the 2HA-FBXO22 cDNA and treated with DMSO or 1 μM SP3N for 16 h. For **(b, c)** the BFP/mCherry ratio was normalized to DMSO and the data is the mean ± s.d. of  $n = 3$  biological replicates. **d** Co-immunoprecipitation

of 2HA-FBXO22 and Nluc-3xFlag-FKBP12 following treatment with DMSO, 1 μM dFKBP1, 1 μM or 10 μM SP3N or 1 μM SP3Nac for 4 h in the presence of 1 μM carfilzomib. Samples without carfilzomib were used as controls. IP immunoprecipitation. \*unspecific band. Representative image of  $n = 3$  independent experiments. **e** Schematic representation of the NanoLuc® Binary Technology (NanoBIT) assay. Upon treatment with molecules that induce proximity of the N-terminal LgBIT-FKBP12 and N-terminal SmBIT-FBXO22 fusions, an active Nluc enzyme is formed that can generate luminescence. **f**, **g** NanoBIT® assays in HEK293T co-transfected with LgBIT-FKBP12 and SmBIT-FBXO22 fusions, pre-treated with 1 μM carfilzomib and Vivazine substrate before treatment with the indicated compounds. Fold change of luminescence is normalized to timepoint 0, right before the treatment. Mean ± s.d. of  $n = 3$  technical replicates; representative of  $n = 3$  biological replicates. **f** Dose-response for complex formation. Luminescence was monitored after 5 min, 10 min, 30 min and every hour up to 4 h, post-treatment. **g** Competition assay with SLF. Luminescence was monitored every hour up to 4 h, post-treatment.

histone methyltransferase NSD2<sup>33</sup>. In brief, Nie et al. could demonstrate that UNC8732 acts as a precursor that is metabolized to a potent aldehyde by amine oxidases present in the fetal calf serum (FCS) in the cell culture media. To test if SP3N follows a similar mechanism (Fig. 3a), we treated cells with SP3N in full media containing 10% FCS or in Opti-MEM without FCS, for 8 h and tested degradation. Indeed, FKBP12 degradation only occurred in media with FCS, suggesting that SP3N might undergo a similar metabolic conversion towards an active species (Fig. 3b). To confirm the presence of the SP3N-derived aldehyde (SP3CHO) and the dependence on FCS for this metabolic step, we treated KBM7 cells with SP3N in IMDM + 10% FCS or Opti-MEM without FCS and used ultra-performance liquid chromatography-mass spectrometry (UPLC-MS/MS) to detect the formation of the aldehyde species. Our results reveal the detection of SP3CHO already at 6 h of incubation, and only in conditions containing FCS (Fig. 3c). Taken together, these results indicate that SP3N undergoes an FCS-dependent metabolic step towards an active aldehyde species. The requirement of FCS for the activity of the alkylamine degrader insinuates the involvement of extracellular amine oxidases in the

conversion of SP3N to SP3CHO. To further test this hypothesis, we incubated SP3N with recombinant porcine diamine oxidase (DAO) and subsequently treated KBM7 cells with this solution in media without FCS. Supporting the notion of an involvement of diamine oxidases in the metabolic conversion, DAO pre-treatment of SP3N was sufficient to convert it into an active degrader (Fig. 3d). We next performed a time-course treatment of SP3N with DAO and used UPLC-MS/MS to quantify SP3CHO levels. Confirming the involvement of DAO in this metabolic conversion, we quantified increasing amounts of SP3CHO over time and only upon treatment with the enzyme (Supplementary Fig. 3a).

To confirm that the aldehyde is the active species, we synthesized SP3CHO, as well as the hydrolytically labile, protected aldehyde bisulfite adduct of SP2N (SP2CHOP; given technical challenges in directly synthesizing SP2CHO). In cellular degradation assays, in the presence of FCS, both aldehyde species outperform their matched alkylamine analog (Fig. 3e, Supplementary Fig. 3b). This suggests that metabolic conversion might act as a rate-limiting step (Fig. 3c). Moreover, in contrast to SP3N and SP2N, FKBP12 degradation induced by SP3CHO and SP2CHOP is independent of FCS (Fig. 3e,



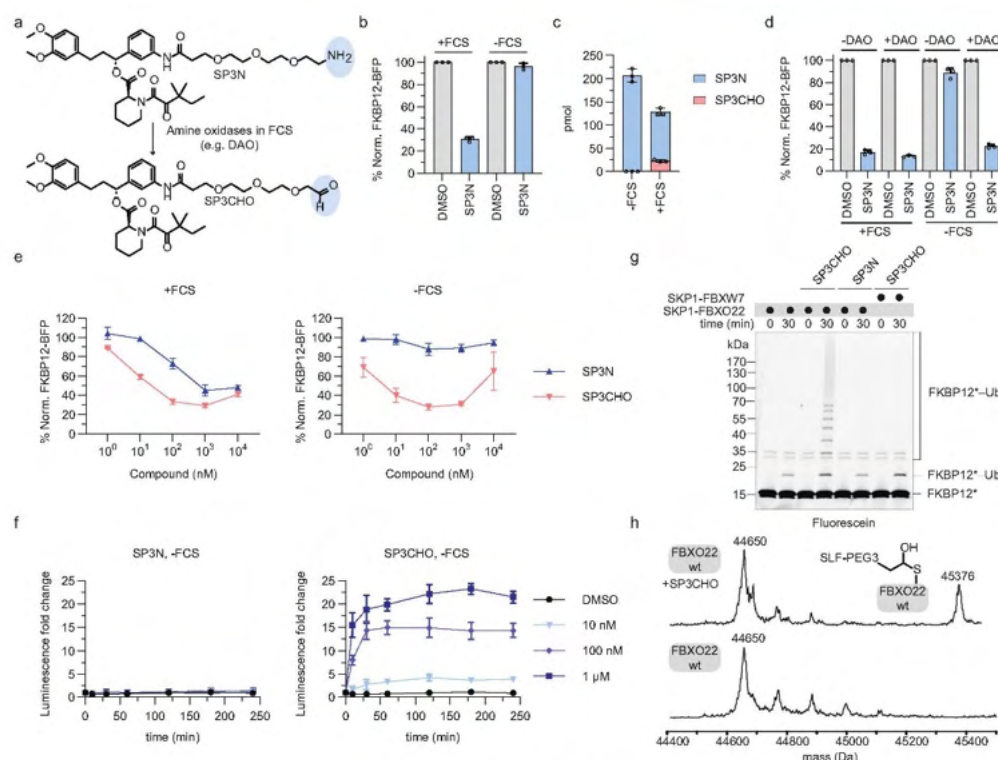


**Fig. 3 | SP3N is a precursor metabolized to an active aldehyde. a** Structures of SP3N and the SP3CHO metabolite, DAO diamine oxidase. **b** Flow-cytometry based degradation assay. KBM7 iCas9 FKBP12-BFP-P2A-mCherry reporter cells were treated with DMSO or 1  $\mu$ M SP3N in IMDM + 10% FCS or Opti-MEM + FCS for 8 h. **c** Quantification of SP3N and SP3CHO (pmol) using UPLC-MS/MS, in KBM7 iCas9 cells. 1  $\mu$ M SP3N was added in IMDM + 10% FCS or Opti-MEM + FCS and incubated at 37  $^{\circ}$ C for 6 h. Mean  $\pm$  s.d. of  $n = 3$  technical replicates. **d** Flow-cytometry based degradation assay with porcine diamine oxidase (DAO). 10  $\mu$ M of SP3N were incubated with 40  $\mu$ g DAO in PBS for 4 h. KBM7 iCas9 FKBP12-BFP-P2A-mCherry reporter cells were treated with the pre-incubated solution in Opti-MEM + 10% FCS or Opti-MEM + FCS, for 16 h. **e** Flow-cytometry based degradation assay in KBM7 iCas9 FKBP12-BFP-P2A-mCherry reporter cells in IMDM + 10% FCS or Opti-MEM + FCS treated with DMSO or the indicated concentrations of SP3N or SP3CHO for 6 h. **f** NanoBIT assay as described in Fig. 2e. Before treatment, the cells were washed

with PBS and the indicated concentrations of SP3N or SP3CHO were added to the cells in Opti-MEM + FCS. The luminescence was monitored after 10 min, 30 min and every hour up to 4 h post-treatment and normalized to timepoint 0. Mean  $\pm$  s.d. of  $n = 3$  technical replicates; representative plot of  $n = 3$  biological replicates. **g** In vitro ubiquitylation assay of fluorescently labeled FKBP12 with activated (i.e. neddylated) SCF<sup>FBXO22</sup> in the presence of 10  $\mu$ M SP3N or SP3CHO. The neddylated SCF<sup>FBXO22</sup> is used as negative control. Representative image of  $n = 2$  biological replicates.

**h** Intact mass spectrometry for the identification of FBXO22-SP3CHO complex formation. 20  $\mu$ M FBXO22-SKP1 complex were incubated with 100  $\mu$ M SP3CHO for 10 min and analyzed with LC-MS. The spectra of FBXO22 and FBXO22-SP3CHO are shown;  $n = 2$  biological replicates. Expected mass for FBXO22: 44652 Da and for FBXO22-SP3CHO adduct: 45374 Da. For the flow cytometry-based degradation assays (b, d, e), the BFP/mCherry ratio was normalized to DMSO and the data is the mean  $\pm$  s.d. of  $n = 3$  biological replicates.

Supplementary Fig. 3b). Interestingly, SP3CHO is slightly more potent and shows a more pronounced hook effect (a phenomenon typically observed with PROTACs) in the absence of FCS (Fig. 3e). UPLC-MS/MS based, targeted quantification of SP3CHO levels after short cellular treatment revealed significantly elevated levels of SP3CHO in cells treated in media lacking FCS as a plausible mechanism for this differential potency (Supplementary Fig. 3c). Moreover, as our data indicates that the aldehyde metabolite mediates the degradation, we sought to confirm that it also induces proximity between FBXO22 and FKBP12, independent of FCS availability. To this end, we employed the aforementioned NanoBIT<sup>®</sup> assay and monitored real-time complex formation. In line with our hypothesis, our findings revealed that SP3CHO induces dose-dependent ternary complex formation irrespective of FCS availability. In contrast, SP3N failed to induce

interactions in FCS-deprived media, further supporting that SP3CHO is the active SP3N metabolite (Fig. 3f, Supplementary Fig. 3d).

To reconstitute the proposed mechanism in vitro, we purified recombinantly expressed activated (i.e. neddylated) SCF<sup>FBXO22</sup> (Supplementary Fig. 3e), and FKBP12, and performed ubiquitylation assays with or without compound treatment. In support of a precursor mechanism of action, SP3N treatment was insufficient to induce poly-ubiquitylation of FKBP12. In contrast, SP3CHO treatment prompted clear poly-ubiquitylation of FKBP12 by SCF<sup>FBXO22</sup>, but not by an unrelated CRL E3 ligase (neddylated SCF<sup>FBXO22</sup>) (Fig. 3g). Similar results were observed with SP2C10p, which induced FKBP12 poly-ubiquitylation, while SP2N did not show any effects in vitro (Supplementary Fig. 3f). Given the electrophilic nature of SP3CHO and considering recent findings with the aforementioned NSD2 degrader UNC8732, we surmised that SP3CHO can form an adduct with FBXO22 via a covalent

and reversible hemithioacetal. Indeed, intact mass spectrometry clearly revealed a mass corresponding to the SP3CHO-adducted FBXO22 (Fig. 3h). Having established that SP3N covalently adducts FBXO22, and based on another recent report that established SCF<sup>FBXO22</sup> as a ligase that can be harnessed with a covalent, chloroacetamide containing PROTAC, we wanted to investigate if we could replace the aldehyde with alternative warheads and synthesized four additional electrophilic compounds, namely the SP3-chloroacetamide, the SP3-acrylamide and the respective SP2-based analogs<sup>37</sup>. Interestingly, none of these compounds exhibited robust FKBP12 degradation, indicating that these SLF-based aldehydes are favored over the other SLF-based electrophiles in inducing FBXO22-dependent protein degradation (Supplementary Fig. 3g).

### FBXO22 is recruited through its C326 for degradation

Given the reactivity of the active aldehyde species, we next wanted to assess a possible covalent engagement on FBXO22. To map the functionally required and covalently engaged cysteine residue in FBXO22, we mutated five cysteine residues in the C-terminal region of FBXO22 (amino acids 143–365) that has been reported to play a role in substrate binding<sup>38,39</sup>. To this end, we turned to genetic reconstitution experiments where we re-introduce FBXO22 cysteine mutants in FBXO22 knockout cells and assess their effect on SP3N-induced FKBP12 degradation utilizing the aforementioned FKBP12-BFP-P2A-mCherry stability reporter. SP3N- or SP3CHO-induced degradation was maintained by all FBXO22 mutations with the exception of C326A (Fig. 4a, b, Supplementary Fig. 4a, b). To rule out potential deleterious effects of the C326A mutation on FBXO22, we turned to Nano differential scanning fluorimetry (NanoDSF) which revealed thermal stability (Supplementary Fig. 4c). In addition, FBXO22 WT and C326A are similarly sensitive to pharmacologically induced auto-degradation via COP9 signalosome inhibition (Supplementary Fig. 4d), supporting the notion that the mutant incorporates into a functional SCF complex also in cells<sup>40–42</sup>. Further, an *in vitro* autoubiquitylation assay demonstrated comparable autoubiquitylation of recombinant FBXO22-WT and FBXO22-C326A variants, hence again suggesting intact SCF complex activity (Supplementary Fig. 4e). To orthogonally confirm the relevance of C326, we employed NanoBIT® assays with SmBIT-FBXO22-WT, SmBIT-FBXO22-C326A or SmBIT-FBXO22-C228A mutants. While SP3CHO induced comparable bioluminescence levels for FBXO22-WT and the C228A negative control mutant, no induction of bioluminescence and hence no evidence for ternary complex formation could be observed when assaying the C326A mutant (Fig. 4c, Supplementary Fig. 4f). Further corroborating that C326 is essential for the molecular recognition of SP3CHO, SCF<sup>FBXO22-C326A</sup> failed to induce ubiquitylation on FKBP12 in *in vitro* assays (Fig. 4d). Likewise, intact MS analysis of SKP1-FBXO22-C326A treated with SP3CHO revealed no evidence of adduct formation (Fig. 4e). To confirm the proteome-wide selective engagement by SP3CHO, we performed global reactive cysteine profiling in HEK293T cell lysates by TMT-ABPP<sup>43,44</sup>. This revealed that approximately 30% of FBXO22-C326 was engaged by SP3CHO. No other FBXO22 Cys residues were detected as engaging SP3CHO (Supplementary Fig. 4g, h, Supplementary Data 4). Notably, SP3CHO generally exhibited low reactivity with 5 other Cys (HDAC1-C100, GPX4-C102, TARSI-C254, PSMB1-C82;S9 and PPAT-C503). Taken together, our results reveal C326 as the site of covalent binding by SP3CHO that is functionally required for ternary complex formation, ubiquitylation and degradation.

### Alkylamine-based degraders functionally depend on FBXO22

To explore the potential generalizability of exploiting FBXO22 for targeted protein degradation, we extended our experiments to two recently reported primary alkylamine-tethered degraders targeting either NSD2 or XIAP, as well as a set of alkylamine-tethered analogues targeting BRD4 (Fig. 4f and Supplementary Fig. 5a)<sup>32–34</sup>. Supporting a

general role of FBXO22 in the mechanism of action of alkylamine-based degraders, no target degradation was observed in FBXO22 KO cells. In contrast, reconstitution with FBXO22-WT re-sensitized KO cells to target destabilization by the NSD2, XIAP and FKBP12 targeting degraders. Notably, reconstitution with FBXO22-C326A failed to re-establish target degradability, suggesting a shared functional dependency on this key residue. Together, these findings support the broader applicability of a TPD strategy whereby target-binding ligands can be equipped with flexible alkylamines to recruit the SCF<sup>FBXO22</sup> ligase for target ubiquitylation and ensuing degradation by the proteasome. Interestingly, a set of alkylamine-based analogues building off the BET-bromodomain inhibitor JQ1 did not degrade BRD4, a target that is frequently utilized as proof of concept for prototypical degraders that co-opt novel E3 ligases (Supplementary Fig. 5a). While immunoblot analysis of the BRD4 transcriptional target MYC implies cellular target engagement of this set of analogues, co-IP experiments reveal a lack of ternary complex formation as a likely reason for the observed lack of degradation (Supplementary Fig. 5 b, c). In sum, these data suggest that the concept of alkylamine-base degraders is generalizable yet will require optimization on a target-by-target level.

### Discussion

Here, we report the serendipitous identification of SP3N, a degrader of the prolyl isomerase FKBP12, which features a minimal design where the known FKBP12 ligand SLF is equipped with an alkylamine extension that conveys the observed degradation properties. Orthogonal mechanistic characterization via quantitative proteomics, functional genomics and biochemical reconstitutions led us to identify that SP3N-induced degradation is highly specific and depends on the recruitment of the SCF<sup>FBXO22</sup> ligase. Further, we employ metabolomics to reveal that SP3N is a precursor that is metabolically converted into an active aldehyde species (SP3CHO) via amine oxidases. Coupling targeted mutagenesis studies with genetic rescue experiments, we identify C326 in the C-terminal putative substrate binding domain of FBXO22 as critical for SP3N/SP3CHO-induced FKBP12 degradation. Further corroborating the critical role of C326, we observe that mutating C326 completely abrogates drug-induced proximity of FKBP12 and FBXO22 in intact cells. Likewise, recombinant FBXO22-C326A is incapable of inducing FKBP12 polyubiquitylation. Lastly, we could extend our findings around SP3N to two recently reported degraders of XIAP and NSD2 that feature a similar alkylamine design<sup>32–34</sup>. Akin to SP3N, both compounds require FBXO22 for target degradation and appear similarly dependent on C326 in this process. Of note, the NSD2-based degrader UNC8732 has also been reported to be subject to metabolization into an aldehyde species<sup>33</sup>. We thus surmise that this metabolic conversion of primary amine tethered precursors into reactive aldehyde species is a general phenomenon.

Expanding the reach of targeted protein degradation to additional E3 ligases has recently been a very active area of research. Fragment-based chemoproteomics as well as focused mechanism of action campaigns have unlocked several E3 ligases, including DCAF11, DCAF16, RNF4 or RNF114 for chemical exploration<sup>24–27,34,45</sup>. Nevertheless, less than 3% of the around 600 E3 ligases encoded in the human genome can be coopted with small-molecule ligands. Among the successfully liganded E3 ligases, a critical evaluation will be required to understand if the identified chemical matter can be progressed towards selective compounds that fulfill probe-like criteria<sup>46</sup>. Likewise, further research will be required to understand which of those E3 ligases provides a tangible differentiation from CRBN and VHL, the two E3 ligases that are harnessed by clinically approved or evaluated MGDs and PROTACs. Aside from potentially addressing and overcoming resistance mechanisms to CRBN- and VHL-based degraders<sup>16–19,47</sup>, or from expanding the toolbox of degron-tag approaches<sup>48–50</sup>, the disclosed mechanism of FBXO22 dependent,



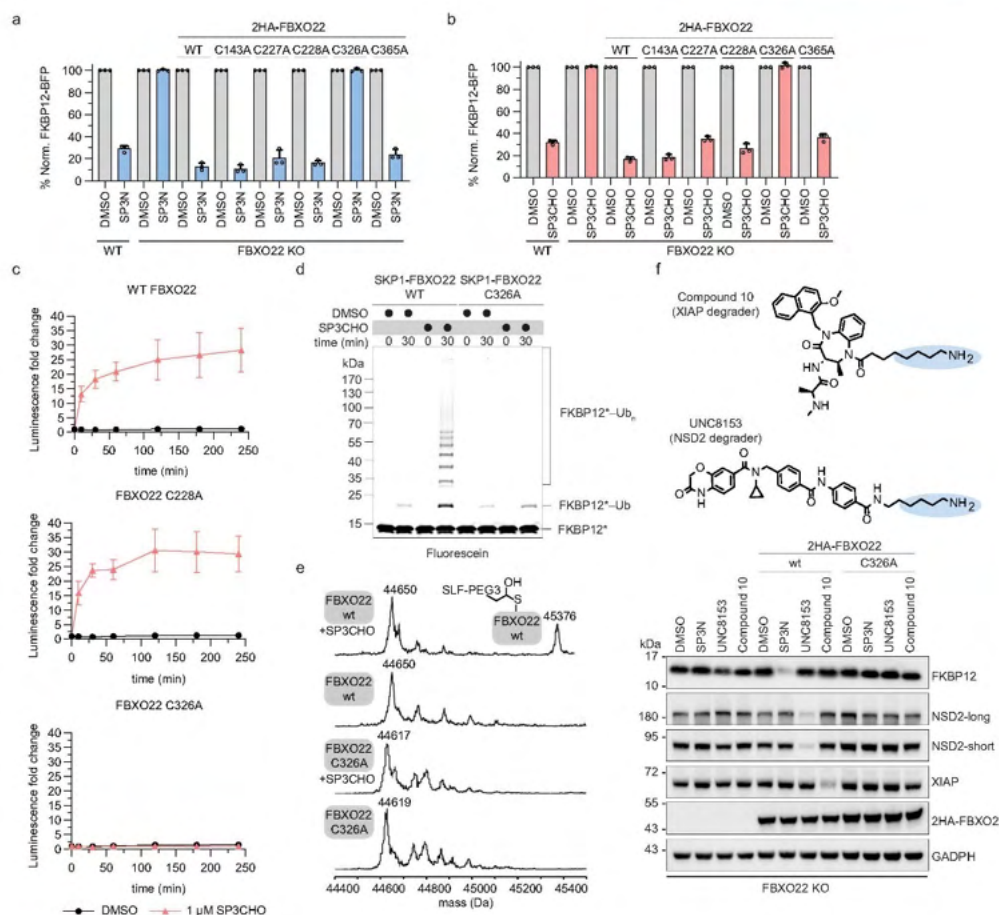


**Fig. 4 | FBXO22-C326 is crucial for the degradation induced by SP3N and other alkylamine-tethered degraders.** **a**, **b** Flow-cytometry based degradation assays in HEK293T FKBP12-BFP-P2A-mCherry single FBXO22 KO clone transfected with WT, C143A, C227A, C228A, C326A or C365A mutant 2HA-FBXO22 cDNAs. Cells were treated with DMSO or 1  $\mu$ M SP3N for 16 h (**a**) and with DMSO or 1  $\mu$ M SP3CHO for 8 h (**b**). Untransfected WT or FBXO22 KO cells were used as controls. The BFP/mCherry ratio was normalized to DMSO for each cell line. Mean  $\pm$  s.d. of  $n = 3$  biological replicates. **c** NanoBIT assay in HEK293T cells co-transfected with LgBIT-FKBP12 and SmBIT-FBXO22-WT, SmBIT-FBXO22-C228A or SmBIT-FBXO22-C326A and treated with DMSO or 1  $\mu$ M SP3CHO, in Opti-MEM + FCS. The luminescence was monitored after 10 min, 30 min and every hour up to 4 h post-treatment. Mean  $\pm$  s.d. of  $n = 3$  technical replicates; representative plot of  $n = 3$  biological replicates. **d** In vitro ubiquitylation assay of fluorescently labeled FKBP12 with SCF<sup>FBXO22</sup> WT

or SCF<sup>FBXO22-C326A</sup> in the presence of DMSO or 10  $\mu$ M SP3CHO. Representative image of  $n = 2$  biological replicates. **e** Intact mass spectrometry of FBXO22-WT versus FBXO22-C326A for SP3CHO binding. 20  $\mu$ M SKP1-FBXO22-WT or SKP1-FBXO22-C326A were incubated with 100  $\mu$ M SP3CHO for 10 min and analyzed with LC-MS. The spectra of SKP1-FBXO22-WT + SP3CHO or SKP1-FBXO22-C326A + SP3CHO are shown. Expected mass for FBXO22: 44652 Da. Expected mass for FBXO22-SP3CHO adduct: 45374 Da. Expected mass for FBXO22 C326A: 44619 Da. **f** Immunoblot of HEK293T FKBP12-BFP-P2A-mCherry FBXO22 KO untransfected cells or cells transfected with the 2HA-FBXO22-WT cDNA or 2HA-FBXO22-C326A cDNA followed by treatment with DMSO, 5  $\mu$ M SP3N, 5  $\mu$ M UNC8153 (NSD2 degrader) or 5  $\mu$ M Compound 10 (XIAP degrader) for 16 h. GAPDH is the loading control. Western blots are representative of  $n = 3$  biological replicates.

alkylamine-based degraders offers some points of differentiation that warrant further exploration.

First, FBXO22 has a well-established role in carcinogenesis and its expression is associated with poor survival in several cancer types<sup>31</sup>. While it is broadly expressed in most tissues, reports of increased levels of expression in certain cancer types, such as lung adenocarcinoma or ovarian cancers, might enable increased degradation efficiencies specifically in malignant cells, which could result in an

expanded therapeutic index<sup>32,33</sup>. This is further supported by TCGA data that indicates the elevated expression levels in tumor tissue as a differentiating characteristic compared to CRBN, the most frequently pursued E3 ligase for TPD applications (Supplementary Fig. 5d, e). Second, the required precursor conversion is another layer of tumor specificity that could be exploited. Certain cancer types such as colorectal cancer or hepatocellular carcinoma exhibit upregulation of specific amine oxidases, which could enable elevated rates of degrader

precursor conversion in tumors, even though general metabolic liabilities of primary amines would need to be considered<sup>54–56</sup>. Future studies should explore experimental approaches that better reflect the physiological context in which amine oxidases function. One potential avenue would be the use of ex vivo or in vivo models that better mimic the tumor microenvironment and allow for the assessment of tumor-restricted amine-to-aldehyde conversion and target degradation.

Our data, alongside the data reported in Nie et al. clearly highlight an essential functional role of the solvent-accessible Cys326 in the C-terminal domain of FBXO22<sup>33,57,58</sup>. However, future research including a full structural elucidation will be required to dissect the determinants of molecular recognition of the highly flexible alkylamine tail. Moreover, structural understanding will be key to empower rational ligand optimization. This is of particular interest in light of recent findings by Basu et al. highlighting that additional cysteine residues (C227, C228) of FBXO22 are in principle ligandable with chloroacetamide-based compounds<sup>37</sup>. In addition, a more granular understanding of the underpinning molecular recognition will be instrumental to explain limitations in the generalizability of the alkylamine degrader approach. For instance, while alkylamine-based degraders could be leveraged against FKBP12, NSD2, and XIAP, an informer set of alkylamines conjugated to the BET bromodomain ligand JQ1 failed to induce proximity and ensuing degradation of the BET protein BRD4, a target that is otherwise frequently utilized for degrader proof of concept studies.

In conclusion, data presented in this manuscript, together with corroborating evidence from other studies, highlight alkylamine conjugation as a strategy to develop small-molecule precursor degraders that mechanistically converge on harnessing the SCF<sup>FBXO22</sup> ligase and harbor the potential to be active against a broad spectrum of targets. As such, we expect the presented data to establish motivation for focused FBXO22 ligand discovery and degrader optimization efforts as well as for understanding a putative physiological relevance of reprogramming FBXO22.

## Methods

### Cell culture

KBM7 inducible Cas9 (iCas9) cells (gift from Johannes Zuber / IMP - Research Institute of Molecular Pathology) were cultured in IMDM (Gibco, 21980032) and 293T cells (ATCC, CRL-3216) or Lenti-X 293T (Clontech, 632180) in DMEM (Gibco, 41965062), both supplemented with 100 U ml<sup>-1</sup> penicillin/streptomycin (Sigma-Aldrich, P4333) and 10% fetal calf serum (FCS, Gibco, A5256701), unless specified otherwise. Cells were grown at 37 °C and 5% CO<sub>2</sub> humidified incubator.

### Plasmids/oligonucleotides

For the engineering of the FKBP12-BFP-P2A-mCherry reporter, FKBP12 (Twist Biosciences) was cloned into a pRRL lentiviral vector containing a 3xV5-mTagBFP coupled to mCherry with a P2A self-cleaving peptide for normalization. The BRD4short(s)-BFP-P2A-mCherry stability reporter used in this study has been previously published<sup>31,59</sup>. For the cloning of pLenti6.2-Nluc-3xFlag-FKBP12 or 2HA-FBXO22, 3xFlag-FKBP12-(wt or NLS) (Twist Biosciences) or FBXO22 with synonymous mutations in the PAM and seed sequences (Twist Biosciences) were cloned into the pLenti6.2-Nluc-cdb (Addgene, #87078) or the pLEX-2HA-P2A-puro, using Gateway™ (BP Clonase II, 11789020 and LR Clonase™ II, 11791100 both from Invitrogen) and according to the manufacturer's protocol. Cloning of the pBit2.1-SmBiT-FBXO22 and pBit1.1-N-LgBiT-FKBP12 was achieved by restriction enzyme-based cloning. Briefly, FBXO22 or FKBP12 were PCR amplified (Q5 DNA polymerase, NEB, B9027S) from the 2HA-FBXO22 or the pLenti6.2-Nluc-3xFlag-FKBP12 plasmids, respectively, using primers with appropriate restriction enzyme sites. The amplified FBXO22 or FKBP12 fragments were inserted in the restriction enzyme-digested pBit2.1-N-SmBiT or pBit1.1-N-LgBiT (Promega, N2014) vectors and ligated using

T4 DNA Ligase (NEB, M0202S) according to the manufacturer's protocol. For the cysteine-mutant 2HA-FBXO22 and SmBiT-FBXO22 plasmids, the 2HA-FBXO22-wt or SmBiT-FBXO22-wt plasmids were mutated using Q5 site-directed mutagenesis (New England Biolabs, E0552), according to the manufacturer's protocol and using oligonucleotides designed with NEBaseChanger (v2.4.2). All plasmids and oligonucleotides/primers used in this study are shown in Supplementary Tables 1 and 2, respectively, and the UPS-focused sgRNA library used for the FACS-based CRISPR/Cas9 stability screen is shown in Supplementary Data 2.

### Compounds

The inhibitor carfilzomib (Cay17554) is from Biomol and JQ1 (1268524-70-4) is from AmBeed. The inhibitors MLN4924 (HY-70062) and TAK243 (HY-100487) and the degraders dFKBP1 (HY-103634), Compound 10 (XIAP degrader-1, HY-115865) and dBet6 (HY-112588) were all purchased from MedChemExpress.

### Virus production and transductions

Lenti-X 293T cells at 70–90% confluency were transfected with the desired lentiviral plasmids and the packaging plasmids (pCMV8.74 helper, Addgene #22036 and pMD2.G envelope, Addgene #12259) using polyethylenimine (PEI MAX® MW 40,000, Polysciences, 24765). The virus was collected and clarified using 0.45 µm Whatman Puradisc Syringe Filter (cytiva, WH6756-2504). Different dilutions of viral suspension were added to the cells and the cell/virus suspension was centrifuged at 900 g for 45 min and 33 °C.

### Clonal FBXO22 knock-out cell line

To generate clonal FBXO22 knock-out cell line, HEK293T FKBP12-BFP-P2A-mCherry cells were transduced with plasmids expressing the sgRNA 'GATCCAGGTTACGCTCCGAT' targeting FBXO22. After G418 (Sigma-Aldrich, A1720) selection, the cells were transfected with pSpCas9(BB)-2A-Puro (PX459) v2.0 (Addgene, #62988) plasmid using PEI. 48 h post-transfection, single clones were seeded in 96 well plates using CytoFLEX LX sorter (Beckman Coulter) and grown for 2 weeks at 37 °C and 5% CO<sub>2</sub> humidified incubator. Several single clones were screened for FBXO22 protein levels using western blot assay and validated with functional rescue assays with the SP3N degrader.

### Flow-cytometry-based degradation assays

KBM7 iCas9 or HEK293T cells expressing FKBP12-BFP-P2A-mCherry reporter or BRD4short-BFP-P2A-mCherry reporter were seeded in 24 well plates at seeding densities of 0.5 or 0.25 × 10<sup>6</sup> cells ml<sup>-1</sup>, respectively. The working dilutions of compounds were prepared freshly in media, using 1000x stock solutions in DMSO (Sigma-Aldrich, D1435). For competition experiments the cells were pre-treated with 1 µM Carfilzomib, 1 µM MLN4924 or 500 nM TAK243 for 1 h before the addition of SP3N or co-treated with different concentrations of SLF and SP3N. Post-treatment, cells were collected into Falcon® 5 ml Round Bottom Polystyrene Test Tubes (Corning, 352052) and directly measured with BD LSRFortessa™ Cell Analyzer (BD Biosciences).

### Western blot analysis

Cells, post-treatment with the compounds described in the figure legends, were collected in ice-cold Dulbecco's phosphate-buffered saline (PBS, Gibco, 14190144), washed 2x with PBS and lysed with RIPA buffer (150 mM NaCl, 1% TritonX-100, 0.5% Sodium deoxycholate, 0.1% Sodium dodecyl sulfate, 50 mM Tris pH 8) freshly supplemented with benzonase Nuclease (Merck Millipore, 70746) and Halt™ Protease Inhibitor Cocktail, EDTA-Free (100X) (Thermo Fisher Scientific, 78425). The protein concentration was determined using the Pierce™ BCA Protein Assay (Thermo Fisher Scientific, 23225) and 20 µg of lysate with 4X Bolt™ LDS Sample Buffer (Thermo Fisher Scientific, B0007) supplemented with 10% 2-Mercaptoethanol (Sigma-Aldrich, M3148)



was loaded per lane of NuPAGE 4–12% bis-tris gels (Invitrogen, NP0329PK2). Proteins were transferred to nitrocellulose membranes (Cytiva, 10600002), blocked at room temperature (RT) with 5% dry non-fat milk in Tris-buffered saline-Tween-20 (TBS-T, 50 mM Tris-Cl, pH 7.5, 150 mM NaCl, 0.1% Tween-20) and incubated with primary antibodies overnight at 4 °C. The following day, the membranes were incubated with HRP-conjugated secondary antibodies for 1 h at RT. The membranes were imaged with ChemiDoc™ Touch Imaging System-system (Bio-Rad), using ECL (Amersham, RPN2106). Primary antibodies used: anti- $\alpha$ Tubulin DM1A (T9026, Sigma-Aldrich, 1:5000), anti-NSD2 29D1 (Ab-75357, Abcam, 1:1000), anti-FKBP12 H-5 (sc-133067, 1:1000), anti-FBXO22 FF-7 (sc-100736, 1:400), anti-XIAP E-2 (sc-55551, 1:200) and anti-GADPH O411 (sc-47724, 1:5000) all purchased from SantaCruz Biotechnology, anti-cMYC D84C12 (#5605, 1:1000), anti-HA-Tag C29F4 (#3724, 1:1000), anti-BRD4 E2A7X (#13440, 1:2000), anti-CRBN D8H3S (#71810, 1:1000) and anti-V5 D3H8Q (#13202, 1:1000) from Cell Signaling Technology, anti-Flag M2 (F1804, Sigma-Aldrich, 1:1000) and anti-BRD3 (#A302-368A, Bethyl Laboratories, 1:1000). Secondary antibodies used: anti-rabbit IgG, HRP-linked (#7074, 1:10000) and anti-mouse IgG, HRP-linked (#7076, 1:10000) both from Cell Signaling Technology.

#### Co-immunoprecipitation of FBXO22-FKBP12, FBXO22-BRD4s or CRBN-BRD4s

HEK293T or HEK393T Nluc-3xFlag-FKBP12 cells were seeded in 10 cm dishes ( $6 \times 10^6$  cells/dish) and incubated overnight at 37 °C to attach. The following day, each 10 cm dish was transiently transfected with 3  $\mu$ g of the appropriate constructs as specified in the figure legends using PEI for 18 h, before being expanded into  $2 \times 10$  cm dishes. 48 h post-transfection cells were pre-treated with DMSO or carfilzomib for 1 h and then co-treated for 4 h with the appropriate compounds specified in the figure legends. Post-treatment, cells were collected and washed 3x with ice-cold PBS, and lysed in 250  $\mu$ l of lysis buffer (50 mM Tris-HCl pH 7.4, 150 mM NaCl, 0.1% Triton-X-100, 1 mM EDTA, 5 mM MgCl<sub>2</sub>, 5% glycerol) freshly supplemented with the 100X Halt™ Protease Inhibitor Cocktail for 20 min on ice. Lysates were cleared at 20,000 rcf spinning down for 20 min and the lysate was normalized with BCA. 200  $\mu$ g of protein/condition were boiled with 4x LDS at 95 °C for 5 min (Input fraction). In the meantime, 20  $\mu$ l of Pierce Anti-HA Magnetic Beads (Thermo Fisher Scientific, 88836) per condition were washed with TBS. 1 mg of lysate, adjusted to 200  $\mu$ l with lysis buffer was incubated with 20  $\mu$ l beads overnight at 4 °C on rotating wheel. The following day, the beads were separated from the flow-through using a magnetic rack, washed 3x with TBS-T and eluted in 2X Bolt™ LDS Sample Buffer by boiling at 95 °C for 10 min. Western-blot analysis was performed as described above, with 20  $\mu$ g input and 10% of the IP fraction loaded to 4–12% Bis-Tris gels.

#### NanoLuc® Binary Technology (NanoBit) complementation assay

$8 \times 10^5$  HEK293T cells/well were seeded in 6-well plates overnight to attach before being transfected with 500 ng of each plasmid SmBit-FBXO22 and IgBit-FKBP12, or SmBit FBXO22 C228A/C326A and IgBit-FKBP12 using PEI. The cells were incubated overnight and then seeded into 96-well flat, black bottom plates (Costar) at a density of  $0.5 \times 10^5$ /well. The next day, media was removed, cells were gently washed twice with PBS and fresh Opti-MEM I Reduced Serum Medium (Gibco, 31985062) with or without FCS supplemented with 1  $\mu$ M carfilzomib and 1:20 Vivazine™ (Promega, N2581) was added onto the cells and let to calibrate for 1.5–2 h. Before treating with the desired compounds, baseline luminescence was measured at timepoint 0, using VICTOR™ Multilabel Plate Reader (Perkin Elmer). After treatment, the luminescence was measured with 2 s interval at timepoints indicated in the figure legends.

#### Diamine oxidase treatments

Diamine Oxidase from porcine kidney (Sigma-Aldrich, D7876) was prepared fresh in PBS at a concentration of 10 mg ml<sup>-1</sup>. For the time/dose-dependent SP3CHO quantification experiments in PBS, 10  $\mu$ M SP3N were incubated with 40  $\mu$ g diluted DAO in final volume of 100  $\mu$ l PBS, at 37 °C and 5% CO<sub>2</sub> humidified incubator. The metabolites were extracted by adding 200  $\mu$ l MeOH and subjected to UPLC-MS/MS analysis. For the FACS-based degradation experiments with cells, 10  $\mu$ M SP3N were treated with DAO as above, for 4 h at 37 °C and 5% CO<sub>2</sub> humidified incubator. The DAO-pretreated SP3N solution was added (1:10) on  $0.5 \times 10^6$  KBM7 iCas9 cells with the FKBP12-BFP-P2A-mCherry reporter that were washed 3x with PBS to remove FCS and resuspended in Opti-MEM -FCS or Opti-MEM supplemented with 10% FCS. Degradation was measured 16 h post-treatment using FACS.

#### Design and construction of a ubiquitin-focused sgRNA library

A custom-made focused sgRNA library targeting 1301 ubiquitin-associated human genes with 6 sgRNAs per gene was designed based on the VBC score<sup>60</sup>. Predicted 20mer sgRNA sequences containing a G in the first three 5'-positions were trimmed to the first G at the 5'-end, while others were extended by a 5'-G, resulting in final sgRNA sequences of 18–21 nt in length. The sequences were synthesized as DNA oligo pool (Twist Bioscience) with overhangs and primer binding sites for cloning as previously described<sup>60</sup> and cloned into pLentiV1-PBS69-U6-sgRNA-IT-EF1as-Thy1.1-P2A-Neo. To this end, the DNA oligo pool was amplified using Q5 High-Fidelity DNA Polymerase (New England Biolabs, M0491) in 48 parallel 50  $\mu$ l PCR reactions, each containing 10  $\mu$ l 5X Q5 Reaction Buffer, 1  $\mu$ l dNTP (10 mM each), 2.5  $\mu$ l forward primer (10  $\mu$ M), 2.5  $\mu$ l reverse primer (10  $\mu$ M), 1 ng oligo pool template, and 0.5  $\mu$ l Q5 High-Fidelity Polymerase, using the following thermocycler conditions: 98 °C for 30 s; 14 cycles of 98 °C for 10 s, 70 °C for 30 s; final extension at 72 °C for 2 min. The generated amplicons were purified using the QIAquick PCR Purification kit (Qiagen, 28104) according to the manufacturer's recommendations and used in 10 parallel Golden Gate Assembly reactions, each containing 5 ng purified sgRNA amplicon, 200 ng BsmBI (New England Biolabs, R0739) pre-cut and column purified pLentiV1-PBS69-U6-sgRNA-IT-EF1as-Thy1.1-P2A-Neo vector, 1  $\mu$ l FastDigest Esp3I (Thermo Fisher Scientific, FD0454), 1  $\mu$ l T7 Ligase (New England Biolabs, M0318), 2  $\mu$ l FastDigest Buffer (Thermo Fisher Scientific, B64), 1 mM DTT (Roche, 1019777001) and 1 mM ATP (Thermo Fisher Scientific, R0441), all to 20  $\mu$ l final reaction volume with H<sub>2</sub>O and incubated in a thermocycler with the following conditions: 37 °C for 5 min and 23 °C for 5 min for 40 cycles. Pooled ligations were incubated with 2  $\mu$ l BsmBI and incubated 2 h at 55 °C and subsequently stored at 4 °C. Pooled ligations were purified by Phenol extraction followed by EtOH precipitation and electroporation into MegaX DH10B T1 (Invitrogen, C640003) with a BioRad Pulser II (Bio-Rad) as recommended by the manufacturer. After 1 h recovery at 37 °C, a dilution series of bacteria was plated to ensure a minimum representation of at least 5000 bacterial colonies per sgRNA. The bacteria were grown at 32 °C on LB agar containing 100  $\mu$ g ml<sup>-1</sup> ampicillin for 16 h and the following day, colonies were scraped, recovered in LB broth by shaking at 220 RPM under antibiotic selection at 32 °C for 5 h. Plasmid DNA was extracted using the NucleoBond Midi prep kit (Macherey-Nagel, REF740410.50).

#### FACS-based CRISPR/Cas9 knock-out FKBP12 stability screen

The FACS-based CRISPR/Cas9 FKBP12-BFP stability screen was performed as previously described<sup>31</sup>. Briefly, the lentiviral library containing the UPS-focused sgRNA library (Supplementary Data 2) was generated as described above and used to transduce KBM7 doxycyclin (DOX)-inducibleCas9 (iCas9) FKBP12-BFP-P2A-mCherry cells at a multiplicity of infection (MOI) of 0.1 and 1000x library representation. 10 days post-selection with G418 (1 mg ml<sup>-1</sup>),  $50 \times 10^6$  cells were DOX-induced (0.4  $\mu$ g ml<sup>-1</sup>, PanReac AppliChem, A2951) for 3 days and



treated with DMSO, 100 nM dFKBP1 or 250 nM SP3N (1000x stocks in DMSO) for 16 h in 2 biological replicates.

Post-treatment, cells were incubated with anti-CD90.1/Thy1.1-APC (BioLegend, 202526, 1:400), Zombie NIR™ Fixable Viability Dye (BioLegend, 423105, 1:1000) and Human TruStain FcX™ Fc Receptor Blocking Solution (BioLegend, 422301, 1:400), for 10 min at 4 °C, fixed with BD Fixation buffer 4% (Thermo Scientific™ Pierce™, BD 554655) for 45 min at 4 °C, protected from light and stored in PBS + 5% FCS + 1 mM EDTA overnight at 4 °C. The next day, cells were sorted on a BD FACSAria™ Fusion (BD Biosciences) using a 100 µm nozzle. The aggregates were excluded based on the forward scatter and side scatter channels and the live cells (Zombie NIR) were gated for Cas9<sup>+</sup>Thy1.1-APC<sup>+</sup> (Supplementary Fig. 6a). In this population, the fractions FKBP12<sup>high</sup> (5–8%), FKBP12<sup>mid</sup> (30–35%) and FKBP12<sup>low</sup> (5–8%) were sorted based on the FKBP12-BFP-mCherry expression levels, at a library representation of at least 1200x.

### Library preparation

Next-generation sequencing (NGS) library preparation of sorted cell fractions was performed as previously described<sup>34,59</sup>. Briefly, the sorted fractions were lysed in lysis buffer (10 mM Tris-HCl, 150 mM NaCl, 10 mM EDTA, 0.1% SDS), supplemented with proteinase K (1:100, New England Biolabs, P81075) and SDS (1:100) and incubated overnight at 55 °C. After treatment with DNase-free RNase digest (Thermo Fisher Scientific, EN0531), the gDNA was extracted using 2 rounds of extraction with phenol (Sigma-Aldrich, P4557) followed by precipitation with isopropanol (Sigma-Aldrich, I9516) overnight at –20 °C.

To generate barcoded NGS libraries a two-step PCR protocol and AmpliTaq Gold DNA polymerase (Thermo Fischer Scientific, 4311806) were used, with the first PCR step to introduce unique barcodes to each sample and the second PCR step to introduce the standard Illumina adapters. Mag-Bind® TotalPure NGS beads (Omega BIO-TEK, M1378) were used to purify the amplified DNA, which was pooled and sequenced on a HiSeq 3500 platform (Illumina).

### Screen analysis

The screen analysis was performed using the crispr-process-nf Nextflow workflow, from <https://zenodo.org/records/11445611> and the crispr-mageck-nf Nextflow workflow from <https://zenodo.org/records/11445588> as previously described<sup>34</sup>. The median normalized read counts calculated with MAGeCK (0.5.9)<sup>61</sup> were used to compare the FKBP12<sup>high</sup> or FKBP12<sup>low</sup> versus the respective FKBP12<sup>mid</sup>, per treatment.

### Analysis of *FBXO22* and *CRBN* expression in cancer versus healthy tissues

For the comparison of the expression profiles of *FBXO22* and *CRBN* in healthy and cancer tissues, we extracted mRNA expression data from the Gene Expression Profiling Interactive Analysis, GEPIA2<sup>62</sup>, an online platform for integrating RNA sequencing data from The Cancer Genome Atlas (TCGA, <https://www.cancer.gov/tcga>) and the Genotype-Tissue Expression project of normal tissues (GTEx, <https://gtexportal.org/home/>).

### Sample preparation and TMT-labeling

Frozen HEK293T pellets were lysed using 8 M urea and 200 mM EPPS at pH 8.5 with protease inhibitors. Samples were then sonicated using a probe sonicator (twenty 0.5-s pulses at level 3). The total amount of protein per sample was determined using a BCA assay. A total of 50 µg of protein was aliquoted for each condition. Protein extracts were reduced using 5-Tris (2-carboxyethyl) phosphine hydrochloride (TCEP) for 15 min at RT. Samples were then treated with 10 mM iodoacetamide for 30 min in the dark at RT followed by precipitation using chloroform/methanol as previously described<sup>63</sup>.

After precipitation, samples were digested overnight using LysC and trypsin (1:100 enzyme/protein ratio) at 37 °C using a ThermoMixer set to 1,200 rpm. Following overnight digestion, peptides were labeled with TMTpro 16-plex reagents at a 1:2 ratio by mass (peptides/TMT reagents) for 1 h with constant shaking at 1,200 rpm. Excess TMT reagent was quenched using hydroxylamine (0.3% final concentration) for 15 min at RT. Next, samples were mixed 1:1 across all TMT channels and the pooled sample was fully dried in a Speedvac.

### Basic pH reversed-phase fractionation of TMT-labeled peptides

A 100-mg Sep-Pak solid-phase extraction cartridge was used to desalt the dried, pooled peptide sample, as previously described<sup>63</sup>. The desalted peptide sample was dried in the Speedvac, resuspended (10 mM ammonium bicarbonate, 5% acetonitrile, pH 8.0 buffer) and fractionated into a 96-deep-well plate with basic pH reversed-phase HPLC using an Agilent 300 extend C18 column, and a 50 min linear gradient in 13–43% buffer (10 mM ammonium bicarbonate, 90% acetonitrile, pH 8.0) at a flow rate of 0.250 ml min<sup>–1</sup>. The fractionated peptide mixture was combined into 24 fractions as previously described, and 12 non-adjacent fractions were desalted using StageTips<sup>63</sup>. 40% of the sample (resuspended in 10 µl of 5% acetonitrile 5% FA) was injected for analysis on an Orbitrap Lumos utilizing a high-resolution MS2-based method.

### Liquid chromatography and tandem mass spectrometry

For the mass spectrometry data collection, Orbitrap Fusion Lumos instruments coupled to a Proxeon NanoLC-1200 UHPLC were used. Peptide separation was achieved with a capillary column (35 cm long, 100 µm diameter) packed with Accucore 150 resin (2.6 µm, 150 Å; ThermoFisher Scientific), at a flow rate of 425 nL min<sup>–1</sup>. The MS1 spectrum was acquired (Orbitrap analysis, resolution 60,000, 350–1350 Th, automatic gain control (AGC) target 100%, maximum injection time 118 ms), for ~90 min per fraction, followed by the high-resolution MS2 stage consisting of fragmentation by higher energy collisional dissociation (HCD, normalized collision energy 35%) and analysis using the Orbitrap (AGC 200%, maximum injection time 120 ms, isolation window 0.6 Th, resolution 50,000). Data acquisition was performed using the FAIMSpro with the following parameters: dispersion voltage (DV): 5,000 V; compensation voltages (CVs): –40V, –60V, and –80V; TopSpeed parameter: 1 sec per CV.

### Mass spectrometry data analysis

For data searches the open-source Comet algorithm (release 2019010), following a previously described pipeline, and a customized FASTA-formatted database incorporating common contaminants and reversed sequences (Uniprot Human, 2021), were used<sup>64–67</sup>. The ensuing parameters were employed: 50 PPM precursor tolerance, fully tryptic peptides, fragment ion tolerance of 0.02 Da, a static modification by TMTPro16 (+304.2071 Da) on lysine and peptide N-termini, carbamidomethylation of cysteine residues (+57.0214 Da) included as static modification and oxidation of methionine residues (+15.9949 Da) included as a variable modification. To achieve a false discovery rate (FDR) of <1%, the peptide spectral matches were filtered using linear discriminant analysis with a target-decoy strategy. Further filtration ensured a final protein-level FDR of 1% at the dataset level, and proteins were grouped. Reporter ion intensities were adjusted to rectify impurities during the synthesis of different TMT reagents in alignment with the specifications of the manufacturer. Each MS2 spectrum required a total sum signal-to-noise (S/N) of all reporter ions of 160 for quantification. The S/N measurements of peptides corresponding to proteins were summed and normalized to ensure equal loading across all channels. Finally, protein abundance measurements were scaled to achieve a summed signal-to-noise for each protein across all channels equaled 100 (relative abundance measurement).



### In-lysate reactive cysteine profiling

The streamlined reactive cysteine profiling was performed as described in previous work<sup>43,44</sup>. Briefly HEK293T cells were grown in DMEM (Corning) supplemented with 10% FBS and 1% Penicillin/Streptomycin to near confluent, collected, washed twice with cold PBS and were resuspended with lysis buffer (PBS, pH 7.4, 0.1% NP-40) and sequentially homogenized by syringe equipped with 21-gauge needle and probe sonicator (5 min, 3-s on, 5-s off, 50% amp) on ice. Soluble native proteome was collected after centrifugation at 1400 g for 5 min and protein concentration was measured by BCA assay.

To profile reactive cysteine, 15  $\mu$ L lysate (2  $\mu$ g/ $\mu$ L), containing 30  $\mu$ g HEK293T native proteome with spike-in of 0.15  $\mu$ g recombinant FBXO22-SKP1, was loaded into 96-well plate. 5  $\mu$ L of compound solution in lysis buffer was added to the plate for final concentrations as described in figure legend and incubated for 1 h at RT. 5  $\mu$ L of DBIA solution in lysis buffer was added to a concentration of 500  $\mu$ M and incubated in the dark for 1 h at RT. 3  $\mu$ L SP3 beads (1:1 mixture of hydrophobic and hydrophilic type, 50 mg mL<sup>-1</sup>, Cytiva) and 30  $\mu$ L -98% ethanol supplemented with 20 mM DTT were added to the plate and incubated for 15 min with mild shaking. Beads were washed once with 200  $\mu$ L 80% ethanol and resuspended in 25  $\mu$ L lysis buffer supplemented with 20 mM IAA and incubated in the dark for 30 min with vigorous shaking. 50  $\mu$ L -98% ethanol supplemented with 20 mM DTT were added to the mixture followed by beads-based clean-up and 2x washes using 80% ethanol. 30  $\mu$ L 200 mM EPPS buffer (pH 8.5) containing 0.3  $\mu$ g Lys-C were added to the remaining beads. After 3 h incubation at RT, 5  $\mu$ L EPPS buffer containing 0.3  $\mu$ g trypsin was added and incubated with beads at 37 °C overnight. To the mixture of digested peptides and beads, 9  $\mu$ L acetonitrile and 6  $\mu$ L TMT (10  $\mu$ g/ $\mu$ L) reagent were sequentially added, followed by gentle mixing at RT for 60 min. The reaction was quenched by adding 7  $\mu$ L 5% hydroxylamine and all TMT-labeled samples were combined, dried using a SpeedVac and then desalted using a 100-mg Sep-Pak column.

The desalted TMT-labeled peptides were resuspended in 460  $\mu$ L of 100 mM HEPES buffer (pH 7.4), 80  $\mu$ L Pierce™ High Capacity Streptavidin Agarose (Thermo Fisher Scientific, 20359) were added and the mixture was incubated at RT for 3 h. The resulting mixture was then loaded on a Ultrafree-MC centrifugal filter (hydrophilic PTFE, 0.22  $\mu$ m pore size) and centrifuged at 1000 g for 30 seconds. Beads were washed sequentially with 300  $\mu$ L 100 mM HEPES (pH 7.4) with 0.05% NP-40 twice, 350  $\mu$ L 100 mM HEPES (pH 7.4) three times and 400  $\mu$ L H<sub>2</sub>O once. Peptides were eluted sequentially by 1) elution buffer (80% acetonitrile, 0.1% formic acid) with 20-min incubation at RT, 2) elution buffer with 20-min incubation; 3) elution buffer with 10-min incubation at 72 °C. The combined eluent was dried in a SpeedVac and desalted via StageTip prior to LC-FAIMS-MS/MS analysis.

### LC-FAIMS-MS/MS analysis

Enriched cysteines resuspended in 5% ACN and 5% FA were separated on a capillary column (100  $\mu$ m diameter, packed with 30 cm of Accucore 150 resin), using a 180-min method on a Proxeon NanoLC-1200 UPLC system. Data collection was performed using a high-resolution MS/MS method on an Orbitrap Eclipse mass spectrometer connected to a FAIMS Pro. A 2-shots analysis workflow was followed using a set of three FAIMS compensation voltages (CVs): 1) -60V, -45V and -35V and 2) -70V, -55V and -30V. MS1 scans were collected in the Orbitrap (resolution setting of 60 K, mass range of 400–1600  $m/z$ , AGC at 100%, maximum injection time of 50 ms). Data-dependent MS2 scans were acquired in Top Speed mode (cycle time of 1 s, HCD with collision energy of 36) and were collected in the Orbitrap (resolution of 50 K, fixed scan range of 110–2000  $m/z$ , and 500% AGC with maximum injection time of 86 ms). A dynamic exclusion of 120 s with a mass tolerance of  $\pm$ 10 p.p.m was chosen. The flowthrough was separated using a 60-min method and analyzed by FAIMS-MS/MS in data-dependent analysis in similar setting as analyzing cysteine samples.

### Data analysis for cysteine identification, localization, and quantification

A workflow similar to the mass spectrometry data analysis above was followed. The raw files were searched using the Comet search engine (ver. 2019.01.5)<sup>68</sup> with the Uniprot human proteome database (downloaded 11/24/2021) with contaminants and reverse decoy sequences appended. The following parameters were used: precursor error tolerance: 50 p.p.m., fragment error tolerance: 0.9 Da, static modifications: Cys carboxyamidomethylation (+57.0215) and TMTpro (+304.2071) on Lys side chains and peptide N-termini, variable modifications: methionine oxidation (+15.9949) and DBIA-modification on cysteine residues (+239.1628). Peptide spectral matches were filtered to a peptide FDR of <1%<sup>64,65</sup>, and further filtered to obtain a 1% protein FDR at the entire dataset level<sup>69</sup>. Cysteine-modified peptides were filtered for site localization using the AScorePro algorithm with a cutoff of 13 ( $P < 0.05$ ) as previously described<sup>66,70</sup>. Only unique peptides and cysteine sites were summarized from all PSMs and reported. To quantify TMT reporters in each MS2 spectrum, a total sum signal-to-noise ratio of all reporter ions totaling 180 (for TMTPro 18-plex) was required with <3 missing values. To address variations in loading, quantitative values were normalized to ensure an equal sum of signal for all proteins across each channel.

### Protein expression and purification

All proteins were of human origin. Ubiquitin was expressed tag-less in BL21(DE3) RIL *E. coli* cells. UBA1 was expressed as a GST-TEV fusion in *Spodoptera frugiperda* cells. Following glutathione-affinity purification and TEV protease cleavage the protein was further purified using ion exchange and size exclusion chromatography. UBE2L3, UBE2R2 and ARIH1 were expressed as GST-TEV fusions in BL21(DE3) RIL. Following glutathione-affinity purification and TEV protease cleavage the protein was further purified using ion exchange and size exclusion chromatography. CUL1 and GST-TEV-RBX1 were co-expressed in *Spodoptera frugiperda* cells using two baculoviruses. Following glutathione-affinity purification and TEV protease cleavage the protein was further purified using ion exchange and size exclusion chromatography. CUL1-RBX1 complex was neddylated using previously described procedures<sup>71</sup>. FBXO22 and SKP1 were cloned into a bicistronic pAcBacDual-based vector, as follows. FBXO22 was cloned downstream of Strep-tag II-TEV under control of the polyhedron promoter. SKP1 was placed downstream of the p10 promoter. SKP1-Fbox protein complexes were expressed in *Spodoptera frugiperda* cells. Following Strep-tag II affinity purification, Strep-tag II was removed by treatment with TEV-protease at 4 °C. The protein was further purified by ion exchange and size exclusion chromatography in 25 mM HEPES, 150 mM NaCl, 2 mM DTT, pH 7.5. The C326A mutant of FBXO22 was prepared by Quikchange (Agilent, 200513). FKBP12 was cloned downstream of GST-TEV into pGEX with a Gly-Ser motif at the TEV-cleavage site. The Gly-Ser motif was used as a handle for labeling of FKBP12 with a fluorescent peptide by sortase-mediated transpeptidation<sup>72</sup>. The protein was expressed in BL21 (DE3) RIL *E. coli*. Following glutathione affinity purification and TEV-mediated cleavage, FKBP12 was further purified using size exclusion chromatography.

### Peptides

Peptide was prepared by the Max Planck Institute of Biochemistry Core Facility (>90% purity) and used as received. The peptide to fluorescently label FKBP12 had the following sequence: Carboxyfluorescein-GSGGLPETGG.

### Fluorescent labeling of FKBP12

FKBP12 (100  $\mu$ M) was mixed with fluorescent peptide (200  $\mu$ M) in 50 mM Tris, 150 mM NaCl, 1 mM TCEP, 10 mM Ca(OAc)<sub>2</sub>, pH 7.5. SrtA 4 M (10  $\mu$ M) was added and the reaction was incubated for 5 h at 4 °C. The reaction product was purified by size exclusion chromatography.



**Multiturnover ubiquitylation assay**

Fluorescent-FKBP12 (0.5  $\mu$ M), CUL1-NEDD8-RBX1 (0.5  $\mu$ M), FBXO22-SKP1 (0.5  $\mu$ M), ARIH1 (0.4  $\mu$ M), UBE2L3 (2.0  $\mu$ M) and UBE2R2 (2.0  $\mu$ M) were mixed with buffer (50 mM HEPES, 100 mM NaCl, 7.5 mM  $MgCl_2$ , 5 mM ATP, 0.5 mg ml<sup>-1</sup> BSA, pH 7.5) and either DMSO or compounds (10  $\mu$ M). The reaction was initiated by the addition of UBA1 (0.1  $\mu$ M). The reaction was allowed to proceed at RT and time points were removed at 0 and 30 min, quenched by mixing with 3x SDS-PAGE buffer (150 mM Tris-HCl, 20 vol% glycerol, 30 mM EDTA, 4% SDS and 4 vol%  $\beta$ -mercaptoethanol). Time points were resolved on hand-cast 4–22% SDS-PAGE gels. Gels were visualized on a Typhoon 9410 Imager (Cytiva).

**Pulse-chase autoubiquitylation of FBXO22**

UBE2L3 (10  $\mu$ M) was charged with fluorescent-ubiquitin (15  $\mu$ M) by UBA1 (0.4  $\mu$ M) in 25 mM HEPES, 100 mM NaCl, pH 7.5 in the presence of  $MgCl_2$  (5 mM) and ATP (1 mM) at RT. The charging reaction was allowed to proceed for 15 min before quenching with aprotinase (8 U ml<sup>-1</sup>) for 5 min at 4 °C. UBE2L3-UB\* (0.4  $\mu$ M) was added to ARIH1 (0.3  $\mu$ M), CUL1-NEDD8 (0.5  $\mu$ M), SKP1-FBXO22 (0.5  $\mu$ M). Time points were removed at indicated times and resolved by SDS-PAGE analysis and in-gel fluorescence analysis.

**Intact Mass determination of FBXO22-compound complex**

FBXO22-SKP1 variants (20  $\mu$ M) were mixed with buffer (25 mM HEPES, 100 mM NaCl, pH 7.5). 100  $\mu$ M of the respective compound were added and the mixture was incubated for 10 min on ice prior to ESI-LCMS analysis. LCMS analysis for intact mass determination was carried out on a microTOF Bruker Daltonik instrument equipped with an Agilent 1100 HPLC system. Samples were resolved on a Phenomenex AerisTM 3.6  $\mu$ m WIDEPORE C4 100 mm $\times$ 2.1 mm ID, 200 Å pore size column with eluents H<sub>2</sub>O + 0.05 vol% TFA (Buffer A) and MeCN + 0.05 vol% TFA (Buffer B). Elution was achieved with a Buffer B gradient of 20–95% over 16 min at a flow rate of 250  $\mu$ l/min. MS mode was set to positive detection and a mass range of 800–3000  $m/z$ . Raw MS data was analyzed in CompassTM Data Analysis software from Bruker Daltonik and deconvoluted with “Maximum Entropy”.

**nanodSF**

SKP1-FBXO22, wt and C326A, were diluted with 25 mM HEPES, 150 mM NaCl, 1 mM TCEP, pH 7.5 to 2.7  $\mu$ M. Protein heat denaturation was measured using nanodSF (Prometheus, Nanotemper). 10  $\mu$ l of protein solution was loaded in each capillary. Tryptophan fluorescence was measured at 330 and 350 nm with 40% gain. Following temperature stabilization at 20 °C for 20 min, heat denaturation was measured at a rate of 1 °C/min. Measurements were performed in duplicates.

**Ultra-performance liquid chromatography-mass spectrometry (UPLC-MS/MS) for SP3N and SP3CHO**

80% methanol cell extracts (or solutions without cells) were evaporated to dryness using a soft nitrogen flow. Samples were reconstituted with 50  $\mu$ l of HPLC-grade methanol and vortexed. Samples were analyzed by UPLC-MS/MS using a Waters Acquity UHPLC system coupled to a Waters Xevo TQMS triple quadrupole mass spectrometer. The conditions for the equipment were optimized before the sample analysis to obtain the best selectivity and sensitivity. The analytes were separated using reverse phase liquid chromatography on an Agilent ZORBAX Eclipse Plus C18 Rapid Resolution HD (1.8  $\mu$ m, 2.1  $\times$  50 mm) analytical column equipped with a pre-column, running a gradient with solvent A (water with 0.1% formic acid) and solvent B (acetonitrile with 0.1% formic acid), and keeping the column compartment at 40 °C. The mass spectrometer was run in positive electrospray ionization (ESI) mode, monitoring 2 MRM transitions per compound: for SP3CHO  $m/z$  727.404 > 472.26 and 727.404 > 99.02; for SP3N 728.628 > 473.409 and 728.628 > 270.223; and for SP3Nac 770.638 > 515.436 and 770.638 > 86.043. For the absolute quantification of the compounds, a

10-point external calibration curve was recorded using neat standards, from 0.04 to 10,000 nM. Excellent linearity was obtained in all the range ( $R^2$  > 0.996). Quantification was executed using the software TargetLynx XS V4 S2 SCN986.

**Reporting summary**

Further information on research design is available in the Nature Portfolio Reporting Summary linked to this article.

**Data availability**

The mass spectrometry data for the global proteomics generated in this study have been deposited in the ProteomeXchange Consortium via the PRIDE partner repository with the accession identifier PXD049330<sup>73</sup>. The mass spectrometry data for the TMT-ABPP experiment have been deposited in the ProteomeXchange Consortium with the accession identifier PXD051803. Source data of all graphs and uncropped gels and blots are provided in the “Source Data” file. Source data for Figs. 1e, 2a, Supplementary Fig. 2a and Supplementary Fig. 4g, h are included in Supplementary Data 1–4. The gating strategies applied for FACS analyses and cell sorting are provided in Supplementary Fig. 6. Source data are provided with this paper.

**Code availability**

The code for the analysis of the FACS-based CRISPR-KO screens is available on GitHub [<https://zenodo.org/records/11445588>, <https://zenodo.org/records/11445611>].

**References**

- Ito, T. et al. Identification of a primary target of thalidomide teratogenicity. *Science* **327**, 1345–1350 (2010).
- Kronke, J. et al. Lenalidomide causes selective degradation of IKZF1 and IKZF3 in multiple myeloma cells. *Science* **343**, 301–305 (2014).
- Lu, G. et al. The myeloma drug lenalidomide promotes the cereblon-dependent destruction of Ikaros proteins. *Science* **343**, 305–309 (2014).
- Sievers, Q. L. et al. Defining the human C2H2 zinc finger degrader targeted by thalidomide analogs through CRBN. *Science* **362**, eaat0572 (2018).
- Han, T. et al. Anticancer sulfonamides target splicing by inducing RBM39 degradation via recruitment to DCAF15. *Science* **356**, eaal3755 (2017).
- Toriki, E. S. et al. Rational chemical design of molecular glue degraders. *ACS Cent. Sci.* **9**, 915–926 (2023).
- Mayor-Ruiz, C. et al. Rational discovery of molecular glue degraders via scalable chemical profiling. *Nat. Chem. Biol.* **16**, 1199–1207 (2020).
- Hanzl, A. et al. E3-specific degrader discovery by dynamic tracing of substrate receptor abundance. *J. Am. Chem. Soc.* **145**, 1176–1184 (2023).
- Ng, A. et al. Discovery of Molecular Glue Degradors via Isogenic Morphological Profiling. *ACS Chem. Biol.* **18**, 2464–2473 (2023).
- Mason, J. W. et al. DNA-encoded library-enabled discovery of proximity-inducing small molecules. *Nat. Chem. Biol.* <https://doi.org/10.1038/s41589-023-01458-4> (2023).
- Liu, S. et al. Rational screening for cooperativity in small-molecule inducers of protein–protein associations. *bioRxiv* <https://doi.org/10.1101/2023.05.22.541439> (2023).
- Sakamoto, K. M. et al. Protacs: chimeric molecules that target proteins to the Skp1-Cullin-F box complex for ubiquitination and degradation. *Proc. Natl Acad. Sci. USA* **98**, 8554–8559 (2001).
- O’Brien Laramy, M. N., Luthra, S., Brown, M. F. & Bartlett, D. W. Delivering on the promise of protein degraders. *Nat. Rev. Drug Discov.* **22**, 410–427 (2023).
- Békés, M., Langley, D. R. & Crews, C. M. PROTAC targeted protein degraders: the past is prologue. *Nat. Rev. Drug Discov.* **21**, 181–200 (2022).



15. Kramer, L. T. & Zhang, X. Expanding the landscape of E3 ligases for targeted protein degradation. *Curr. Res. Chem. Biol.* **2**, 100020 (2022).
16. Gooding, S. et al. Multiple cereblon genetic changes are associated with acquired resistance to lenalidomide or pomalidomide in multiple myeloma. *Blood* **137**, 232–237 (2021).
17. Barrio, S. et al. IKZF1/3 and CRL4 CRBN E3 ubiquitin ligase mutations and resistance to immunomodulatory drugs in multiple myeloma. *Haematologica* **105**, E237–E241 (2020).
18. Hanzl, A. et al. Functional E3 ligase hotspots and resistance mechanisms to small-molecule degraders. *Nat. Chem. Biol.* **19**, 323–333, <https://doi.org/10.1038/s41589-022-01177-2> (2023).
19. Ottis, P. et al. Cellular resistance mechanisms to targeted protein degradation converge toward impairment of the engaged ubiquitin transfer pathway. *ACS Chem. Biol.* **14**, 2215–2223 (2019).
20. Khan, S. et al. A selective BCL-XL PROTAC degrader achieves safe and potent antitumor activity. *Nat. Med.* **25**, 1938–1947 (2019).
21. Bondeson, D. P. et al. Lessons in PROTAC design from selective degradation with a promiscuous warhead. *Cell Chem. Biol.* **25**, 78–87.e5 (2018).
22. Huang, H. T. et al. A chemoproteomic approach to query the degradable kinome using a multi-kinase degrader. *Cell Chem. Biol.* <https://doi.org/10.1016/j.chembiol.2017.10.005> (2017).
23. Smith, B. E. et al. Differential PROTAC substrate specificity dictated by orientation of recruited E3 ligase. *Nat. Commun.* **10**, 131 (2019).
24. Zhang, X. et al. DCAF11 supports targeted protein degradation by electrophilic proteolysis-targeting chimeras. *J. Am. Chem. Soc.* **143**, 5141–5149 (2021).
25. Zhang, X., Crowley, V. M., Wucherpfennig, T. G., Dix, M. M. & Cravatt, B. F. Electrophilic PROTACs that degrade nuclear proteins by engaging DCAF16. *Nat. Chem. Biol.* **15**, 737–746 (2019).
26. Ward, C. C. et al. Covalent ligand screening uncovers a RNF4 E3 ligase recruiter for targeted protein degradation applications. *ACS Chem. Biol.* **14**, 2430–2440 (2019).
27. Luo, M. et al. Chemoproteomics-enabled discovery of covalent RNF114-based degraders that mimic natural product function. *Cell Chem. Biol.* **28**, 559–566.e15 (2021).
28. Hickey, C. M. et al. Co-opting the E3 ligase KLHDC2 for targeted protein degradation by small molecules. *Nat. Struct. Mol. Biol.* **31**, 311–322 (2024).
29. Shergalis, A. G. et al. CRISPR screen reveals BRD2/4 molecular glue-like degrader via recruitment of DCAF16. *ACS Chem. Biol.* **18**, 331–339 (2023).
30. Hassan, M. M. et al. Exploration of the tunability of BRD4 degradation by DCAF16 Trans-labelling covalent glues. *bioRxiv* <https://doi.org/10.1101/2023.10.07.561308> (2023).
31. Hsia, O. et al. Targeted protein degradation via intramolecular bivalent glues. *Nature* **627**, 204–211 (2024).
32. den Besten, W. et al. Primary amine tethered small molecules promote the degradation of X-linked inhibitor of apoptosis protein. *J. Am. Chem. Soc.* **143**, 10571–10575 (2021).
33. Nie, D. Y. et al. Recruitment of FBXO22 for targeted degradation of NSD2. *bioRxiv* <https://doi.org/10.1101/2023.11.01.564830> (2023).
34. Hanley, R. P. et al. Discovery of a potent and selective targeted NSD2 degrader for the reduction of H3K36me2. *J. Am. Chem. Soc.* **145**, 8176–8188 (2023).
35. Harper, J. W. & Schulman, B. A. Cullin-RING ubiquitin ligase regulatory circuits: a quarter century beyond the F-box hypothesis. *Annu. Rev. Biochem.* **90**, 403–429 (2021).
36. Winter, G. E. et al. DRUG DEVELOPMENT. Phthalimide conjugation as a strategy for in vivo target protein degradation. *Science* **348**, 1376–1381 (2015).
37. Basu, A. A. et al. A CRISPR activation screen identifies FBXO22 as an E3 ligase supporting targeted protein degradation. *bioRxiv* <https://doi.org/10.1101/2023.09.15.557708> (2023).
38. Zhang, L. et al. FBXO22 promotes the development of hepatocellular carcinoma by regulating the ubiquitination and degradation of p21. *J. Exp. Clin. Cancer Res.* **38**, 101 (2019).
39. Johmura, Y., Harris, A. S., Ohta, T. & Nakanishi, M. FBXO22, an epigenetic multiplexer coordinating senescence, hormone signaling, and metastasis. *Cancer Sci.* **111**, 2718–2725 (2020).
40. Schlierf, A. et al. Targeted inhibition of the COP9 signalosome for treatment of cancer. *Nat. Commun.* **7**, 13166 (2016).
41. Mayor-Ruiz, C. et al. Plasticity of the Cullin-RING ligase repertoire shapes sensitivity to ligand-induced protein degradation. *Mol. Cell* **75**, 849–858.e8 (2019).
42. Henneberg, L. T. et al. Activity-based profiling of cullin-RING E3 networks by conformation-specific probes. *Nat. Chem. Biol.* **19**, 1513–1523 (2023).
43. Kuljanin, M. et al. Reimagining high-throughput profiling of reactive cysteines for cell-based screening of large electrophile libraries. *Nat. Biotechnol.* **39**, 630–641 (2021).
44. Yang, K. et al. Accelerating multiplexed profiling of protein-ligand interactions: High-throughput plate-based reactive cysteine profiling with minimal input. *Cell Chem. Biol.* **31**, 565–576.e4 (2024).
45. Xue, G. et al. Discovery of a drug-like, natural product-inspired DCAF11 ligand chemotype. *Nat. Commun.* **14**, 7908 (2023).
46. Arrowsmith, C. H. et al. The promise and peril of chemical probes. *Nat. Chem. Biol.* **11**, 536–541 (2015).
47. Shirasaki, R. et al. Functional genomics identify distinct and overlapping genes mediating resistance to different classes of heterobifunctional degraders of oncoproteins. *Cell Rep.* **34**, 108532 (2021).
48. Nabet, B. et al. The dTAG system for immediate and target-specific protein degradation. *Nat. Chem. Biol.* **14**, 431–441 (2018).
49. Bond, A. G. et al. Development of BromoTag: a ‘bump-and-hole’-PROTAC system to induce potent, rapid, and selective degradation of tagged target proteins. *J. Med. Chem.* <https://doi.org/10.1021/acs.jmedchem.1c01532> (2021).
50. Nabet, B. et al. Rapid and direct control of target protein levels with VHL-recruiting dTAG molecules. *Nat. Commun.* **11**, 4687 (2020).
51. Cheng, J. et al. Emerging role of FBXO22 in carcinogenesis. *Cell Death Discov.* **6**, 66 (2020).
52. Zhu, X.-N. et al. FBXO22 mediates polyubiquitination and inactivation of LKB1 to promote lung cancer cell growth. *Cell Death Dis.* **10**, 486 (2019).
53. Li, M. et al. FBXO22 promotes growth and metastasis and inhibits autophagy in epithelial ovarian cancers via the MAPK/ERK pathway. *Front. Pharm.* **12**, 778698 (2021).
54. Liu, F. et al. Increased AOC1 expression promotes cancer progression in colorectal cancer. *Front. Oncol.* **11**, 657210 (2021).
55. Ding, Q. et al. Downregulation of amine oxidase copper containing 1 inhibits tumor progression by suppressing IL-6/JAK/STAT3 pathway activation in hepatocellular carcinoma. *Oncol. Lett.* **22**, 857 (2021).
56. Xu, F. et al. AOC1 contributes to tumor progression by promoting the AKT and EMT pathways in gastric cancer. *Cancer Manag Res* **12**, 1789–1798 (2020).
57. Jumper, J. et al. Highly accurate protein structure prediction with AlphaFold. *Nature* **596**, 583–589 (2021).
58. Varadi, M. et al. AlphaFold Protein Structure Database: massively expanding the structural coverage of protein-sequence space with high-accuracy models. *Nucleic Acids Res.* **50**, D439–D444 (2022).
59. de Almeida, M. et al. AKIRIN2 controls the nuclear import of proteasomes in vertebrates. *Nature* **599**, 491–496 (2021).
60. Michlits, G. et al. Multilayered VBC score predicts sgRNAs that efficiently generate loss-of-function alleles. *Nat. Methods* **17**, 708–716 (2020).
61. Li, W. et al. MAGECK enables robust identification of essential genes from genome-scale CRISPR/Cas9 knockout screens. *Genome Biol.* **15**, 554 (2014).

62. Tang, Z., Kang, B., Li, C., Chen, T. & Zhang, Z. GEPIA2: an enhanced web server for large-scale expression profiling and interactive analysis. *Nucleic Acids Res.* **47**, W556–W560 (2019).
63. Navarrete-Perea, J., Yu, Q., Gygi, S. P. & Paulo, J. A. Streamlined tandem mass tag (SL-TMT) protocol: an efficient strategy for quantitative (phospho)proteome profiling using tandem mass tag-synchronous precursor selection-MS3. *J. Proteome Res.* **17**, 2226–2236 (2018).
64. Huttlin, E. L. et al. A tissue-specific atlas of mouse protein phosphorylation and expression. *Cell* **143**, 1174–1189 (2010).
65. Elias, J. E. & Gygi, S. P. Target-decoy search strategy for increased confidence in large-scale protein identifications by mass spectrometry. *Nat. Methods* **4**, 207–214 (2007).
66. Beausoleil, S. A., Villén, J., Gerber, S. A., Rush, J. & Gygi, S. P. A probability-based approach for high-throughput protein phosphorylation analysis and site localization. *Nat. Biotechnol.* **24**, 1285–1292 (2006).
67. McAlister, G. C. et al. Increasing the multiplexing capacity of TMTs using reporter ion isotopologues with isobaric masses. *Anal. Chem.* **84**, 7469–7478 (2012).
68. Eng, J. K., Jahan, T. A. & Hoopmann, M. R. Comet: an open-source sequence database search tool. *Proteomics* **13**, 22–24 (2013).
69. Savitski, M. M., Wilhelm, M., Hahne, H., Kuster, B. & Bantscheff, M. A scalable approach for protein false discovery rate estimation in large proteomic data sets. *Mol. Cell. Proteom.* **14**, 2394–2404 (2015).
70. Gassaway, B. M. et al. A multi-purpose, regenerable, proteome-scale, human phosphoserine resource for phosphoproteomics. *Nat. Methods* **19**, 1371–1375 (2022).
71. Scott, D. C. et al. Two distinct types of E3 ligases work in unison to regulate substrate ubiquitylation. *Cell* **166**, 1198–1214.e24 (2016).
72. Jeong, H.-J., Abhiraman, G. C., Story, C. M., Ingram, J. R. & Dougan, S. K. Generation of Ca<sup>2+</sup>-independent sortase A mutants with enhanced activity for protein and cell surface labeling. *PLoS ONE* **12**, e0189068 (2017).
73. Perez-Riverol, Y. et al. The PRIDE database resources in 2022: a hub for mass spectrometry-based proteomics evidences. *Nucleic Acids Res.* **50**, D543–D552 (2022).

## Acknowledgements

CeMM and the Winter lab are supported by the Austrian Academy of Sciences. The Winter lab is further supported by funding from the European Research Council (ERC) under the European Union's Horizon 2020 research and innovation program (grant agreement 851478), as well as by funding from the Austrian Science Fund (FWF, projects P7909, P36746 and P5918723) and an Aspire Award from the Mark Foundation for Cancer Research. This work in the Schulman lab was supported by the Max Planck Society, and the European Research Council (ERC) under the European Union's Horizon 2020 research and innovation program (grant agreement No 789016-NEDD8Activate). J.F. is supported by a postdoctoral fellowship from the Peter und Traudl Engelhorn-Stiftung. We thank the Core Facility Flow Cytometry of the Medical University of Vienna for access to flow cytometry instruments and assistance with flow cytometric cell sorting as well as the CeMM Biomedical Sequencing Facility for NGS sample processing, sequencing, and data curation. We are grateful to all the members of the Winter lab for helpful discussions. We thank Stephan Uebel and the Biochemistry Core Facility of Max Planck Institute of Biochemistry for peptide synthesis and Maria Victoria Sanchez Caballero, Barbara Steigenberger and the Mass Spectrometry Core Facility of Max Planck Institute of Biochemistry for intact mass analysis. We thank Susanne von Gronau for protein expression in insect cells.

## Author contributions

C.K. designed and executed most of the described experiments, analyzed data, wrote the manuscript, and made figures. J.A.C. synthesized compounds. J.F. performed in vitro ubiquitylation assays and intact MS. J.L. produced recombinant neddylated SCF<sup>FKC22</sup> and FKBP12 and performed preliminary in vitro biochemical experiments. F.O. developed the NanoBiT assay. K.D. and J.A.P. performed and analyzed the global proteome experiment. K.Y. performed and analyzed the Cys-ABPP proteome-wide profiling. G.T. synthesized compounds. C.S.H. performed mutagenesis studies. M.H. developed the FKBP12 stability reporter. N.S.S. supported CRISPR screens. J.S.A. performed metabolomics experiments. M.F. cloned UPS-focused sgRNA library. F.A. annotated UPS-focused sgRNA library. J.T.H. supervised and analyzed metabolomics experiments. J.Z. supervised UPS-focused sgRNA library design. S.K. supervised metabolomics. S.P.G. supervised proteomics experiments. B.A.S. supervised in vitro experiments. G.E.W. conceptualized the study, wrote the manuscript, and has overall responsibility for the presented study.

## Competing interests

S.K. and G.E.W. are scientific founders and shareholders of Proxygen and Solgate. G.E.W. is on the Scientific Advisory Board of Nexo Therapeutics. The Winter lab received research funding from Pfizer. B.A.S. is a member of the scientific advisory boards of Proxygen and BioTheryX, and a co-inventor of intellectual property licensed to Cinsano. The remaining authors declare no competing interests.

## Additional information

**Supplementary information** The online version contains supplementary material available at <https://doi.org/10.1038/s41467-024-49739-3>.

**Correspondence** and requests for materials should be addressed to Georg E. Winter.

**Peer review information** *Nature Communications* thanks the anonymous reviewer(s) for their contribution to the peer review of this work. A peer review file is available.

**Reprints and permissions information** is available at <http://www.nature.com/reprints>

**Publisher's note** Springer Nature remains neutral with regard to jurisdictional claims in published maps and institutional affiliations.

**Open Access** This article is licensed under a Creative Commons Attribution 4.0 International License, which permits use, sharing, adaptation, distribution and reproduction in any medium or format, as long as you give appropriate credit to the original author(s) and the source, provide a link to the Creative Commons licence, and indicate if changes were made. The images or other third party material in this article are included in the article's Creative Commons licence, unless indicated otherwise in a credit line to the material. If material is not included in the article's Creative Commons licence and your intended use is not permitted by statutory regulation or exceeds the permitted use, you will need to obtain permission directly from the copyright holder. To view a copy of this licence, visit <http://creativecommons.org/licenses/by/4.0/>.

© The Author(s) 2024



## Supplementary Information

### Alkylamine-tethered molecules recruit FBXO22 for targeted protein degradation

#### Authors

Chrysanthi Kagiou<sup>1</sup>, Jose Antonio Cisneros<sup>1</sup>, Jakob Farnung<sup>2</sup>, Joanna Liwocha<sup>2</sup>, Fabian Offensperger<sup>1</sup>, Kevin Dong<sup>3</sup>, Ka Yang<sup>3</sup>, Gary Tin<sup>1</sup>, Christina S. Horstmann<sup>1,4</sup>, Matthias Hinterndorfer<sup>1</sup>, Joao A. Paulo<sup>3</sup>, Natalie S. Scholes<sup>1</sup>, Juan Sanchez Avila<sup>1</sup>, Michaela Fellner<sup>5</sup>, Florian Andersch<sup>5</sup>, J. Thomas Hannich<sup>1</sup>, Johannes Zuber<sup>5</sup>, Stefan Kubicek<sup>1</sup>, Steven P. Gygi<sup>3</sup>, Brenda A. Schulman<sup>2</sup>, Georg E. Winter<sup>1,#</sup>

#### Affiliations

<sup>1</sup>CeMM Research Center for Molecular Medicine of the Austrian Academy of Sciences, 1090 Vienna, Austria

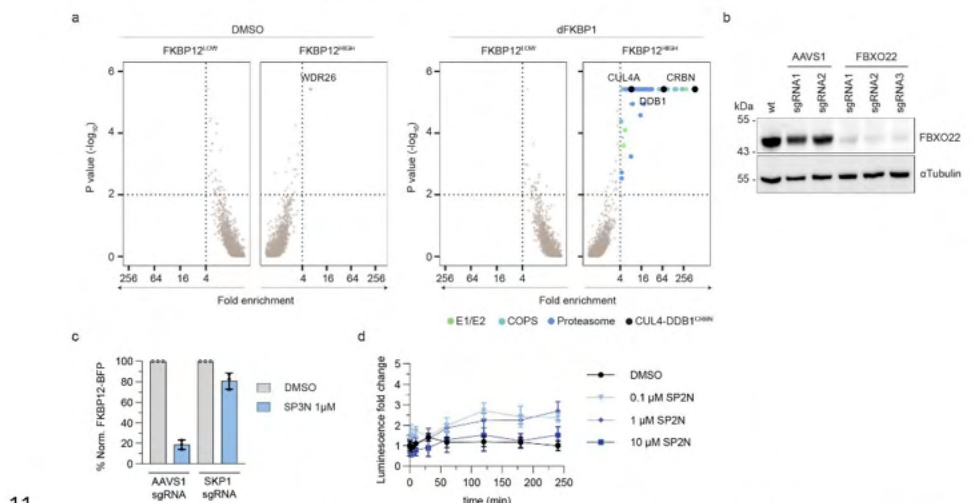
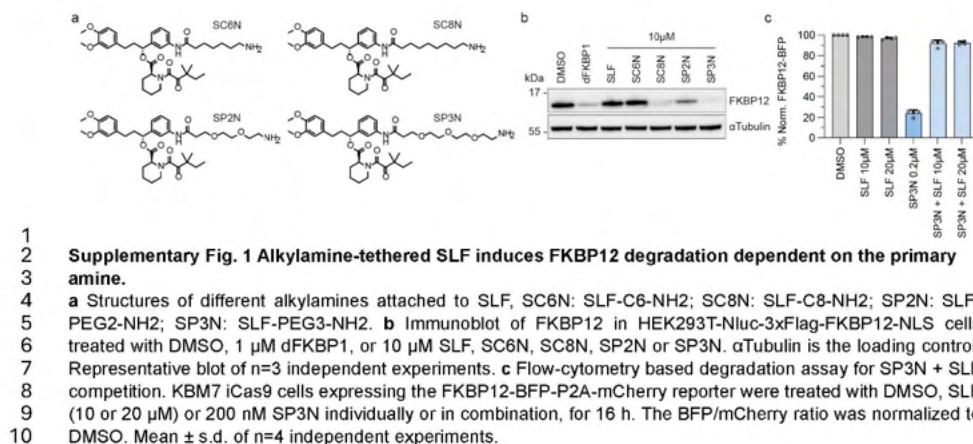
<sup>2</sup>Department of Molecular Machines and Signaling, Max Planck Institute of Biochemistry, Am Klopferspitz 18, 82152, Martinsried, Germany

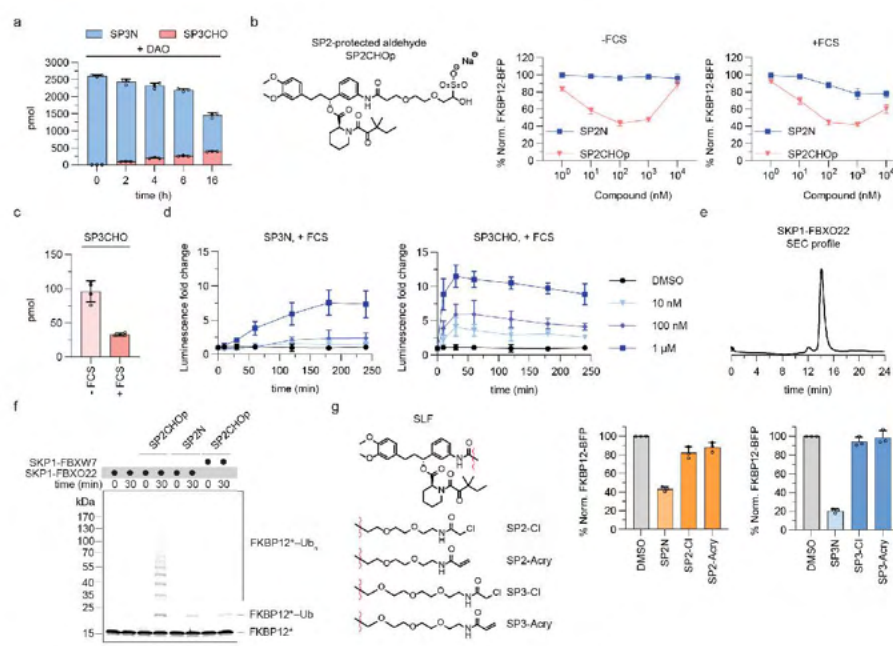
<sup>3</sup>Department of Cell Biology, Harvard Medical School, Boston, MA, USA

<sup>4</sup>St. Anna Children's Cancer Research Institute, Vienna, Austria

<sup>5</sup>Research Institute of Molecular Pathology, Vienna BioCenter, 1030 Vienna, Austria.

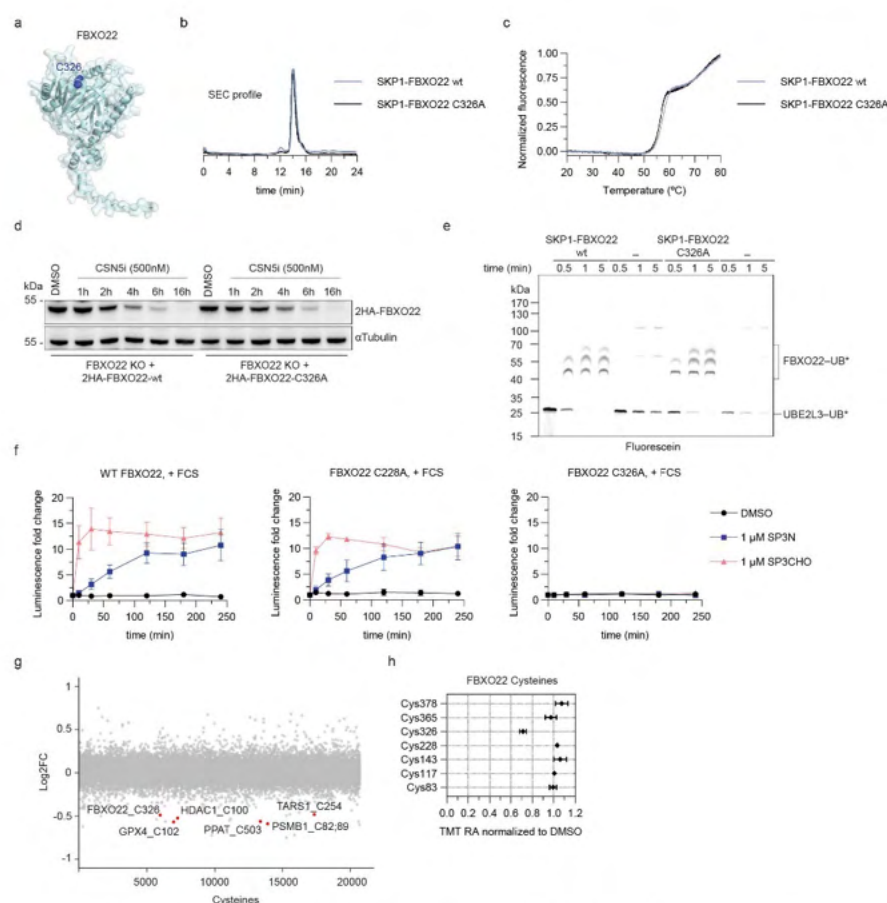
#correspondence to gwinter@cemm.oeaw.ac.at





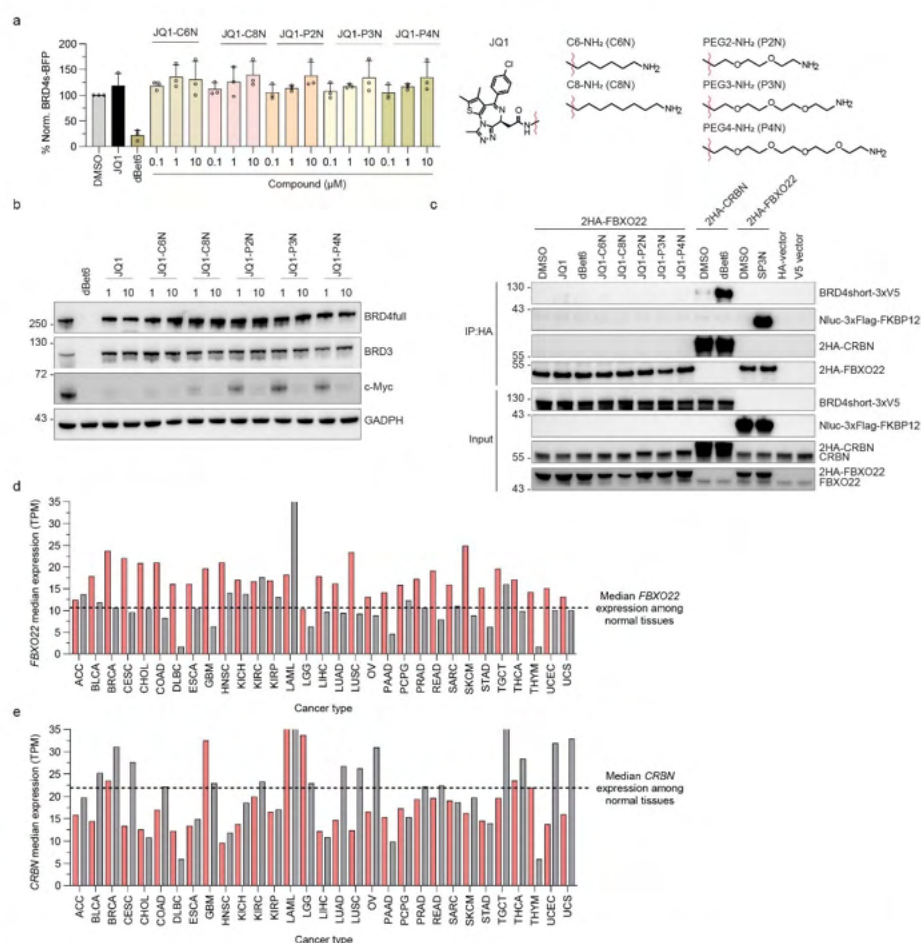
**Supplementary Fig. 3 The alkylamines are metabolized to active aldehydes.**

**a** Quantification of SP3N and SP3CHO (pmol) using UPLC-MS/MS, in PBS. 10  $\mu$ M SP3N were added in PBS with 40  $\mu$ g DAO and incubated for 0-16 h at 37  $^{\circ}$ C. Conditions without DAO were used as controls. Mean  $\pm$  s.d. of n=3 technical replicates. **b** Flow-cytometry based degradation assay in KBM7 iCas9 with the FKBP12-BFP-P2A-mCherry reporter washed to remove FCS, resuspended in IMDM + 10% FCS or Opti-MEM - FCS and treated with DMSO, SP2N or SP2CHO protected aldehyde adduct (SP3CHOp) at the indicated concentrations for 6 h. **c** Quantification of intracellular SP3CHO (pmol) in medium -/+ FCS. KBM7 iCas9 FKBP12-BFP-P2A-mCherry FBXO22 KO cells were treated with 1  $\mu$ M SP3CHO in OptiMEM -/+ FCS for 5 min and the SP3CHO levels were quantified using UPLC-MS/MS. Mean  $\pm$  s.d. of n=4 technical replicates. **d** NanoBiT assay as described in Fig. 3f. Before treatment, the cells were washed 3x with PBS and the indicated concentrations of SP3N or SP3CHO were added to the cells in Opti-MEM + 10% FCS. The luminescence was monitored after 10 min, 30 min and every hour up to 4h post-treatment. Fold-change is calculated based on the luminescence at timepoint 0, right before the treatments. Mean  $\pm$  s.d. of n=3 technical replicates; representative of n=3 independent experiments. **e** Size exclusion chromatography (SEC) profile of the recombinant SKP1-FBXO22-WT. Relative absorbance over time is shown. **f** *In vitro* multi-turnover ubiquitylation assay of fluorescently labeled FKBP12 with SKP1-FBXO22 in the presence of DMSO, 10  $\mu$ M SP2N or 10  $\mu$ M SP2CHOp. SKP1-FBXW7 was used as negative control. Representative blot of n=2 independent experiments. **g** Flow-cytometry based degradation assay in KBM7 iCas9 with the FKBP12-BFP-P2A-mCherry reporter treated with DMSO or 10  $\mu$ M SP2N, SP2-acrylamide (SP2-Acry), SP2-chloroacetamide (SP2-Cl), SP3N, SP3-Acry or SP3-Cl for 16 h. For all the flow-cytometry based degradation assays (b, g), the BFP/mCherry ratio was normalized to DMSO and the data is the mean  $\pm$  s.d. from n = 3 biological replicates.



**Supplementary Fig. 4 FBXO22-C326 is crucial for the degradation induced by SP3N/SP3CHO.**  
**a** AlphaFold prediction of FBXO22 structure with C326 highlighted in blue. **b** Comparison of SEC profiles of SKP1-FBXO22-WT and SKP1-FBXO22-C326A. Relative absorbance over time is shown. **c** Normalized fluorescence data from nano differential scanning fluorimetry (NanoDSF) of SKP1-FBXO22-WT and SKP1-FBXO22-C326A. Heat denaturation was measured at a rate of 1 °C/min. Measurements were performed in duplicates. **d** Immunoblot of 2HA-FBXO22-WT or 2HA-FBXO22-C326A in HEK293T-FKBP12-BFP-P2A-mCherry FBXO22 KO single clone transduced with 2HA-FBXO22-WT or -C326A cDNAs. Cells were treated with DMSO or 500 nM CSN5i-03 for 1-16 h.  $\alpha$ Tubulin is the loading control. Representative plot of n=2 independent experiments. **e** Pulse-chase *in vitro* autoubiquitylation assay of FBXO22 with SKP1-FBXO22-WT and SKP1-FBXO22-C326A. UB\*: fluorescent ubiquitin. Representative blot from n=2 independent experiments. **f** NanoBiT assay in HEK293T cells co-transfected with LgBiT-FKBP12 and SmBiT-FBXO22-WT, SmBiT-FBXO22-C228A or SmBiT-FBXO22-C326A and treated with DMSO, 1  $\mu$ M SP3N or 1  $\mu$ M SP3CHO. The luminescence was monitored after 10 min, 30 min and every hour up to 4 h post-treatment. Mean  $\pm$  s.d. of n=3 technical replicates; representative of n=3 independent experiments. **g** Proteome-wide TMT-ABPP profiling of SP3CHO in HEK293T cell lysates spiked with 0.15  $\mu$ g recombinant SKP1-FBXO22 and treated with 40  $\mu$ M SP3CHO for 1.5 h. More than 20,000 cysteine sites were quantified. Log2 fold-changes (Log2FC) were calculated based on the DMSO treated cells. Red dots represent cysteine sites with Log2FC < -0.45 and -logPvalue > 2. Data from n=3 replicates. **h** TMT relative abundances (RA) of the quantified FBXO22 cysteines in the TMT-ABPP as described in g. RA are normalized to DMSO. Mean  $\pm$  s.d. of n=3 replicates.

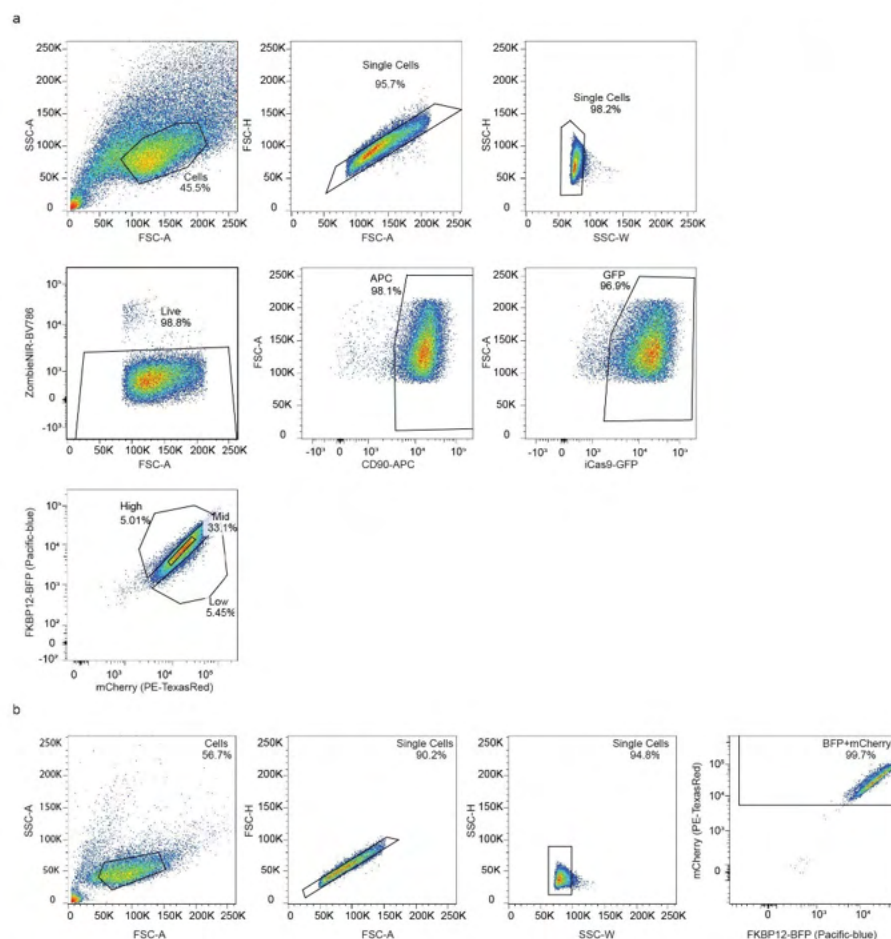




**Supplementary Fig. 5 Expandability of co-opting FBXO22.**

**a** Flow-cytometry based degradation assay in KBM7 iCas9 BRD4(short)-BFP-P2A-mCherry cells treated with DMSO, 10 μM JQ1, 1 μM dBet6 or the indicated concentrations of the different alkylamine-tethered JQ1 molecules for 16 h. Mean ± s.d. of n=3 biological replicates. **b** Immunoblot of endogenous BRD4, BRD3 and c-Myc in KBM7 iCas9 FKBP12-BFP-P2A-mCherry cells treated with DMSO, 1 μM dBet6, 1 or 10 μM JQ1 and 1 μM or 10 μM of the JQ1-alkylamines for 16 h. GAPDH is the loading control. Representative blot of n=2 experiments. **c** Co-immunoprecipitation of 2HA-FBXO22 and BRD4s-3xV5 following treatment with DMSO, 1 μM dBet6, 10 μM JQ1 or 10 μM of the indicated JQ1-alkylamines, for 4 h in the presence of 1 μM carfilzomib. Co-immunoprecipitation of 2HA-FBXO22 with Nluc-3xFlag-FKBP12 upon treatment with 10 μM SP3N or of 2HA-CRBN with BRD4s-3xV5 upon treatment with 1 μM dBet6 were used as positive controls. Transfection with only HA-empty vector or V5-empty vector were used as negative controls for the IPs. Representative blot of n=2 experiments. IP: immunoprecipitation, IB: immunoblot. **d**, **e** Comparisons of the median gene expression (TPM; transcripts per million) of FBXO22 (**d**) or CRBN (**e**) in different cancer tissues and the respective normal tissues extracted from TCGA and GTEx using GEPIA2. Gray bars: Normal tissues. Red bars: Cancer tissues. Dotted horizontal line: the median FBXO22 or CRBN levels among all healthy tissues. ACC, Adrenocortical carcinoma; BLCA, Bladder Urothelial Carcinoma; BRCA, Breast invasive carcinoma; CESC, Cervical squamous cell carcinoma and endocervical adenocarcinoma; CHOL, Cholangio carcinoma; COAD, Colon adenocarcinoma; DLBC, Lymphoid Neoplasm Diffuse Large B-cell Lymphoma; ESCA, Esophageal carcinoma; GBM, Glioblastoma multiforme; HNSC, Head and Neck squamous cell carcinoma; KICH, Kidney Chromophobe; KIRC, Kidney renal clear cell carcinoma; KIRP, Kidney renal papillary cell carcinoma; LAML, Acute Myeloid Leukemia; LGG, Brain Lower Grade Glioma;

1 LIHC, Liver hepatocellular carcinoma; LUAD, Lung adenocarcinoma; LUSC, Lung squamous cell carcinoma; OV,  
2 Ovarian serous cystadenocarcinoma; PAAD Pancreatic adenocarcinoma; PCPG, Pheochromocytoma and  
3 Paraganglioma; PRAD, Prostate adenocarcinoma; READ, Rectum adenocarcinoma; SARC, Sarcoma; SKCM,  
4 Skin Cutaneous Melanoma; STAD, Stomach adenocarcinoma; TGCT, Testicular Germ Cell Tumors; THCA, Thyroid  
5 carcinoma; THYM, Thymoma; UCEC, Uterine Corpus Endometrial Carcinoma; UCS, Uterine Carcinosarcoma.  
6



**Supplementary Fig. 6 Gating strategy for flow cytometry sorting and analysis.**

**a** Gating strategy for sorting the FACS-based FKBP12-BFP stability CRISPR/iCas9 screen cells (fixed), as in Fig. 2a and Supplementary Fig. 2a. The viable cells were separated from debris using forward scatter area (FSC-A) vs. side scatter area (SSC-A). Single cells were separated from aggregates using FSC-A vs. forward scatter height (FSC-H) and side scatter width (SSC-W) vs. side scatter height (SSC-H). Zombie-NIR staining (BV786) vs FSC-A was used to exclude the dead cells and the CD90-APC<sup>+</sup> (sgRNA library) and iCas9-GFP<sup>+</sup> cells were sorted into FKBP12<sup>LOW</sup>, FKBP12<sup>MID</sup> and FKBP12<sup>HIGH</sup> based on the FKBP12-BFP (Pacific-blue) vs mCherry (PE-TexasRed) scatter plots. The gates were dynamically adjusted at 5-8% FKBP12<sup>LOW</sup> and FKBP12<sup>HIGH</sup> and at 30-35% for FKBP12<sup>MID</sup>. **b** Gating strategy for all FACS-based degradation assays in (live) cells with the FKBP12-BFP-P2A-mCherry reporter. Live cells were separated from debris and aggregates as described in **a**. The BFP<sup>+</sup>mCherry<sup>+</sup> population was used to compare the BFP/mCherry ratios among different conditions.

1 **Supplementary tables**

2 **Supplementary Table 1. Plasmids**

| Plasmid   | Description                                      |
|---|--|
| pRRL-SFFV-FKBP12-mTagBFP-P2A-mCherry              | FKBP12 fluorescent stability reporter            |
| pRRL-SFFV-BRD4s-mTagBFP-P2A-mCherry               | BRD4s fluorescent stability reporter (V5-tagged) |
| pRRL-SFFV-BRD4s-P2A-mCherry                       | BRD4s without BFP (V5-tagged)                    |
| pRRL-U6-sgRNA-EF1 $\alpha$ -Thy1.1-P2A-NeoR       | sgRNA cloning vector                             |
| pRRL-U6-sg1.FBXO22-IT-EF1 $\alpha$ -Thy1-P2A-NeoR | sgRNA 1 targeting FBXO22                         |
| pRRL-U6-sg2.FBXO22-IT-EF1 $\alpha$ -Thy1-P2A-NeoR | sgRNA 2 targeting FBXO22                         |
| pRRL-U6-sg3.FBXO22-IT-EF1 $\alpha$ -Thy1-P2A-NeoR | sgRNA 3 targeting FBXO22                         |
| pRRL-U6-sg1.SKP1-IT-EF1 $\alpha$ -Thy1-P2A-NeoR   | sgRNA 1 targeting SKP1                           |
| pRRL-U6-sg1.AAVS1-IT-EF1 $\alpha$ -Thy1-P2A-NeoR  | sgRNA 1 targeting AAVS1                          |
| pRRL-U6-sg2.AAVS1-IT-EF1 $\alpha$ -Thy1-P2A-NeoR  | sgRNA 2 targeting AAVS1                          |
| pLEX_puro-P2A-2HA_DEST_N-terminal                 | 2HA cloning vector                               |
| pLEX_puro-P2A-HA_FBXO22sgResistant_N-terminal     | 2HA-FBXO22 cDNA                                  |
| pLEX_puro-P2A-HA_CRBN_N-terminal                  | 2HA-CRBN cDNA                                    |
| pLenti6.2-Nanoluc-ccdB                            | Nanoluciferase cloning vector                    |
| pLenti6.2-NLuc-3xFlag-FKBP12                      | IP experiments/ WB                               |
| pLEX-2HA-FBXO22.C143A.sgRes-P2A-puro              | 2HA-FBXO22 mutant cDNA                           |
| pLEX-2HA-FBXO22.C227A.sgRes-P2A-puro              | 2HA-FBXO22 mutant cDNA                           |
| pLEX-2HA-FBXO22.C228A.sgRes-P2A-puro              | 2HA-FBXO22 mutant cDNA                           |
| pLEX-2HA-FBXO22.C326A.sgRes-P2A-puro              | 2HA-FBXO22 mutant cDNA                           |
| pLEX-2HA-FBXO22.C365A.sgRes-P2A-puro              | 2HA-FBXO22 mutant cDNA                           |
| pBiT2.1_SmBiT-FBXO22.WT                           | NanoBiT assay - WT FBXO22                        |
| pBiT2.1_SmBiT-FBXO22.C228A                        | NanoBiT assay - mutant FBXO22                    |
| pBiT2.1_SmBiT-FBXO22.C326A                        | NanoBiT assay - mutant FBXO22                    |
| pBiT1.1-C_LgBiT_FKBP12                            | NanoBiT assay - FKBP12                           |

3  
4  
5  
6  
7  
8  
9  
10  
11  
12  
13  
14  
15  
16  
17  
18  
19  
20  
21  
22  
23  
24  
25  
26  
27  
28  
29  
30  
31

**Supplementary Table 2.** Oligonucleotides & primers

| Oligo/primer       | 5-3 Sequence   | Description                                      |
|--------------------|--|--|
| FBXO22 sgRNA 1     | GCCAGGTTACTCAACACGA  | Depletion of FBXO22                              |
| FBXO22 sgRNA 2     | GCCATGTAAAGAACTGTATG   | Depletion of FBXO22                              |
| FBXO22 sgRNA 3     | GATCCAGGTTACGCTCCGAT   | Depletion of FBXO22                              |
| SKP1 sgRNA         | GTGACTATTAAGACCATGT  | Depletion of SKP1                                |
| AAVS1 sgRNA 1      | GTCACCAATCCTGTCCCTAG   | Depletion of AAVS1                               |
| AAVS1 sgRNA 2      | GGGGCCACTAGGGACAGGAT   | Depletion of AAVS1                               |
| attB_FBXO22_fw     | GGGGACAAGTTTGTACAAAAAAGC<br>AGGCTTAATGGAGCCGGTAGGCTG               | Gateway cloning 2HA FBXO22                       |
| attB_FBXO22_rv     | GGGGACCACTTTGTACAAGAAAGC<br>TGGGTTTTATTAGATGACCCAGAT<br>GTATGAGTGC | Gateway cloning 2HA-FBXO22                       |
| N-SmBiT-FBXO22_fw  | GGTGGTCTCGAGATGGAGCCGGTAG  | Restriction enzyme-based cloning of SmBiT-FBXO22 |
| N-SmBiT-FBXO22_rv  | AATAATCTCGAGTTATTTAGATGACCCAGATG                                   | Restriction enzyme-based cloning of SmBiT-FBXO22 |
| Q5_FBXO22-C143A_fw | CCCCAAACAAGCGCAAGTCCTTGGG  | FBXO22 cDNA Q5 mutagenesis                       |
| Q5_FBXO22-C143A_rv | AATAGCTTCTCAAGGGC  | FBXO22 cDNA Q5 mutagenesis                       |
| Q5_FBXO22-C227A_fw | TGGTTATAATGCGTGTAAGGTGGGAGC  | FBXO22 cDNA Q5 mutagenesis                       |
| Q5_FBXO22-C227A_rv | TGGTTATAATGCGTGTAAGGTGGGAGC  | FBXO22 cDNA Q5 mutagenesis                       |
| Q5_FBXO22-C228A_fw | TTATAATTGCGCGAAGGTGGGAGCC<br>AGTAATTATC                            | FBXO22 cDNA Q5 mutagenesis                       |
| Q5_FBXO22-C228A_rv | CCAAAGACAAGGACC  | FBXO22 cDNA Q5 mutagenesis                       |
| Q5_FBXO22-C326A_fw | CATGTTTGCAGCGGTTGGCAGGG  | FBXO22 cDNA Q5 mutagenesis                       |
| Q5_FBXO22-C326A_rv | AAGCCAATGGTGTATG   | FBXO22 cDNA Q5 mutagenesis                       |
| Q5_FBXO22-C365A_fw | AGAAATTGAGCGGATCGGATAGTCACTGG                                      | FBXO22 cDNA Q5 mutagenesis                       |
| Q5_FBXO22-C365A_rv | CCATTTCCAAAGAAGCC  | FBXO22 cDNA Q5 mutagenesis                       |

2

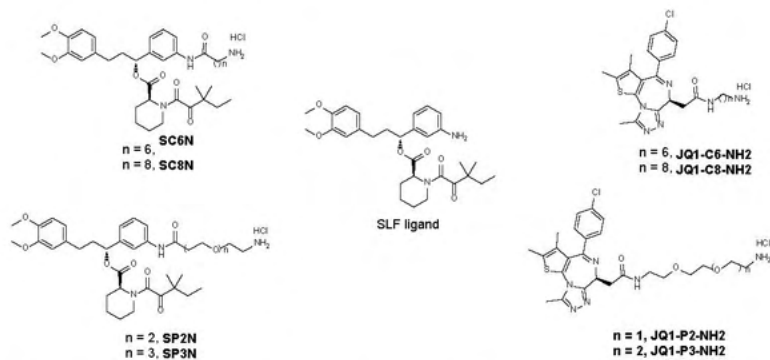
### Supplementary Methods

#### Chemistry

#### General Information

All starting materials, solvents, and reagents used were purchased from commercial sources unless stated otherwise, with no further purification. Reactions were monitored by thin-layer chromatography (TLC) using pre-coated silica gel plates F-254 and visualized using UV light and/or ninhydrin. Proton nuclear magnetic resonance ( $^1\text{H}$  NMR) spectra and carbon nuclear magnetic resonance ( $^{13}\text{C}$  NMR) spectra were recorded on Bruker AV III 600, AV NEO 600 and AV III HD 700 instruments from the NMR Facility of the University of Vienna. Chemical shifts ( $\delta$ ) are expressed in parts per million (ppm). Data for  $^1\text{H}$  NMR were denoted as follows: chemical shift, multiplicity (s, singlet; d, doublet; dd, doublet of doublets; t, triplet; m, multiplet; bs, broad singlet) coupling constant ( $J$ ) in Hertz (Hz) and integration. Data for both  $^1\text{H}$  and  $^{13}\text{C}$  NMR spectra were referenced to the corresponding deuterated solvent. Column chromatography was carried out using Biotage Selekt over Biotage Sfar Silica D column cartridges employing Merck silica gel (Kieselgel 60, 63-200  $\mu\text{m}$ ). Low resolution mass determinations MS were performed using electrospray ionization (ESI) on Bruker amaZon speed ETD while HR-MS (ESI-TOF) analyses were performed on Bruker timsTOF flex at the MS Facility of the University of Vienna.

**SC6N, SC8N, SP2N, SP3N, JQ1-C6-NH2, JQ1-C8-NH2, JQ1-P2-NH2, JQ1-P3-NH2, JQ1-P4-NH2** and **SLF ligand** were provided by WuXi App Tech:



- 1
- 2 **(R)-1-(3-(7-aminoheptanamido)phenyl)-3-(3,4-dimethoxyphenyl)propyl (S)-1-(3,3-dimethyl-2-**  
3 **oxopentanoyl)piperidine-2-carboxylate (SC6N).** <sup>1</sup>H NMR (700 MHz, CDCl<sub>3</sub>) δ 8.89 (bs, 1H), 8.16 (bs, 3H), 7.66 – 7.59 (m, 2H), 7.24 (t, *J* = 8.0 Hz, 1H), 6.99 (d, *J* = 7.4 Hz, 1H), 6.77 – 6.74 (m, 1H), 6.69 –  
4 6.63 (m, 2H), 5.77 (dd, *J* = 7.9, 5.4 Hz, 1H), 5.31 – 5.27 (m, 1H), 3.84 (s, 3H), 3.82 (s, 3H), 3.36 – 3.30  
5 (m, 1H), 3.19 – 3.12 (m, 1H), 3.01 – 2.94 (m, 2H), 2.76 – 2.63 (m, 2H), 2.63 – 2.55 (m, 1H), 2.55 – 2.49  
6 (m, 1H), 2.39 – 2.32 (m, 3H), 2.25 – 2.18 (m, 1H), 2.10 – 2.02 (m, 1H), 1.78 – 1.61 (m, 7H), 1.49 – 1.38  
7 (m, 3H), 1.38 – 1.28 (m, 3H), 1.21 (s, 3H), 1.20 (s, 3H), 0.87 (t, *J* = 7.5 Hz, 3H). <sup>13</sup>C NMR (176 MHz,  
8 CDCl<sub>3</sub>) δ 208.4, 172.5, 169.6, 167.2, 148.8, 147.3, 140.7, 138.8, 133.5, 129.1, 121.6, 120.2, 119.5,  
9 117.6, 111.8, 111.3, 77.2, 67.1, 55.9, 55.8, 51.3, 46.7, 44.3, 40.0, 38.8, 38.3, 36.8, 32.5, 31.2, 27.9,  
10 26.8, 26.3, 25.5, 24.9, 23.3, 21.0, 8.7. HRMS (ESI) (*m/z*) [*M*+*H*]<sup>+</sup> C<sub>37</sub>H<sub>54</sub>N<sub>3</sub>O<sub>7</sub> calc. 652.3956, found  
11 652.3960.  
12
- 13 **(R)-1-(3-(9-aminononanamido)phenyl)-3-(3,4-dimethoxyphenyl)propyl (S)-1-(3,3-dimethyl-2-**  
14 **oxopentanoyl)piperidine-2-carboxylate (SC8N).** <sup>1</sup>H NMR (700 MHz, CDCl<sub>3</sub>) δ 8.80 (bs, 1H), 8.13  
15 (bs, 3H), 7.69 – 7.64 (m, 1H), 7.60 – 7.55 (m, 1H), 7.26 (t, *J* = 7.9 Hz, 2H), 7.00 (t, *J* = 7.6 Hz, 1H), 6.77  
16 – 6.74 (m, 1H), 6.68 – 6.63 (m, 2H), 5.78 (dd, *J* = 7.9, 5.5 Hz, 1H), 5.31 – 5.27 (m, 1H), 3.84 (s, 3H),  
17 3.83 (s, 3H), 3.35 – 3.29 (m, 1H), 3.29 – 3.21 (m, 2H), 3.15 – 3.09 (m, 1H), 3.00 – 2.93 (m, 2H), 2.62 –  
18 2.49 (m, 2H), 2.43 – 2.32 (m, 3H), 2.25 – 2.17 (m, 1H), 2.09 – 2.02 (m, 1H), 1.77 – 1.60 (m, 7H), 1.48  
19 – 1.42 (m, 1H), 1.40 – 1.25 (m, 8H), 1.21 (s, 6H), 0.88 (t, *J* = 7.5 Hz, 3H). <sup>13</sup>C NMR (176 MHz, CDCl<sub>3</sub>)  
20 δ 208.6, 172.7, 169.5, 167.1, 148.8, 147.3, 140.7, 138.7, 133.5, 129.2, 121.8, 120.2, 119.5, 117.6, 111.7,  
21 111.3, 76.7, 55.9, 55.8, 51.3, 46.8, 44.2, 40.0, 38.2, 37.3, 32.5, 31.1, 28.7, 28.5, 28.3, 27.2, 26.2, 26.0,  
22 25.5, 24.9, 23.3, 23.3, 21.0, 8.7. HRMS (ESI) (*m/z*) [*M*+*H*]<sup>+</sup> C<sub>39</sub>H<sub>58</sub>N<sub>3</sub>O<sub>7</sub> calc. 680.4269, found  
23 680.4262.
- 24 **(R)-1-(3-(3-(2-(2-aminoethoxy)ethoxy)propanamido)phenyl)-3-(3,4-dimethoxyphenyl)propyl (S)-**  
25 **1-(3,3-dimethyl-2-oxopentanoyl)piperidine-2-carboxylate (SP2N).** <sup>1</sup>H NMR (700 MHz, CDCl<sub>3</sub>) δ  
26 9.40 (bs, 1H), 7.95 (bs, 3H), 7.74 (s, 1H), 7.68 (d, *J* = 7.9 Hz, 1H), 7.26 (t, *J* = 67.9 Hz, 1H), 7.00 (d, *J* =  
27 7.7 Hz, 1H), 6.79 – 6.74 (m, 1H), 6.70 – 6.63 (m, 2H), 5.73 (dd, *J* = 8.3, 5.2 Hz, 1H), 5.29 – 5.26 (m,  
28 1H), 3.85 (s, 3H), 3.83 (s, 3H), 3.73 – 3.66 (m, 2H), 3.62 – 3.56 (m, 4H), 3.36 – 3.29 (m, 1H), 3.24 –  
29 3.16 (m, 1H), 3.12 – 3.05 (m, 2H), 2.76 – 2.67 (m, 2H), 2.66 – 2.49 (m, 4H), 2.43 – 2.34 (m, 1H), 2.28  
30 – 2.17 (m, 1H), 2.11 – 2.02 (m, 1H), 1.80 – 1.57 (m, 5H), 1.51 – 1.42 (m, 1H), 1.42 – 1.32 (m, 1H), 1.19  
31 (s, 3H), 1.18 (s, 3H), 0.85 (t, *J* = 7.5 Hz, 3H). <sup>13</sup>C NMR (176 MHz, CDCl<sub>3</sub>) δ 208.2, 170.2, 169.8, 167.4,  
32 148.8, 147.3, 140.7, 138.9, 133.5, 129.2, 121.7, 120.2, 119.5, 117.6, 111.7, 111.3, 77.1, 70.2, 69.8, 67.3,  
33 66.3, 55.9, 55.8, 51.5, 46.7, 44.2, 39.6, 38.2, 37.6, 32.4, 31.3, 26.4, 24.9, 23.3, 23.1, 21.1, 8.7. HRMS  
34 (ESI) (*m/z*) [*M*+*H*]<sup>+</sup> C<sub>37</sub>H<sub>54</sub>N<sub>3</sub>O<sub>9</sub> calc. 684.3855, found 684.3846.
- 35 **(R)-1-(3-(3-(2-(2-aminoethoxy)ethoxy)ethoxy)propanamido)phenyl)-3-(3,4-**  
36 **dimethoxyphenyl)propyl (S)-1-(3,3-dimethyl-2-oxopentanoyl)piperidine-2-carboxylate (SP3N).**  
37 <sup>1</sup>H NMR (700 MHz, CDCl<sub>3</sub>) δ 9.57 (bs, 1H), 7.93 (bs, 3H), 7.76 (s, 1H), 7.69 (d, *J* = 7.8 Hz, 1H), 7.26 (t,  
38 *J* = 7.9 Hz, 1H), 7.01 (d, *J* = 7.5 Hz, 1H), 6.79 – 6.75 (m, 1H), 6.70 – 6.64 (m, 2H), 5.75 (dd, *J* = 8.2,  
39 5.3 Hz, 1H), 5.33 – 5.29 (m, 1H), 3.85 (s, 3H), 3.84 (s, 3H), 3.75 – 3.71 (m, 2H), 3.64 – 3.60 (m, 6H),  
40 3.58 – 3.54 (m, 2H), 3.37 – 3.32 (m, 1H), 3.22 – 3.17 (m, 1H), 3.10 – 3.03 (m, 2H), 2.84 – 2.77 (m, 2H),  
41 2.64 – 2.58 (m, 1H), 2.58 – 2.51 (m, 1H), 2.44 – 2.34 (m, 3H), 2.26 – 2.19 (m, 1H), 2.11 – 2.03 (m, 1H),  
42 1.80 – 1.59 (m, 5H), 1.53 – 1.43 (m, 1H), 1.43 – 1.32 (m, 2H), 1.21 (s, 3H), 1.20 (s, 3H), 0.87 (t, *J* = 7.5



1 Hz, 3H). <sup>13</sup>C NMR (176 MHz, CDCl<sub>3</sub>) δ 208.2, 170.5, 169.6, 167.3, 148.8, 147.3, 140.7, 138.9, 133.5,  
2 129.1, 121.7, 120.2, 119.5, 117.6, 111.7, 111.3, 76.9, 70.1, 69.9 (2C), 69.6, 67.3, 66.6, 55.9, 55.8, 51.5,  
3 46.7, 44.2, 39.8, 38.3, 37.7, 32.4, 31.3, 26.4, 24.9, 23.4, 23.2, 21.1, 8.7. HRMS (ESI) (m/z) [M+H]<sup>+</sup>  
4 C<sub>39</sub>H<sub>58</sub>N<sub>3</sub>O<sub>10</sub> calc. 728.4117, found 728.4102.

5 **(S)-N-(6-aminohexyl)-2-(4-(4-chlorophenyl)-2,3,9-trimethyl-6H-thieno[3,2-f][1,2,4]triazolo[4,3-  
6 a][1,4]diazepin-6-yl)acetamide (JQ1-C6-NH<sub>2</sub>)**. <sup>1</sup>H NMR (700 MHz, CDCl<sub>3</sub>) δ 8.14 (bs, 3H), 8.06 (bs,  
7 1H), 7.53 – 7.43 (m, 2H), 7.36 – 7.33 (m, 2H), 4.84 (t, J = 7.0 Hz, 1H), 3.67 – 3.59 (m, 1H), 3.58 – 3.50  
8 (m, 1H), 3.36 – 3.29 (m, 1H), 3.20 – 3.13 (m, 1H), 2.98 – 2.90 (m, 2H), 2.85 (s, 3H), 2.41 (s, 3H), 1.76  
9 – 1.68 (m, 2H), 1.63 (s, 3H), 1.57 – 1.49 (m, 2H), 1.43 – 1.32 (m, 4H). <sup>13</sup>C NMR (176 MHz, CDCl<sub>3</sub>) δ  
10 169.6, 165.9, 154.7, 151.0, 138.1, 134.4, 133.1, 131.9, 131.6, 131.0, 130.4, 128.9, 53.3, 39.5, 39.1,  
11 36.9, 28.3, 26.7, 25.6, 25.4, 14.4, 13.3, 11.9. HRMS (ESI) (m/z) [M+H]<sup>+</sup> C<sub>25</sub>H<sub>32</sub>CIN<sub>6</sub>OS, calc.  
12 499.2041, found 499.2050.

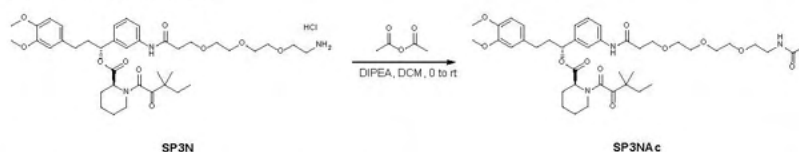
13 **(S)-N-(8-amino-octyl)-2-(4-(4-chlorophenyl)-2,3,9-trimethyl-6H-thieno[3,2-f][1,2,4]triazolo[4,3-  
14 a][1,4]diazepin-6-yl)acetamide (JQ1-C8-NH<sub>2</sub>)**. <sup>1</sup>H NMR (600 MHz, CDCl<sub>3</sub>) δ 8.09 (bs, 3H), 7.90 (bs,  
15 1H), 7.55 – 7.46 (m, 2H), 7.39 – 7.34 (m, 2H), 4.87 (t, J = 7.0 Hz, 1H), 3.68 – 3.56 (m, 2H), 3.31 – 3.22  
16 (m, 2H), 2.92 – 2.86 (m, 2H), 2.82 (s, 3H), 2.41 (s, 3H), 1.72 – 1.64 (m, 2H), 1.63 (s, 3H), 1.56 – 1.49  
17 (m, 2H), 1.39 – 1.33 (m, 4H), 1.32 – 1.28 (m, 4H). <sup>13</sup>C NMR (151 MHz, CDCl<sub>3</sub>) δ 169.4, 166.5, 154.4,  
18 151.1, 138.6, 133.7, 133.1, 132.8, 131.7, 131.4, 129.7, 128.9, 53.1, 39.9, 39.4, 36.4, 28.7, 27.9, 27.9,  
19 26.7, 25.9, 25.4, 14.4, 13.2, 11.8. HRMS (ESI) (m/z) [M+H]<sup>+</sup> C<sub>27</sub>H<sub>36</sub>CIN<sub>6</sub>OS, calc. 527.2354, found  
20 527.2349.

21 **(S)-N-(2-(2-(2-aminoethoxy)ethoxy)ethyl)-2-(4-(4-chlorophenyl)-2,3,9-trimethyl-6H-thieno[3,2-  
22 f][1,2,4]triazolo[4,3-a][1,4]diazepin-6-yl)acetamide (JQ1-P2-NH<sub>2</sub>)**. <sup>1</sup>H NMR (600 MHz, CDCl<sub>3</sub>) δ 8.51  
23 (bs, 1H), 8.09 (s, 3H), 7.64 – 7.57 (m, 2H), 7.40 – 7.37 (m, 2H), 5.12 – 5.06 (m, 1H), 3.82 – 3.61 (m,  
24 9H), 3.53 – 3.43 (m, 3H), 3.19 – 3.10 (m, 2H), 3.00 (s, 3H), 2.42 (s, 3H), 1.60 (s, 3H). <sup>13</sup>C NMR (151  
25 MHz, CDCl<sub>3</sub>) δ 169.4, 167.0, 153.8, 152.2, 140.9, 139.8, 135.6, 134.6, 133.5, 132.4, 131.3, 129.0, 70.0  
26 (2C), 69.5, 66.5, 52.3, 39.8, 39.6, 34.8, 14.4, 13.4, 12.1. HRMS (ESI) (m/z) [M+H]<sup>+</sup> C<sub>25</sub>H<sub>32</sub>CIN<sub>6</sub>O<sub>3</sub>S,  
27 calc. 531.1940, found 531.1950.

28 **(S)-N-(2-(2-(2-(2-aminoethoxy)ethoxy)ethoxy)ethyl)-2-(4-(4-chlorophenyl)-2,3,9-trimethyl-6H-  
29 thieno[3,2-f][1,2,4]triazolo[4,3-a][1,4]diazepin-6-yl)acetamide (JQ1-P3-NH<sub>2</sub>)**. <sup>1</sup>H NMR (600 MHz,  
30 CDCl<sub>3</sub>) δ 8.56 (bs, 1H), 8.12 (bs, 3H), 7.70 – 7.58 (m, 2H), 7.44 – 7.35 (m, 2H), 5.21 – 5.08 (m, 1H),  
31 3.91 – 3.82 (m, 1H), 3.81 – 3.70 (m, 3H), 3.70 – 3.59 (m, 10H), 3.56 – 3.40 (m, 2H), 3.12 – 3.03 (m,  
32 2H), 2.98 (s, 3H), 2.42 (s, 3H), 1.57 (s, 3H). <sup>13</sup>C NMR (151 MHz, CDCl<sub>3</sub>) δ 169.2, 166.9, 153.6, 152.6,  
33 140.6, 135.2, 134.6, 133.1, 132.8, 130.6, 129.2, 128.4, 70.5, 70.2, 69.8 (2C), 69.7, 66.6, 52.1, 39.8,  
34 39.6, 34.2, 14.7, 13.6, 12.2. HRMS (ESI) (m/z) [M+H]<sup>+</sup> C<sub>27</sub>H<sub>36</sub>CIN<sub>6</sub>O<sub>4</sub>S calc. 575.2202, found  
35 575.2213.

36 **(S)-N-(14-amino-3,6,9,12-tetraoxatetradecyl)-2-(4-(4-chlorophenyl)-2,3,9-trimethyl-6H-thieno[3,2-  
37 f][1,2,4]triazolo[4,3-a][1,4]diazepin-6-yl)acetamide (JQ1-P4-NH<sub>2</sub>)**. <sup>1</sup>H NMR (600 MHz, CDCl<sub>3</sub>) δ 8.68  
38 (bs, 1H), 7.97 (bs, 3H), 7.65 – 7.56 (m, 2H), 7.40 – 7.32 (m, 2H), 5.35 – 5.27 (m, 1H), 3.92 – 3.85 (m,  
39 1H), 3.85 – 3.75 (m, 3H), 3.71 – 3.59 (m, 14H), 3.58 – 3.48 (m, 1H), 3.46 – 3.38 (m, 1H), 3.16 – 3.05  
40 (m, 5H), 2.42 (s, 3H), 1.49 (s, 3H). <sup>13</sup>C NMR (151 MHz, CDCl<sub>3</sub>) δ 168.8, 167.0, 153.2, 153.0, 141.0,  
41 135.5, 135.2, 133.6, 133.1, 129.0, 128.8, 127.7, 70.2, 70.1, 70.1, 70.0, 70.0, 69.9, 69.8, 66.8, 51.4,  
42 40.0, 39.3, 33.2, 14.3, 13.5, 12.3. HRMS (ESI) (m/z) [M+H]<sup>+</sup> C<sub>29</sub>H<sub>40</sub>CIN<sub>6</sub>O<sub>5</sub>S calc. 619.2464, found  
43 619.2460.

#### 44 Synthesis of SP3NAc

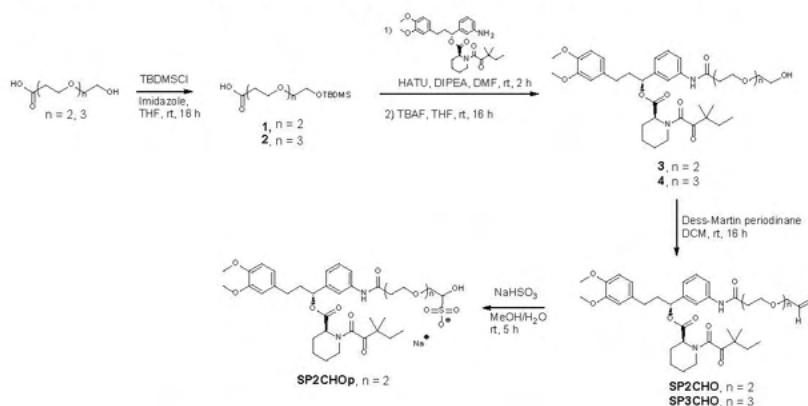


45  
46 To a solution of **SP3N** hydrochloride salt (20 mg, 0.026 mmol) in dichloromethane (0.5 mL), acetic  
47 anhydride (3.7 μL, 1.5 eq) is added at 0 °C and the reaction stirred at room temperature for 1 h until no  
48 starting material is observed. The mixture is diluted with dichloromethane and washed with water, 1.0  
49 N HCl and brine. The organic layer is dried over anhydrous Na<sub>2</sub>SO<sub>4</sub>, filtered and concentrated under

1 reduced pressure. The desired compound is purified by flash-chromatography using  
2 dichloromethane/methanol.

3 **(R)-3-(3,4-dimethoxyphenyl)-1-(3-(2-oxo-6,9,12-trioxa-3-azapentadecan-15-amido)phenyl)propyl**  
4 **(S)-1-(3,3-dimethyl-2-oxopentanoyl)piperidine-2-carboxylate (SP3NAC)**. 12 mg. 60%. White  
5 powder. <sup>1</sup>H NMR (600 MHz, CDCl<sub>3</sub>) δ 8.65 (bs, 1H), 7.58 (bs, 1H), 7.57 – 7.53 (m, 1H), 7.28 (t, *J* = 7.8  
6 Hz, 1H), 7.03 (d, *J* = 7.5 Hz, 1H), 6.80 – 6.74 (m, 1H), 6.72 – 6.64 (m, 2H), 6.19 (s, 1H), 5.78 (dd, *J* =  
7 8.0, 5.5 Hz, 1H), 5.32 – 5.29 (m, 1H), 3.88 – 3.82 (m, 8H), 3.72 – 3.66 (m, 4H), 3.65 – 3.61 (m, 2H),  
8 3.58 – 3.54 (m, 2H), 3.48 (t, *J* = 5.1 Hz, 2H), 3.40 – 3.31 (m, 3H), 3.21 – 3.11 (m, 1H), 2.65 (t, *J* = 5.8  
9 Hz, 2H), 2.62 – 2.57 (m, 1H), 2.57 – 2.49 (m, 1H), 2.38 – 2.33 (m, 1H), 2.29 – 2.19 (m, 1H), 2.10 – 2.03  
10 (m, 1H), 1.94 (s, 3H), 1.78 – 1.59 (m, 5H), 1.51 – 1.42 (m, 1H), 1.41 – 1.31 (m, 2H), 1.23 (s, 2H), 1.22  
11 (s, 3H), 0.89 (t, *J* = 7.5 Hz, 3H). <sup>13</sup>C NMR (176 MHz, CDCl<sub>3</sub>) δ 208.4, 170.5, 170.0, 169.7, 167.3, 149.0,  
12 147.4, 140.9, 138.8, 133.6, 129.2, 122.0, 120.3, 119.7, 117.9, 111.9, 111.4, 76.8, 70.6, 70.4 (2C), 70.2,  
13 69.9, 67.2, 56.1, 56.0, 51.4, 46.9, 44.3, 39.5, 38.3, 38.1, 32.6, 31.3, 26.5, 25.1, 23.5, 23.4, 23.3, 21.2,  
14 8.9. HRMS (ESI) (*m/z*) [*M*+Na]<sup>+</sup> C<sub>41</sub>H<sub>59</sub>N<sub>3</sub>O<sub>11</sub> calc. 792.4042, found 792.4035.

15 **Synthesis of aldehydes SP2CHO-SP3CHO and protected aldehyde SP2CHOp.**



16

17 **Synthesis of carboxylic acids 1-2**

18 To a solution of hydroxy carboxylic acid (100 mg) in THF (0.5 M), imidazole (1.4 eq.) is added and stirred  
19 for 30 min at room temperature. TBDMSCl (1.4 eq.) is added and the reaction stirred at room  
20 temperature for 16 h until no starting material is observed. The mixture is diluted with ethyl acetate and  
21 washed with water and brine. The organic layer is dried over anhydrous Na<sub>2</sub>SO<sub>4</sub>, filtered, and  
22 concentrated under reduced pressure. The resulting compounds are used for the next step without  
23 further purification.

24 **2,2,3,3-tetramethyl-4,7,10-trioxa-3-silatridecan-13-oic acid (1)**. 120 mg. 87%. Colorless oil. <sup>1</sup>H NMR  
25 (600 MHz, CDCl<sub>3</sub>) δ 3.75 (t, *J* = 5.2 Hz, 2H), 3.67 – 3.63 (m, 4H), 3.62 – 3.59 (m, 2H), 3.56 (d, *J* = 5.1  
26 Hz, 2H), 2.58 (t, *J* = 3.4 Hz, 2H), 0.87 (s, 9H), 0.05 (s, 6H). <sup>13</sup>C NMR (151 MHz, CDCl<sub>3</sub>) δ 177.2, 70.2,  
27 69.8, 67.3, 66.3, 62.6, 36.8, 25.9, 18.1, -4.7, -4.8. MS (ESI) (*m/z*) [*M*-H]<sup>-</sup> C<sub>13</sub>H<sub>27</sub>O<sub>5</sub>Si calc. 291.17,  
28 found 291.16.

29 **2,2,3,3-tetramethyl-4,7,10,13-tetraoxa-3-silahexadecan-16-oic acid (2)**. 150 mg. 99%. Colorless oil.  
30 <sup>1</sup>H NMR (600 MHz, CDCl<sub>3</sub>) δ 3.80 (t, *J* = 5.2 Hz, 2H), 3.72 – 3.68 (m, 2H), 3.67 – 3.60 (m, 8H), 3.56 (t,  
31 *J* = 5.1 Hz, 2H), 2.63 (t, *J* = 3.4 Hz, 2H), 0.89 (s, 9H), 0.07 (s, 6H). MS (ESI) (*m/z*) [*M*-H]<sup>-</sup> C<sub>15</sub>H<sub>31</sub>O<sub>6</sub>Si  
32 calc. 335.20, found 335.19.

33 **Synthesis of alcohols 3-4.**

34 A mixture of carboxylic acids 1 or 2 (1.4 eq.), SLF ligand (1.0 eq.), HATU (1.9 eq.) and DIPEA (1.0 eq.)  
35 in DMF (0.5 M) is stirred at room temperature until completion for 2 hours. The reaction is diluted with  
36 ethyl acetate and washed with water, sat. NH<sub>4</sub>Cl and brine. The organic layer is dried over anhydrous  
37 Na<sub>2</sub>SO<sub>4</sub>, filtered and concentrated under reduced pressure. After purification by flash chromatography  
38 using hexane/ethyl acetate the resulting compound is dissolved in THF (0.2 M) and 1.0 M solution of

11



1 TBAF in THF (1.5 eq) is added dropwise at 0 °C. The reaction is allowed to warm to room temperature  
2 and stirred for 16 hours until no starting material is observed. The reaction is quenched with water and  
3 extracted with ethyl acetate. Organic layer is dried over Na<sub>2</sub>SO<sub>4</sub>, filtered and concentrated under  
4 reduced pressure. Desired compounds are used for the next step without further purification.

5 **(R)-3-(3,4-dimethoxyphenyl)-1-(3-(3-(2-(2-hydroxyethoxy)ethoxy)propanamido)phenyl)propyl**  
6 **(S)-1-(3,3-dimethyl-2-oxopentanoyl)piperidine-2-carboxylate (3)**. Yellow oil. <sup>1</sup>H NMR (600 MHz,  
7 CDCl<sub>3</sub>) δ 8.61 (bs, 1H), 7.63 (d, *J* = 8.0 Hz, 1H), 7.51 (s, 1H), 7.30 (t, *J* = 7.9 Hz, 1H), 7.04 (d, *J* = 7.6  
8 Hz, 1H), 6.80 – 6.75 (m, 1H), 6.70 – 6.64 (m, 2H), 5.78 (dd, *J* = 7.9, 5.6 Hz, 1H), 5.33 – 5.30 (m, 1H),  
9 3.87 – 3.82 (m, 8H), 3.72 – 3.66 (m, 6H), 3.63 – 3.58 (m, 2H), 3.38 – 3.31 (m, 1H), 3.18 – 3.11 (m, 1H),  
10 2.66 (t, *J* = 5.5 Hz, 2H), 2.63 – 2.57 (m, 1H), 2.57 – 2.50 (m, 1H), 2.39 – 2.33 (m, 1H), 2.28 – 2.20 (m,  
11 1H), 2.09 – 2.04 (m, 1H), 1.76 – 1.60 (m, 5H), 1.52 – 1.42 (m, 1H), 1.41 – 1.32 (m, 1H), 1.23 (s, 3H),  
12 1.22 (s, 3H), 0.89 (t, *J* = 7.5 Hz, 3H). <sup>13</sup>C NMR (176 MHz, CDCl<sub>3</sub>) δ 208.2, 170.2, 169.7, 167.3, 148.8,  
13 147.3, 140.7, 138.9, 133.5, 129.1, 121.6, 120.2, 119.5, 117.7, 111.7, 111.3, 77.1, 70.0, 69.2, 67.3, 66.3,  
14 60.3, 55.9, 55.8, 51.5, 46.7, 44.2, 38.3, 37.4, 32.4, 31.3, 26.4, 24.9, 23.3, 23.1, 21.1, 8.7. MS (ESI) (m/z) [M+Na]<sup>+</sup> C<sub>37</sub>H<sub>52</sub>N<sub>2</sub>O<sub>10</sub> calc. 707.36, found 707.48.

16 **(R)-3-(3,4-dimethoxyphenyl)-1-(3-(3-(2-(2-**  
17 **hydroxyethoxy)ethoxy)ethoxy)propanamido)phenyl)propyl** **(S)-1-(3,3-dimethyl-2-**  
18 **oxopentanoyl)piperidine-2-carboxylate (4)**. Yellow oil. <sup>1</sup>H NMR (600 MHz, CDCl<sub>3</sub>) δ 8.81 (bs, 1H),  
19 7.63 (s, 1H), 7.52 (d, *J* = 8.0 Hz, 1H), 7.28 (t, *J* = 7.8 Hz, 1H), 7.03 (d, *J* = 7.8 Hz, 1H), 6.79 – 6.75 (m,  
20 1H), 6.71 – 6.64 (m, 2H), 5.78 (dd, *J* = 8.0, 5.6 Hz, 1H), 5.32 – 5.29 (m, 1H), 3.85 (s, 3H), 3.84 (s, 3H),  
21 3.82 (t, *J* = 5.5 Hz, 2H), 3.71 – 3.68 (m, 2H), 3.68 – 3.66 (m, 4H), 3.65 – 3.61 (m, 4H), 3.58 – 3.56 (m,  
22 2H), 3.38 – 3.31 (m, 1H), 3.18 – 3.14 (m, 1H), 2.64 (t, *J* = 5.8 Hz, 2H), 2.62 – 2.57 (m, 1H), 2.57 – 2.48  
23 (m, 1H), 2.39 – 2.32 (m, 1H), 2.29 – 2.20 (m, 1H), 2.11 – 2.03 (m, 1H), 1.77 – 1.64 (m, 5H), 1.49 – 1.44  
24 (m, 1H), 1.38 – 1.32 (m, 1H), 1.23 (s, 3H), 1.21 (s, 3H), 0.89 (t, *J* = 7.4 Hz, 3H). <sup>13</sup>C NMR (176 MHz,  
25 CDCl<sub>3</sub>) δ 208.2, 170.1, 169.6, 167.2, 148.8, 147.3, 140.7, 138.8, 133.5, 129.1, 121.8, 120.2, 119.6,  
26 117.7, 111.7, 111.3, 76.8, 69.9 (2C), 69.6, 68.7, 67.3, 66.6, 60.2, 55.9, 55.8, 51.5, 46.7, 44.2, 38.3, 37.9,  
27 32.4, 31.3, 26.4, 24.9, 23.4, 23.2, 21.1, 8.7. MS (ESI) (m/z) [M+Na]<sup>+</sup> C<sub>39</sub>H<sub>56</sub>N<sub>2</sub>O<sub>11</sub> calc. 751.38, found  
28 751.50.

#### 29 Synthesis of aldehydes **SP2CHO** and **SP3CHO**

30 To a solution of alcohols **3** or **4** (1.0 eq) in dichloromethane (0.1 M), Dess Martin periodinane (1.2 eq.)  
31 is added portion wise at room temperature. The reaction slowly turns red and is stirred until no alcohol  
32 is observed in TLC (around 2-3 h). 1 mL of 10% Na<sub>2</sub>S<sub>2</sub>O<sub>3</sub> is added and stirred for 30 minutes, followed  
33 by dilution with dichloromethane and separation of layer. Organic layer is washed with water and brine,  
34 dried over Na<sub>2</sub>SO<sub>4</sub>, filtered and concentrated under reduced pressure. Desired compounds are purified  
35 by flash chromatography using ethyl acetate/methanol as solvents. Since **SP2CHO** was not pure  
36 enough according to NMR, we proceed to its transformation into the corresponding hydroxysulfonate  
37 sodium salt.

38 **(R)-3-(3,4-dimethoxyphenyl)-1-(3-(3-(2-(2-oxoethoxy)ethoxy)propanamido)phenyl)propyl** **(S)-1-**  
39 **(3,3-dimethyl-2-oxopentanoyl)piperidine-2-carboxylate (SP2CHO)**. 50 mg. 85%. Dark yellow oil. <sup>1</sup>H  
40 NMR (600 MHz, CDCl<sub>3</sub>) δ 9.65 (bs, 1H), 8.51 (bs, 1H), 7.59 (d, 1H), 7.51 (s, 1H), 7.29 (t, *J* = 8.0 Hz  
41 1H), 7.03 (d, *J* = 7.7 Hz, 1H), 6.79 – 6.76 (m, 1H), 6.69 – 6.66 (m, 2H), 5.76 (dd, *J* = 8.0, 5.0 Hz, 1H),  
42 5.33 – 5.30 (m, 1H), 4.16 (d, *J* = 2.9 Hz, 2H), 3.88 – 3.80 (m, 8H), 3.77 – 3.74 (m, 2H), 3.73 – 3.68 (m,  
43 2H), 3.36 – 3.31 (m, 1H), 3.17 – 3.10 (m, 1H), 2.66 (t, *J* = 5.6 Hz, 2H), 2.64 – 2.56 (m, 1H), 2.56 – 2.51  
44 (m, 1H), 2.38 – 2.32 (m, 1H), 2.27 – 2.19 (m, 1H), 2.09 – 2.02 (m, 1H), 1.77 – 1.58 (m, 5H), 1.48 – 1.42  
45 (m, 1H), 1.41 – 1.31 (m, 1H), 1.23 (s, 3H), 1.22 (s, 3H), 0.89 (t, *J* = 7.5 Hz, 3H). MS (ESI) (m/z) [M+Na]<sup>+</sup>  
46 C<sub>37</sub>H<sub>50</sub>N<sub>2</sub>O<sub>10</sub> calc. 705.33, found 705.50.

47 **(R)-3-(3,4-dimethoxyphenyl)-1-(3-(3-(2-(2-**  
48 **oxoethoxy)ethoxy)ethoxy)propanamido)phenyl)propyl** **(S)-1-(3,3-dimethyl-2-**  
49 **oxopentanoyl)piperidine-2-carboxylate (SP3CHO)**. 26 mg. 42%. Yellow oil. <sup>1</sup>H NMR (600 MHz,  
50 CDCl<sub>3</sub>) δ 9.65 (bs, 1H), 8.64 (bs, 1H), 7.60 (s, 1H), 7.51 (d, *J* = 8.4 Hz, 1H), 7.28 (t, *J* = 7.8 Hz, 1H),  
51 7.04 (d, *J* = 7.5 Hz, 1H), 6.79 – 6.75 (m, 1H), 6.69 – 6.65 (m, 2H), 5.78 (dd, *J* = 8.0, 5.4 Hz, 1H), 5.34  
52 – 5.30 (m, 1H), 4.08 (s, 2H), 3.88 – 3.81 (m, 8H), 3.72 – 3.63 (m, 8H), 3.38 – 3.32 (m, 1H), 3.19 – 3.14  
53 (m, 1H), 2.67 (t, *J* = 5.7 Hz, 2H), 2.62 – 2.57 (m, 1H), 2.57 – 2.51 (m, 1H), 2.39 – 2.33 (m, 1H), 2.26 –  
54 2.20 (m, 1H), 2.10 – 2.06 (m, 1H), 1.77 – 1.61 (m, 5H), 1.51 – 1.42 (m, 1H), 1.41 – 1.33 (m, 1H), 1.23  
55 (s, 3H), 1.22 (s, 3H), 0.89 (t, *J* = 7.5 Hz, 3H). <sup>13</sup>C NMR (176 MHz, CDCl<sub>3</sub>) δ 208.2, 200.8, 169.9, 169.6,  
56 167.1, 148.9, 147.3, 140.7, 138.7, 133.5, 129.1, 121.9, 120.1, 119.6, 117.9, 111.7, 111.3, 76.7, 76.7,

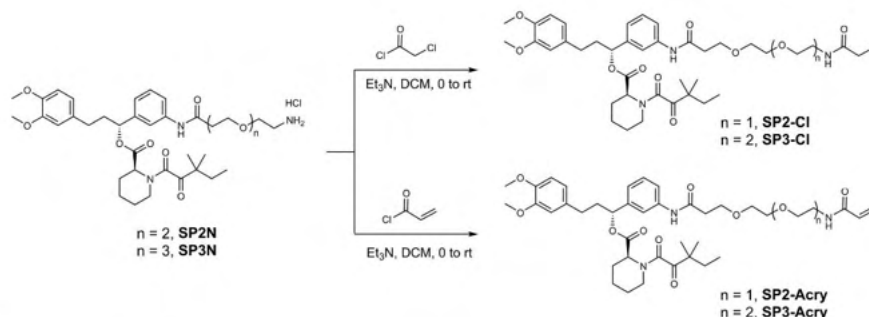
1 71.1, 70.6, 70.4, 70.2, 67.0, 55.9, 55.8, 51.2, 46.7, 44.2, 38.2, 38.0, 32.5, 31.2, 26.3, 25.0, 23.4, 23.2,  
2 21.1, 8.7. HRMS (ESI) (m/z) [M+Na]<sup>+</sup> C<sub>39</sub>H<sub>54</sub>N<sub>2</sub>O<sub>11</sub> calc. 749.3620, found 749.3606.

3 Synthesis of hydroxysulfonate salt **SP2CHOp**.

4 To a solution of **SP2CHO** (50 mg, 0.07 mmol) in methanol (0.14 mL) 0.02 mL of 3.3 M solution of  
5 NaHSO<sub>3</sub> is added dropwise at room temperature. The reaction is stirred for 5 hours until no starting  
6 material is observed by TLC. Solvent is evaporated under reduced pressure and the residue is washed  
7 with diethyl ether and dichloromethane/ether (1:1). The resulting pale-yellow solid is collected and dried.

8 **Sodium 2-(2-(3-((3-(R)-3-(3,4-dimethoxyphenyl)-1-((S)-1-(3,3-dimethyl-2-oxopentano-  
9 oxopentano-1-yl)piperidine-2-carbonyloxy)propyl)phenyl)amino)-3-oxopropoxy)ethoxy)-1-  
10 hydroxyethane-1-sulfonate (SP2CHOp)**. 30 mg, 54%. Pale yellow powder. <sup>1</sup>H NMR (600 MHz,  
11 DMSO) δ 10.01 (s, 1H), 7.75–7.70 (m, 1H), 7.47 (d, J = 7.5 Hz, 1H), 7.29 (t, J = 7.4 Hz, 1H), 7.01 (d, J =  
12 7.8 Hz, 1H), 6.85 (d, J = 8.2 Hz, 1H), 6.80–6.73 (m, 1H), 6.68 (d, J = 7.9 Hz, 1H), 5.63 (dd, J =  
13 8.7, 4.8 Hz, 1H), 5.53–5.46 (m, 1H), 5.17–5.09 (m, 1H), 4.06–3.99 (m, 1H), 3.78 (d, J = 10.0 Hz,  
14 1H), 3.75–3.66 (m, 7H), 3.52–3.26 (m, 6H), 3.19–3.15 (m, 1H), 2.57–2.49 (m, 6H), 2.25–2.19 (m,  
15 1H), 2.14–2.10 (m, 1H), 2.04–1.99 (m, 1H), 1.73–1.54 (m, 5H), 1.37–1.31 (m, 1H), 1.24–1.19 (m,  
16 1H), 1.16 (s, 3H), 1.14 (s, 3H), 0.80 (t, J = 7.4 Hz, 3H). <sup>13</sup>C NMR (176 MHz, CDCl<sub>3</sub>) δ 208.0, 170.1,  
17 169.7, 167.3, 148.8, 147.3, 140.7, 138.9, 133.5, 129.0, 121.5, 120.2, 119.4, 117.7, 111.8, 111.3, 81.7,  
18 77.1, 70.2, 69.5, 67.3, 67.1, 55.9, 55.8, 51.4, 46.7, 44.2, 38.3, 37.3, 32.4, 31.3, 26.5, 24.9, 23.4, 23.1,  
19 21.2, 8.7. HRMS (ESI) (m/z) [M+Na]<sup>+</sup> C<sub>37</sub>H<sub>52</sub>N<sub>2</sub>O<sub>13</sub>S (sulfonic acid) calc. 787.3082, found 787.3087.

20 Synthesis of **SP2-Cl**, **SP2-Acry**, **SP3-Cl** and **SP3-Acry**.



21

22 To a solution of **SP2N** or **SP3N** hydrochloride salt (10–20 mg) in dichloromethane (0.1 M), triethylamine  
23 (2.5 eq) is added at 0 °C and the mixture stirred at 0 °C for 30 min. Corresponding acid chloride (1.2 eq)  
24 is added and the reaction stirred at room temperature for 2–3 h until no starting material is observed.  
25 The mixture is diluted with dichloromethane and washed with water, 1.0 N HCl and brine. The organic  
26 layer is dried over anhydrous Na<sub>2</sub>SO<sub>4</sub>, filtered and concentrated under reduced pressure. The desired  
27 compound is purified by flash-chromatography using dichloromethane/methanol.

28 **(R)-1-(3-(3-(2-(2-(2-chloroacetamido)ethoxy)ethoxy)propanamido)phenyl)-3-(3,4-  
29 dimethoxyphenyl)propyl (S)-1-(3,3-dimethyl-2-oxopentano-1-yl)piperidine-2-carboxylate (SP2-Cl)**.  
30 15 mg, 70%. White powder. <sup>1</sup>H NMR (600 MHz, CDCl<sub>3</sub>) δ 8.53 (bs, 1H), 7.58 (d, J = 8.4 Hz, 1H), 7.52  
31 (s, 1H), 7.29 (t, J = 8.0 Hz, 1H), 7.04 (d, J = 7.6 Hz, 1H), 6.96 (bs, 1H), 6.79–6.75 (m, 1H), 6.70–6.65  
32 (m, 2H), 5.77 (dd, J = 8.0, 5.5 Hz, 1H), 5.33–5.30 (m, 1H), 3.98 (s, 2H), 3.86 (s, 3H), 3.84 (s, 3H), 3.74  
33 –3.65 (m, 6H), 3.59 (t, J = 5.3 Hz, 2H), 3.48–3.44 (m, 2H), 3.37–3.32 (m, 1H), 3.17–3.11 (m, 1H),  
34 2.66 (t, J = 5.7 Hz, 2H), 2.63–2.57 (m, 1H), 2.57–2.51 (m, 1H), 2.38–2.33 (m, 1H), 2.28–2.19 (m,  
35 1H), 2.10–2.03 (m, 1H), 1.77–1.60 (m, 5H), 1.50–1.42 (m, 1H), 1.41–1.33 (m, 1H), 1.23 (s, 3H),  
36 1.22 (s, 3H), 0.89 (t, J = 7.5 Hz, 3H). <sup>13</sup>C NMR (151 MHz, CDCl<sub>3</sub>) δ 207.32, 168.77, 168.65, 166.08,  
37 165.14, 147.86, 146.30, 139.79, 137.59, 132.45, 128.19, 120.89, 119.15, 118.47, 116.81, 110.73,  
38 110.28, 75.62, 69.23, 69.03, 68.38, 65.96, 54.91, 54.83, 50.21, 45.74, 43.22, 41.60, 38.36, 37.15, 36.95,  
39 31.49, 30.15, 25.27, 23.96, 22.36, 22.25, 20.03, 7.75. HRMS (ESI) (m/z) [M+Na]<sup>+</sup> C<sub>39</sub>H<sub>54</sub>CIN<sub>3</sub>O<sub>10</sub>  
40 calc. 782.3390, found 782.3383.

41 **(R)-1-(3-(3-(2-(2-(2-acrylamidoethoxy)ethoxy)propanamido)phenyl)-3-(3,4-dimethoxyphenyl)propyl  
42 (S)-1-(3,3-dimethyl-2-oxopentano-1-yl)piperidine-2-carboxylate (SP2-Acry)**. 12 mg, 58%. White

13

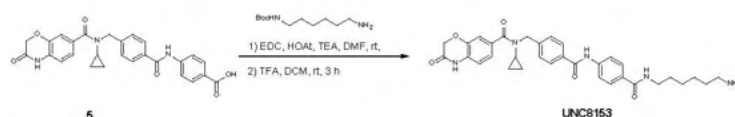
1 powder. <sup>1</sup>H NMR (600 MHz, CDCl<sub>3</sub>) δ 8.61 (bs, 1H), 7.65 (d, *J* = 8.2 Hz, 1H), 7.47 (s, 1H), 7.29 (t, *J* =  
2 8.0 Hz, 1H), 7.03 (d, *J* = 7.7 Hz, 1H), 6.78 – 6.75 (m, 1H), 6.69 – 6.65 (m, 2H), 6.27 (bs, 1H), 6.23 (dd,  
3 *J* = 17.0, 1.5 Hz, 1H), 6.03 (dd, *J* = 17.0, 10.0 Hz, 1H), 5.76 (dd, *J* = 7.9, 5.5 Hz, 1H), 5.56 (dd, *J* = 10.3,  
4 1.5 Hz, 1H), 5.33 – 5.29 (m, 1H), 3.86 (s, 3H), 3.84 (s, 3H), 3.72 (q, *J* = 7.0 Hz, 2H), 3.69 – 3.64 (m,  
5 4H), 3.58 (t, *J* = 5.2 Hz, 2H), 3.51 – 3.43 (m, 2H), 3.38 – 3.31 (m, 1H), 3.18 – 3.09 (m, 1H), 2.65 (t, *J* =  
6 5.7 Hz, 2H), 2.63 – 2.58 (m, 1H), 2.58 – 2.52 (m, 1H), 2.38 – 2.33 (m, 1H), 2.28 – 2.20 (m, 1H), 2.10 –  
7 2.03 (m, 1H), 1.77 – 1.60 (m, 5H), 1.49 – 1.42 (m, 1H), 1.40 – 1.33 (m, 1H), 1.23 (s, 3H), 1.22 (s, 3H),  
8 0.89 (t, *J* = 7.5 Hz, 3H). <sup>13</sup>C NMR (151 MHz, CDCl<sub>3</sub>) δ 207.3, 168.9, 168.7, 166.1, 164.7, 147.9, 146.3,  
9 139.7, 137.6, 132.4, 129.7, 128.2, 125.4, 120.8, 119.2, 118.6, 116.8, 110.7, 110.3, 75.6, 69.2, 68.9,  
10 68.7, 65.8, 54.9, 54.8, 50.2, 45.7, 43.2, 38.0, 37.1, 36.9, 31.5, 30.1, 25.3, 23.9, 22.3, 22.3, 20.0, 7.7.  
11 HRMS (ESI) (*m/z*) [M+Na]<sup>+</sup> C<sub>40</sub>H<sub>55</sub>N<sub>3</sub>O<sub>10</sub> calc. 760.3780, found 760.3769.

12 **(R)-1-(3-(1-chloro-2-oxo-6,9,12-trioxa-3-azapentadecan-15-amido)phenyl)-3-(3,4-**  
13 **dimethoxyphenyl)propyl (S)-1-(3,3-dimethyl-2-oxopentanoyl)piperidine-2-carboxylate (SP3-CI).**  
14 7 mg, 68%. <sup>1</sup>H NMR (600 MHz, CDCl<sub>3</sub>) δ 8.59 (bs, 1H), 7.60 (s, 1H), 7.52 (d, *J* = 8.0 Hz, 1H), 7.29 (t, *J* =  
15 7.8 Hz, 1H), 7.05 (d, *J* = 7.4 Hz, 1H), 6.98 (bs, 1H), 6.81 – 6.75 (m, 1H), 6.75 – 6.62 (m, 2H), 5.78  
16 (dd, *J* = 7.8, 5.6 Hz, 1H), 5.35 – 5.27 (m, 1H), 4.02 (s, 2H), 3.88 – 3.80 (m, 8H), 3.73 – 3.66 (m, 4H),  
17 3.65 – 3.62 (m, 2H), 3.61 – 3.56 (m, 2H), 3.56 – 3.50 (m, 2H), 3.48 – 3.43 (m, 2H), 3.39 – 3.32 (m, 1H),  
18 3.22 – 3.13 (m, 1H), 2.68 – 2.62 (m, 2H), 2.62 – 2.57 (m, 1H), 2.57 – 2.51 (m, 1H), 2.39 – 2.34 (m, 1H),  
19 2.27 – 2.19 (m, 1H), 2.11 – 2.03 (m, 1H), 1.77 – 1.71 (m, 5H), 1.51 – 1.42 (m, 1H), 1.41 – 1.32 (m, 1H),  
20 1.24 (s, 3H), 1.22 (s, 3H), 0.89 (t, *J* = 7.5 Hz, 3H). <sup>13</sup>C NMR (151 MHz, CDCl<sub>3</sub>) δ 208.2, 169.9, 169.6,  
21 167.1, 166.0, 148.9, 147.3, 140.8, 138.7, 133.5, 129.1, 121.9, 120.2, 119.6, 117.9, 111.8, 111.3, 76.7,  
22 70.5, 70.4, 70.3 (2C), 69.3, 67.1, 55.9, 55.8, 51.2, 46.7, 44.2, 42.6, 39.6, 38.2, 38.0, 32.5, 31.2, 26.3,  
23 25.0, 23.4, 23.2, 21.1, 8.7. HRMS (ESI) (*m/z*) [M+Na]<sup>+</sup> C<sub>41</sub>H<sub>58</sub>N<sub>3</sub>O<sub>11</sub> calc. 826.3652, found  
24 826.3660.

25 **(R)-3-(3,4-dimethoxyphenyl)-1-(3-(3-oxo-7,10,13-trioxa-4-aza-hexadec-1-en-16-**  
26 **amido)phenyl)propyl (S)-1-(3,3-dimethyl-2-oxopentanoyl)piperidine-2-carboxylate (SP3-Acry).** 4  
27 mg, 40%. <sup>1</sup>H NMR (600 MHz, CDCl<sub>3</sub>) δ 8.64 (bs, 1H), 7.60 – 7.54 (m, 2H), 7.29 (t, *J* = 7.8 Hz, 1H), 7.04  
28 (d, *J* = 7.7 Hz, 1H), 6.79 – 6.75 (m, 1H), 6.71 – 6.65 (m, 2H), 6.36 (bs, 1H), 6.27 (d, *J* = 17.1 Hz, 1H),  
29 6.09 (dd, *J* = 17.1, 10.3 Hz, 1H), 5.78 (dd, *J* = 8.0, 5.4 Hz, 1H), 5.61 (d, *J* = 10.3 Hz, 1H), 5.33 – 5.29  
30 (m, 1H), 3.88 – 3.82 (m, 8H), 3.72 – 3.66 (m, 4H), 3.66 – 3.61 (m, 2H), 3.60 – 3.55 (m, 2H), 3.53 (t, *J* =  
31 5.2 Hz, 2H), 3.48 – 3.45 (m, 2H), 3.38 – 3.33 (m, 1H), 3.20 – 3.13 (m, 1H), 2.65 (t, *J* = 5.7 Hz, 2H), 2.63  
32 – 2.57 (m, 1H), 2.57 – 2.51 (m, 1H), 2.38 – 2.34 (m, 1H), 2.27 – 2.20 (m, 1H), 2.10 – 2.04 (m, 1H), 1.77  
33 – 1.63 (m, 5H), 1.49 – 1.41 (m, 1H), 1.41 – 1.33 (m, 1H), 1.23 (s, 3H), 1.22 (s, 3H), 0.89 (t, *J* = 7.5 Hz,  
34 3H). <sup>13</sup>C NMR (151 MHz, CDCl<sub>3</sub>) δ 208.2, 169.9, 169.7, 169.6, 167.1, 148.9, 147.3, 140.7, 138.7, 133.5,  
35 130.7, 129.1, 126.6, 121.9, 120.2, 119.6, 117.9, 111.8, 111.3, 76.6, 70.5, 70.3 (2C), 70.1, 69.7, 67.1,  
36 55.9, 55.8, 51.3, 46.7, 44.2, 39.4, 38.2, 37.9, 32.5, 31.2, 26.3, 25.0, 23.4, 23.2, 21.1, 8.7. HRMS (ESI)  
37 (*m/z*) [M+Na]<sup>+</sup> C<sub>42</sub>H<sub>59</sub>N<sub>3</sub>O<sub>11</sub> calc. 804.4042, found 804.4037.

### 38 Synthesis of UNC8153.

39



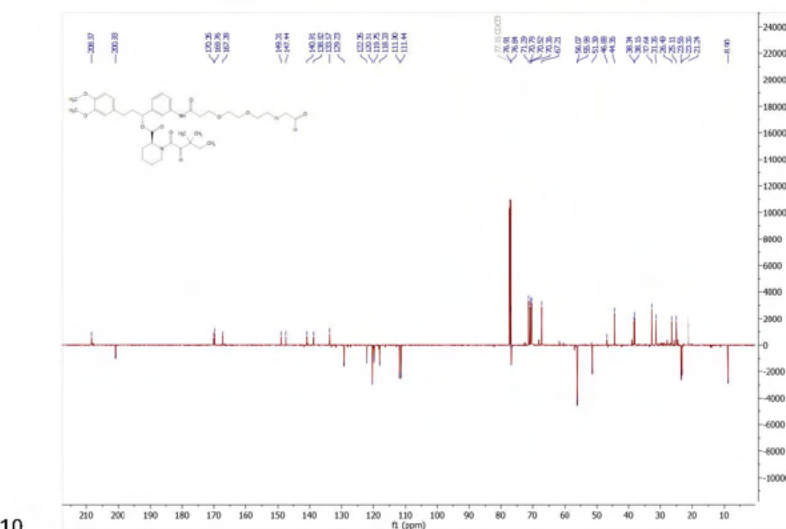
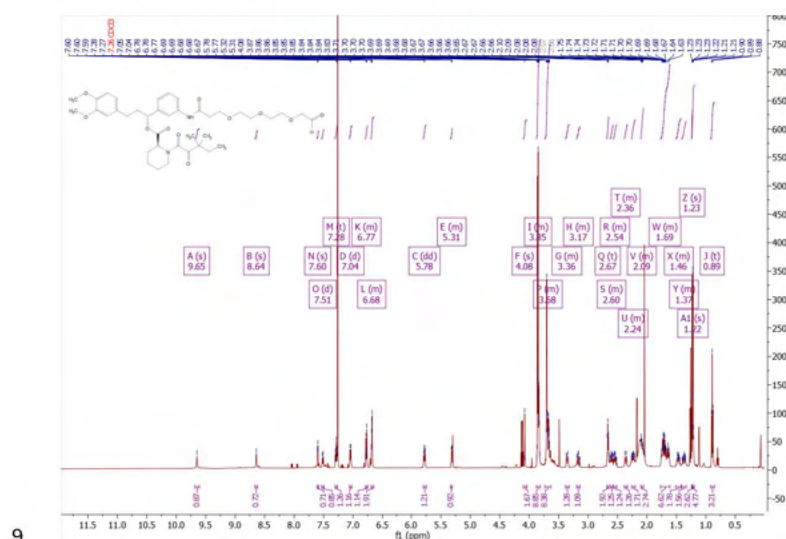
40

41

42 **N-4-((4-((6-aminohexyl)carbamoyl)phenyl)carbamoyl)benzyl)-N-cyclopropyl-3-oxo-3,4-dihydro-**  
43 **2H-benzo[b][1,4]oxazine-7-carboxamide 2,2,2-trifluoroacetate (UNC8153).** Synthesized according  
44 to reported procedure.<sup>1</sup> Briefly, a mixture of carboxylic acid **5** (100 mg, 0.2 mmol, 1.0 eq.), tert-butyl  
45 (6-aminohexyl)carbamate (67 mg, 0.3 mmol, 1.5 eq.), HOAt (42 mg, 0.3 mmol, 1.5 eq.), EDC (59 mg,  
46 0.3 mmol 1.5 eq.) and triethylamine (112 μL, 0.8 mmol, 4.0 eq) in DMF (0.5 M) is stirred at room  
47 temperature until completion for 2 hours. The reaction is diluted with ethyl acetate and washed with  
48 water, sat. NH<sub>4</sub>Cl and brine. The organic layer is dried over anhydrous Na<sub>2</sub>SO<sub>4</sub>, filtered and  
49 concentrated under reduced pressure. After purification by flash-chromatography using  
50 dichloromethane/methanol, the corresponding Boc-protected molecule is diluted in dichloromethane  
51 and trifluoroacetic acid is added at 0 °C and the reaction stirred at rt for 3 h. Volatiles are removed under

1 reduced pressure and the desired compound purified by flash chromatography using  
 2 dichloromethane/methanol. 60 mg. 40%. Characterization data correspond to those previously  
 3 reported.  $^1\text{H}$  NMR (600 MHz, MeOD)  $\delta$  7.96 (d,  $J$  = 8.3 Hz, 2H), 7.85 – 7.83 (m, 4H), 7.50 (d,  $J$  = 7.9  
 4 Hz, 2H), 7.20 (d,  $J$  = 8.1 Hz, 1H), 7.17 (d,  $J$  = 1.8 Hz, 1H), 6.96 (d,  $J$  = 8.0 Hz, 1H), 4.83 (s, 2H), 4.62  
 5 (s, 2H), 3.40 (t,  $J$  = 7.1 Hz, 2H), 2.93 (t,  $J$  = 7.6 Hz, 2H), 2.87 – 2.79 (m, 1H), 1.72 – 1.64 (m, 4H), 1.50  
 6 – 1.41 (m, 4H), 0.69 – 0.61 (m, 2H), 0.60 – 0.51 (m, 2H). MS (ESI) ( $m/z$ )  $[\text{M}+\text{H}]^+$  C<sub>33</sub>H<sub>38</sub>N<sub>5</sub>O<sub>5</sub> calc.  
 7 584.29, found 584.33.

8  $^1\text{H}$ -NMR and  $^{13}\text{C}$ -NMR spectra of SP3CHO.



Supplementary References

- 1 1. Hanley, R. P. *et al.* Discovery of a Potent and Selective Targeted NSD2 Degradator for the  
2 Reduction of H3K36me2. *J Am Chem Soc* **145**, 8176–8188 (2023).  
3

### 3. Discussion

In this study, we discovered a novel degrader class that is characterized by its simplistic design: the modification of a protein ligand or inhibitor with a small aliphatic tail ending in a primary amine was sufficient to convert it into an active degrader (Kagiou et al., 2024). What began as a rationally designed screening strategy, ultimately resulted in an unexpected degrader mechanism. Our initial objective was to construct a library of SLF-linked-covalent scout fragments that could potentially recruit novel E3s to induce degradation of an FKBP12-Nluc reporter system. During the screening, we observed that one of the starting materials for the synthesis of our library, SP3N itself induced degradation (Preliminary Data Fig. 1E). This unanticipated finding led us to investigate its mechanism of action, ultimately revealing FBXO22 recruitment.

CRISPR screening, proteomics and biochemical assays revealed that SP3N selectively degraded FKBP12 by recruitment of the SCF-FBXO22 complex, an E3 ligase that was not previously amenable to hijacking. Targeted metabolomics demonstrated an intriguing mechanism: the amine-containing molecule is a precursor requiring metabolic conversion for its activity. Extensive investigations demonstrated the dependency of SP3N activity by amine oxidases that catalyze amine-to-aldehyde conversion resulting in the active molecule, named SP3CHO. Synthesizing the active compound enabled subsequent in vitro biochemical reconstitutions and further mechanistic investigations. Given the electrophilic nature of aldehydes, we performed mutagenesis studies that revealed C326 in FBXO22 as an essential amino acid for SP3N-FBXO22 complex formation and FKBP12 degradation. Detection of an FBXO22-SP3CHO adduct by intact-MS, further supported a potential covalent mechanism. Our study not only identified a previously non-PROTACable E3 ligase but also elucidated the mechanism of action of an alternative class of PROTACs with minimal design.

#### 3.1 Alkylamine-based molecules as a novel class of degraders

This novel class of degraders could offer key advantages for degrader development in TPD. The reduced structural complexity of alkylamine-based degraders allows for simplicity in modifying an existing ligand or inhibitor, potentially making medicinal chemistry efforts more streamlined. Additionally, the need for large bifunctional PROTACs, which suffer from poor permeability and suboptimal pharmacokinetics (Edmondson et al., 2019), would be circumvented. The modular nature of the design suggests that many known inhibitors could

be transformed into degraders by adding a primary amine tail. However, given the limited experience with these compounds, extensive structure-activity-relationship (SAR) assays may still be required to optimize binding and degradation, similarly to classical PROTAC design (Bondeson et al., 2018).

Of note, our attempts to expand the mechanism to BRD4 degraders using JQ1-alkylamines were not fruitful, underscoring the need for better understanding of the mechanistic determinants of degradation. While treatment experiments demonstrated that JQ1-alkylamines entered the cells – as they inhibited signaling similarly to JQ1 inhibitor – they failed to induce BRD4 degradation. One potential explanation might be the existence of conformational hindrances that prevent a productive ternary FBXO22-JQ1-alkylamine-BRD4 complex. In support of this hypothesis, immunoprecipitation experiments failed to reveal FBXO22-BRD4 interaction. We speculate that, similarly to PROTAC design, factors such as linker length and composition significantly affect ternary complex assembly and POI accessibility for ubiquitination.

Our work aligns with a parallel study by Nie and colleagues, on conceptually similar NSD2 degraders (Nie et al., 2024). In brief, attachment of alkylamine tails to an NSD2 inhibitor transformed it into an FBXO22-mediated degrader. With elegant biochemical and MS-based experiments they showed the metabolic conversion of the primary amine to an aldehyde, highlighting the expandability of this mechanism to other targets. Both our study and the one from Nie et al, demonstrated evidence that XIAP degraders act via the same mechanism, potentially disproving the proposed small-molecule-ubiquitination mechanism (den Besten et al., 2021). Nevertheless, as this theory was not experimentally tested, and in line with a recent preprint that small molecules can, in fact, be ubiquitinated, we cannot completely disregard it (W. Li et al., 2024). The mechanistic convergence of the activity of alkylamine-tethered degraders supports this strategy as a robust way to co-opt FBXO22 for degradation.

Given the novelty of this mechanism and the limited number of characterized degraders, several mechanistic aspects remain unexplored. Therefore, future structural studies alongside SAR analyses of various linkers and POIs, could inform on potential unifying principles, as well as unique case-by-case characteristics, to facilitate broader applications.

The recruitment of FBXO22 by SP3N, together with two parallel studies by Basu and colleagues (Basu et al., 2024) and Nie and colleagues (Nie et al., 2024), mark a significant



step forward in expanding the repertoire of hijackable E3 ligases for TPD. As this ligase has not been previously targeted, its broader applicability remains uncertain. However, its addition to the E3 ligase toolbox offers exciting opportunities, particularly given its relevance in cancer biology.

### **3.2 FBXO22's role in cancer and implications**

FBXO22 has been reported to have various roles in tumor-related processes, with context- and substrate-dependent pro- or anti-tumorigenic effects (J. Bai et al., 2019; F. Guo et al., 2019; Shen et al., 2024; Tian et al., 2015; Wu et al., 2017; Long Zhang et al., 2019; Zheng et al., 2020; Zhu et al., 2019). In some cancers, FBXO22's endogenous roles could promote anti-tumor effects (J. Bai et al., 2019; F. Guo et al., 2019; Wu et al., 2017; Zheng et al., 2020). For instance, FBXO22-mediated degradation of the oncogenic proteins human double minute 2 (HDM2) in breast cancer or CD147 in cisplatin resistant tumors, have been correlated with metastasis inhibition and treatment re-sensitization, respectively (J. Bai et al., 2019; Wu et al., 2017). In renal cell carcinoma, FBXO22 has been associated with better survival and anti-angiogenic effects, although its precise molecular targets were not identified in this context (F. Guo et al., 2019). Interestingly, in ER+ breast cancers, FBXO22 is a key determinant of the antagonistic response of compounds acting as selective estrogen receptor modulators (SERMs), mainly via the lysine demethylase KDM4B turnover (Johmura et al., 2018). These antitumor effects could be tied back to FBXO22's reported role in senescence, where it binds to KDM4A and induces methylated p53 degradation, corroborating the senescent/antiproliferative phenotype (Johmura et al., 2016).

Conversely, FBXO22 can also contribute to tumor progression depending on its binding partners and cancer type (Shen et al., 2024; Tian et al., 2015; Long Zhang et al., 2019; Zhu et al., 2019). Elevated levels of FBXO22 in hepatocellular carcinoma have been associated with poor prognosis, with underlying molecular events including the degradation of tumor suppressor factors such as p21 or Krüppel-like factor 4 (KLF4) (Tian et al., 2015; Long Zhang et al., 2019). In addition, FBXO22 has emerged as an angiogenesis- and metastasis-promoting factor in malignant melanoma and glioblastoma, possibly via the degradation of VHL, a direct regulator of the angiogenic factor HIF1 $\alpha$  (Shen et al., 2024). Intriguingly, in lung cancer, FBXO22 was correlated with poor prognosis, not by degrading its target, the tumor-suppressive liver kinase B1 (LKB1), but by impairing its activity through polyubiquitination (Zhu et al., 2019).

Taken together, these studies support a context-dependent role of FBXO22 in tumorigenesis, highlighting the importance of understanding its endogenous substrates and molecular networks in different cancer types. Interestingly, even within the same cancer type, FBXO22's role can vary, for instance in breast cancer, it promotes primary tumor growth but inhibits epithelial–mesenchymal transition (EMT) and metastasis (Sun et al., 2018).

The multifaceted roles of FBXO22 in cancer highlight its context-specific potential as a novel E3 ligase for TPD-based strategies. Our analysis demonstrated that FBXO22 is frequently upregulated in certain tumor types, presenting an opportunity for tumor-selective targeting, while sparing healthy tissues with lower expression. In addition, given that FBXO22 could degrade tumor suppressors (i.e. KLF4) (Tian et al., 2015), TPD strategies utilizing FBXO22 could offer dual antitumorigenic benefits. For instance, an FBXO22-based oncogene degrader would, on the one hand, eliminate the tumorigenic drivers, and on the other hand shield tumor suppressors from their endogenous turnover. The feasibility of this “dual activity” strategy has already been shown with PROTACs targeting the MDM2-p53 pathway, resulting in release of the tumor suppressor p53 from negative regulation (Hines et al., 2019).

Despite the potential benefits of the dual activity strategy, it is important to note that global disruptions on FBXO22's networks might induce unwanted cell toxicities. However, our global proteomics experiments did not demonstrate any effects on the previously reported FBXO22 endogenous substrates - potentially explained by the modest SP3CHO-FBXO22 occupancy we observed in ABPP or intact-MS.

To fully explore the therapeutic applicability of FBXO22 in cancer, future studies should focus on clinically relevant targets and physiological *in vivo* models. These studies could allow monitoring the precise molecular events, tumor growth and metastasis upon degrader treatment and in correlation with FBXO22's context-dependent roles, to achieve optimal drug efficacy with minimal off-target effects.

### **3.3 FBXO22's role in redox homeostasis and implications**

Beyond FBXO22's role in cancer, FBXO22 is heavily involved in redox homeostasis through the regulation of its substrate, BTB and CNC homology 1 (BACH1) (Lignitto et al., 2019). BACH1 is a transcription factor that competes with NRF2, a major antioxidative-response factor, for heme regulation (Cai et al., 2022; Nishizawa et al., 2023). Heme is a porphyrin derivative, required for the activity of many proteins (Gallio et al., 2021). Despite its

crucial effects, heme release under oxidative stress has been shown to generate free radicals further contributing to the unwanted oxidative stress (Cai et al., 2022). Cells employ an elegant antioxidant heme response pathway which releases heme oxygenase -1 (HO-1) to catabolize free heme. Briefly, under normal conditions, the E3 ligase KEAP1 continuously degrades NRF2, but in oxidative stress, KEAP1 is inhibited, and NRF2 is free to drive the expression of antioxidative genes including HO-1. In the meantime, BACH1 suppresses HO-1, unless heme levels increase, prompting BACH1 degradation (Zenke-Kawasaki et al., 2007), an event required for NRF2 accessibility to HO-1 (Nishizawa et al., 2023).

The regulation of BACH1 has been shown to be mediated by the ubiquitin proteasome system with two critical SCF-type E3 ligases controlling its levels - FBXO22 and F-Box and leucine rich repeat protein 17 (FBXL17) (Lignitto et al., 2019; Tan et al., 2013). Recently, after the publication of our work, two studies reported the structures of FBXO22-BACH1 and FBXL17-BACH1, revealing the mechanistic underpinnings of BACH1 regulation in unprecedented detail (Cao et al., 2024; Goretzki et al., 2024). Both studies suggested that FBXO22 and FBXL17 have complementary functions for BACH1 recognition, with FBXO22 recognizing quaternary structures of BACH1, while FBXL17 destabilized monomers. Interestingly, it was suggested that upon heme increase, BACH1 is released from the DNA as a quaternary complex that can be recognized by FBXO22. Subsequently, depending on the oxidative stress load, oxidation of critical amino acids on BACH1 could occur, destabilizing the ternary structure and therefore bypassing recognition by FBXO22. The destabilized BACH1 was demonstrated to be recognized by FBXL17 that takes over its degradation, revealing a finetuned “ligase switch” mechanism, with BACH1 amino-acid oxidation as sensory events (Cao et al., 2024; Goretzki et al., 2024).

Despite insights into BACH1 regulation, no consensus degron has been reported driving the universal recognition of substrates by FBXO22. While binding to BACH1 relies on a structural degron (Cao et al., 2024; Goretzki et al., 2024), another reported substrate, the Bcl2-associated athanogene 3 (BAG3) is only recognized when phosphorylated, suggesting an alternative phosphodegron-dependent mechanism (Liu et al., 2022). These findings indicate that FBXO22's substrate recognition might be context-dependent and thus not easily generalizable across all substrates.

This substrate variability raises the question of how FBXO22 recognizes FKBP12 in the presence of SP3CHO. We suspect that BACH1 and BAG3 recognition mechanisms by

FBXO22 differ from the FKBP12 recruitment by SP3CHO, as both seem to occur via domains distant from C326 and they involve either structural or PTM-modified degrons (Cao et al., 2024; Goretzki et al., 2024; Liu et al., 2022). Of note, our attempts for ternary complex detection at high resolution with Cryo-EM were challenging, potentially due to the high flexibility of the complex or the observed low occupancy. Therefore, further structural investigations will be needed to clarify the precise mode of recruitment.

The important role of FBXO22 for BACH1 regulation under oxidative stress might offer an additional avenue for a “dual activity” strategy utilizing FBXO22’s endogenous circuits. Redirecting FBXO22 from BACH1 towards degrading an oncogene could have two effects: on the one hand, the oncogene degradation would inhibit tumor growth and on the other hand, BACH1 would keep suppressing the antioxidative response. This could in turn enhance tumor-sensitivity to oxidative-stress-inducing therapies, such as ionizing radiation and chemotherapy (Gorrini et al., 2013).

The feasibility of a dual degradation-and-redox-homeostasis-targeting strategy has been shown in in vitro neurodegenerative models, where hijacking KEAP1 facilitated both Tau degradation and NRF2 release (Lu et al., 2018). However, in the context of tumorigenesis, the broader role of FBXO22 in antioxidative responses is poorly defined. Furthermore, there is a lack of proof-of-concept studies demonstrating the potential benefit of combinatorial PROTAC-based degraders and oxidative-stress-inducing therapies. Further investigations are needed to assess whether FBXO22-based PROTACs in combination with ROS-induction could enhance tumor vulnerability.

### **3.4 FBXO22’s liability to covalent engagement and implications**

Another key finding of our study is that the interaction between FBXO22-C326 and SP3CHO falls into the category of reversible covalent interactions (Kiely-Collins et al., 2021; Serafimova et al., 2012). The aldehyde likely reacts with the thiol group of C326 to form a hemiacetal adduct, that contributes to reversible binding. Covalent interaction was supported by our mutagenesis experiments showing the C326 is required for the degradation and by the in vitro intact-mass-spectrometry assays which detected the SP3CHO-FBXO22 adduct in a C326A-dependent fashion. However, the theoretically suspected reversibility has not been directly tested, and future work should focus on experiments to confirm and characterize this interaction. For instance, compound washout experiments or co-treatments with reducing agents could inform on the persistence or reversibility of the interaction. Furthermore,

biophysical assays for monitoring adduct formation and dissociation could give additional insights into the kinetics of the binding and release of SP3CHO.

The reversibility of the interaction differentiates the aldehydes from other irreversible covalent warheads such as acrylamides or chloroacetamides (Kiely-Collins et al., 2021). Interestingly, parallel to our work, Basu and colleagues, following a different route, discovered electrophilic PROTACs that recruit FBXO22 via an alternative mechanism, making their compounds the only other FBXO22 reported ligands (Basu et al., 2024). In brief, by employing CRISPR transcriptional activation studies they demonstrated that chloroacetamide and acrylamide electrophilic warheads attached to SLF could recruit FBXO22 via joint engagement of two cysteines, C227 and C228. These compounds have several differences to the alkylamine degraders: i) they require two cysteine residues for their activity ii) they are potent electrophiles that might pose the risk of off-target engagement iii) they require transcriptional activation of FBXO22 for their activity, even in 293T cells, in which we show that endogenous levels are adequate for degradation with our compounds.

In contrast to the report by Basu and colleagues, when we tested compounds where the aldehyde moiety of SP3CHO was exchanged for a chloroacetamide or acrylamide warhead, we observed no degradation activity, suggesting that at least in our system, the aldehyde allowed for optimal interactions. To gain insights into the structural features of FBXO22, we relied on high-confidence AlphaFold predictions (Jumper et al., 2021; Varadi et al., 2024), which suggested that C326 is a solvent exposed residue potentially making it accessible to the aldehyde. Nevertheless, structural elucidation of the FBXO22-SP3CHO-FKBP12 ternary complex would be ideal to understand the interactions at the atomic level and with high resolution.

The recent findings reporting the only available to-date ligands of FBXO22 suggest that its engagement can be achieved through different electrophiles, highlighting its potential for broader applicability in TPD (Basu et al., 2024; Nie et al., 2024). The discovered liability of several FBXO22 cysteines for electrophilic engagement sets FBXO22 as an attractive target for future screening efforts to identify improved ligands. For instance, large-scale covalent fragment or DNA-encoded library (DEL) screens can significantly enhance the throughput of discovery (Peterson and Liu, 2023; Resnick et al., 2019; Satz et al., 2022).

Furthermore, coupling fragment screens to functional readouts could, on the one hand, potentiate the identification of improved FBXO22 binders and, on the other hand, facilitate the discovery of molecular glues that induce novel PPIs via FBXO22. Combined, these efforts could reveal deeper mechanistic insights underlying the FBXO22-ligand interactions, provide modular scaffolds for further optimization, and ultimately expand the FBXO22 targeting landscape. These future studies can help address the other major limitations in expanding the undruggable space, as they employ discovery campaigns on the basis of the E3 ligase, rather than a selective POI. Studies on IMiDs and CRBN have shown that changes on the IMiD scaffold allow tunability of neosubstrate degradation (Brennan et al., 2024; Nowak et al., 2023; Yamanaka et al., 2023), so it remains to see if similar principles apply for FBXO22.

### **3.5 Metabolic liability of alkylamine-tethered molecules and implications**

One of the key findings of our study, and in accordance with the parallel report by Nie and colleagues (Nie et al., 2024), is that alkylamine-based-degrader activity relies on amine oxidases that catalyze the conversion to the aldehyde species. Amine oxidases share the general capability of catalyzing the oxidative deamination of amine substrates, however they comprise a diverse group of enzymes with distinct cofactor dependencies, substrate specificities and tissue distributions (Toninello et al., 2006). They can be broadly classified into two groups determined by the cofactors required for their activity, namely copper-containing amine oxidases (CAOs) and flavin adenine dinucleotide (FAD)-containing amine oxidases (FAOs) (Klinman et al., 1991; Toninello et al., 2006).

CAOs depend on copper and topaquinone, a tyrosine derivative, for their catalytic activity (Janes et al., 1990). Three human CAOs have been reported, the amine-oxidase copper-containing AOC1, AOC2 and AOC3 (Schwelberger, 2010). AOC1, also referred to as diamine oxidase (DAO) or histaminase is the primary oxidase of histamine, putrescine or other diamines (Biegański et al., 1983). It is involved in the catabolism of biogenic diamines and mainly expressed in small intestine, kidneys and placenta, where it regulates inflammatory processes. AOC2 is mainly expressed in the retina and is poorly characterized (Imamura et al., 1997). Finally, AOC3 also called semicarbazide-sensitive oxidase (SSAO) or vascular adhesion protein-1 (VAP-1), mainly catalyzes the conversion of primary amines (Salmi and Jalkanen, 2017). It is expressed in tissues like vascular endothelium, adipocytes or smooth muscle cells and has been implicated in leukocyte extravasation and adhesion. Elevated

levels of AOC3 have been linked to several malignancies, mainly through overactivation leading to oxidative stress (Chen et al., 2023).

On the other hand, FAOs utilize FAD or derivatives as cofactors and include the mitochondrial monoamine oxidases (MAO-A and MAO-B), the lysine demethylases LSD1 and LSD2 as well as several polyamine oxidases (Kaludercic et al., 2011; Perillo et al., 2020). The monoamine oxidases are both localized on the outer mitochondrial membrane and are involved in neurotransmitter catabolism (serotonin, dopamine etc). MAO-A, in particular, has been implicated in prostate cancer, breast or neuroendocrine tumors, making it a potential drug target (Y. Ma et al., 2024). LSD1 (KDM1A) and LSD2 (KDM1B) are epigenetic regulators that mainly demethylate histone H3 (Anand and Marmorstein, 2007). LSD1 overexpression has been reported in multiple cancers, with LSD1 inhibitors being actively pursued in clinical trials (Perillo et al., 2020). Lastly, polyamine oxidases including spermine oxidase (SMO), and N-acetylpolyamine oxidase (PAO or PAOX), catabolize the polyamines spermine and spermidine (Salvi and Tavladoraki, 2020). Polyamines are essential for proliferation and are often in high demand by highly proliferating tumors, reinforcing the link between polyamine metabolism and oncogenesis (Holbert et al., 2022). Given the widespread physiological functions of AOs, their frequent overexpression in certain cancers, and the correlation to poor prognosis make them potential therapeutic targets (Toninello et al., 2006).

Since the established roles of AOs in cancer, our findings highlighting the AO-mediated activation of the alkylamine-based degraders could be exploited for tumor-selective drug delivery. For instance, overexpression of secreted or membrane-bound AOs on certain types of tumors could be harnessed to drive the local formation of the active aldehyde-based degrader in a more selective manner (Ding et al., 2021; Liu et al., 2021; Xu et al., 2020). In addition, as diverse AOs have preferential substrate specificity, we might have the possibility to modify the alkylamine tail, towards desired specificity of certain AOs, those known to be overexpressed in tumors. These strategies could potentially benefit tumor selectivity or efficacy, as the conversion would be accelerated in the tissues containing more of these AOs, sparing healthy tissues of off-target effects (Cha et al., 2018).

Therefore, future studies could be focused on finetuning the composition and structure of the alkylamine tails to achieve amine-oxidase dependent therapeutic effects. In addition, to better understand the efficacy of such strategies, more physiologically relevant models need to be employed, for instance in vivo tumor models with elevated AOs, such as metastatic



breast cancer (Cha et al., 2018; Cox et al., 2016). These studies are crucial for assessing the system-wide effects of such treatments and whether there would be an added benefit employing AOs.

Conversely, the metabolic liability of the alkylamine-based degraders to AOs might pose challenges in drug development mainly due to the unpredictability of the pharmacokinetic properties of the amine-to-aldehyde conversion (Shu et al., 2008). This might require extensive optimization with in vivo studies that would not guarantee translatability to human clinical trials. Therefore, direct synthesis of the active aldehyde could address this issue, especially when moving closer to clinical applications. We have shown that the aldehyde presents increased potency likely by bypassing the need for AO-mediated conversion. Metabolomics experiments to quantify SP3CHO upon SP3N treatment with FCS demonstrated that only a small fraction of the amine was converted to the aldehyde, supporting that this metabolic step is the main bottleneck. Thus, even though aldehydes might pose synthetic hurdles due to potential instability, benefits arising from obtaining the active compound tip the balance towards that direction.

It is important to mention that in our cell line models, the activity of the alkylamine-based degraders was dependent on non-physiological AOs, either presumably the bovine serum amine oxidase (BSAO, the main amine oxidase reported in FCS) or the recombinant porcine DAO. Interestingly, despite both belonging to the copper-dependent family, they seem to have distinct substrate preferences. BSAO is a SSAO, more closely related to the human AOC3, with specificity for primary amines (Stolen et al., 2004), while DAO is the porcine equivalent of the human AOC1 (or DAO), with histamine as main substrate (McGrath et al., 2009). Our results showed that both could catalyze the conversion, although only DAO was used as a purified recombinant protein. This suggests that, in our experimental conditions, i) despite distinct substrate preferences, overlapping substrate specificities between BSAO and DAO might exist, ii) in vitro settings with purified DAO could lead to promiscuous activity even for non-primary substrates iii) we cannot exclude that FCS might contain other AOs. Notably, none of our metabolomics experiments showed complete conversion, indicating that while SP3N is a substrate for these enzymes, it is not an optimal one, corroborating the hypothesis that AOs could act on non-canonical substrates to a limited extent (Binda et al., 2002). Interestingly, Nie and colleagues (Nie et al., 2024) showed a higher conversion rate of the NSD2-targeting alkylamine-tethered degrader to the aldehyde, suggesting that substrate

preference for AOs might be dependent on the aliphatic tail's composition combined with the overall compound structure, underscoring the need for case-by-case optimization.

Collectively, future studies to refine this approach for cancer treatment should focus on optimizing the alkylamine scaffolds for modulating the metabolism by preferential AOs in parallel to developing in vivo models to assess conversion in the tumor microenvironment. Ultimately, while metabolic instability could pose a challenge, harnessing AO activity for tumor-selective conversion might represent an exciting avenue for precision medicine.

### **3.6 FBXO22 expands the TPD toolbox**

One of the major challenges in the search for novel E3 ligases for TPD is the lack of available small-molecule ligands that can be used to recruit E3s (Kannt and Đikić, 2021; Liu et al., 2023; Rodríguez-Gimeno and Galdeano, 2024). Our study has successfully introduced a generalizable strategy for recruiting FBXO22, an E3 ligase that at the time of this study, had not been harnessed for TPD. Adding FBXO22 in the E3 ligase arsenal could address some of the current limitations arising from the predominant use of the “standard” E3 ligases CRBN and VHL in PROTAC design. For instance, FBXO22 can support the efforts to circumvent CRBN-dependent tumor resistance (Gooding et al., 2021; Hanzl et al., 2023; Lu Zhang et al., 2019). Simplicity in the design could possibly allow for straightforward modification of existing CRBN-based PROTACs, enabling rapid adaptations. In addition, in contrast to CRBN's ubiquitous expression, the differential expression patterns of FBXO22 in healthy versus tumor cells could be utilized for tumor-selective targeting (Shen et al., 2024; Tian et al., 2015; Long Zhang et al., 2019). Finally, as discussed above, harnessing the endogenous FBXO22 regulatory circuits could achieve stronger effects and potentially mitigate resistance occurrences, due to multifaceted system dependency.

Beyond introducing FBXO22 as a novel E3 ligase for TPD, our study highlights the value of screening strategies with covalent fragments and degradation as a functional readout for “scouting” novel E3 ligases, adding to several successful fragment-based E3 identifications (Lim et al., 2024; Luo et al., 2021; Ward et al., 2019; Zhang et al., 2021, 2019). While the identification of FBXO22 was serendipitous, arising from the unexpected activity of the starting material rather than the intended bifunctional molecules, preliminary data suggest that additional hijackable E3 could be uncovered.

Building on these insights, future studies will focus on expanding our screening methodology in two directions:

i) by performing the screen in different cellular backgrounds such as diverse cell types or healthy versus tumor cells, aiming at identifying selective degradation. This strategy can support the identification of E3s that might be overexpressed or are active in selective contexts, offering the chance to further diversify the toolbox for TPD, and

ii) by adjusting our reporter system to monitor cell-compartment specific-TPD. A study by Simpson and colleagues, focusing on assessing PROTAC-induced degradation of synthetic POI-chimeras linked to various localization signals, demonstrated that the subcellular localization of a POI affects susceptibility to degradation (Simpson et al., 2022). This suggests that in order to expand the targetable space towards differentially localized proteins we need to potentially identify E3s with distinct localization patterns. Using our FKBP12-reporter system is a powerful and highly modular tool that combined with our library of heterobifunctional scout molecules could pave the way for further exploration of E3 ligases, that will be the main focus of future research.

Taken together, our findings highlight how chemical modifications combined with strategic screening can uncover novel E3 ligases and mechanistic insights for TPD. Our work unveils an unexpected mechanism to hijack the E3 ligase FBXO22, via metabolically converting alkylamine-tethered molecules into active aldehyde-containing degraders. The simplified design of these “minimal” PROTACs offers potential advantages for TPD, however further studies are needed to assess the broader applicability. Integrating future structural studies, degrader scaffold optimization and in vivo validation, could broaden the scope of TPD by offering tumor specificity and mechanistic diversity. By revealing the unexpected roles of alkylamine-tethered molecules, delineating the AO-dependent activation and achieving recruitment of a previously non-PROTACable E3 ligase, this work offers a starting point for broader TPD innovation.

### **3.7 Conclusion and outlook**

The discovery of alkylamine-based degraders engaging FBXO22 is an intriguing example of how minimal chemical modifications can reveal novel E3 ligases and degradation mechanisms for TPD. Yet, this work represents only a small fraction of the larger opportunity space for broadening the chemical and biological scope of TPD. Looking beyond the standard

E3 ligases CRBN and VHL, the field will benefit from richer repertoire of E3 ligases with distinct expression profiles, subcellular localizations and substrate specificities. This expansion can address the challenges that TPD faces, including tumor resistance occurrences, while boosting specificity and reaching more previously “undruggable” targets.

From a chemical perspective, our findings highlight the promise of leveraging simple structural scaffolds that rely on metabolic conversion to form active effector compounds. Many examples from inhibitor-drug design as well as recent examples from TPD support that metabolic conversion is a generalizable principle that can reveal novel mechanistic insights and potential therapeutic windows (Nie et al., 2024; Zhuang et al., 2024). Future studies might systematically couple alkylamine tails to known protein binders or fragment libraries for high-throughput screening in diverse cellular contexts. By combining these explorations with chemoproteomics (leveraging the covalent nature of aldehydes) and machine learning-driven design, could reveal plausible hijackable E3 ligases, or foster the identification of novel molecular glues.

Beyond oncology, where AOs and FBXO22 offer opportunities to explore cancer-specific applications, other areas such as neurodegenerative diseases may also benefit from expanded TPD approaches. Understanding the roles of ligases in a broader physiological context, such as redox homeostasis, may create novel dual effect therapies. Ultimately, refining TPD by identifying underutilized ligases and designing flexible chemistries to exploit them would be critical for next-generation therapeutics.

As the TPD field matures, it increasingly highlights the broader power of chemically induced proximity (CIP) for diverse biological outcomes. While degradation remains a leading application of CIP, many related strategies are emerging where proximity induction leads to a wide range of effects such as PPI-induced inhibition, PTM changes, stabilization, or transcriptional rewiring (Gourisankar et al., 2023; Liu and Ciulli, 2023; Stanton et al., 2018). As mentioned in the introduction, early advances in CIP directed the development of TPD, now the lessons learnt from TPD research, especially through extensive structural and biochemical characterizations, could guide the next generation of CIP strategies. As our understanding of proximity-driven pharmacology deepens, future therapeutics will likely combine multiple CIP strategies to achieve context-dependent outcomes.

In the coming years, the integration of high-throughput screening, structural biology and in vivo validation will expand the catalogue of E3s, optimize compound scaffolds and reveal novel generalizable CIP mechanisms. By pushing the boundaries, TPD will continue to support the broader CIP landscape, demonstrating how small molecules can mediate diverse interactions and manipulate cellular functions in unprecedented ways. By integrating this growing knowledge and expanding our understanding, CIP could transform future targeted therapeutics.

## **4. Materials and Methods**

The materials and methods used for the results of this thesis are described in detail in the attached published manuscript and the respective published supplementary information.



## References

- Ahn, G., Banik, S.M., Miller, C.L., Riley, N.M., Cochran, J.R., Bertozzi, C.R., 2021. LYACs that engage the asialoglycoprotein receptor for targeted protein degradation. *Nat Chem Biol* 17, 937–946. <https://doi.org/10.1038/s41589-021-00770-1>
- Anand, R., Marmorstein, R., 2007. Structure and Mechanism of Lysine-specific Demethylase Enzymes. *Journal of Biological Chemistry* 282, 35425–35429. <https://doi.org/10.1074/jbc.R700027200>
- Angers, S., Li, T., Yi, X., MacCoss, M.J., Moon, R.T., Zheng, N., 2006. Molecular architecture and assembly of the DDB1–CUL4A ubiquitin ligase machinery. *Nature* 443, 590–593. <https://doi.org/10.1038/nature05175>
- Asatsuma-Okumura, T., Ando, H., De Simone, M., Yamamoto, J., Sato, T., Shimizu, N., Asakawa, K., Yamaguchi, Y., Ito, T., Guerrini, L., Handa, H., 2019. p63 is a cereblon substrate involved in thalidomide teratogenicity. *Nat Chem Biol* 15, 1077–1084. <https://doi.org/10.1038/s41589-019-0366-7>
- Bachmair, A., Finley, D., Varshavsky, A., 1986. In Vivo Half-Life of a Protein Is a Function of Its Amino-Terminal Residue. *Science* (1979) 234, 179–186. <https://doi.org/10.1126/science.3018930>
- Backus, K.M., Correia, B.E., Lum, K.M., Forli, S., Horning, B.D., González-Páez, G.E., Chatterjee, S., Lanning, B.R., Teijaro, J.R., Olson, A.J., Wolan, D.W., Cravatt, B.F., 2016. Proteome-wide covalent ligand discovery in native biological systems. *Nature* 534, 570–574. <https://doi.org/10.1038/nature18002>
- Baek, K., Metivier, R.J., Burman, S.S.R., Bushman, J.W., Yoon, H., Lumpkin, R.J., Abeja, D.M., Lakshminarayan, M., Yue, H., Ojeda, S., Verano, A.L., Gray, N.S., Donovan, K.A., Fischer, E.S., 2024. Unveiling the hidden interactome of CRBN molecular glues with chemoproteomics. *bioRxiv* 2024.09.11.612438. <https://doi.org/10.1101/2024.09.11.612438>
- Bai, J., Wu, K., Cao, M.-H., Yang, Y., Pan, Y., Liu, H., He, Y., Itahana, Y., Huang, L., Zheng, J.-N., Pan, Z.-Q., 2019. SCFFBXO22 targets HDM2 for degradation and modulates breast cancer cell invasion and metastasis. *Proceedings of the National Academy of Sciences* 116, 11754–11763. <https://doi.org/10.1073/pnas.1820990116>
- Bai, L., Zhou, H., Xu, R., Zhao, Y., Chinnaswamy, K., McEachern, D., Chen, J., Yang, C.-Y., Liu, Z., Wang, M., Liu, L., Jiang, H., Wen, B., Kumar, P., Meagher, J.L., Sun, D., Stuckey, J.A., Wang, S., 2019. A Potent and Selective Small-Molecule Degradator of STAT3 Achieves Complete Tumor Regression In Vivo. *Cancer Cell* 36, 498–511.e17. <https://doi.org/10.1016/j.ccell.2019.10.002>
- Banaszynski, L.A., Liu, C.W., Wandless, T.J., 2005. Characterization of the FKBP·Rapamycin·FRB Ternary Complex. *J Am Chem Soc* 127, 4715–4721. <https://doi.org/10.1021/ja043277y>

- Banaszynski, L.A., Wandless, T.J., 2006. Conditional Control of Protein Function. *Chem Biol* 13, 11–21. <https://doi.org/https://doi.org/10.1016/j.chembiol.2005.10.010>
- Banik, S.M., Pedram, K., Wisnovsky, S., Ahn, G., Riley, N.M., Bertozzi, C.R., 2020. Lysosome-targeting chimaeras for degradation of extracellular proteins. *Nature* 584, 291–297. <https://doi.org/10.1038/s41586-020-2545-9>
- Bartlett, D.W., Gilbert, A.M., 2022. Translational PK–PD for targeted protein degradation. *Chem Soc Rev* 51, 3477–3486. <https://doi.org/10.1039/D2CS00114D>
- Bartlett, J.B., Dredge, K., Dalglish, A.G., 2004. The evolution of thalidomide and its IMiD derivatives as anticancer agents. *Nat Rev Cancer* 4, 314–322. <https://doi.org/10.1038/nrc1323>
- Bashore, C., Prakash, S., Johnson, M.C., Conrad, R.J., Kekessie, I.A., Scales, S.J., Ishisoko, N., Kleinheinz, T., Liu, P.S., Popovych, N., Weckslar, A.T., Zhou, L., Tam, C., Zilberleyb, I., Srinivasan, R., Blake, R.A., Song, A., Staben, S.T., Zhang, Y., Arnott, D., Fairbrother, W.J., Foster, S.A., Wertz, I.E., Ciferri, C., Dueber, E.C., 2023. Targeted degradation via direct 26S proteasome recruitment. *Nat Chem Biol* 19, 55–63. <https://doi.org/10.1038/s41589-022-01218-w>
- Basu, A.A., Zhang, C., Riha, I.A., Magassa, A., Campos, M.A., Caldwell, A.G., Ko, F., Zhang, X., 2024. A CRISPR activation screen identifies FBXO22 supporting targeted protein degradation. *Nat Chem Biol* 20, 1608–1616. <https://doi.org/10.1038/s41589-024-01655-9>
- Baur, M., Gneist, M., Owa, T., Dittrich, C., 2007. Clinical complete long-term remission of a patient with metastatic malignant melanoma under therapy with indisulam (E7070). *Melanoma Res* 17.
- Beck, M., Topf, M., Frazier, Z., Tjong, H., Xu, M., Zhang, S., Alber, F., 2011. Exploring the spatial and temporal organization of a cell's proteome. *J Struct Biol* 173, 483–496. <https://doi.org/https://doi.org/10.1016/j.jsb.2010.11.011>
- Békés, M., Langley, D.R., Crews, C.M., 2022. PROTAC targeted protein degraders: the past is prologue. *Nat Rev Drug Discov*. <https://doi.org/10.1038/s41573-021-00371-6>
- Belcher, B.P., Ward, C.C., Nomura, D.K., 2023. Ligandability of E3 Ligases for Targeted Protein Degradation Applications. *Biochemistry* 62, 588–600. <https://doi.org/10.1021/acs.biochem.1c00464>
- Belshawl, P.J., Spencer, D.M., Crabtree, G.R., Schreiber, S.L., 1996. Controlling programmed cell death with a cyclophilincyclosporin-based chemical inducer of dimerization. *Chem Biol* 3, 731–738. [https://doi.org/https://doi.org/10.1016/S1074-5521\(96\)90249-5](https://doi.org/https://doi.org/10.1016/S1074-5521(96)90249-5)
- Biegański, T., Kusche, J., Lorenz, W., Hesterberg, R., Stahlknecht, C.-D., Feussner, K.-D., 1983. Distribution and properties of human intestinal diamine oxidase and its relevance for the histamine catabolism. *Biochimica et Biophysica Acta (BBA) - General Subjects* 756, 196–203. [https://doi.org/https://doi.org/10.1016/0304-4165\(83\)90092-2](https://doi.org/https://doi.org/10.1016/0304-4165(83)90092-2)

- Binda, C., Mattevi, A., Edmondson, D.E., 2002. Structure-Function Relationships in Flavoenzyme-dependent Amine Oxidations: A COMPARISON OF POLYAMINE OXIDASE AND MONOAMINE OXIDASE\*. *Journal of Biological Chemistry* 277, 23973–23976. <https://doi.org/https://doi.org/10.1074/jbc.R200005200>
- Bond, A.G., Muñoz i Ordoño, M., Bisbach, C.M., Craigon, C., Makukhin, N., Caine, E.A., Nagala, M., Urh, M., Winter, G.E., Riching, K.M., Ciulli, A., 2024. Leveraging Dual-Ligase Recruitment to Enhance Protein Degradation via a Heterotrivalent Proteolysis Targeting Chimera. *J Am Chem Soc* 146, 33675–33711. <https://doi.org/10.1021/jacs.4c11556>
- Bondeson, D.P., Mares, A., Smith, I.E.D., Ko, E., Campos, S., Miah, A.H., Mulholland, K.E., Routly, N., Buckley, D.L., Gustafson, J.L., Zinn, N., Grandi, P., Shimamura, S., Bergamini, G., Faeltch-Savitski, M., Bantscheff, M., Cox, C., Gordon, D.A., Willard, R.R., Flanagan, J.J., Casillas, L.N., Votta, B.J., den Besten, W., Famm, K., Kruidenier, L., Carter, P.S., Harling, J.D., Churcher, I., Crews, C.M., 2015. Catalytic in vivo protein knockdown by small-molecule PROTACs. *Nat Chem Biol* 11, 611–617. <https://doi.org/10.1038/nchembio.1858>
- Bondeson, D.P., Smith, B.E., Burslem, G.M., Buhimschi, A.D., Hines, J., Jaime-Figueroa, S., Wang, J., Hamman, B.D., Ishchenko, A., Crews, C.M., 2018. Lessons in PROTAC Design from Selective Degradation with a Promiscuous Warhead. *Cell Chem Biol* 25, 78-87.e5. <https://doi.org/https://doi.org/10.1016/j.chembiol.2017.09.010>
- Bouvier, C., Lawrence, R., Cavallo, F., Xolalpa, W., Jordan, A., Hjerpe, R., Rodriguez, M.S., 2024. Breaking Bad Proteins—Discovery Approaches and the Road to Clinic for Degraders. *Cells*. <https://doi.org/10.3390/cells13070578>
- Brennan, P.J., Saunders, R.E., Spanou, M., Serafini, M., Sun, L., Heger, G.P., Konopacka, A., Beveridge, R.D., Gordon, L., Bunally, S.B., Saudemont, A., Benowitz, A.B., Martinez-Fleites, C., Queisser, M.A., An, H., Deane, C.M., Hann, M.M., Brayshaw, L.L., Conway, S.J., 2024. Orthogonal IMiD-Degron Pairs Induce Selective Protein Degradation in Cells. *bioRxiv* 2024.03.15.585309. <https://doi.org/10.1101/2024.03.15.585309>
- Buckley, D.L., Van Molle, I., Gareiss, P.C., Tae, H.S., Michel, J., Noblin, D.J., Jorgensen, W.L., Ciulli, A., Crews, C.M., 2012. Targeting the von Hippel–Lindau E3 Ubiquitin Ligase Using Small Molecules To Disrupt the VHL/HIF-1 $\alpha$  Interaction. *J Am Chem Soc* 134, 4465–4468. <https://doi.org/10.1021/ja209924v>
- Buetow, L., Huang, D.T., 2016. Structural insights into the catalysis and regulation of E3 ubiquitin ligases. *Nat Rev Mol Cell Biol* 17, 626–642. <https://doi.org/10.1038/nrm.2016.91>
- Bussiere, D.E., Xie, L., Srinivas, H., Shu, W., Burke, A., Be, C., Zhao, J., Godbole, A., King, D., Karki, R.G., Hornak, V., Xu, F., Cobb, J., Carte, N., Frank, A.O., Frommlet, A., Graff, P., Knapp, M., Fazal, A., Okram, B., Jiang, S., Michellys, P.-Y., Beckwith, R., Voshol, H., Wiesmann, C., Solomon, J.M., Paulk, J., 2020. Structural basis of indisulam-mediated RBM39 recruitment to DCAF15 E3 ligase complex. *Nat Chem Biol* 16, 15–23. <https://doi.org/10.1038/s41589-019-0411-6>

- Cai, L., Arbab, A.S., Lee, T.J., Sharma, A., Thomas, B., Igarashi, K., Raju, R.P., 2022. BACH1-Hemoxygenase-1 axis regulates cellular energetics and survival following sepsis. *Free Radic Biol Med* 188, 134–145. <https://doi.org/https://doi.org/10.1016/j.freeradbiomed.2022.06.005>
- Caianiello, D.F., Zhang, M., Ray, J.D., Howell, R.A., Swartzel, J.C., Branham, E.M.J., Chirkin, E., Sabbasani, V.R., Gong, A.Z., McDonald, D.M., Muthusamy, V., Spiegel, D.A., 2021. Bifunctional small molecules that mediate the degradation of extracellular proteins. *Nat Chem Biol* 17, 947–953. <https://doi.org/10.1038/s41589-021-00851-1>
- Cao, S., Garcia, S.F., Shi, Huigang, James, E.I., Kito, Y., Shi, Hui, Mao, H., Kaisari, S., Rona, G., Deng, S., Goldberg, H. V, Ponce, J., Ueberheide, B., Lignitto, L., Guttman, M., Pagano, M., Zheng, N., 2024. Recognition of BACH1 quaternary structure degrons by two F-box proteins under oxidative stress. *Cell* 187, 7568–7584.e22. <https://doi.org/10.1016/j.cell.2024.10.012>
- Cao, S., Kang, S., Mao, H., Yao, J., Gu, L., Zheng, N., 2022. Defining molecular glues with a dual-nanobody cannabidiol sensor. *Nat Commun* 13, 815. <https://doi.org/10.1038/s41467-022-28507-1>
- Cha, Yoon Jin, Jung, Woo Hee, Koo, Ja Seung, 2018. Site-specific expression of amine oxidases in breast cancer metastases. *Tumor Biology* 40, 1010428318776822. <https://doi.org/10.1177/1010428318776822>
- Chamberlain, P.P., Lopez-Girona, A., Miller, K., Carmel, G., Pagarigan, B., Chie-Leon, B., Rychak, E., Corral, L.G., Ren, Y.J., Wang, M., Riley, M., Delker, S.L., Ito, T., Ando, H., Mori, T., Hirano, Y., Handa, H., Hakoshima, T., Daniel, T.O., Cathers, B.E., 2014. Structure of the human Cereblon-DB1-lenalidomide complex reveals basis for responsiveness to thalidomide analogs. *Nat Struct Mol Biol* 21, 803–809. <https://doi.org/10.1038/nsmb.2874>
- Chau, V., Tobias, J.W., Bachmair, A., Marriott, D., Ecker, D.J., Gonda, D.K., Varshavsky, A., 1989. A Multiubiquitin Chain Is Confined to Specific Lysine in a Targeted Short-Lived Protein. *Science* (1979) 243, 1576–1583. <https://doi.org/10.1126/science.2538923>
- Chen, S.-C., Fan, K.-C., Yen, I.-W., Yang, C.-Y., Lin, C.-H., Hsu, C.-Y., Lyu, Y.-P., Juan, H.-C., Lin, H.-H., Lin, M.-S., Shih, S.-R., Li, H.-Y., Kuo, C.-H., 2023. Serum vascular adhesion protein-1 is associated with twelve-year risk of incident cancer, cancer mortality, and all-cause mortality: a community-based cohort study. *Front Oncol* Volume 13-2023.
- Cheng, B., Li, H., Peng, X., Chen, J., Shao, C., Kong, Z., 2025. Recent advances in developing targeted protein degraders. *Eur J Med Chem* 284, 117212. <https://doi.org/https://doi.org/10.1016/j.ejmech.2024.117212>
- Chini, A., Fonseca, S., Fernández, G., Adie, B., Chico, J.M., Lorenzo, O., García-Casado, G., López-Vidriero, I., Lozano, F.M., Ponce, M.R., Micol, J.L., Solano, R., 2007. The JAZ family of repressors is the missing link in jasmonate signalling. *Nature* 448, 666–671. <https://doi.org/10.1038/nature06006>

- Chirnomas, D., Hornberger, K.R., Crews, C.M., 2023. Protein degraders enter the clinic — a new approach to cancer therapy. *Nat Rev Clin Oncol* 20, 265–278.  
<https://doi.org/10.1038/s41571-023-00736-3>
- Ciechanover, A., Heller, H., Elias, S., Haas, A.L., Hershko, A., 1980. ATP-dependent conjugation of reticulocyte proteins with the polypeptide required for protein degradation. *Proceedings of the National Academy of Sciences* 77, 1365–1368.  
<https://doi.org/10.1073/pnas.77.3.1365>
- Clift, D., McEwan, W.A., Labzin, L.I., Konieczny, V., Mogessie, B., James, L.C., Schuh, M., 2017. A Method for the Acute and Rapid Degradation of Endogenous Proteins. *Cell* 171, 1692–1706.e18. <https://doi.org/10.1016/j.cell.2017.10.033>
- Cohen, E., Quistad, G.B., Casida, J.E., 1996. Cytotoxicity of nimbolide, epoxyazadiradione and other limonoids from neem insecticide. *Life Sci* 58, 1075–1081.  
[https://doi.org/https://doi.org/10.1016/0024-3205\(96\)00061-6](https://doi.org/https://doi.org/10.1016/0024-3205(96)00061-6)
- Copeland, R.A., Pompliano, D.L., Meek, T.D., 2006. Drug–target residence time and its implications for lead optimization. *Nat Rev Drug Discov* 5, 730–739.  
<https://doi.org/10.1038/nrd2082>
- Cox, T.R., Gartland, A., Erler, J.T., 2016. Lysyl Oxidase, a Targetable Secreted Molecule Involved in Cancer Metastasis. *Cancer Res* 76, 188–192. <https://doi.org/10.1158/0008-5472.CAN-15-2306>
- Crowley, V.M., Thielert, M., Cravatt, B.F., 2021. Functionalized Scout Fragments for Site-Specific Covalent Ligand Discovery and Optimization. *ACS Cent Sci* 7, 613–623.  
<https://doi.org/10.1021/acscentsci.0c01336>
- de Wispelaere, M., Du, G., Donovan, K.A., Zhang, T., Eleuteri, N.A., Yuan, J.C., Kalabathula, J., Nowak, R.P., Fischer, E.S., Gray, N.S., Yang, P.L., 2019. Small molecule degraders of the hepatitis C virus protease reduce susceptibility to resistance mutations. *Nat Commun* 10, 3468. <https://doi.org/10.1038/s41467-019-11429-w>
- den Besten, W., Verma, K., Yamazoe, S., Blaquiere, N., Phung, W., Izrael-Tomasevic, A., Mulvihill, M.M., Helgason, E., Prakash, S., Goncharov, T., Vucic, D., Dueber, E., Fairbrother, W.J., Wertz, I., Yu, K., Staben, S.T., 2021. Primary Amine Tethered Small Molecules Promote the Degradation of X-Linked Inhibitor of Apoptosis Protein. *J Am Chem Soc* 143, 10571–10575.  
<https://doi.org/10.1021/jacs.1c05269>
- Deng, Z., Catlett, J., Lee, Y., Wu, Q., Xu, Z., Xie, L., Chen, X., Xiong, Y., Kaniskan, H.Ü., Jin, J., 2025. Harnessing the SPOP E3 Ubiquitin Ligase via a Bridged Proteolysis Targeting Chimera (PROTAC) Strategy for Targeted Protein Degradation. *J Med Chem* 68, 8634–8647.  
<https://doi.org/10.1021/acs.jmedchem.5c00295>
- Ding, Q., Lin, D., Zhou, Y., Li, F., Lai, J., Duan, J., Chen, J., Jiang, C., 2021. Downregulation of amine oxidase copper containing 1 inhibits tumor progression by suppressing IL-

- 6/JAK/STAT3 pathway activation in hepatocellular carcinoma. *Oncol Lett* 22. <https://doi.org/10.3892/ol.2021.13118>
- Dohmen, R.J., Wu, P., Varshavsky, A., 1994. Heat-Inducible Degron: a Method for Constructing Temperature-Sensitive Mutants. *Science* (1979) 263, 1273–1276. <https://doi.org/10.1126/science.8122109>
- Dong, G., Ding, Y., He, S., Sheng, C., 2021. Molecular Glues for Targeted Protein Degradation: From Serendipity to Rational Discovery. *J Med Chem* 64, 10606–10620. <https://doi.org/10.1021/acs.jmedchem.1c00895>
- Dong, J., Ma, F., Cai, M., Cao, F., Li, H., Liang, H., Li, Y., Ding, G., Li, J., Cheng, X., Qin, J.-J., 2024. Heat Shock Protein 90 Interactome-Mediated Proteolysis Targeting Chimera (HIM-PROTAC) Degrading Glutathione Peroxidase 4 to Trigger Ferroptosis. *J Med Chem* 67, 16712–16736. <https://doi.org/10.1021/acs.jmedchem.4c01518>
- Donovan, K.A., An, J., Nowak, R.P., Yuan, J.C., Fink, E.C., Berry, B.C., Ebert, B.L., Fischer, E.S., 2018. Thalidomide promotes degradation of SALL4, a transcription factor implicated in Duane Radial Ray syndrome. *Elife* 7, e38430. <https://doi.org/10.7554/eLife.38430>
- Donovan, K.A., Ferguson, F.M., Bushman, J.W., Eleuteri, N.A., Bhunia, D., Ryu, S., Tan, L., Shi, K., Yue, H., Liu, X., Dobrovolsky, D., Jiang, B., Wang, J., Hao, M., You, I., Teng, M., Liang, Y., Hatcher, J., Li, Z., Manz, T.D., Groendyke, B., Hu, W., Nam, Y., Sengupta, S., Cho, H., Shin, I., Agius, M.P., Ghobrial, I.M., Ma, M.W., Che, J., Buhrlage, S.J., Sim, T., Gray, N.S., Fischer, E.S., 2020. Mapping the Degradable Kinome Provides a Resource for Expedited Degradation Development. *Cell* 183, 1714–1731.e10. <https://doi.org/https://doi.org/10.1016/j.cell.2020.10.038>
- Du, G., Jiang, J., Henning, N.J., Safaee, N., Koide, E., Nowak, R.P., Donovan, K.A., Yoon, H., You, I., Yue, H., Eleuteri, N.A., He, Z., Li, Z., Huang, H.T., Che, J., Nabet, B., Zhang, T., Fischer, E.S., Gray, N.S., 2022. Exploring the target scope of KEAP1 E3 ligase-based PROTACs. *Cell Chem Biol* 29, 1470–1481.e31. <https://doi.org/10.1016/j.chembiol.2022.08.003>
- Du, G., Jiang, J., Wu, Q., Henning, N.J., Donovan, K.A., Yue, H., Che, J., Lu, W., Fischer, E.S., Bardeesy, N., Zhang, T., Gray, N.S., 2021. Discovery of a Potent Degradation for Fibroblast Growth Factor Receptor 1/2. *Angewandte Chemie International Edition* 60, 15905–15911. <https://doi.org/https://doi.org/10.1002/anie.202101328>
- Du, X., Volkov, O.A., Czerwinski, R.M., Tan, H., Huerta, C., Morton, E.R., Rizzi, J.P., Wehn, P.M., Xu, R., Nijhawan, D., Wallace, E.M., 2019. Structural Basis and Kinetic Pathway of RBM39 Recruitment to DCAF15 by a Sulfonamide Molecular Glue E7820. *Structure* 27, 1625–1633.e3. <https://doi.org/https://doi.org/10.1016/j.str.2019.10.005>
- Edmondson, S.D., Yang, B., Fallan, C., 2019. Proteolysis targeting chimeras (PROTACs) in ‘beyond rule-of-five’ chemical space: Recent progress and future challenges. *Bioorg Med Chem Lett* 29, 1555–1564. <https://doi.org/https://doi.org/10.1016/j.bmcl.2019.04.030>

- Emadi, A., Gore, S.D., 2010. Arsenic trioxide — An old drug rediscovered. *Blood Rev* 24, 191–199. <https://doi.org/https://doi.org/10.1016/j.blre.2010.04.001>
- Filippakopoulos, P., Qi, J., Picaud, S., Shen, Y., Smith, W.B., Fedorov, O., Morse, E.M., Keates, T., Hickman, T.T., Felletar, I., Philpott, M., Munro, S., McKeown, M.R., Wang, Y., Christie, A.L., West, N., Cameron, M.J., Schwartz, B., Heightman, T.D., La Thangue, N., French, C.A., Wiest, O., Kung, A.L., Knapp, S., Bradner, J.E., 2010. Selective inhibition of BET bromodomains. *Nature* 468, 1067–1073. <https://doi.org/10.1038/nature09504>
- Fischer, E.S., Böhm, K., Lydeard, J.R., Yang, H., Stadler, M.B., Cavadini, S., Nagel, J., Serluca, F., Acker, V., Lingaraju, G.M., Tichkule, R.B., Schebesta, M., Forrester, W.C., Schirle, M., Hassiepen, U., Ottl, J., Hild, M., Beckwith, R.E.J., Harper, J.W., Jenkins, J.L., Thomä, N.H., 2014. Structure of the DDB1–CRBN E3 ubiquitin ligase in complex with thalidomide. *Nature* 512, 49–53. <https://doi.org/10.1038/nature13527>
- Foley, K.P., Ye, L., Wang, M., Ying, C., Yin, W., Zhang, L., Ying, W., 2021. Abstract 971: Chaperone-mediated protein degradation (CHAMP): A novel technology for tumor-targeted protein degradation. *Cancer Res* 81, 971. <https://doi.org/10.1158/1538-7445.AM2021-971>
- Forte, N., Dovala, D., Hesse, M.J., McKenna, J.M., Tallarico, J.A., Schirle, M., Nomura, D.K., 2023. Targeted Protein Degradation through E2 Recruitment. *ACS Chem Biol* 18, 897–904. <https://doi.org/10.1021/acscchembio.3c00040>
- Fralish, Z., Chen, A., Khan, S., Zhou, P., Reker, D., 2024. The landscape of small-molecule prodrugs. *Nat Rev Drug Discov* 23, 365–380. <https://doi.org/10.1038/s41573-024-00914-7>
- Franks, M.E., Macpherson, G.R., Figg, W.D., 2004. Thalidomide. *The Lancet* 363, 1802–1811. [https://doi.org/https://doi.org/10.1016/S0140-6736\(04\)16308-3](https://doi.org/https://doi.org/10.1016/S0140-6736(04)16308-3)
- Gadd, M.S., Testa, A., Lucas, X., Chan, K.-H., Chen, W., Lamont, D.J., Zengerle, M., Ciulli, A., 2017. Structural basis of PROTAC cooperative recognition for selective protein degradation. *Nat Chem Biol* 13, 514–521. <https://doi.org/10.1038/nchembio.2329>
- Gallio, A.E., Fung, S.S.-P., Cammack-Najera, A., Hudson, A.J., Raven, E.L., 2021. Understanding the Logistics for the Distribution of Heme in Cells. *JACS Au* 1, 1541–1555. <https://doi.org/10.1021/jacsau.1c00288>
- Gandhi, A.K., Kang, J., Havens, C.G., Conklin, T., Ning, Y., Wu, L., Ito, T., Ando, H., Waldman, M.F., Thakurta, A., Klippel, A., Handa, H., Daniel, T.O., Schafer, P.H., Chopra, R., 2014. Immunomodulatory agents lenalidomide and pomalidomide co-stimulate T cells by inducing degradation of T cell repressors Ikaros and Aiolos via modulation of the E3 ubiquitin ligase complex CRL4. *Br J Haematol* 164, 811–821. <https://doi.org/https://doi.org/10.1111/bjh.12708>
- Gao, X., Burris III, H.A., Vuky, J., Dreicer, R., Sartor, A.O., Sternberg, C.N., Percent, I.J., Hussain, M.H.A., Rezazadeh Kalebasty, A., Shen, J., Heath, E.I., Abesada-Terk, G., Gandhi, S.G., McKean, M., Lu, H., Berghorn, E., Gedrich, R., Chirnomas, S.D., Vogelzang, N.J., Petrylak, D.P., 2022. Phase 1/2 study of ARV-110, an androgen receptor (AR) PROTAC degrader, in



- metastatic castration-resistant prostate cancer (mCRPC). *Journal of Clinical Oncology* 40, 17. [https://doi.org/10.1200/JCO.2022.40.6\\_suppl.017](https://doi.org/10.1200/JCO.2022.40.6_suppl.017)
- Gao, Y., Jiang, B., Kim, H., Berberich, M.J., Che, J., Donovan, K.A., Hatcher, J.M., Huerta, F., Kwiatkowski, N.P., Liu, Y., Liuni, P.P., Metivier, R.J., Murali, V.K., Nowak, R.P., Zhang, T., Fischer, E.S., Gray, N.S., Jones, L.H., 2023. Catalytic Degraders Effectively Address Kinase Site Mutations in EML4-ALK Oncogenic Fusions. *J Med Chem* 66, 5524–5535. <https://doi.org/10.1021/acs.jmedchem.2c01864>
- Gheysen, M., Punie, K., Wildiers, H., Neven, P., 2024. Oral SERDs changing the scenery in hormone receptor positive breast cancer, a comprehensive review. *Cancer Treat Rev* 130, 102825. <https://doi.org/https://doi.org/10.1016/j.ctrv.2024.102825>
- Ghidini, A., Cléry, A., Halloy, F., Allain, F.H.T., Hall, J., 2021. RNA-PROTACs: Degradors of RNA-Binding Proteins. *Angewandte Chemie International Edition* 60, 3163–3169. <https://doi.org/https://doi.org/10.1002/anie.202012330>
- Ghosh, P., Dahms, N.M., Kornfeld, S., 2003. Mannose 6-phosphate receptors: new twists in the tale. *Nat Rev Mol Cell Biol* 4, 202–213. <https://doi.org/10.1038/nrm1050>
- Goldstein, G., Scheid, M., Hammerling, U., Schlesinger, D.H., Niall, H.D., Boyse, E.A., 1975. Isolation of a polypeptide that has lymphocyte-differentiating properties and is probably represented universally in living cells. *Proceedings of the National Academy of Sciences* 72, 11–15. <https://doi.org/10.1073/pnas.72.1.11>
- Good, M.C., Zalatan, J.G., Lim, W.A., 2011. Scaffold Proteins: Hubs for Controlling the Flow of Cellular Information. *Science* (1979) 332, 680–686. <https://doi.org/10.1126/science.1198701>
- Gooding, S., Ansari-Pour, N., Towfic, F., Ortiz Estévez, M., Chamberlain, P.P., Tsai, K.-T., Flynt, E., Hirst, M., Rozelle, D., Dhiman, P., Neri, P., Ramasamy, K., Bahlis, N., Vyas, P., Thakurta, A., 2021. Multiple cereblon genetic changes are associated with acquired resistance to lenalidomide or pomalidomide in multiple myeloma. *Blood* 137, 232–237. <https://doi.org/10.1182/blood.2020007081>
- Goretzki, B., Khoshouei, M., Schröder, M., Penner, P., Egger, L., Stephan, C., Argoti, D., Dierlamm, N., Rada, J.M., Kapps, S., Müller, C.S., Thiel, Z., Mutlu, M., Tschopp, C., Furkert, D., Freuler, F., Haenni, S., Tenaillon, L., Knapp, B., Hinniger, A., Hoppe, P., Schmidt, E., Gutmann, S., Iurlaro, M., Ryzhakov, G., Fernández, C., 2024. Dual BACH1 regulation by complementary SCF-type E3 ligases. *Cell* 187, 7585–7602.e25. <https://doi.org/10.1016/j.cell.2024.11.006>
- Gorrini, C., Harris, I.S., Mak, T.W., 2013. Modulation of oxidative stress as an anticancer strategy. *Nat Rev Drug Discov* 12, 931–947. <https://doi.org/10.1038/nrd4002>
- Gosavi, P.M., Ngan, K.C., Yeo, M.J.R., Su, C., Li, J., Lue, N.Z., Hoenig, S.M., Liao, B.B., 2022. Profiling the Landscape of Drug Resistance Mutations in Neosubstrates to Molecular Glue Degradors. *ACS Cent Sci* 8, 417–429. <https://doi.org/10.1021/acscentsci.1c01603>

- Gosink, M.M., Vierstra, R.D., 1995. Redirecting the specificity of ubiquitination by modifying ubiquitin-conjugating enzymes. *Proceedings of the National Academy of Sciences* 92, 9117–9121. <https://doi.org/10.1073/pnas.92.20.9117>
- Gourisankar, S., Krokhotin, A., Ji, W., Liu, X., Chang, C.-Y., Kim, S.H., Li, Z., Wenderski, W., Simanauskaite, J.M., Yang, H., Vogel, H., Zhang, T., Green, M.R., Gray, N.S., Crabtree, G.R., 2023. Rewiring cancer drivers to activate apoptosis. *Nature* 620, 417–425. <https://doi.org/10.1038/s41586-023-06348-2>
- Gowans, F.A., Forte, N., Hatcher, J., Huang, O.W., Wang, Y., Altamirano Poblano, B.E., Wertz, I.E., Nomura, D.K., 2024. Covalent Degradation of the Oncogenic Transcription Factor  $\beta$ -Catenin. *J Am Chem Soc* 146, 16856–16865. <https://doi.org/10.1021/jacs.4c05174>
- Gray, W.M., Carlos Del Pozo, J., Walker, L., Hobbie, L., Risseuw, E., Banks, T., Crosby, W.L., Yang, M., Ma, H., Estelle, M., 1999. Identification of an SCF ubiquitin-ligase complex required for auxin response in *Arabidopsis thaliana*.
- Gray, W.M., Kepinski, S., Rouse, D., Leyser, O., Estelle, M., 2001. Auxin regulates SCFTIR1-dependent degradation of AUX/IAA proteins. *Nature* 414, 271–276. <https://doi.org/10.1038/35104500>
- Guo, F., Liu, J., Han, X., Zhang, X., Lin, T., Wang, Y., Bai, J., Han, J., 2019. FBXO22 suppresses metastasis in human renal cell carcinoma via inhibiting MMP-9-mediated migration and invasion and VEGF-mediated angiogenesis. *Int J Biol Sci* 15, 647–656. <https://doi.org/10.7150/ijbs.31293>
- Guo, Z., Hong, S.Y., Wang, J., Rehan, S., Liu, W., Peng, H., Das, M., Li, W., Bhat, S., Peiffer, B., Ullman, B.R., Tse, C.M., Tarmakova, Z., Schiene-Fischer, C., Fischer, G., Coe, I., Paavilainen, V.O., Sun, Z., Liu, J.O., 2019. Rapamycin-inspired macrocycles with new target specificity. *Nat Chem* 11, 254–263. <https://doi.org/10.1038/s41557-018-0187-4>
- Haid, R.T.U., Reichel, A., 2025. PK/PD modeling of targeted protein degraders: Charting new waters and navigating the shallows. *Drug Discov Today* 30, 104311. <https://doi.org/https://doi.org/10.1016/j.drudis.2025.104311>
- Hamilton, E.P., Schott, A.F., Nanda, R., Lu, H., Keung, C.F., Gedrich, R., Parameswaran, J., Han, H.S., Hurvitz, S.A., 2022. ARV-471, an estrogen receptor (ER) PROTAC degrader, combined with palbociclib in advanced ER+/human epidermal growth factor receptor 2–negative (HER2–) breast cancer: Phase 1b cohort (part C) of a phase 1/2 study. *Journal of Clinical Oncology* 40, TPS1120–TPS1120. [https://doi.org/10.1200/JCO.2022.40.16\\_suppl.TPS1120](https://doi.org/10.1200/JCO.2022.40.16_suppl.TPS1120)
- Han, T., Goralski, M., Gaskill, N., Capota, E., Kim, J., Ting, T.C., Xie, Y., Williams, N.S., Nijhawan, D., 2017. Anticancer sulfonamides target splicing by inducing RBM39 degradation via recruitment to DCAF15. *Science* (1979) 356. <https://doi.org/10.1126/science.aal3755>
- Hanley, R.P., Nie, D.Y., Tabor, J.R., Li, F., Sobh, A., Xu, C., Barker, N.K., Dilworth, D., Hajian, T., Gibson, E., Szewczyk, M.M., Brown, P.J., Barsyte-Lovejoy, D., Herring, L.E., Wang, G.G., Licht, J.D., Vedadi, M., Arrowsmith, C.H., James, L.I., 2023. Discovery of a Potent and

- Selective Targeted NSD2 Degradator for the Reduction of H3K36me2. *J Am Chem Soc* 145, 8176–8188. <https://doi.org/10.1021/jacs.3c01421>
- Hanzl, A., Casement, R., Imrichova, H., Hughes, S.J., Barone, E., Testa, A., Bauer, S., Wright, J., Brand, M., Ciulli, A., Winter, G.E., 2023. Functional E3 ligase hotspots and resistance mechanisms to small-molecule degraders. *Nat Chem Biol* 19, 323–333. <https://doi.org/10.1038/s41589-022-01177-2>
- Hanzl, A., Inghelram, C., Schmitt, S., Thomä, N.H., 2025. Primed for degradation: How weak protein interactions enable molecular glue degraders. *Curr Opin Struct Biol* 92, 103052. <https://doi.org/https://doi.org/10.1016/j.sbi.2025.103052>
- Harper, J.W., Schulman, B.A., 2021. Cullin-RING Ubiquitin Ligase Regulatory Circuits: A Quarter Century Beyond the F-Box Hypothesis 52. <https://doi.org/10.1146/annurev-biochem-090120>
- Hassan, M.M., Li, Y.-D., Ma, M.W., Teng, M., Byun, W.S., Puvar, K., Lumpkin, R., Sandoval, B., Rutter, J.C., Jin, C.Y., Wang, M.Y., Xu, S., Schmoker, A.M., Cheong, H., Groendyke, B.J., Qi, J., Fischer, E.S., Ebert, B.L., Gray, N.S., 2024. Exploration of the tunability of BRD4 degradation by DCAF16 trans-labelling covalent glues. *Eur J Med Chem* 279, 116904. <https://doi.org/https://doi.org/10.1016/j.ejmech.2024.116904>
- Hatakeyama, S., Yada, M., Matsumoto, M., Ishida, N., Nakayama, K.-I., 2001. U Box Proteins as a New Family of Ubiquitin-Protein Ligases\*. *Journal of Biological Chemistry* 276, 33111–33120. <https://doi.org/https://doi.org/10.1074/jbc.M102755200>
- He, Y., Koch, R., Budamagunta, V., Zhang, P., Zhang, Xuan, Khan, S., Thummuri, D., Ortiz, Y.T., Zhang, Xin, Lv, D., Wiegand, J.S., Li, W., Palmer, A.C., Zheng, G., Weinstock, D.M., Zhou, D., 2020. DT2216—a Bcl-xL-specific degrader is highly active against Bcl-xL-dependent T cell lymphomas. *J Hematol Oncol* 13, 95. <https://doi.org/10.1186/s13045-020-00928-9>
- Hennes, E., Lucas, B., Scholes, N.S., Cheng, X.-F., Scott, D.C., Bischoff, M., Reich, K., Gasper, R., Lucas, M., Xu, T.T., Pulvermacher, L.-M., Dötsch, L., Imrichova, H., Brause, A., Naredla, K.R., Sievers, S., Kumar, K., Janning, P., Gersch, M., Murray, P.J., Schulman, B.A., Winter, G.E., Ziegler, S., Waldmann, H., 2025. Identification of a Monovalent Pseudo-Natural Product Degradator Class Supercharging Degradation of IDO1 by its native E3 KLHDC3. *bioRxiv* 2024.07.10.602857. <https://doi.org/10.1101/2024.07.10.602857>
- Henning, N.J., Manford, A.G., Spradlin, J.N., Brittain, S.M., Zhang, E., McKenna, J.M., Tallarico, J.A., Schirle, M., Rape, M., Nomura, D.K., 2022. Discovery of a Covalent FEM1B Recruiter for Targeted Protein Degradation Applications. *J Am Chem Soc* 144, 701–708. <https://doi.org/10.1021/jacs.1c03980>
- Hershko, A., Ciechanover, A., 1998. THE UBIQUITIN SYSTEM, *Annu. Rev. Biochem.*
- Hershko, A., Ciechanover, A., Heller, H., Haas, A.L., Rose, I.A., 1980. Proposed role of ATP in protein breakdown: conjugation of protein with multiple chains of the polypeptide of ATP-

- dependent proteolysis. *Proceedings of the National Academy of Sciences* 77, 1783–1786. <https://doi.org/10.1073/pnas.77.4.1783>
- Hickey, C.M., Digianantonio, K.M., Zimmermann, K., Harbin, A., Quinn, C., Patel, A., Gareiss, P., Chapman, A., Tiberi, B., Dobrodziej, J., Corradi, J., Cacace, A.M., Langley, D.R., Békés, M., 2024. Co-opting the E3 ligase KLHDC2 for targeted protein degradation by small molecules. *Nat Struct Mol Biol* 31, 311–322. <https://doi.org/10.1038/s41594-023-01146-w>
- Hilmi, K., Nader, H., Rodrigo, M.-S., Mohamed, E.-E., Houssam, I., Chantal, D., Martine, B., Maria Johanna, R., Michel, B., Pierre, T., James L., G., and Mader, S., 2012. Role of SUMOylation in Full Antiestrogenicity. *Mol Cell Biol* 32, 3823–3837. <https://doi.org/10.1128/MCB.00290-12>
- Hines, J., Lartigue, S., Dong, H., Qian, Y., Crews, C.M., 2019. MDM2-Recruiting PROTAC Offers Superior, Synergistic Antiproliferative Activity via Simultaneous Degradation of BRD4 and Stabilization of p53. *Cancer Res* 79, 251–262. <https://doi.org/10.1158/0008-5472.CAN-18-2918>
- Hinterndorfer, M., Spiteri, V.A., Ciulli, A., Winter, G.E., 2025. Targeted protein degradation for cancer therapy. *Nat Rev Cancer*. <https://doi.org/10.1038/s41568-025-00817-8>
- Ho, S.N., Biggar, S.R., Spencer, D.M., Schreiber, S.L., Crabtree, G.R., 1996. Dimeric ligands define a role for transcriptional activation domains in reinitiation. *Nature* 382, 822–826. <https://doi.org/10.1038/382822a0>
- Hoi, D.M., Junker, S., Junk, L., Schwechel, K., Fischel, K., Podlesinski, D., Hawkins, P.M.E., van Geelen, L., Kaschani, F., Leodolter, J., Morreale, F.E., Kleine, S., Guha, S., Rumpel, K., Schmiedel, V.M., Weinstabl, H., Meinhart, A., Payne, R.J., Kaiser, M., Hartl, M., Boehmelt, G., Kazmaier, U., Kalscheuer, R., Clausen, T., 2023. Clp-targeting BacPROTACs impair mycobacterial proteostasis and survival. *Cell* 186, 2176–2192.e22. <https://doi.org/10.1016/j.cell.2023.04.009>
- Holbert, C.E., Cullen, M.T., Casero, R.A., Stewart, T.M., 2022. Polyamines in cancer: integrating organismal metabolism and antitumour immunity. *Nat Rev Cancer* 22, 467–480. <https://doi.org/10.1038/s41568-022-00473-2>
- Hong, S.H., Divakaran, A., Osa, A., Huang, O.W., Wertz, I.E., Nomura, D.K., 2024. Exploiting the Cullin E3 Ligase Adaptor Protein SKP1 for Targeted Protein Degradation. *ACS Chem Biol* 19, 442–450. <https://doi.org/10.1021/acscchembio.3c00642>
- Hsia, O., Hinterndorfer, M., Cowan, A.D., Iso, K., Ishida, T., Sundaramoorthy, R., Nakasone, M.A., Imrichova, H., Schätz, C., Rukavina, A., Husnjak, K., Wegner, M., Correa-Sáez, A., Craigon, C., Casement, R., Maniaci, C., Testa, A., Kaulich, M., Dikic, I., Winter, G.E., Ciulli, A., 2024. Targeted protein degradation via intramolecular bivalent glues. *Nature* 627, 204–211. <https://doi.org/10.1038/s41586-024-07089-6>
- Hsu, J.H.-R., Rasmusson, T., Robinson, J., Pacht, F., Read, J., Kawatkar, S., O’Donovan, D.H., Bagal, S., Code, E., Rawlins, P., Argryou, A., Tomlinson, R., Gao, N., Zhu, X., Chiarparin, E.,

- Jacques, K., Shen, M., Woods, H., Bednarski, E., Wilson, D.M., Drew, L., Castaldi, M.P., Fawell, S., Bloecher, A., 2020. EED-Targeted PROTACs Degrade EED, EZH2, and SUZ12 in the PRC2 Complex. *Cell Chem Biol* 27, 41-46.e17. <https://doi.org/10.1016/j.chembiol.2019.11.004>
- Huibregtse1, J.M., Scheffner, M., Howley, P.M., 1991. A cellular protein mediates association of p53 with the E6 oncoprotein of human papillomavirus types 16 or 18, *The EMBO Journal*.
- Imamura, Y., Kubota, R., Wang, Y., Asakawa, S., Kudoh, J., Mashima, Y., Oguchi, Y., Shimizu, N., 1997. Human Retina-Specific Amine Oxidase (RAO): cDNA Cloning, Tissue Expression, and Chromosomal Mapping. *Genomics* 40, 277–283. <https://doi.org/https://doi.org/10.1006/geno.1996.4570>
- Ishida, T., Ciulli, A., 2021. E3 Ligase Ligands for PROTACs: How They Were Found and How to Discover New Ones. *SLAS Discovery* 26, 484–502. <https://doi.org/10.1177/2472555220965528>
- Ito, T., Ando, H., Suzuki, T., Ogura, T., Hotta, K., Imamura, Y., Yamaguchi, Y., Handa, H., 2010. Identification of a Primary Target of Thalidomide Teratogenicity. *Science* (1979) 327, 1345–1350. <https://doi.org/10.1126/science.1177319>
- Itoh, Y., Ishikawa, M., Kitaguchi, R., Okuhira, K., Naito, M., Hashimoto, Y., 2012. Double protein knockdown of cIAP1 and CRABP-II using a hybrid molecule consisting of ATRA and IAPs antagonist. *Bioorg Med Chem Lett* 22, 4453–4457. <https://doi.org/https://doi.org/10.1016/j.bmcl.2012.04.134>
- Itoh, Y., Ishikawa, M., Kitaguchi, R., Sato, S., Naito, M., Hashimoto, Y., 2011a. Development of target protein-selective degradation inducer for protein knockdown. *Bioorg Med Chem* 19, 3229–3241. <https://doi.org/https://doi.org/10.1016/j.bmc.2011.03.057>
- Itoh, Y., Kitaguchi, R., Ishikawa, M., Naito, M., Hashimoto, Y., 2011b. Design, synthesis and biological evaluation of nuclear receptor-degradation inducers. *Bioorg Med Chem* 19, 6768–6778. <https://doi.org/https://doi.org/10.1016/j.bmc.2011.09.041>
- Janes, S.M., Mu, D., Wemmer, D., Smith, A.J., Kaur, S., Maltby, D., Burlingame, A.L., Klinman, J.P., 1990. A New Redox Cofactor in Eukaryotic Enzymes: 6-Hydroxydopa at the Active Site of Bovine Serum Amine Oxidase. *Science* (1979) 248, 981–987. <https://doi.org/10.1126/science.2111581>
- Jevtić, P., Haakonsen, D.L., Rapé, M., 2021. An E3 ligase guide to the galaxy of small-molecule-induced protein degradation. *Cell Chem Biol* 28, 1000–1013. <https://doi.org/https://doi.org/10.1016/j.chembiol.2021.04.002>
- Ji, C.H., Kim, H.Y., Lee, M.J., Heo, A.J., Park, D.Y., Lim, S., Shin, S., Ganipiseti, S., Yang, W.S., Jung, C.A., Kim, K.Y., Jeong, E.H., Park, S.H., Bin Kim, S., Lee, S.J., Na, J.E., Kang, J.I., Chi, H.M., Kim, H.T., Kim, Y.K., Kim, B.Y., Kwon, Y.T., 2022. The AUTOTAC chemical biology platform for targeted protein degradation via the autophagy-lysosome system. *Nat Commun* 13, 904. <https://doi.org/10.1038/s41467-022-28520-4>

- Johmura, Y., Maeda, I., Suzuki, N., Wu, W., Goda, A., Morita, M., Yamaguchi, K., Yamamoto, M., Nagasawa, S., Kojima, Y., Tsugawa, K., Inoue, N., Miyoshi, Y., Osako, T., Akiyama, F., Maruyama, R., Inoue, J. ichiro, Furukawa, Y., Ohta, T., Nakanishi, M., 2018. Fbxo22-mediated KDM4B degradation determines selective estrogen receptor modulator activity in breast cancer. *Journal of Clinical Investigation* 128, 5603–5619. <https://doi.org/10.1172/JCI121679>
- Johmura, Y., Sun, J., Kitagawa, K., Nakanishi, K., Kuno, T., Naiki-Ito, A., Sawada, Y., Miyamoto, T., Okabe, A., Aburatani, H., Li, S., Miyoshi, I., Takahashi, S., Kitagawa, M., Nakanishi, M., 2016. SCFFbxo22-KDM4A targets methylated p53 for degradation and regulates senescence. *Nat Commun* 7, 10574. <https://doi.org/10.1038/ncomms10574>
- Jones, L.H., 2018. Small-Molecule Kinase Downregulators. *Cell Chem Biol* 25, 30–35. <https://doi.org/https://doi.org/10.1016/j.chembiol.2017.10.011>
- Jumper, J., Evans, R., Pritzel, A., Green, T., Figurnov, M., Ronneberger, O., Tunyasuvunakool, K., Bates, R., Žídek, A., Potapenko, A., Bridgland, A., Meyer, C., Kohl, S.A.A., Ballard, A.J., Cowie, A., Romera-Paredes, B., Nikolov, S., Jain, R., Adler, J., Back, T., Petersen, S., Reiman, D., Clancy, E., Zielinski, M., Steinegger, M., Pacholska, M., Berghammer, T., Bodenstein, S., Silver, D., Vinyals, O., Senior, A.W., Kavukcuoglu, K., Kohli, P., Hassabis, D., 2021. Highly accurate protein structure prediction with AlphaFold. *Nature* 596, 583–589. <https://doi.org/10.1038/s41586-021-03819-2>
- Kabir, M., Qin, L., Luo, K., Xiong, Y., Sidi, R.A., Park, K.-S., Jin, J., 2024. Discovery and Characterization of a Novel Cereblon-Recruiting PRC1 Bridged PROTAC Degradar. *J Med Chem* 67, 6880–6892. <https://doi.org/10.1021/acs.jmedchem.4c00538>
- Kaefer, A., Yang, J., Noertersheuser, P., Mensing, S., Humerickhouse, R., Awni, W., Xiong, H., 2014. Mechanism-based pharmacokinetic/pharmacodynamic meta-analysis of navitoclax (ABT-263) induced thrombocytopenia. *Cancer Chemother Pharmacol* 74, 593–602. <https://doi.org/10.1007/s00280-014-2530-9>
- Kagiou, C., Cisneros, J.A., Farnung, J., Liwocha, J., Offensperger, F., Dong, K., Yang, K., Tin, G., Horstmann, C.S., Hinterndorfer, M., Paulo, J.A., Scholes, N.S., Sanchez Avila, J., Fellner, M., Andersch, F., Hannich, J.T., Zuber, J., Kubicek, S., Gygi, S.P., Schulman, B.A., Winter, G.E., 2024. Alkylamine-tethered molecules recruit FBXO22 for targeted protein degradation. *Nat Commun* 15, 5409. <https://doi.org/10.1038/s41467-024-49739-3>
- Kaludercic, N., Carpi, A., Menabò, R., Di Lisa, F., Paolocci, N., 2011. Monoamine oxidases (MAO) in the pathogenesis of heart failure and ischemia/reperfusion injury. *Biochimica et Biophysica Acta (BBA) - Molecular Cell Research* 1813, 1323–1332. <https://doi.org/https://doi.org/10.1016/j.bbamcr.2010.09.010>
- Kanemaki, M., Sanchez-Diaz, A., Gambus, A., Labib, K., 2003. Functional proteomic identification of DNA replication proteins by induced proteolysis in vivo. *Nature* 423, 720–724. <https://doi.org/10.1038/nature01692>

- Kaneshige, A., Bai, L., Wang, Mi, McEachern, D., Meagher, J.L., Xu, R., Wang, Y., Jiang, W., Metwally, H., Kirchhoff, P.D., Zhao, L., Jiang, H., Wang, Meilin, Wen, B., Sun, D., Stuckey, J.A., Wang, S., 2023. A selective small-molecule STAT5 PROTAC degrader capable of achieving tumor regression in vivo. *Nat Chem Biol* 19, 703–711. <https://doi.org/10.1038/s41589-022-01248-4>
- Kannt, A., Đikić, I., 2021. Expanding the arsenal of E3 ubiquitin ligases for proximity-induced protein degradation. *Cell Chem Biol.* <https://doi.org/10.1016/j.chembiol.2021.04.007>
- Kholodenko, B.N., 2006. Cell-signalling dynamics in time and space. *Nat Rev Mol Cell Biol* 7, 165–176. <https://doi.org/10.1038/nrm1838>
- Kiely-Collins, H., Winter, G.E., Bernardes, G.J.L., 2021. The role of reversible and irreversible covalent chemistry in targeted protein degradation. *Cell Chem Biol.* <https://doi.org/10.1016/j.chembiol.2021.03.005>
- King, E.A., Cho, Y., Hsu, N.S., Dovala, D., McKenna, J.M., Tallarico, J.A., Schirle, M., Nomura, D.K., 2023. Chemoproteomics-enabled discovery of a covalent molecular glue degrader targeting NF- $\kappa$ B. *Cell Chem Biol* 30, 394-402.e9. <https://doi.org/https://doi.org/10.1016/j.chembiol.2023.02.008>
- Klinman, J.P., Dooley, D.M., Duine, J.A., Knowles, P.F., Mondovi, B., Villafranca, J.J., 1991. Status of the cofactor identity in copper oxidative enzymes. *FEBS Lett* 282, 1–4. [https://doi.org/https://doi.org/10.1016/0014-5793\(91\)80431-2](https://doi.org/https://doi.org/10.1016/0014-5793(91)80431-2)
- Kozicka, Z., Suchyta, D.J., Focht, V., Kempf, G., Petzold, G., Jentzsch, M., Zou, C., Di Genua, C., Donovan, K.A., Coomar, S., Cigler, M., Mayor-Ruiz, C., Schmid-Burgk, J.L., Häussinger, D., Winter, G.E., Fischer, E.S., Słabicki, M., Gillingham, D., Ebert, B.L., Thomä, N.H., 2024. Design principles for cyclin K molecular glue degraders. *Nat Chem Biol* 20, 93–102. <https://doi.org/10.1038/s41589-023-01409-z>
- Krönke, J., Fink, E.C., Hollenbach, P.W., MacBeth, K.J., Hurst, S.N., Udeshi, N.D., Chamberlain, P.P., Mani, D.R., Man, H.W., Gandhi, A.K., Svinkina, T., Schneider, R.K., McConkey, M., Järås, M., Griffiths, E., Wetzler, M., Bullinger, L., Cathers, B.E., Carr, S.A., Chopra, R., Ebert, B.L., 2015. Lenalidomide induces ubiquitination and degradation of CK1 $\alpha$  in del(5q) MDS. *Nature* 523, 183–188. <https://doi.org/10.1038/nature14610>
- Krönke, J., Udeshi, N.D., Narla, A., Grauman, P., Hurst, S.N., McConkey, M., Svinkina, T., Heckl, D., Comer, E., Li, X., Ciarlo, C., Hartman, E., Munshi, N., Schenone, M., Schreiber, S.L., Carr, S.A., Ebert, B.L., 2014. Lenalidomide Causes Selective Degradation of IKZF1 and IKZF3 in Multiple Myeloma Cells. *Science* (1979) 343, 301–305. <https://doi.org/10.1126/science.1244851>
- KyungWon, H., Xiaobo, Z., Hiroyuki, H., Je-Yoel, C., A, L.T., Jianping, J., J, W.H., Karl, M., 2007. Human Papillomavirus Type 16 E7 Oncoprotein Associates with the Cullin 2 Ubiquitin Ligase Complex, Which Contributes to Degradation of the Retinoblastoma Tumor Suppressor. *J Virol* 81, 9737–9747. <https://doi.org/10.1128/jvi.00881-07>



- Landré, V., Rotblat, B., Melino, S., Bernassola, F., Melino, G., 2014. Screening for E3-Ubiquitin ligase inhibitors: challenges and opportunities, *Oncotarget*.
- Lechtenberg, B.C., Rajput, A., Sanishvili, R., Dobaczewska, M.K., Ware, C.F., Mace, P.D., Riedl, S.J., 2016. Structure of a HOIP/E2~ubiquitin complex reveals RBR E3 ligase mechanism and regulation. *Nature* 529, 546–550. <https://doi.org/10.1038/nature16511>
- Lee, S., Hu, L., 2020. Nrf2 activation through the inhibition of Keap1–Nrf2 protein–protein interaction. *Medicinal Chemistry Research* 29, 846–867. <https://doi.org/10.1007/s00044-020-02539-y>
- Lévy, F., Johnston, J.A., Varshavsky, A., 1999. Analysis of a conditional degradation signal in yeast and mammalian cells. *Eur J Biochem* 259, 244–252. <https://doi.org/https://doi.org/10.1046/j.1432-1327.1999.00024.x>
- Li, L., Mi, D., Pei, H., Duan, Q., Wang, X., Zhou, W., Jin, J., Li, D., Liu, M., Chen, Y., 2020. In vivo target protein degradation induced by PROTACs based on E3 ligase DCAF15. *Signal Transduct Target Ther* 5, 129. <https://doi.org/10.1038/s41392-020-00245-0>
- Li, T., Robert, E.I., van Breugel, P.C., Strubin, M., Zheng, N., 2010. A promiscuous  $\alpha$ -helical motif anchors viral hijackers and substrate receptors to the CUL4–DDB1 ubiquitin ligase machinery. *Nat Struct Mol Biol* 17, 105–111. <https://doi.org/10.1038/nsmb.1719>
- Li, W., Garcia-Rivera, E.M., Mitchell, D.C., Chick, J.M., Maetani, M., Knapp, J.M., Matthews, G.M., Shirasaki, R., de Matos Simoes, R., Viswanathan, V., Pulice, J.L., Rees, M.G., Roth, J.A., Gygi, S.P., Mitsiades, C.S., Kadoch, C., Schreiber, S.L., Ostrem, J.M.L., 2024. Highly specific intracellular ubiquitination of a small molecule. *bioRxiv* 2024.01.26.577493. <https://doi.org/10.1101/2024.01.26.577493>
- Li, Y., Bao, K., Sun, J., Ge, R., Zhang, Q., Zhang, B., Yan, X., Li, J., Shi, F., Zhang, M., Zang, J., Liu, M., Zhou, J., Mi, W., Xie, S., Chen, D., Shi, L., Dong, C., 2025. Design of PROTACs utilizing the E3 ligase GID4 for targeted protein degradation. *Nat Struct Mol Biol*. <https://doi.org/10.1038/s41594-025-01537-1>
- Li, Y.-D., Ma, M.W., Hassan, M.M., Hunkeler, M., Teng, M., Puvar, K., Rutter, J.C., Lumpkin, R.J., Sandoval, B., Jin, C.Y., Schmoker, A.M., Ficarro, S.B., Cheong, H., Metivier, R.J., Wang, M.Y., Xu, S., Byun, W.S., Groendyke, B.J., You, I., Sigua, L.H., Tavares, I., Zou, C., Tsai, J.M., Park, P.M.C., Yoon, H., Majewski, F.C., Sperling, H.T., Marto, J.A., Qi, J., Nowak, R.P., Donovan, K.A., Stabicki, M., Gray, N.S., Fischer, E.S., Ebert, B.L., 2024. Template-assisted covalent modification underlies activity of covalent molecular glues. *Nat Chem Biol* 20, 1640–1649. <https://doi.org/10.1038/s41589-024-01668-4>
- Li, Z., Chenggang, Z., Yu, D., Yiyan, F., and Lu, B., 2020. ATTEC: a potential new approach to target proteinopathies. *Autophagy* 16, 185–187. <https://doi.org/10.1080/15548627.2019.1688556>

- Li, Z., Ma, S., Zhang, L., Zhang, S., Ma, Z., Du, L., Li, M., 2023. Targeted Protein Degradation Induced by HEMTACs Based on HSP90. *J Med Chem* 66, 733–751. <https://doi.org/10.1021/acs.jmedchem.2c01648>
- Liberles, S.D., Diver, S.T., Austin, D.J., Schreiber, S.L., 1997. Inducible gene expression and protein translocation using nontoxic ligands identified by a mammalian three-hybrid screen. *Proceedings of the National Academy of Sciences* 94, 7825–7830. <https://doi.org/10.1073/pnas.94.15.7825>
- Lignitto, L., LeBoeuf, S.E., Homer, H., Jiang, S., Askenazi, M., Karakousi, T.R., Pass, H.I., Bhutkar, A.J., Tsigos, A., Ueberheide, B., Sayin, V.I., Papagiannakopoulos, T., Pagano, M., 2019. Nrf2 Activation Promotes Lung Cancer Metastasis by Inhibiting the Degradation of Bach1. *Cell* 178, 316–329.e18. <https://doi.org/10.1016/j.cell.2019.06.003>
- Lim, M., Cong, T. Do, Orr, L.M., Toriki, E.S., Kile, A.C., Papatzimas, J.W., Lee, E., Lin, Y., Nomura, D.K., 2024. DCAF16-Based Covalent Handle for the Rational Design of Monovalent Degraders. *ACS Cent Sci* 10, 1318–1331. <https://doi.org/10.1021/acscentsci.4c00286>
- Lipinski, C.A., Lombardo, F., Dominy, B.W., Feeney, P.J., 1997. Experimental and computational approaches to estimate solubility and permeability in drug discovery and development settings. *Adv Drug Deliv Rev* 23, 3–25. [https://doi.org/https://doi.org/10.1016/S0169-409X\(96\)00423-1](https://doi.org/10.1016/S0169-409X(96)00423-1)
- Liu, F., Ou, W., Tang, W., Huang, Z., Zhu, Z., Ding, W., Fu, J., Zhu, Y., Liu, C., Xu, W., Du, P., 2021. Increased AOC1 Expression Promotes Cancer Progression in Colorectal Cancer. *Front Oncol* Volume 11-2021.
- Liu, J., Farmer, J.D., Lane, W.S., Friedman, J., Weissman, I., Schreiber, S.L., 1991. Calcineurin Is a Common Target of Cyclophilin-Cyclosporin A and FKBP-FK506 Complexes, *Cell*.
- Liu, P., Cong, X., Liao, S., Jia, X., Wang, X., Dai, W., Zhai, L., Zhao, L., Ji, J., Ni, D., Liu, Z., Chen, Y., Pan, L., Liu, W., Zhang, J., Huang, M., Liu, B., Tan, M., 2022. Global identification of phospho-dependent SCF substrates reveals a FBXO22 phosphodegron and an ERK-FBXO22-BAG3 axis in tumorigenesis. *Cell Death Differ* 29, 1–13. <https://doi.org/10.1038/s41418-021-00827-7>
- Liu, X., Ciulli, A., 2023. Proximity-Based Modalities for Biology and Medicine. *ACS Cent Sci* 9, 1269–1284. <https://doi.org/10.1021/acscentsci.3c00395>
- Liu, Y., Yang, J., Wang, T., Luo, M., Chen, Y., Chen, C., Ronai, Z., Zhou, Y., Ruppin, E., Han, L., 2023. Expanding PROTACtable genome universe of E3 ligases. *Nat Commun* 14, 6509. <https://doi.org/10.1038/s41467-023-42233-2>
- Livingston, J.A., Blay, J.-Y., Trent, J., Valverde, C., Agulnik, M., Gounder, M., Le Cesne, A., McKean, M., Wagner, M.J., Stacchiotti, S., Agresta, S., Quintás-Cardama, A., Reilly, S.A., Healy, K., Hickman, D., Zhao, T., Ballesteros-Perez, A., Khalil, A., Collins, M.P., Piel, J., Horrigan, K., Lefkovith, A., Innis, S., Lazar, A.J., Cote, G.M., Wagner, A.J., 2025. A Phase I Study of FHD-609, a Heterobifunctional Degradator of Bromodomain-Containing Protein 9,

- in Patients with Advanced Synovial Sarcoma or SMARCB1-Deficient Tumors. *Clinical Cancer Research* 31, 628–638. <https://doi.org/10.1158/1078-0432.CCR-24-2583>
- Long, X., Nephew, K.P., 2006. Fulvestrant (ICI 182,780)-dependent Interacting Proteins Mediate Immobilization and Degradation of Estrogen Receptor- $\alpha$ ; \*. *Journal of Biological Chemistry* 281, 9607–9615. <https://doi.org/10.1074/jbc.M510809200>
- Lopez-Girona, A., Mendy, D., Ito, T., Miller, K., Gandhi, A.K., Kang, J., Karasawa, S., Carmel, G., Jackson, P., Abbasian, M., Mahmoudi, A., Cathers, B., Rychak, E., Gaidarova, S., Chen, R., Schafer, P.H., Handa, H., Daniel, T.O., Evans, J.F., Chopra, R., 2012. Cereblon is a direct protein target for immunomodulatory and antiproliferative activities of lenalidomide and pomalidomide. *Leukemia* 26, 2326–2335. <https://doi.org/10.1038/leu.2012.119>
- Lu, G., Middleton, R.E., Sun, H., Naniong, M.V., Ott, C.J., Mitsiades, C.S., Wong, K.K., Bradner, J.E., Kaelin, W.G., 2014. The myeloma drug lenalidomide promotes the cereblon-dependent destruction of ikaros proteins. *Science* (1979) 343, 305–309. <https://doi.org/10.1126/science.1244917>
- Lu, H., Zhou, Q., He, J., Jiang, Z., Peng, C., Tong, R., Shi, J., 2020. Recent advances in the development of protein–protein interactions modulators: mechanisms and clinical trials. *Signal Transduct Target Ther* 5, 213. <https://doi.org/10.1038/s41392-020-00315-3>
- Lu, M., Liu, T., Jiao, Q., Ji, J., Tao, M., Liu, Y., You, Q., Jiang, Z., 2018. Discovery of a Keap1-dependent peptide PROTAC to knockdown Tau by ubiquitination-proteasome degradation pathway. *Eur J Med Chem* 146, 251–259. <https://doi.org/https://doi.org/10.1016/j.ejmech.2018.01.063>
- Lu, P., Cheng, Y., Xue, L., Ren, X., Xu, X., Chen, C., Cao, L., Li, J., Wu, Q., Sun, S., Hou, J., Jia, W., Wang, W., Ma, Y., Jiang, Z., Li, C., Qi, X., Huang, N., Han, T., 2024. Selective degradation of multimeric proteins by TRIM21-based molecular glue and PROTAC degraders. *Cell* 187, 7126–7142.e20. <https://doi.org/10.1016/j.cell.2024.10.015>
- Luo, M., Spradlin, J.N., Boike, L., Tong, B., Brittain, S.M., McKenna, J.M., Tallarico, J.A., Schirle, M., Maimone, T.J., Nomura, D.K., 2021. Chemoproteomics-enabled discovery of covalent RNF114-based degraders that mimic natural product function. *Cell Chem Biol* 28, 559–566.e15. <https://doi.org/10.1016/j.chembiol.2021.01.005>
- Luo, Z., Tzivion, G., Belshaw, P.J., Vavvas, D., Marshall, M., Avruch, J., 1996. Oligomerization activates c-Raf-1 through a Ras-dependent mechanism. *Nature* 383, 181–185. <https://doi.org/10.1038/383181a0>
- Lv, L., Chen, P., Cao, L., Li, Y., Zeng, Z., Cui, Y., Wu, Q., Li, J., Wang, J.-H., Dong, M.-Q., Qi, X., Han, T., 2020. Discovery of a molecular glue promoting CDK12-DDB1 interaction to trigger cyclin K degradation. *Elife* 9, e59994. <https://doi.org/10.7554/eLife.59994>
- Ma, L., Zhang, K., Huang, Z., Guo, Y., Liu, N., Chen, J., Wang, X., Liu, Y., Li, M., Li, J., Yang, C., Liu, S., Yang, G., 2024. Development of Novel Silicon-Based Hydrophobic Tags (SiHyT) for

- Targeted Proteins Degradation. *J Med Chem*.  
<https://doi.org/10.1021/acs.jmedchem.4c02273>
- Ma, Y., Chen, H., Li, H., Zhao, Z., An, Q., Shi, C., 2024. Targeting monoamine oxidase A: a strategy for inhibiting tumor growth with both immune checkpoint inhibitors and immune modulators. *Cancer Immunology, Immunotherapy* 73, 48. <https://doi.org/10.1007/s00262-023-03622-0>
- Mahon, C., Krogan, N.J., Craik, C.S., Pick, E., 2014. Cullin E3 Ligases and their rewiring by viral factors. *Biomolecules*. <https://doi.org/10.3390/biom4040897>
- Mallery, D.L., McEwan, W.A., Bidgood, S.R., Towers, G.J., Johnson, C.M., James, L.C., 2010. Antibodies mediate intracellular immunity through tripartite motif-containing 21 (TRIM21). *Proceedings of the National Academy of Sciences* 107, 19985–19990. <https://doi.org/10.1073/pnas.1014074107>
- Mares, A., Miah, A.H., Smith, I.E.D., Rackham, M., Thawani, A.R., Cryan, J., Haile, P.A., Votta, B.J., Beal, A.M., Capriotti, C., Reilly, M.A., Fisher, D.T., Zinn, N., Bantscheff, M., MacDonald, T.T., Vossenkamper, A., Dace, P., Churcher, I., Benowitz, A.B., Watt, G., Denyer, J., Scott-Stevens, P., Harling, J.D., 2020. Extended pharmacodynamic responses observed upon PROTAC-mediated degradation of RIPK2. *Commun Biol* 3, 140. <https://doi.org/10.1038/s42003-020-0868-6>
- Mario, C., Michelino, D.L., Komal, J., Xichun, H., Sylvain, L., Anne, P., Claudio, Z., Jiuwei, C., Marina, C., Timucin, C., J, J.K., Christian, F., Tetsuhiro, Y., Alvaro, R.-L., Ahmet, S., Andrea, F., Valentina, G., Andrea, M., Marie-Ange, M.-R., Umut, D., Yongqiang, Z., Olga, V., R, L.D., Marcella, M., Janaki, P., Xin, Z., P, H.E., 2025. Vepdegestrant, a PROTAC Estrogen Receptor Degradar, in Advanced Breast Cancer. *New England Journal of Medicine* 0. <https://doi.org/10.1056/NEJMoa2505725>
- Martinez-Zapien, D., Ruiz, F.X., Poirson, J., Mitschler, A., Ramirez, J., Forster, A., Cousido-Siah, A., Masson, M., Pol, S. Vande, Podjarny, A., Travé, G., Zanier, K., 2016. Structure of the E6/E6AP/p53 complex required for HPV-mediated degradation of p53. *Nature* 529, 541–545. <https://doi.org/10.1038/nature16481>
- Matyskiela, M.E., Lu, G., Ito, T., Pagarigan, B., Lu, C.-C., Miller, K., Fang, W., Wang, N.-Y., Nguyen, D., Houston, J., Carmel, G., Tran, T., Riley, M., Nosaka, L., Lander, G.C., Gaidarova, S., Xu, S., Ruchelman, A.L., Handa, H., Carmichael, J., Daniel, T.O., Cathers, B.E., Lopez-Girona, A., Chamberlain, P.P., 2016. A novel cereblon modulator recruits GSPT1 to the CRL4CRBN ubiquitin ligase. *Nature* 535, 252–257. <https://doi.org/10.1038/nature18611>
- Matyskiela, M.E., Zhu, J., Baughman, J.M., Clayton, T., Slade, M., Wong, H.K., Danga, K., Zheng, X., Labow, M., LeBrun, L., Lu, G., Chamberlain, P.P., Thompson, J.W., 2020. Cereblon Modulators Target ZBTB16 and Its Oncogenic Fusion Partners for Degradation via Distinct Structural Degrons. *ACS Chem Biol* 15, 3149–3158. <https://doi.org/10.1021/acscchembio.0c00674>

- Mayor-Ruiz, C., Bauer, S., Brand, M., Kozicka, Z., Siklos, M., Imrichova, H., Kalthener, I.H., Hahn, E., Seiler, K., Koren, A., Petzold, G., Fellner, M., Bock, C., Müller, A.C., Zuber, J., Geyer, M., Thomä, N.H., Kubicek, S., Winter, G.E., 2020. Rational discovery of molecular glue degraders via scalable chemical profiling. *Nat Chem Biol* 16, 1199–1207. <https://doi.org/10.1038/s41589-020-0594-x>
- McGrath, A.P., Hilmer, K.M., Collyer, C.A., Shepard, E.M., Elmore, B.O., Brown, D.E., Dooley, D.M., Guss, J.M., 2009. Structure and Inhibition of Human Diamine Oxidase. *Biochemistry* 48, 9810–9822. <https://doi.org/10.1021/bi9014192>
- Melchert, M., List, A., 2007. The thalidomide saga. *Int J Biochem Cell Biol* 39, 1489–1499. <https://doi.org/https://doi.org/10.1016/j.biocel.2007.01.022>
- Meyers, M., Cismoski, S., Panidapu, A., Chie-Leon, B., Nomura, D.K., 2024. Targeted Protein Degradation through Recruitment of the CUL4 Complex Adaptor Protein DDB1. *ACS Chem Biol* 19, 58–68. <https://doi.org/10.1021/acscchembio.3c00487>
- Michnick, S.W., Rosen, M.K., Wandless, T.J., Karplus, M., Schreiber, S.L., 1991. Solution Structure of FKBP, a Rotamase Enzyme and Receptor for FK506 and Rapamycin. *Science* (1979) 252, 836–839. <https://doi.org/10.1126/science.1709301>
- Montoya, S., Bourcier, J., Noviski, M., Lu, H., Thompson, M.C., Chirino, A., Jahn, J., Sondhi, A.K., Gajewski, S., Tan, Y.S. (May), Yung, S., Urban, A., Wang, E., Han, C., Mi, X., Kim, W.J., Sievers, Q., Auger, P., Bousquet, H., Brathaban, N., Bravo, B., Gessner, M., Guiducci, C., Iuliano, J.N., Kane, T., Mukerji, R., Reddy, P.J., Powers, J., Sanchez Garcia de los Rios, M., Ye, J., Barrientos Risso, C., Tsai, D., Pardo, G., Notti, R.Q., Pardo, A., Affer, M., Nawaratne, V., Totiger, T.M., Pena-Velasquez, C., Rhodes, J.M., Zelenetz, A.D., Alencar, A., Roeker, L.E., Mehta, S., Garippa, R., Linley, A., Soni, R.K., Skånland, S.S., Brown, R.J., Mato, A.R., Hansen, G.M., Abdel-Wahab, O., Taylor, J., 2024. Kinase-impaired BTK mutations are susceptible to clinical-stage BTK and IKZF1/3 degrader NX-2127. *Science* (1979) 383, eadi5798–eadi5798. <https://doi.org/10.1126/science.adi5798>
- Morreale, F.E., Kleine, S., Leodolter, J., Junker, S., Hoi, D.M., Ovchinnikov, S., Okun, A., Kley, J., Kurzbauer, R., Junk, L., Guha, S., Podlesinski, D., Kazmaier, U., Boehmelt, G., Weinstabl, H., Rumpel, K., Schmiedel, V.M., Hartl, M., Haselbach, D., Meinhart, A., Kaiser, M., Clausen, T., 2022. BacPROTACs mediate targeted protein degradation in bacteria. *Cell* 185, 2338–2353.e18. <https://doi.org/https://doi.org/10.1016/j.cell.2022.05.009>
- Mutvei, A.P., Nagiec, M.J., Blenis, J., 2023. Balancing lysosome abundance in health and disease. *Nat Cell Biol* 25, 1254–1264. <https://doi.org/10.1038/s41556-023-01197-7>
- Naito, M., 2022. Targeted protein degradation and drug discovery. *The Journal of Biochemistry* 172, 61–69. <https://doi.org/10.1093/jb/mvac041>
- Nawaz, Z., Lonard, D.M., Dennis, A.P., Smith, C.L., O'Malley, B.W., 1999. Proteasome-dependent degradation of the human estrogen receptor. *Proceedings of the National Academy of Sciences* 96, 1858–1862. <https://doi.org/10.1073/pnas.96.5.1858>

- Nguyen, N.T., Hanieh, H., Nakahama, T., Kishimoto, T., 2013. The roles of aryl hydrocarbon receptor in immune responses. *Int Immunol* 25, 335–343. <https://doi.org/10.1093/intimm/dxt011>
- Nie, D.Y., Tabor, J.R., Li, J., Kuter, M., St-Germain, J., Hanley, R.P., Wolf, E., Paulakonis, E., Kenney, T.M.G., Duan, S., Shrestha, S., Owens, D.D.G., Maitland, M.E.R., Pon, A., Szewczyk, M., Lamberto, A.J., Menes, M., Li, F., Penn, L.Z., Barsyte-Lovejoy, D., Brown, N.G., Barsotti, A.M., Stamford, A.W., Collins, J.L., Wilson, D.J., Raught, B., Licht, J.D., James, L.I., Arrowsmith, C.H., 2024. Recruitment of FBXO22 for targeted degradation of NSD2. *Nat Chem Biol* 20, 1597–1607. <https://doi.org/10.1038/s41589-024-01660-y>
- Nishimura, K., Fukagawa, T., Takisawa, H., Kakimoto, T., Kanemaki, M., 2009. An auxin-based degron system for the rapid depletion of proteins in nonplant cells. *Nat Methods* 6, 917–922. <https://doi.org/10.1038/nmeth.1401>
- Nishizawa, H., Yamanaka, M., Igarashi, K., 2023. Ferroptosis: regulation by competition between NRF2 and BACH1 and propagation of the death signal. *FEBS J* 290, 1688–1704. <https://doi.org/https://doi.org/10.1111/febs.16382>
- Nowak, R.P., Che, J., Ferrao, S., Kong, N.R., Liu, H., Zervas, B.L., Jones, L.H., 2023. Structural rationalization of GSPT1 and IKZF1 degradation by thalidomide molecular glue derivatives. *RSC Med Chem* 14, 501–506. <https://doi.org/10.1039/D2MD00347C>
- Nowak, R.P., DeAngelo, S.L., Buckley, D., He, Z., Donovan, K.A., An, J., Safaei, N., Jedrychowski, M.P., Ponthier, C.M., Ishoey, M., Zhang, T., Mancias, J.D., Gray, N.S., Bradner, J.E., Fischer, E.S., 2018. Plasticity in binding confers selectivity in ligand-induced protein degradation. *Nat Chem Biol* 14, 706–714. <https://doi.org/10.1038/s41589-018-0055-y>
- Ohoka, N., Okuhira, K., Ito, M., Nagai, K., Shibata, N., Hattori, T., Ujikawa, O., Shimokawa, K., Sano, O., Koyama, R., Fujita, H., Teratani, M., Matsumoto, H., Imaeda, Y., Nara, H., Cho, N., Naito, M., 2017. In Vivo Knockdown of Pathogenic Proteins via Specific and Nongenetic Inhibitor of Apoptosis Protein (IAP)-dependent Protein Erasers (SNIPERs)\*. *Journal of Biological Chemistry* 292, 4556–4570. <https://doi.org/https://doi.org/10.1074/jbc.M116.768853>
- Ohoka, N., Tsuji, G., Shoda, T., Fujisato, T., Kurihara, M., Demizu, Y., Naito, M., 2019. Development of Small Molecule Chimeras That Recruit AhR E3 Ligase to Target Proteins. *ACS Chem Biol* 14, 2822–2832. <https://doi.org/10.1021/acscchembio.9b00704>
- Ohtake, F., Baba, A., Takada, I., Okada, M., Iwasaki, K., Miki, H., Takahashi, S., Kouzmenko, A., Nohara, K., Chiba, T., Fujii-Kuriyama, Y., Kato, S., 2007. Dioxin receptor is a ligand-dependent E3 ubiquitin ligase. *Nature* 446, 562–566. <https://doi.org/10.1038/nature05683>
- Okuhira, K., Demizu, Y., Hattori, T., Ohoka, N., Shibata, N., Nishimaki-Mogami, T., Okuda, H., Kurihara, M., Naito, M., 2013. Development of hybrid small molecules that induce degradation of estrogen receptor- $\alpha$  and necrotic cell death in breast cancer cells. *Cancer Sci* 104, 1492–1498. <https://doi.org/https://doi.org/10.1111/cas.12272>

- Okuhira, K., Ohoka, N., Sai, K., Nishimaki-Mogami, T., Itoh, Y., Ishikawa, M., Hashimoto, Y., Naito, M., 2011. Specific degradation of CRABP-II via cIAP1-mediated ubiquitylation induced by hybrid molecules that crosslink cIAP1 and the target protein. *FEBS Lett* 585, 1147–1152. <https://doi.org/https://doi.org/10.1016/j.febslet.2011.03.019>
- Otten, E.G., Werner, E., Crespillo-Casado, A., Boyle, K.B., Dharamdasani, V., Pathe, C., Santhanam, B., Randow, F., 2021. Ubiquitylation of lipopolysaccharide by RNF213 during bacterial infection. *Nature* 594, 111–116. <https://doi.org/10.1038/s41586-021-03566-4>
- Padovani, C., Jevtić, P., Rapé, M., 2022. Quality control of protein complex composition. *Mol Cell* 82, 1439–1450. <https://doi.org/https://doi.org/10.1016/j.molcel.2022.02.029>
- Paulk, J., 2021. Lysosome-targeting chimeras evolve. *Nat Chem Biol* 17, 931–933. <https://doi.org/10.1038/s41589-021-00835-1>
- Perillo, B., Tramontano, A., Pezone, A., Migliaccio, A., 2020. LSD1: more than demethylation of histone lysine residues. *Exp Mol Med* 52, 1936–1947. <https://doi.org/10.1038/s12276-020-00542-2>
- Peterson, A.A., Liu, D.R., 2023. Small-molecule discovery through DNA-encoded libraries. *Nat Rev Drug Discov* 22, 699–722. <https://doi.org/10.1038/s41573-023-00713-6>
- Petzold, G., Fischer, E.S., Thomä, N.H., 2016. Structural basis of lenalidomide-induced CK1 $\alpha$  degradation by the CRL4CRBN ubiquitin ligase. *Nature* 532, 127–130. <https://doi.org/10.1038/nature16979>
- Petzold, G., Gainza, P., Annunziato, S., Lamberto, I., Trenh, P., McAllister, L., Demarco, B., Schwander, L., Bunker, R.D., Zlotosch, M., SriRamaratnam, R., Gilberto, S., Langousis, G., Donckele, E.J., Quan, C., Strande, V., Donatis, G.M. De, Alabi, S.B., Alers, J., Matysik, M., Staehly, C., Dubois, A., Osmont, A., Garskovas, M., Lyon, D., Wiedmer, L., Oleinikovas, V., Lieberherr, R., Rubin, N.T., Lam, D.T., Widlund, N.I., Ritzén, A., Caceres, R.M., Vigil, D., Tsai, J., Wallace, O., Peluso, M., Sadok, A., Paterson, A.M., Zarayskiy, V., Fasching, B., Bonenfant, D., Warmuth, M., Castle, J., Townson, S.A., 2024. Mining the CRBN Target Space Redefines Rules for Molecular Glue-induced Neosubstrate Recognition. *bioRxiv* 2024.10.07.616933. <https://doi.org/10.1101/2024.10.07.616933>
- Pickart, C.M., 2001. MECHANISMS UNDERLYING UBIQUITINATION.
- Pike, A., Williamson, B., Harlfinger, S., Martin, S., McGinnity, D.F., 2020. Optimising proteolysis-targeting chimeras (PROTACs) for oral drug delivery: a drug metabolism and pharmacokinetics perspective. *Drug Discov Today* 25, 1793–1800. <https://doi.org/https://doi.org/10.1016/j.drudis.2020.07.013>
- Pla-Prats, C., Thomä, N.H., 2022. Quality control of protein complex assembly by the ubiquitin–proteasome system. *Trends Cell Biol* 32, 696–706. <https://doi.org/https://doi.org/10.1016/j.tcb.2022.02.005>



- Plechanovová, A., Jaffray, E.G., Tatham, M.H., Naismith, J.H., Hay, R.T., 2012. Structure of a RING E3 ligase and ubiquitin-loaded E2 primed for catalysis. *Nature* 489, 115–120. <https://doi.org/10.1038/nature11376>
- Pliatsika, D., Blatter, C., Riedl, R., 2024. Targeted protein degradation: current molecular targets, localization, and strategies. *Drug Discov Today* 29, 104178. <https://doi.org/https://doi.org/10.1016/j.drudis.2024.104178>
- Pohl, C., Dikic, I., 2019. Cellular quality control by the ubiquitin-proteasome system and autophagy. *Science* (1979) 366, 818–822. <https://doi.org/10.1126/science.aax3769>
- Poirson, J., Cho, H., Dhillon, A., Haider, S., Imrit, A.Z., Lam, M.H.Y., Alerasool, N., Lacoste, J., Mizan, L., Wong, C., Gingras, A.-C., Schramek, D., Taipale, M., 2024. Proteome-scale discovery of protein degradation and stabilization effectors. *Nature* 628, 878–886. <https://doi.org/10.1038/s41586-024-07224-3>
- Poling, L.L., Coccoziello, D., He, M., Hurh, E., Lobbardi, R., Jackson, K.L., Fisher, S.L., Pollock, R.M., 2023. CFT8634, a Clinical Stage BRD9 Bi DAC™ Degradar, Is Active in a Subset of Multiple Myeloma Cell Line Models and Synergistic When Combined with Pomalidomide. *Blood* 142, 6594. <https://doi.org/10.1182/blood-2023-174555>
- Pruneda, J.N., Littlefield, P.J., Soss, S.E., Nordquist, K.A., Chazin, W.J., Brzovic, P.S., Klevit, R.E., 2012. Structure of an E3:E2~Ub Complex Reveals an Allosteric Mechanism Shared among RING/U-box Ligases. *Mol Cell* 47, 933–942. <https://doi.org/https://doi.org/10.1016/j.molcel.2012.07.001>
- Pruschy, M.N., Spencer, D.M., Kapoor, T.M., Miyake, H., Crabtree, G.R., Schreiber, S.L., 1994. Mechanistic studies of a signaling pathway activated by the organic dimerizer FK1012. *Chem Biol* 1, 163–172. [https://doi.org/10.1016/1074-5521\(94\)90006-X](https://doi.org/10.1016/1074-5521(94)90006-X)
- Qilu Pharmaceutical Co., Ltd., 2023. Trial of QLH12016 in Patients With Metastatic Castration Resistant Prostate Cancer (NCT05973149).
- Resnick, E., Bradley, A., Gan, Jinrui, Douangamath, A., Krojer, T., Sethi, R., Geurink, P.P., Aimon, A., Amitai, G., Bellini, D., Bennett, J., Fairhead, M., Fedorov, O., Gabizon, R., Gan, Jin, Guo, J., Plotnikov, A., Reznik, N., Ruda, G.F., Díaz-Sáez, L., Straub, V.M., Szommer, T., Velupillai, S., Zaidman, D., Zhang, Y., Coker, A.R., Dowson, C.G., Barr, H.M., Wang, C., Huber, K.V.M., Brennan, P.E., Ovaa, H., von Delft, F., London, N., 2019. Rapid Covalent-Probe Discovery by Electrophile-Fragment Screening. *J Am Chem Soc* 141, 8951–8968. <https://doi.org/10.1021/jacs.9b02822>
- Rodríguez-Gimeno, A., Galdeano, C., 2024. Drug Discovery Approaches to Target E3 Ligases. *ChemBioChem*. <https://doi.org/10.1002/cbic.202400656>
- Rodriguez-Gonzalez, A., Cyrus, K., Salcius, M., Kim, K., Crews, C.M., Deshaies, R.J., Sakamoto, K.M., 2008. Targeting steroid hormone receptors for ubiquitination and degradation in breast and prostate cancer. *Oncogene* 27, 7201–7211. <https://doi.org/10.1038/onc.2008.320>

- Rotin, D., Kumar, S., 2009. Physiological functions of the HECT family of ubiquitin ligases. *Nat Rev Mol Cell Biol* 10, 398–409. <https://doi.org/10.1038/nrm2690>
- Roy, N., Wyseure, T., Lo, I.-C., Metzger, J., Eissler, C.L., Bernard, S.M., Bok, I., Snead, A.N., Parker, A., Green, J.C., Inloes, J., Jacinto, S.R., Kuenzi, B., Horning, B.D., Ibrahim, N., Grabow, S., Panda, H., Bhatt, D.P., Saeidi, S., Zolkind, P., Rush, Z., Negri, K., Williams, H.N., Walton, E., Pastuszka, M.K., Sigler, J.J., Tran, E., Hee, K., McLaughlin, J., Ambrus-Aikelin, G., Pollock, J., Abraham, R.T., Kinsella, T.M., Simon, G.M., Major, M.B., Weinstein, D.S., Patricelli, M.P., 2024. Suppression of NRF2-dependent cancer growth by a covalent allosteric molecular glue. *bioRxiv* 2024.10.04.616592. <https://doi.org/10.1101/2024.10.04.616592>
- Rui, H., Ashton, K.S., Min, J., Wang, C., Potts, P.R., 2023. Protein-protein interfaces in molecular glue-induced ternary complexes: classification, characterization, and prediction. *RSC Chem Biol*. <https://doi.org/10.1039/d2cb00207h>
- Sabatini, D.M., Erdjument-Bromage, H., Lui, M., Tempst, P., Snyder, S.H., 1994. RAFT1: A mammalian protein that binds to FKBP12 in a rapamycin-dependent fashion and is homologous to yeast TORs. *Cell* 78, 35–43. [https://doi.org/10.1016/0092-8674\(94\)90570-3](https://doi.org/10.1016/0092-8674(94)90570-3)
- Safe, S., Cheng, Y., Jin, U.-H., 2017. The aryl hydrocarbon receptor (AhR) as a drug target for cancer chemotherapy. *Curr Opin Toxicol* 2, 24–29. <https://doi.org/https://doi.org/10.1016/j.cotox.2017.01.012>
- Sakamoto, K.M., Kim, K.B., Kumagai, A., Mercurio, F., Crews, C.M., Deshaies, R.J., 2001. Protacs: Chimeric molecules that target proteins to the Skp1–Cullin–F box complex for ubiquitination and degradation. *Proceedings of the National Academy of Sciences* 98, 8554–8559. <https://doi.org/10.1073/pnas.141230798>
- Sakamoto, K.M., Kim, K.B., Verma, R., Ransick, A., Stein, B., Crews, C.M., Deshaies, R.J., 2003. Development of Protacs to Target Cancer-promoting Proteins for Ubiquitination and Degradation\*. *Molecular & Cellular Proteomics* 2, 1350–1358. <https://doi.org/https://doi.org/10.1074/mcp.T300009-MCP200>
- Salmi, M., Jalkanen, S., 2017. Vascular Adhesion Protein-1: A Cell Surface Amine Oxidase in Translation. *Antioxid Redox Signal* 30, 314–332. <https://doi.org/10.1089/ars.2017.7418>
- Salvi, D., Tavladoraki, P., 2020. The tree of life of polyamine oxidases. *Sci Rep* 10, 17858. <https://doi.org/10.1038/s41598-020-74708-3>
- Samarasinghe, K.T.G., An, E., Genuth, M.A., Chu, L., Holley, S.A., Crews, C.M., 2022. OligoTRAFTACs: A generalizable method for transcription factor degradation. *RSC Chem Biol* 3, 1144–1153. <https://doi.org/10.1039/D2CB00138A>
- Sasso, J.M., Tenchov, R., Wang, D., Johnson, L.S., Wang, X., Zhou, Q.A., 2023. Molecular Glues: The Adhesive Connecting Targeted Protein Degradation to the Clinic. *Biochemistry* 62, 601–623. <https://doi.org/10.1021/acs.biochem.2c00245>

- Satz, A.L., Brunschweiler, A., Flanagan, M.E., Gloger, A., Hansen, N.J. V, Kuai, L., Kunig, V.B.K., Lu, X., Madsen, D., Marcaurelle, L.A., Mulrooney, C., O'Donovan, G., Sakata, S., Scheuermann, J., 2022. DNA-encoded chemical libraries. *Nature Reviews Methods Primers* 2, 3. <https://doi.org/10.1038/s43586-021-00084-5>
- Schneekloth, A.R., Pucheault, M., Tae, H.S., Crews, C.M., 2008. Targeted intracellular protein degradation induced by a small molecule: En route to chemical proteomics. *Bioorg Med Chem Lett* 18, 5904–5908. <https://doi.org/https://doi.org/10.1016/j.bmcl.2008.07.114>
- Schneekloth, J.S.Jr., Fonseca, F.N., Koldobskiy, M., Mandal, A., Deshaies, R., Sakamoto, K., Crews, C.M., 2004. Chemical Genetic Control of Protein Levels: Selective in Vivo Targeted Degradation. *J Am Chem Soc* 126, 3748–3754. <https://doi.org/10.1021/ja039025z>
- Scholes, N.S., Bertoni, M., Comajuncosa-Creus, A., Kladnik, K., Frommelt, F., Hinterndorfer, M., Razumkov, H., Prokofeva, P., Schwalm, M.P., Imrichova, H., Barone, E., Schätz, C., Rukavina, A., Koren, A., Kubicek, S., Knapp, S., Gray, N.S., Superti-Furga, G., Kuster, B., Aloy, P., Winter, G.E., 2024. Inhibitor-induced supercharging of kinase turnover via endogenous proteolytic circuits. *bioRxiv* 2024.07.10.602881. <https://doi.org/10.1101/2024.07.10.602881>
- Schreiber, S.L., 2019. A Chemical Biology View of Bioactive Small Molecules and a Binder-Based Approach to Connect Biology to Precision Medicines. *Isr J Chem* 59, 52–59. <https://doi.org/https://doi.org/10.1002/ijch.201800113>
- Schreiber, S.L., 1992. ImmunophilinSensitive Protein Phosphatase Action in Cell Signaling Pathways, *Cell*.
- Schröder, M., Renatus, M., Liang, X., Meili, F., Zoller, T., Ferrand, S., Gauter, F., Li, X., Sigoillot, F., Gleim, S., Stachyra, T.-M., Thomas, J.R., Begue, D., Khoshouei, M., Lefeuve, P., Andraos-Rey, R., Chung, B., Ma, R., Pinch, B., Hofmann, A., Schirle, M., Schmiedeberg, N., Imbach, P., Gorses, D., Calkins, K., Bauer-Probst, B., Maschlej, M., Niederst, M., Maher, R., Henault, M., Alford, J., Ahrne, E., Tordella, L., Hollingworth, G., Thomä, N.H., Vulpetti, A., Radimerski, T., Holzer, P., Carbonneau, S., Thoma, C.R., 2024. DCAF1-based PROTACs with activity against clinically validated targets overcoming intrinsic- and acquired-degrader resistance. *Nat Commun* 15, 275. <https://doi.org/10.1038/s41467-023-44237-4>
- Schwelberger, H.G., 2010. Structural organization of mammalian copper-containing amine oxidase genes. *Inflammation Research* 59, 223–225. <https://doi.org/10.1007/s00011-009-0135-2>
- Sekine, K., Takubo, K., Kikuchi, R., Nishimoto, M., Kitagawa, M., Abe, F., Nishikawa, K., Tsuruo, T., Naito, M., 2008. Small Molecules Destabilize cIAP1 by Activating Auto-ubiquitylation\*. *Journal of Biological Chemistry* 283, 8961–8968. <https://doi.org/https://doi.org/10.1074/jbc.M709525200>
- Serafimova, I.M., Pufall, M.A., Krishnan, S., Duda, K., Cohen, M.S., Maglathlin, R.L., McFarland, J.M., Miller, R.M., Frödin, M., Taunton, J., 2012. Reversible targeting of noncatalytic

- cysteines with chemically tuned electrophiles. *Nat Chem Biol* 8, 471–476.  
<https://doi.org/10.1038/nchembio.925>
- Shah, S.S., Kumar, S., 2021. Adaptors as the regulators of HECT ubiquitin ligases. *Cell Death Differ* 28, 455–472. <https://doi.org/10.1038/s41418-020-00707-6>
- Shah, V.J., Đikić, I., 2022. Localization matters in targeted protein degradation. *Cell Chem Biol.*  
<https://doi.org/10.1016/j.chembiol.2022.09.006>
- Shao, J., Yan, Y., Ding, D., Wang, D., He, Y., Pan, Y., Yan, W., Kharbanda, A., Li, H., Huang, H., 2021. Destruction of DNA-Binding Proteins by Programmable Oligonucleotide PROTAC (O'PROTAC): Effective Targeting of LEF1 and ERG. *Advanced Science* 8, 2102555.  
<https://doi.org/https://doi.org/10.1002/advs.202102555>
- Shen, Z., Dong, T., Yong, H., Deng, C., Chen, C., Chen, X., Chen, M., Chu, S., Zheng, J., Li, Z., Bai, J., 2024. FBXO22 promotes glioblastoma malignant progression by mediating VHL ubiquitination and degradation. *Cell Death Discov* 10. <https://doi.org/10.1038/s41420-024-01919-2>
- Shergalis, A.G., Marin, V.L., Rhee, D.Y., Senaweera, S., McCloud, R.L., Ronau, J.A., Hutchins, C.W., McLoughlin, S., Woller, K.R., Warder, S.E., Vasudevan, A., Reitsma, J.M., 2023. CRISPR Screen Reveals BRD2/4 Molecular Glue-like Degradator via Recruitment of DCAF16. *ACS Chem Biol* 18, 331–339. <https://doi.org/10.1021/acscchembio.2c00747>
- Shu, Y.-Z., Johnson, B.M., Yang, T.J., 2008. Role of Biotransformation Studies in Minimizing Metabolism-Related Liabilities in Drug Discovery. *AAPS J* 10, 178–192.  
<https://doi.org/10.1208/s12248-008-9016-9>
- Sievers, Q.L., Petzold, G., Bunker, R.D., Renneville, A., Stabicki, M., Liddicoat, B.J., Abdulrahman, W., Mikkelsen, T., Ebert, B.L., Thomä, N.H., 2018. Defining the human C2H2 zinc finger degrader targeted by thalidomide analogs through CRBN. *Science* (1979) 362.  
<https://doi.org/10.1126/science.aat0572>
- Simonetta, K.R., Taygerly, J., Boyle, K., Basham, S.E., Padovani, C., Lou, Y., Cummins, T.J., Yung, S.L., von Soly, S.K., Kayser, F., Kuriyan, J., Rape, M., Cardozo, M., Gallop, M.A., Bence, N.F., Barsanti, P.A., Saha, A., 2019. Prospective discovery of small molecule enhancers of an E3 ligase-substrate interaction. *Nat Commun* 10, 1402. <https://doi.org/10.1038/s41467-019-09358-9>
- Simpson, L.M., Glennie, L., Brewer, A., Zhao, J.-F., Crooks, J., Shpiro, N., Sapkota, G.P., 2022. Target protein localization and its impact on PROTAC-mediated degradation. *Cell Chem Biol* 29, 1482-1504.e7. <https://doi.org/10.1016/j.chembiol.2022.08.004>
- Stabicki, M., Kozicka, Z., Petzold, G., Li, Y.-D., Manojkumar, M., Bunker, R.D., Donovan, K.A., Sievers, Q.L., Koepfel, J., Suchyta, D., Sperling, A.S., Fink, E.C., Gasser, J.A., Wang, L.R., Corsello, S.M., Sellar, R.S., Jan, M., Gillingham, D., Scholl, C., Fröhling, S., Golub, T.R., Fischer, E.S., Thomä, N.H., Ebert, B.L., 2020a. The CDK inhibitor CR8 acts as a molecular

- glue degrader that depletes cyclin K. *Nature* 585, 293–297.  
<https://doi.org/10.1038/s41586-020-2374-x>
- Stabicki, M., Yoon, H., Koepfel, J., Nitsch, L., Roy Burman, S.S., Di Genua, C., Donovan, K.A., Sperling, A.S., Hunkeler, M., Tsai, J.M., Sharma, R., Guirguis, A., Zou, C., Chudasama, P., Gasser, J.A., Miller, P.G., Scholl, C., Fröhling, S., Nowak, R.P., Fischer, E.S., Ebert, B.L., 2020b. Small-molecule-induced polymerization triggers degradation of BCL6. *Nature* 588, 164–168. <https://doi.org/10.1038/s41586-020-2925-1>
- Smithells, R.W., Newman, C.G., 1992. Recognition of thalidomide defects. *J Med Genet* 29, 716. <https://doi.org/10.1136/jmg.29.10.716>
- Spencer, D.M., Wandless, T.J., Schreiber, S.L., Crabtree, G.R., 1993. Controlling Signal Transduction with Synthetic Ligands. *Science* (1979) 262, 1019–1024. <https://doi.org/10.1126/science.7694365>
- Spradlin, J.N., Hu, X., Ward, C.C., Brittain, S.M., Jones, M.D., Ou, L., To, M., Proudfoot, A., Ornelas, E., Woldegiorgis, M., Olzmann, J.A., Bussiere, D.E., Thomas, J.R., Tallarico, J.A., McKenna, J.M., Schirle, M., Maimone, T.J., Nomura, D.K., 2019. Harnessing the anti-cancer natural product nimbolide for targeted protein degradation. *Nat Chem Biol* 15, 747–755. <https://doi.org/10.1038/s41589-019-0304-8>
- Stankunas, K., Bayle, J.H., Gestwicki, J.E., Lin, Y.-M., Wandless, T.J., Crabtree, G.R., 2003. Conditional Protein Alleles Using Knockin Mice and a Chemical Inducer of Dimerization. *Mol Cell* 12, 1615–1624. [https://doi.org/https://doi.org/10.1016/S1097-2765\(03\)00491-X](https://doi.org/https://doi.org/10.1016/S1097-2765(03)00491-X)
- Stanton, B.Z., Chory, E.J., Crabtree, G.R., 2018. Chemically induced proximity in biology and medicine. *Science* (1979) 359, eaao5902–eaao5902. <https://doi.org/10.1126/science.aao5902>
- Stolen, C.M., Yegutkin, G.G., Kurkijärvi, R., Bono, P., Alitalo, K., Jalkanen, S., 2004. Origins of Serum Semicarbazide-Sensitive Amine Oxidase. *Circ Res* 95, 50–57. <https://doi.org/10.1161/01.RES.0000134630.68877.2F>
- Sun, R., Xie, H.-Y., Qian, J.-X., Huang, Y.-N., Yang, F., Zhang, F.-L., Shao, Z.-M., Li, D.-Q., 2018. FBXO22 Possesses Both Protumorigenic and Antimetastatic Roles in Breast Cancer Progression. *Cancer Res* 78, 5274–5286. <https://doi.org/10.1158/0008-5472.CAN-17-3647>
- Taipale, M., Krykbaeva, I., Koeva, M., Kayatekin, C., Westover, K.D., Karras, G.I., Lindquist, S., 2012. Quantitative Analysis of Hsp90-Client Interactions Reveals Principles of Substrate Recognition. *Cell* 150, 987–1001. <https://doi.org/https://doi.org/10.1016/j.cell.2012.06.047>
- Takahashi, D., Moriyama, J., Nakamura, T., Miki, E., Takahashi, E., Sato, A., Akaike, T., Itto-Nakama, K., Arimoto, H., 2019. AUTACs: Cargo-Specific Degradation Using Selective Autophagy. *Mol Cell* 76, 797–810.e10. <https://doi.org/10.1016/j.molcel.2019.09.009>

- Tan, M.-K.M., Lim, H.-J., Bennett, E.J., Shi, Y., Harper, J.W., 2013. Parallel SCF Adaptor Capture Proteomics Reveals a Role for SCFFBXL17 in NRF2 Activation via BACH1 Repressor Turnover. *Mol Cell* 52, 9–24. <https://doi.org/10.1016/j.molcel.2013.08.018>
- Tan, X., Calderon-Villalobos, L.I.A., Sharon, M., Zheng, C., Robinson, C. V., Estelle, M., Zheng, N., 2007. Mechanism of auxin perception by the TIR1 ubiquitin ligase. *Nature* 446, 640–645. <https://doi.org/10.1038/nature05731>
- Teo, S.K., Resztak, K.E., Scheffler, M.A., Kook, K.A., Zeldis, J.B., Stirling, D.I., Thomas, S.D., 2002. Thalidomide in the treatment of leprosy. *Microbes Infect* 4, 1193–1202. [https://doi.org/https://doi.org/10.1016/S1286-4579\(02\)01645-3](https://doi.org/https://doi.org/10.1016/S1286-4579(02)01645-3)
- Tian, X., Dai, S., Sun, J., Jin, G., Jiang, S., Meng, F., Li, Y., Wu, D., Jiang, Y., 2015. F-box protein FBXO22 mediates polyubiquitination and degradation of KLF4 to promote hepatocellular carcinoma progression.
- Tong, B., Luo, M., Xie, Y., Spradlin, J.N., Tallarico, J.A., McKenna, J.M., Schirle, M., Maimone, T.J., Nomura, D.K., 2020a. Bardoxolone conjugation enables targeted protein degradation of BRD4. *Sci Rep* 10, 15543. <https://doi.org/10.1038/s41598-020-72491-9>
- Tong, B., Spradlin, J.N., Novaes, L.F.T., Zhang, E., Hu, X., Moeller, M., Brittain, S.M., McGregor, L.M., McKenna, J.M., Tallarico, J.A., Schirle, M., Maimone, T.J., Nomura, D.K., 2020b. A Nimbolide-Based Kinase Degradere Preferentially Degrades Oncogenic BCR-ABL. *ACS Chem Biol* 15, 1788–1794. <https://doi.org/10.1021/acscchembio.0c00348>
- Toninello, A., Pietrangeli, P., De Marchi, U., Salvi, M., Mondovì, B., 2006. Amine oxidases in apoptosis and cancer. *Biochimica et Biophysica Acta (BBA) - Reviews on Cancer* 1765, 1–13. <https://doi.org/https://doi.org/10.1016/j.bbcan.2005.09.001>
- Tsai, J.M., Aguirre, J.D., Li, Y.-D., Brown, J., Focht, V., Kater, L., Kempf, G., Sandoval, B., Schmitt, S., Rutter, J.C., Galli, P., Sandate, C.R., Cutler, J.A., Zou, C., Donovan, K.A., Lumpkin, R.J., Cavadini, S., Park, P.M.C., Sievers, Q., Hatton, C., Ener, E., Regalado, B.D., Sperling, M.T., Słabicki, M., Kim, J., Zon, R., Zhang, Z., Miller, P.G., Belizaire, R., Sperling, A.S., Fischer, E.S., Irizarry, R., Armstrong, S.A., Thomä, N.H., Ebert, B.L., 2023. UBR5 forms ligand-dependent complexes on chromatin to regulate nuclear hormone receptor stability. *Mol Cell* 83, 2753–2767.e10. <https://doi.org/10.1016/j.molcel.2023.06.028>
- Tsai, J.M., Nowak, R.P., Ebert, B.L., Fischer, E.S., 2024. Targeted protein degradation: from mechanisms to clinic. *Nat Rev Mol Cell Biol*. <https://doi.org/10.1038/s41580-024-00729-9>
- Uehara, T., Minoshima, Y., Sagane, K., Sugi, N.H., Mitsuhashi, K.O., Yamamoto, N., Kamiyama, H., Takahashi, K., Kotake, Y., Uesugi, M., Yokoi, A., Inoue, A., Yoshida, T., Mabuchi, M., Tanaka, A., Owa, T., 2017. Selective degradation of splicing factor CAPERα by anticancer sulfonamides. *Nat Chem Biol* 13, 675–680. <https://doi.org/10.1038/nchembio.2363>
- Van Molle, I., Thomann, A., Buckley, D.L., So, E.C., Lang, S., Crews, C.M., Ciulli, A., 2012. Dissecting Fragment-Based Lead Discovery at the von Hippel-Lindau Protein:Hypoxia

- Inducible Factor 1&#x3b1; Protein-Protein Interface. *Chem Biol* 19, 1300–1312.  
<https://doi.org/10.1016/j.chembiol.2012.08.015>
- Varadi, M., Bertoni, D., Magana, P., Paramval, U., Pidruchna, I., Radhakrishnan, M., Tsenkov, M., Nair, S., Mirdita, M., Yeo, J., Kovalevskiy, O., Tunyasuvunakool, K., Laydon, A., Žídek, A., Tomlinson, H., Hariharan, D., Abrahamson, J., Green, T., Jumper, J., Birney, E., Steinegger, M., Hassabis, D., Velankar, S., 2024. AlphaFold Protein Structure Database in 2024: providing structure coverage for over 214 million protein sequences. *Nucleic Acids Res* 52, D368–D375. <https://doi.org/10.1093/nar/gkad1011>
- Venne, A.S., Kollipara, L., Zahedi, R.P., 2014. The next level of complexity: Crosstalk of posttranslational modifications. *Proteomics* 14, 513–524.  
<https://doi.org/https://doi.org/10.1002/pmic.201300344>
- Wallace, A.D., Cidlowski, J.A., 2001. Proteasome-mediated Glucocorticoid Receptor Degradation Restricts Transcriptional Signaling by Glucocorticoids \*. *Journal of Biological Chemistry* 276, 42714–42721. <https://doi.org/10.1074/jbc.M106033200>
- Wang, C., Zhang, Y., Yang, S., Xing, D., 2023. Recent advances of PROTACs technology in neurodegenerative diseases. *Arabian Journal of Chemistry* 16, 105015.  
<https://doi.org/https://doi.org/10.1016/j.arabjc.2023.105015>
- Wang, Y., Wei, T., Zhao, M., Huang, A., Sun, F., Chen, L., Lin, R., Xie, Y., Zhang, M., Xu, S., Sun, Z., Hong, L., Wang, R., Tian, R., Li, G., 2024. Alkenyl oxindole is a novel PROTAC moiety that recruits the CRL4DCAF11 E3 ubiquitin ligase complex for targeted protein degradation. *PLoS Biol* 22, e3002550-.
- Ward, C.C., Kleinman, J.I., Brittain, S.M., Lee, P.S., Chung, C.Y.S., Kim, K., Petri, Y., Thomas, J.R., Tallarico, J.A., McKenna, J.M., Schirle, M., Nomura, D.K., 2019. Covalent Ligand Screening Uncovers a RNF4 E3 Ligase Recruiter for Targeted Protein Degradation Applications. *ACS Chem Biol* 14, 2430–2440. <https://doi.org/10.1021/acscchembio.8b01083>
- Ward, S.P., 1962. Thalidomide and Congenital Abnormalities. *Br Med J* 2, 646.  
<https://doi.org/10.1136/bmj.2.5305.646>
- Weerapana, E., Wang, C., Simon, G.M., Richter, F., Khare, S., Dillon, M.B.D., Bachovchin, D.A., Mowen, K., Baker, D., Cravatt, B.F., 2010. Quantitative reactivity profiling predicts functional cysteines in proteomes. *Nature* 468, 790–795.  
<https://doi.org/10.1038/nature09472>
- Wei, J., Meng, F., Park, K.-S., Yim, H., Velez, J., Kumar, P., Wang, L., Xie, L., Chen, H., Shen, Y., Teichman, E., Li, D., Wang, G.G., Chen, X., Kaniskan, H.Ü., Jin, J., 2021. Harnessing the E3 Ligase KEAP1 for Targeted Protein Degradation. *J Am Chem Soc* 143, 15073–15083.  
<https://doi.org/10.1021/jacs.1c04841>
- Wells, J.A., Kumru, K., 2024. Extracellular targeted protein degradation: an emerging modality for drug discovery. *Nat Rev Drug Discov*. <https://doi.org/10.1038/s41573-023-00833-z>



- Wenzel, D.M., Lissounov, A., Brzovic, P.S., Klevit, R.E., 2011. UBCH7 reactivity profile reveals parkin and HHARI to be RING/HECT hybrids. *Nature* 474, 105–108. <https://doi.org/10.1038/nature09966>
- Wijayarathne, A.L., McDonnell, D.P., 2001. The Human Estrogen Receptor- $\beta$ ; Is a Ubiquitinated Protein Whose Stability Is Affected Differentially by Agonists, Antagonists, and Selective Estrogen Receptor Modulators \*. *Journal of Biological Chemistry* 276, 35684–35692. <https://doi.org/10.1074/jbc.M101097200>
- Wilkinson, K.D., 2005. The discovery of ubiquitin-dependent proteolysis. *Proceedings of the National Academy of Sciences* 102, 15280–15282. <https://doi.org/10.1073/pnas.0504842102>
- Wilkinson, K.D., Urban, M.K., Haas, A.L., 1980. Ubiquitin is the ATP-dependent proteolysis factor I of rabbit reticulocytes. *Journal of Biological Chemistry* 255, 7529–7532. [https://doi.org/10.1016/S0021-9258\(19\)43857-X](https://doi.org/10.1016/S0021-9258(19)43857-X)
- Winter, G.E., Buckley, D.L., Paulk, J., Roberts, J.M., Souza, A., Dhe-Paganon, S., Bradner, J.E., 2015. Phthalimide conjugation as a strategy for in vivo target protein degradation. *Science* (1979) 348, 1376–1381. <https://doi.org/10.1126/science.aab1433>
- Wu, B., Liu, Z.Y., Cui, J., Yang, X.M., Jing, L., Zhou, Y., Chen, Z.N., Jiang, J.L., 2017. F-box protein FBXO22 mediates polyubiquitination and degradation of CD147 to reverse cisplatin resistance of tumor cells. *Int J Mol Sci* 18. <https://doi.org/10.3390/ijms18010212>
- Wu, X., Bayle, J.H., Olson, D., Levine, A.J., 1993. The p53-mdm-2 autoregulatory feedback loop. *Genes Dev* 7, 1126–1132.
- Wurz, R.P., Rui, H., Dellamaggiore, K., Ghimire-Rijal, S., Choi, K., Smither, K., Amegadzie, A., Chen, N., Li, X., Banerjee, A., Chen, Q., Mohl, D., Vaish, A., 2023. Affinity and cooperativity modulate ternary complex formation to drive targeted protein degradation. *Nat Commun* 14, 4177. <https://doi.org/10.1038/s41467-023-39904-5>
- Xiao, Y., He, Z., Li, W., Chen, D., Niu, X., Yang, X., Zeng, W., Wang, M., Qian, Y., Su, Y., Luo, F., Chen, G., Liu, J., Sui, X., Zhou, X., Gao, Y., 2025. A covalent peptide-based lysosome-targeting protein degradation platform for cancer immunotherapy. *Nat Commun* 16, 1388. <https://doi.org/10.1038/s41467-025-56648-6>
- Xiao, Y., Yuan, Y., Liu, Y., Lin, Z., Zheng, G., Zhou, D., Lv, D., 2024. Targeted Protein Degradation: Current and Emerging Approaches for E3 Ligase Deconvolution. *J Med Chem* 67, 11580–11596. <https://doi.org/10.1021/acs.jmedchem.4c00723>
- Xie, S., Zhu, J., Li, J., Zhan, F., Yao, H., Xu, J., Xu, S., 2023. Small-Molecule Hydrophobic Tagging: A Promising Strategy of Druglike Technology for Targeted Protein Degradation. *J Med Chem* 66, 10917–10933. <https://doi.org/10.1021/acs.jmedchem.3c00736>
- Xie, X., Zhang, O., Yeo, M.J.R., Lee, C., Tao, R., Harry, S.A., Payne, N.C., Nam, E., Paul, L., Li, Y., Kwok, H.S., Jiang, H., Mao, H., Hadley, J.L., Lin, H., Batts, M., Gosavi, P.M., D'Angiolella, V.,

- Cole, P.A., Mazitschek, R., Northcott, P.A., Zheng, N., Liao, B.B., 2025. Converging mechanism of UM171 and KBTBD4 neomorphic cancer mutations. *Nature* 639, 241–249. <https://doi.org/10.1038/s41586-024-08533-3>
- Xu, F., Xu, Y., Xiong, J.H., Zhang, J.H., Wu, J., Luo, J., Xiong, J.P., 2020. AOC1 contributes to tumor progression by promoting the AKT and EMT pathways in gastric cancer. *Cancer Manag Res* 12, 1789–1798. <https://doi.org/10.2147/CMAR.S225229>
- Xue, G., Xie, J., Hinterndorfer, M., Cigler, M., Dötsch, L., Imrichova, H., Lampe, P., Cheng, X., Adariani, S.R., Winter, G.E., Waldmann, H., 2023. Discovery of a Drug-like, Natural Product-Inspired DCAF11 Ligand Chemotype. *Nat Commun* 14, 7908. <https://doi.org/10.1038/s41467-023-43657-6>
- Yamanaka, S., Furihata, H., Yanagihara, Y., Taya, A., Nagasaka, T., Usui, M., Nagaoka, K., Shoya, Y., Nishino, K., Yoshida, S., Kosako, H., Tanokura, M., Miyakawa, T., Imai, Y., Shibata, N., Sawasaki, T., 2023. Lenalidomide derivatives and proteolysis-targeting chimeras for controlling neosubstrate degradation. *Nat Commun* 14, 4683. <https://doi.org/10.1038/s41467-023-40385-9>
- Zengerle, M., Chan, K.-H., Ciulli, A., 2015. Selective Small Molecule Induced Degradation of the BET Bromodomain Protein BRD4. *ACS Chem Biol* 10, 1770–1777. <https://doi.org/10.1021/acscchembio.5b00216>
- Zenke-Kawasaki, Y., Yoshihiro, D., Yasutake, K., Tsuyoshi, I., Masae, I., Toshimasa, A., Fuminori, T., Kazuhiro, I., and Igarashi, K., 2007. Heme Induces Ubiquitination and Degradation of the Transcription Factor Bach1. *Mol Cell Biol* 27, 6962–6971. <https://doi.org/10.1128/MCB.02415-06>
- Zhang, D.D., Shih-Ching, L., Janet V., C., Dennis J., T., and Hannink, M., 2004. Keap1 Is a Redox-Regulated Substrate Adaptor Protein for a Cul3-Dependent Ubiquitin Ligase Complex. *Mol Cell Biol* 24, 10941–10953. <https://doi.org/10.1128/MCB.24.24.10941-10953.2004>
- Zhang, Long, Chen, J., Ning, D., Liu, Q., Wang, C., Zhang, Z., Chu, L., Yu, C., Liang, H., Zhang, B., Chen, X., 2019. FBXO22 promotes the development of hepatocellular carcinoma by regulating the ubiquitination and degradation of p21. *Journal of Experimental & Clinical Cancer Research* 38, 101. <https://doi.org/10.1186/s13046-019-1058-6>
- Zhang, Lu, Riley-Gillis, B., Vijay, P., Shen, Y., 2019. Acquired Resistance to BET-PROTACs (Proteolysis-Targeting Chimeras) Caused by Genomic Alterations in Core Components of E3 Ligase Complexes. *Mol Cancer Ther* 18, 1302–1311. <https://doi.org/10.1158/1535-7163.MCT-18-1129>
- Zhang, X., Crowley, V.M., Wucherpfennig, T.G., Dix, M.M., Cravatt, B.F., 2019. Electrophilic PROTACs that degrade nuclear proteins by engaging DCAF16. *Nat Chem Biol* 15, 737–746. <https://doi.org/10.1038/s41589-019-0279-5>
- Zhang, X., Luukkonen, L.M., Eissler, C.L., Crowley, V.M., Yamashita, Y., Schafroth, M.A., Kikuchi, S., Weinstein, D.S., Symons, K.T., Nordin, B.E., Rodriguez, J.L., Wucherpfennig, T.G., Bauer,

- L.G., Dix, M.M., Stamos, D., Kinsella, T.M., Simon, G.M., Baltgalvis, K.A., Cravatt, B.F., 2021. DCAF11 Supports Targeted Protein Degradation by Electrophilic Proteolysis-Targeting Chimeras. *J Am Chem Soc* 143, 5141–5149. <https://doi.org/10.1021/jacs.1c00990>
- Zhang, X., Simon, G.M., Cravatt, B.F., 2025. Implications of frequent hitter E3 ligases in targeted protein degradation screens. *Nat Chem Biol* 21, 474–481. <https://doi.org/10.1038/s41589-024-01821-z>
- Zhang, X., Thummuri, D., He, Y., Liu, X., Zhang, P., Zhou, D., Zheng, G., 2019. Utilizing PROTAC technology to address the on-target platelet toxicity associated with inhibition of BCL-XL. *Chemical Communications* 55, 14765–14768. <https://doi.org/10.1039/C9CC07217A>
- Zhang, Y., Remillard, D., Onubogu, U., Karakyriakou, B., Asiaban, J.N., Ramos, A.R., Bowland, K., Bishop, T.R., Barta, P.A., Nance, S., Durbin, A.D., Ott, C.J., Janiszewska, M., Cravatt, B.F., Erb, M.A., 2023. Collateral lethality between HDAC1 and HDAC2 exploits cancer-specific NuRD complex vulnerabilities. *Nat Struct Mol Biol* 30, 1160–1171. <https://doi.org/10.1038/s41594-023-01041-4>
- Zhao, L., Zhao, J., Zhong, K., Tong, A., Jia, D., 2022. Targeted protein degradation: mechanisms, strategies and application. *Signal Transduct Target Ther* 7, 113. <https://doi.org/10.1038/s41392-022-00966-4>
- Zheng, N., Shabek, N., 2017. Ubiquitin Ligases: Structure, Function, and Regulation 11, 42. <https://doi.org/10.1146/annurev-biochem>
- Zheng, X., Ji, N., Campbell, V., Slavin, A., Zhu, X., Chen, D., Rong, H., Enerson, B., Mayo, M., Sharma, K., Browne, C.M., Klaus, C.R., Li, H., Massa, G., McDonald, A.A., Shi, Y., Sintchak, M., Skouras, S., Walther, D.M., Yuan, K., Zhang, Y., Kelleher, J., Liu, G., Luo, X., Mainolfi, N., Weiss, M.M., 2024. Discovery of KT-474—a Potent, Selective, and Orally Bioavailable IRAK4 Degradator for the Treatment of Autoimmune Diseases. *J Med Chem* 67, 18022–18037. <https://doi.org/10.1021/acs.jmedchem.4c01305>
- Zheng, X.-F., Fiorentino, D., Chen, J., Crabtree, G.R., Schreiber, S.L., 1995. TOR kinase domains are required for two distinct functions, only one of which is inhibited by rapamycin. *Cell* 82, 121–130. [https://doi.org/https://doi.org/10.1016/0092-8674\(95\)90058-6](https://doi.org/https://doi.org/10.1016/0092-8674(95)90058-6)
- Zheng, Y., Chen, H., Zhao, Y., Zhang, X., Liu, J., Pan, Y., Bai, J., Zhang, H., 2020. Knockdown of FBXO22 inhibits melanoma cell migration, invasion and angiogenesis via the HIF-1 $\alpha$ /VEGF pathway. *Invest New Drugs* 38, 20–28. <https://doi.org/10.1007/s10637-019-00761-z>
- Zhong, C., Wang, Z., Li, Z., Li, H., Xu, Q., Wu, W., Liu, C., Fei, Y., Ding, Y., Lu, B., 2024. Mechanisms mediating arylidene-indolinones induced degradation: thoughts on “Discovery of a Drug-like, Natural Product-Inspired, DCAF11 Ligand Chemotype.” *bioRxiv* 2024.03.05.582859-2024.03.05.582859. <https://doi.org/10.1101/2024.03.05.582859>
- Zhou, P., Bogacki, R., McReynolds, L., Howley, P.M., 2000. Harnessing the ubiquitination machinery to target the degradation of specific cellular proteins. *Mol Cell* 6, 751–756. [https://doi.org/10.1016/S1097-2765\(00\)00074-5](https://doi.org/10.1016/S1097-2765(00)00074-5)

- Zhou, X.-L., Zhao, F., Xu, Y.-T., Guan, Y.-Y., Yu, T., Zhang, Y.-Z., Duan, Y.-C., Zhao, Y., 2022. A comprehensive review of BET-targeting PROTACs for cancer therapy. *Bioorg Med Chem* 73, 117033. <https://doi.org/https://doi.org/10.1016/j.bmc.2022.117033>
- Zhu, J., Gianni, M., Kopf, E., Honoré, N., Chelbi-Alix, M., Koken, M., Quignon, F., Rochette-Egly, C., de Thé, H., 1999. Retinoic acid induces proteasome-dependent degradation of retinoic acid receptor  $\alpha$  (RAR $\alpha$ ) and oncogenic RAR $\alpha$  fusion proteins. *Proceedings of the National Academy of Sciences* 96, 14807–14812. <https://doi.org/10.1073/pnas.96.26.14807>
- Zhu, J., Koken, M.H.M., Quignon, F., Chelbi-Alix, M.K., Degos, L., Wang, Z.Y., Chen, Z., de Thé, H., 1997. Arsenic-induced PML targeting onto nuclear bodies: Implications for the treatment of acute promyelocytic leukemia. *Proceedings of the National Academy of Sciences* 94, 3978–3983. <https://doi.org/10.1073/pnas.94.8.3978>
- Zhu, X.-N., He, P., Zhang, L., Yang, S., Zhang, H.-L., Zhu, D., Liu, M.-D., Yu, Y., 2019. FBXO22 mediates polyubiquitination and inactivation of LKB1 to promote lung cancer cell growth. *Cell Death Dis* 10, 486. <https://doi.org/10.1038/s41419-019-1732-9>
- Zhu, Y.X., Braggio, E., Shi, C.-X., Bruins, L.A., Schmidt, J.E., Van Wier, S., Chang, X.-B., Bjorklund, C.C., Fonseca, R., Bergsagel, P.L., Orlowski, R.Z., Stewart, A.K., 2011. Cereblon expression is required for the antimyeloma activity of lenalidomide and pomalidomide. *Blood* 118, 4771–4779. <https://doi.org/10.1182/blood-2011-05-356063>
- Zhu, Y.X., Braggio, E., Shi, C.X., Kortuem, K.M., Bruins, L.A., Schmidt, J.E., Chang, X.B., Langlais, P., Luo, M., Jedlowski, P., LaPlant, B., Laumann, K., Fonseca, R., Bergsagel, P.L., Mikhael, J., Lacy, M., Champion, M.D., Stewart, A.K., 2014. Identification of cereblon-binding proteins and relationship with response and survival after IMiDs in multiple myeloma. *Blood* 124, 536–545. <https://doi.org/10.1182/blood-2014-02-557819>
- Zhuang, Z., Byun, W.S., Chrustowicz, J., Kozicka, Z., Li, V.L., Abeja, D.M., Donovan, K.A., Sepic, S., You, I., Slabicki, M., Fischer, E.S., Hinshaw, S.M., Ebert, B.L., Schulman, B.A., Gray, N.S., 2024. Charged Molecular Glue Discovery Enabled by Targeted Degron Display. <https://doi.org/10.1101/2024.09.24.614843>

## **Appendix & CV**

The manuscript presented in this thesis in Chapter 2.3 was published at Nature Communications and is an open access article distributed under the Creative Commons CC BY licence, permitting unrestricted use, distribution and reproduction, if properly cited.

# Chrysanthi Kagiou

PhD candidate

CeMM

(Research Center for Molecular  
Medicine of the Austrian  
Academy of Sciences)

## CONTACT



+4367764007221



[ckagiou@cemm.at](mailto:ckagiou@cemm.at)



[@CKagiou](https://twitter.com/CKagiou)



[chrysanthi-kagiou-](https://www.linkedin.com/company/chrysanthi-kagiou/)



<https://orcid.org/0000-0002-2795-1194>

## LANGUAGES

Greek – Native speaker

Albanian – Passive speaker

German – A2

English – C2 (Proficiency)

Certificate, Cambridge)

## TECHNICAL SKILLS

### Tissue culture

Extensive culturing experience,  
transfections & transductions, cell  
lines and primary cells

### Genome editing

CRISPR-Cas9 knock-out and  
knock-in  
Prime editing and base editing

### High-throughput screening

CRISPR KO viability screens  
CRISPR-KO coupled with stability  
reporter and FACS sorting  
High-throughput drug screens

## Education

06/2022 – Present

### PhD candidate

Ce-M-M Research Center for Molecular Medicine of the Austrian Academy of Sciences,  
Austria, Supervisor Dr. Georg Winter

09/2020 – 06/2022

### PhD candidate (*discontinued due to laboratory termination*)

Institute of Cancer Research, Medical University of Vienna, Austria, Supervisor Dr. Joanna Loizou

09/2018 – 08/2020

### MSc in Molecular Mechanisms of Disease, (8.63/10 *Cum Laude*)

Radboud University Medical Centre, Nijmegen, Netherlands

10/2013 - 10/2017

### BSc in Biology, 2<sup>nd</sup>/128 graduates in 2016-2017 (8.72/10 *Excellent*)

University of Athens, Greece

## Research Experience

06/2022 – Present

**PhD candidate: Hijacking novel non-PROTACable E3 ligases for targeted protein degradation**, CeMM Research Center for Molecular Medicine of the Austrian Academy of Sciences, Austria, Supervisor Dr. Georg Winter

09/2020 – 06/2022

**PhD candidate (*discontinued due to laboratory termination*): Dissecting cancer associated mutations at single-base resolution**, CeMM & Institute of Cancer Research, Medical University of Vienna, Austria, Supervisor Dr. Joanna Loizou

11/2019 – 07/2020

**MSc Internship: Fever-range hyperthermia as supporting strategy for cancer immunotherapy**, Werner Siemens Imaging Center, Universitätsklinikum Tübingen, Germany, Supervisor Dr. Bettina Weigelin

01/2019 – 07/2019

**MSc Internship: Study of immune checkpoint pathways in immune escape after allogeneic stem cell transplantation**, Laboratory of Hematology, Radboudumc, Nijmegen, The Netherlands, Supervisor Dr. Willemijn Hobo

10/2016 - 10/2017

**BSc Thesis: Role of transcription factor NF-κB in mammalian cardiac myocytes**, Physiology Department, Faculty of Biology, University of Athens, Greece Supervisor Pr. Catherine Gaitanaki

07/2016 - 09/2016

**BSc Internship: Basic applications of histochemical techniques during the function of a Histochemistry Unit**, Biomedical Research Foundation, Academy of Athens (BRFAA), Greece, Supervisor Dr. Stelios Psarras

## Conferences / Certificates

**Ubiquitin and Friends Symposium** (organizing committee), Vienna, May 2025

**Molecular Biology:**  
PCR, Cloning, DNA/RNA isolation

**Flow cytometry:**  
Multicolor flow cytometry, FACS sorting

**Microscopy**  
Live-cell time-lapse, Confocal and epifluorescence, Immunofluorescence staining

**Biochemical assays**  
Western blotting, Immunoprecipitation,

**Luminescence-based assays**  
HiBiT, NanoBiT, Nanoluc, Cell viability assays

**Data analysis**  
CRISPR-KO screen analysis workflow, R for visualization of large data, Basic level for proteomics data analysis (EMBO practical course certificate)

## OTHER SKILLS

**Microsoft Office** ●●●●●

**Graphpad Prism** ●●●●○

**Image analysis** ●●●●○  
(ImageJ, CellProfiler)

**Graphics** ●●●●○  
(Adobe Illustrator)

**Flow cytometry analysis software** ●●●●○  
(FlowJo)

**EMBO Practical Course on Quantitative proteomics: Strategies and tools to probe biology**, EMBL, Heidelberg, March 2025

**EMBO Workshop: Chemical Biology 2024** (poster presentation), EMBL, Heidelberg, September 2024

**CeTPD symposium, Protein Degradation in Focus**, A Special Symposium to Celebrate the Opening of CeTPD in Dundee (poster presentation), Dundee, May 2024

**Precision Genome Engineering**, Keystone, online, April 2022

**FELASA (EU Function B) certificate for Mouse and Rat**. FELASA accredited Nijmegen course 058/17 for person designing projects and procedures, Nijmegen, The Netherlands, November 2019

**3rd European PhD and Postdoc symposium (ENABLE) “Next-generation life scientists: Side by side to break new ground”**, (poster presentation), Nijmegen, November 2019

## Awards & Scholarships

**Studyfund for Molecular Mechanisms of Disease Studies** 2018 - 2020  
Radboud University Medical Centre, Nijmegen, Netherlands

**Scholarship for Master Studies** 2018 - 2020  
Bodossaki Foundation, Athens, Greece

**Sponsorship “The great moment for education”** 2013  
For highest grades at the pan-hellenic university admission examinations. EFG Eurobank Ergasias, Athens, Greece

## Publications

**Kagiou, C.**, Cisneros, J. A., Farnung, J., Liwocha, J., Offensperger, F., Dong, K., Yang, K., Tin, G., Horstmann, C. S., Hinterndorfer, M., Paulo, J. A., Scholes, N. S., Sanchez Avila, J., Fellner, M., Andersch, F., Hannich, J. T., Zuber, J., Kubicek, S., Gygi, S. P., Schulman, B. A., & Winter, G. E. (2024). **Alkylamine-tethered molecules recruit FBXO22 for targeted protein degradation.** *Nature Communications*, 15, Article 5409. <https://doi.org/10.1038/s41467-024-49739-3>

Cigler, M., Imrichova, H., Frommelt, F., Caramelle, L., Depta, L., Rukavina, A., **Kagiou, C.**, Hannich, J. T., Mayor-Ruiz, C., Superti-Furga, G., Sievers, S., Forrester, A., Laraia, L., Waldmann, H., & Winter, G. E. (2025). **Orpinolide disrupts a leukemic dependency on cholesterol transport by inhibiting OSBP.** *Nature Chemical Biology*, 21, 193–202. <https://doi.org/10.1038/s41589-024-01614-4>

Ferreira da Silva, J., Oliveira, G. P., Arasa-Verge, E. A., **Kagiou, C.**, Moreton, A., Timelthaler, G., Jiricny, J., & Loizou, J. I. (2022). **Prime editing efficiency and fidelity are enhanced in the absence of mismatch repair.** *Nature Communications*, 13, Article 760. <https://doi.org/10.1038/s41467-022-28442-1>



